SMART BIOMATERIALS

LOH XIAN JUN
(B.Appl.Sc (Hons.), NUS)

A THESIS SUBMITTED
FOR THE DEGREE OF DOCTOR OF PHILOSOPHY

ACKNOWLEDGEMENTS

I would like to thank my thesis advisor A/Prof Li Jun for his advice, support and invaluable mentoring of my scientific and personal development. I am very grateful for the opportunity to have worked with him for my dissertation. I am appreciative of my Thesis Advisory Committee, A/Prof Zhang Yongwei and Dr Zeng Kaiyang for their helpful comments throughout my candidature. I would like to thank Dr Lim Khiang Wee of Institute of Materials Research and Engineering (IMRE) for closely monitoring my progress and providing important advice during my PhD.

I am thankful for the times I spent with my laboratory members and students in the Institute of Materials Research and Engineering (IMRE) as well as National University of Singapore (NUS). I would treasure the memories of our interactions and discussions for a long time.

My attachment to the Nanomedical Engineering Laboratory in RIKEN, Japan showed me a perspective of the Japanese scientific research. I thank Prof Yoshihiro Ito for his kind hospitality. His vision and encouragement was a source of my motivation when I was working there. I would also like to thank my laboratory colleagues who patiently taught me all the biological characterization techniques I needed for my project.

This research is funded by Agency for Science, Technology and Research (A*STAR) and National University of Singapore. I am grateful to the A*STAR Graduate Scholarship for financial support of my candidature.

Most importantly, I am extremely grateful to my parents, Loh Moi Joo and Lim Joo Gek for always being there for me, for every dinner time discussion of my work, for trying to understand the things that I wrote in my manuscripts and for encouraging and supporting me all the way. I would not have been able to complete this without the both of you. This work is dedicated to my late grandfather, Lim Seak Liang, for taking care of me in my early years, for sparking my creativity in various aspects of my life and for just being around for me during my university days. Words cannot express how much I miss you.

TABLE OF CONTENTS

Chapter 9. Conclusions

SUMMARY

The first part of this thesis focuses on biodegradable multiblock thermoresponsive poly(ether ester urethane)s consisting of poly(ethylene glycol) (PEG), poly(propylene glycol) (PPG) and poly-[(*R*)-3-hydroxybutyrate] (PHB). The thermogelling behaviors of these copolymers as well as the thermodymanic basis of the micelle formation are presented. Sustained protein release is demonstrated with the hydrogels. These copolymers degrade within 1 month to 6 months, depending on the composition and the type of biopolyester incorporated into the copolymer.

Novel thermoresponsive amphiphilic triblock copolymers with two hydrophilic PNIPAAm blocks flanking a central hydrophobic poly[(*R*)-3-hydroxybutyrate] block were synthesized by atom transfer radical polymerization. The water soluble copolymers formed core-corona type micelle aggregates at very low critical micelle concentrations. Using this copolymer, a thermoresponsive substrate was fabricated by drop-coating with an aqueous polymer solution, and used for the attachment and nonenzymatic temperature-induced detachment of human mesenchymal stem cells and mouse embryonic stem (ES) cells. The promising results from the studies show that these copolymers could be utilized as surface modifiers for tissue engineering applications.

In summary, the synthesis of novel “smart biomaterials” and their application in the fields of drug delivery and tissue engineering are described in this thesis.

LIST OF TABLES

LIST OF FIGURES

ABBREVIATIONS

AFM	Atomic Force Microscopy
ALP	Alkaline Phosphatase
ATCC	American Type Culture Collection
ATR-FTIR	Attenuated Total Reflectance – Fourier Transform Infra-Red
ATRP	Atom Transfer Radical Polymerization
BSA	Bovine Serum Albumin
CGC	Critical Gelation Concentration
CMC	Critical Micellization Concentration
CO_2	Carbon dioxide
DLS	Dynamic Light Scattering
DMAAm	Dimethylacrylamide
DMEM	Dulbecco's Minimum Essential Medium
DMSO	Dimethylsulfoxide
DNA	Deoxyribonucleic Acid
DPH	1,6-Diphenyl-1,3,5-Hexatriene
DSC	Differential Scanning Calorimetry
ECM	Extra-Cellular Matrix
EDTA	Ethylenediaminetetraacetic acid
ES cell	Embryonic Stem Cell
FBS	Fetal Bovine Serum
FDA	Food and Drug Administration

FTIR	Fourier Transform Infrared Spectroscopy
GI	Gastrointestinal
GLP	Glucagon-Like Peptide
GMEM	Glasgow Minimum Essential Medium
GPC	Gel Permeation Chromatography
HDI	1,6-Hexamethylene Diisocyanate
hMSC	Human Mesenchymal Stem Cell
HMTETA	1,1,4,7,10,10-hexamethyltriethylenetetramine
IV	Intravenous
LCST	Lower Critical Solution Temperature
LIF	Leukemia Inhibitory Factor
MALDI-TOF	Matrix-Assisted Laser Desorption/Ionization-Time Of Flight
M_n	Number Average Molecular Weight
MTT	3-(4, 5-dimethylthiazol-2-yl)-2,5-diphenyl tetrazolium bromide
M_w	Weight Average Molecular Weight
NMR	Nuclear Magnetic Resonance
PBS	Phosphate Buffer Solution
PCL	Poly(ε-Caprolactone)
PDI	Polydispersity Index
PDLLA	Poly(DL-Lactic Acid)
PEG	Poly(Ethylene Glycol)
PEO	Poly(Ethylene Oxide)

PHB	Poly[(*R*)-3-Hydroxybutyrate]
PHBHHx	Poly(3-hydroxybutyrate-co-3-hydroxyhexanoate)
PLGA	Poly(Lactic-Co-Glycolic Acid)
PMMA	Poly(Methyl Methacrylate)
PNIPAAm	Poly(N-Isopropylacrylamide)
PPF	Poly(Propylene Fumarate)
PPG	Poly(Propylene Glycol)
RT-PCR	Reverse Transcription Polymerase Chain Reaction
SD	Standard Deviation
SEM	Scanning Electron Microscopy
STAT3	Signal Transducer and Activator of Transcription 3
TEM	Transmission Electron Microscopy
TGA	Thermogravimetric Analyser
THF	Tetrahydrofuran
UV-Vis	Ultraviolet-Visible

LIST OF PUBLICATIONS

1. **X. J. Loh**, Y. L. Wu, W. T. J. Seow, M. N. I. Norimzan, Z. X. Zhang, F. J. Xu, E. T. Kang, K. G. Neoh, J. Li, "Micellization and phase transition behavior of thermosensitive poly(N-isopropylacrylamide)–poly(ε-caprolactone)–poly(N-isopropylacrylamide) triblock copolymers" *Polymer*, 49, **2008**, 5084-5094.
2. **X. J. Loh**, Z. X. Zhang, Y. L. Wu, T. S. Lee, J. Li, "Synthesis of novel biodegradable thermoresponsive triblock copolymers based on poly[(R)-3-hydroxybutyrate] and poly(N-isopropylacrylamide) and their formation of thermoresponsive micelles" *Macromolecules*, 42, **2009**, 194-202.
3. **X. J. Loh**, W. C. D. Cheong, J. Li, Y. Ito, "Poly(N-isopropylacrylamide)-poly[(R)-3-hydroxybutyrate]-poly(N-isopropylacrylamide) triblock copolymer as a culture substrate for human mesenchymal stem cells" *Soft Matter*, 5, **2009**, 2937-2946.
4. **X. J. Loh**, J. S. Gong, M. Sakuragi, T. Kitajima, M. Liu, J. Li, Y. Ito, "Surface coating with a thermoresponsive copolymer for the culture and nonenzymatic recovery of mouse embryonic stem cells" *Macromolecular Bioscience*, **2009**, In Press.
5. **X. J. Loh**, S. H. Goh, J. Li "New biodegradable thermogelling copolymers having very low gelation concentrations ", *Biomacromolecules*, 8, **2007**, 585-593
6. **X. J. Loh**, S. H. Goh, J. Li, "Hydrolytic degradation and protein release studies of thermogelling polyurethane copolymers consisting of poly[(R)-3-hydroxybutyrate], poly(ethylene glycol), and poly(propylene glycol). *Biomaterials*, 28, **2007**, 4113-4123.
7. **X. J. Loh**, J. Li, "Biodegradable thermosensitive copolymer hydrogels for drug delivery" (Invited Review). *Expert Opinion on Therapeutic Patents*, 17(8), 2007, 965-977.
8. **X. J. Loh**, Y. X. Tan, Z. Li, L. S. Teo, S. H. Goh, J. Li "Biodegradable thermogelling poly(ester urethane)s consisting of poly(lactic acid) – Thermodynamics of micellization and hydrolytic degradation." *Biomaterials*, 29, **2008**, 2164–2172.
9. **X. J. Loh**, K.B.C. Sng, J. Li, "Synthesis and water-swelling of thermo-responsive poly(ester urethane)s containing polycaprolactone, poly(ethylene glycol) and poly(propylene glycol)." *Biomaterials*, 29, **2008**, 3185-3194.
10. **X. J. Loh**, S. H. Goh, J. Li, "Biodegradable Thermogelling Poly[(R)-3-hydroxybutyrate]-Based Block Copolymers: Micellization, Gelation, and Cytotoxicity and Cell Culture Studies." *Journal of Physical Chemistry B*, 113, **2009**, 11822-11830.

CHAPTER ONE

INTRODUCTION

1.1. Research Background

From time immemorial, man's ingenious use of various natural and synthetic substances to intervene and promote healing in the human body has sown the seeds of the dynamic field of biomaterials. Since the days of the Pharaohs, Egyptians had used linen sutures to close large wounds.[1] The Mayan people of South America had used dental implants made from nacre extracted from seashells to seamlessly integrate into bones.[2] Biomaterials, as we know today, did not exist until after World War II. In 1987, Prof D. F. Williams had defined a biomaterial as "a nonviable material used in a medical device, intended to interact with biological systems." This statement is currently the most endorsed definition of "biomaterial" in literature. [3] Huge strides in the biomaterials community over the last 60 years had seen biomaterials being used in a wide variety of devices such as intraocular lenses, hip/knee prostheses, dental implants, artificial kidneys, artificial hearts, breast implants, vascular grafts, stents, pacemakers and heart valves.[4] Biomaterials have also been used for a variety of applications, such as tissue regeneration, gene delivery, protein assaying, drug delivery and wound healing.[5-7] These advances have helped to improve the quality of life for mankind over the past six decades.

Since about 20 years ago, the direction of biomaterials science has moved towards the control of the properties of a biomaterial based on the environment it is placed in.[8] Such environmentally-sensitive biomaterials are classified as "smart biomaterials" because a change in a particular environmental stimulus, such as temperature, could lead to a change in the property of the material, such as the volume change in a gel. The concept of a smart biomaterial is represented in Figure 1.1.

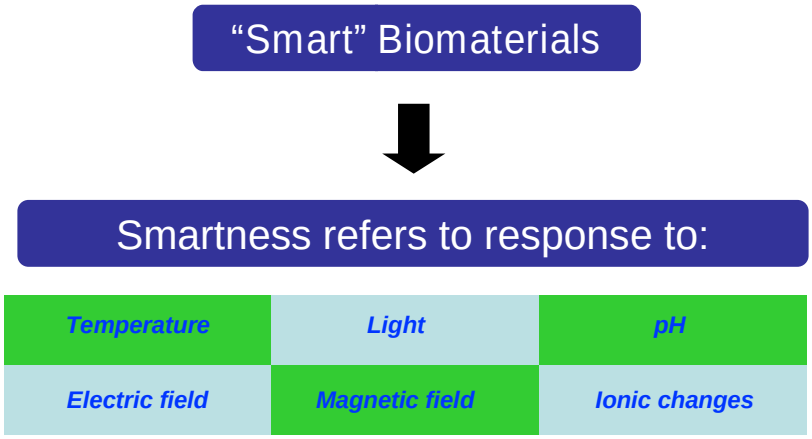

Figure 1.1. Concept of a smart biomaterial

1.2. Objectives and Scope of Study

"Smart biomaterials" are novel materials that can respond to minute external physical, chemical, or biological stimuli, and greatly change their structure, shape, size, morphology, or other physical properties. They have attracted much attention in recent years, with many interesting proposed applications in biomedical areas. The objective of this work is to develop novel smart biomaterials and to investigate the feasibility of their application to biomedical areas such as drug delivery and tissue engineering. The target is to introduce thermoresponsiviness to a biodegradable material and this will be done via 2 different approaches (Figure 1.2).

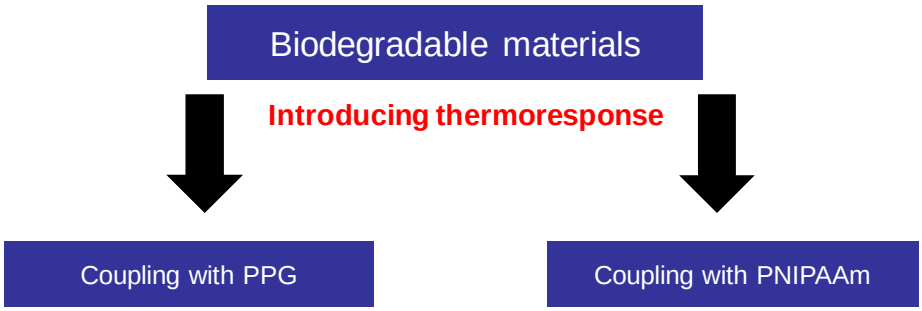

Figure 1.2. Strategy adopted in this work to introduce thermoresponse to a biodegradable material.

The biodegradable biopolyester to be used in this work is poly[(*R*)-3-hydroxybutyrate] (PHB). PHB belongs to a class of biologically synthesized polyesters known as poly[(*R*)-3-hydroxyalkanoate]s.[9-14] PHB has been extracted from genetically modified plants.[15] PHB is a thermoplastic polyester, with mechanical properties close to those of isotactic polypropylene, which can be extruded, molded, and spun using conventional processing equipment. Rising oil prices has seen the increasing popularity of the PHB compared with conventional commodity plastics. Due to its degradable nature, PHB is considered to be an environmentally friendly plastic when compared to its non-degradable counterparts such as polystyrene or polyethylene. These attractive properties have led to the use of PHB as materials in areas such as packaging. PHB degrades to D-3-hydroxybutyrate which is a natural constituent of human blood.[16] As a result of this advantageous property, PHB may be suitable for a variety of biomedical applications, such as uses as drug carriers and tissue engineering scaffolds. Due to its inherent hydrophobicity, PHB is rarely used in applications requiring good water solubility, such as polymeric micelles and gels. The challenge would be in the chemical modification of PHB into a water soluble compound.

The focus of this thesis will be on the design and synthesis of novel amphiphilic block copolymers comprising both biopolyesters and biocompatible polyethers or other polymer

segments. The thermosensitive polymer used will be poly(propylene glycol) (PPG). Through the control of the chemical structures, sequences, block lengths and compositions, the amphiphilic copolymers can be made environmentally sensitive, and can be applied as smart hydrogels as well as micro/nano-capsules for drug delivery and controlled release. Another focus of this project is the design of novel supramolecular structures via the self-assembly of functional block copolymers. In this case, the temperature responsive segment used will be poly(N-isopropylacrylamide) (PNIPAAm). The smart supramolecular structures can be utilized as substrate coating materials for tissue engineering applications, transforming normal cell culture substrates into thermoresponsive substrates for the non-enzymatic detachment of cell sheets from cell culture systems.

Specifically, the objectives of this thesis are:

a. Synthesis and characterization of poly(ester urethane) comprising PEG, PPG and PHB.

b. Study of the self-assembly behavior of the poly(ester urethane)s

c. Evaluation of the hydrolytic degradation, drug release and cyto-compatiblity of the poly(ester urethane)s.

d. Synthesis and characterization of PNIPAAm-PHB-PNIPAAm triblock copolymers.

e. Study of the use of PNIPAAm-PHB-PNIPAAm triblock copolymers as surface substrate modifiers for thermally induced human mesenchymal stem cell detachment.

f. Study of the use of PNIPAAm-PHB-PNIPAAm triblock copolymers as surface substrate modifiers for thermally induced mouse embryonic stem cell detachment

1.3. References

1. Mackenzie, D. *Med. Hist.* **1973,** *17*, 158-168.
2. Westbroek, P; Marin, F. *Nature* **1998**, *392*, 861–862.
3. Williams, D. F. *Definitions in Biomaterials. Proceedings of a Consensus Conference of the European Society for Biomaterials*, Vol. 4, Elsevier, Amsterdam, **1987**.
4. Ratner, B.D.; Hoffman, A.S.; Schoen, F.J.; Lemons, J.E. (eds). *Biomaterials science: An introduction to materials in medicine*, Elsevier, Amsterdam, **2004**.
5. Griffith, L.G.; Naughton, G. *Science* **2002**, *295,* 1009-1014.
6. Langer, R.; Tirrell, D. A. *Nature* **2004**, *428,* 487-492.
7. Langer, R. *Accounts Chem. Res.* **2000**, *33*, 94-101.
8. Hoffman, A. S. *MRS Bulletin* **1991**, *16*, 42-46.
9. Doi, Y., Steinbuchel, A., Eds.; *Biopolymers, Polyesters I-III*; Wiley: New York, 2001; Vols. 3, 3b, and 4.
10. Doi, Y. *Microbial Polyesters*; VCH Publishers: New York, 1990.
11. Anderson, A. J.; Dawes, E. A. *Microbiol. Rev.* **1990**, *54*, 450-472.
12. Dawes, E. A. *Novel Biodegradable Microbial Polymers*; Kluwer: Dordrecht, 1990.
13. Satkowski, M. M.; Melik, D. H.; Autran, J. P.; Green, P. R.; Noda, I.; Schechtman, L. A. In *Biopolymers*; Steinbuchel, A., Doi, Y., Eds.; Wiley-VCH: Wienheim, 2001; p 231.
14. Iwata, T.; Doi, Y. *Macromol. Chem. Phys.* **1999**, *200*, 2429-2442.
15. Purnell, M. P.; Petrasovits, L. A.; Nielsen, L. K.; Brumbley, S. M. *Plant Biotechnol. J.* **2007,** *5,* 173-184.
16. Reusch, R. N. *Can. J. Microbiol.* **1995**, *41*, 50-54.

CHAPTER TWO

LITERATURE REVIEW

2.1. Applications of Smart Biomaterials

There are many examples of successful applications of these "smart biomaterials" in biomedical technology, such as for drug delivery, tissue engineering, protein assaying, protein conjugation, affinity separations and toxin removal.[1-6] These materials extend the field of biomaterials science beyond the conventional implants and medical devices. The major thrust of this thesis is in the synthesis and application of "smart biomaterials" in the fields of drug delivery and tissue engineering as depicted in Figure 2.1. This literature review will give an overview on the use of smart biomaterials in these areas.

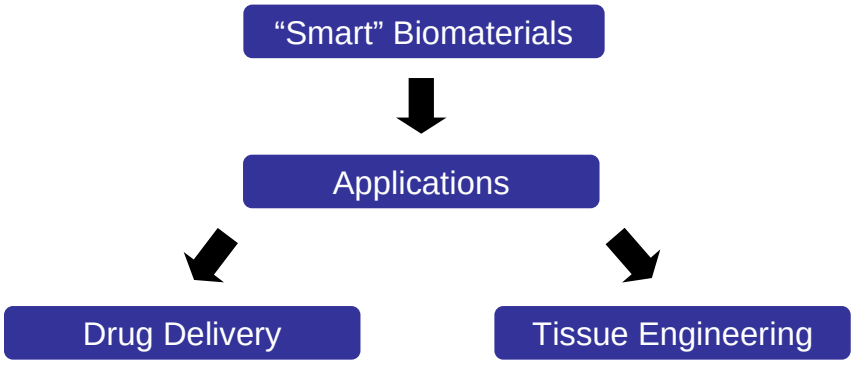

Figure 2.1. Targeted applications of smart biomaterials in this thesis

2.2. Smart Biomaterials for Drug Delivery

Drug delivery poses great challenges to clinicians everywhere. Drugs work at their optimum efficacy when they are maintained at a certain concentration in the blood plasma known as the therapeutic concentration. Below this concentration, the efficacy of the drug decreases and above this concentration, toxicity could result from overdosage.[6] Drugs that are administered by the oral route frequently suffer from losses resulting from first-pass metabolism, reducing the bioavailability of the drug. In cases where the drug suffers from poor oral bioavailability, an alternative method of administration is daily intravenous (IV) infusion. This method, however, increases the risk of infections at the site of administration and could lead to systemic toxicity, as in the case of chemotherapeutic drugs for the treatment of cancer.[7] In order to address these problems, sustained and controllable drug delivery devices have been developed. These devices are modified with stimuli-responsive polymers to enable them to sense variations in the external environment. For example, in the case of a pH-sensitive drug-loaded micelle, the trigger for the release of the drug could be activated by lowering the pH of the external environment. Upon receiving this external feedback, the device responds with a change in its physical properties which could lead to the triggered release of the drug.

In drug delivery applications, stimuli responsive polymers show their response properties under physiological conditions. There is a myriad of approaches which have been reviewed in detail. Common external stimuli include temperature,[8-10] pH,[10] electric fields,[11,12] ionic changes,[13] light[14,15] and magnetic fields[16] (Figure 1.1). Upon stimulation, the polymers could exhibit various responses, for example, a solubility change, a sudden burst in drug release, a change in hydration state, or conformational changes. From a biomedical point of view, the most important and commonly studied stimuli are pH and temperature.[10] In the body, the gastrointestinal (GI) tract exhibits a pH change from acidic in the stomach (pH = 2) to mildly

basic in the intestine (pH = 7–8). Certain drug-loaded oral drug delivery devices have an enteric polymer coating on them. This coating is insoluble at low pH but soluble at physiological pH. These drug delivery devices protect acid-sensitive drugs from gastric juices in the stomach and are able to deliver drugs to the intestine where they are absorbed. Certain cancers as well as inflamed tissues exhibit a different pH compared with the circulation conditions. It has been reported that chronic wounds have pH values between 5.4 and 7.4.[17] The extracellular environment in the tissues of a tumour is reported to be acidic.[18,19] Different regions within a cell also exhibit different pH. This has been exploited for gene delivery applications. Oligo/poly(nucleic acids) are delivered to the cells using cationic polymers which are complexed with the negatively charged nucleic acids. The polymer/gene complexes enter cells by fluid-phase pinocytosis or receptor-mediated endocytosis. As the complex moves from the early endosome towards the lysosomes, it experiences a drop in the pH from 6.2 to 5.0. This drastic decrease in pH has been used to trigger the release of the gene to the cytosol.[20] These cationic polymers are then deprotonated within the endosomes, which triggers endosome membrane disruption and gene release into the cytosol.[21] A dual pH and temperature responsive polymer can become membrane active at either a specific temperature [22] and/or a specific pH.[23] This further enhances the interaction of the polymer with the cell and allows the tailoring for specific cell targeting based on the local temperature and pH on the surface of the cell.

Recently, thermo-sensitive micelles derived from PNIPAAm have been reported.[24-29] PNIPAAm exhibits a lower critical solution temperature (LCST) of 32 to 33 °C, being hydrophilic at low temperatures and precipitating above the critical phase transition temperature. Block copolymers comprising a hydrophobic segment such as poly(methyl methacrylate) (PMMA), poly(10-undecenoic acid) and poly(oleic acid) and hydrophilic PNIPAAm segments have been reported.[26-29] However, these thermoresponsive micelles are non-biodegradable,

raising questions on the elimination of the micelles from the body after its use. In order to address this issue, thermoresponsive poly(N-isopropylacrylamide-*co*-N,N-dimethylacrylamide) (PNIPAAm–PDMAAm) segments have been copolymerized with hydrophobic biodegradable segments such as poly(DL-lactic acid) (PDLLA), poly(ε-caprolactone) (PCL), or poly(lactic-co-glycolic acid) (PLGA).[30-34] Biotinylated poly(N-isopropylacrylamide-*co*-N-(3-dimethylaminopropyl)methacrylamide) which were copolymerized with PCL were reported for cell tracking and drug delivery applications.[34] It was demonstrated that these micelles have a slow rate of drug release at temperatures below the critical phase transition temperature but upon heating to above this temperature, the encapsulated drug is rapidly released.

Emulsions, liposomes, biodegradable microspheres and micelles have a range of shortcomings such as poor stability of the device in the body, the requirement of using toxic organic solvents to incorporate drugs and low drug loading levels. These limitations have restricted the use of these devices in the delivery of drugs. In fact, these shortcomings are particularly severe for the delivery of peptides and proteins, making them unsuitable for the delivery of this class of therapeutic drugs. Recently, there has been increased development in the synthesis and/or isolation of peptides for therapeutic uses. There are various examples, such as glucagon-like peptide-1 (GLP-1) for the control of diabetes, ghrelin for the treatment of obesity, gastrin-releasing peptide used in cancer treatments and defensin, which can be used as an antimicrobial agent.[35-38] The creation of numerous peptide libraries has exponentially increased the number of therapeutic peptides discovered. However, the delivery of peptides to humans remains a problem owing to their short residence half-life due to poor absorption and rapid degradation in the GI tract.[39] In order for peptide therapy to work, a sustained peptide delivery system has to be developed. Biodegradable injectable thermogelling copolymers are attractive candidates as peptide delivery agents. This is due to but not limited to the following reasons.

First, the formulation of the peptide/polymer mixture can be done in an aqueous environment, sidestepping the use of organic solvents, which could denature the peptide and destroy its bioactivity. Second, the method of administration is via the injection route, thus removing the need for surgical implantation of the sustained release device. Third, the system is biodegradable and is removed from the body via the natural excretion route after its intended purpose is achieved. Fourth, such gels are easily sterilized via syringe filtration. Fifth, the high water content of the gel matrix means improved biocompatibility with the site of application. Lastly, the rate of sustained drug release can be easily controlled by adjusting the composition of the formulations.

Biodegradable thermogelling copolymers exhibit a phase change behavior of sol-to-gel-to-sol, sol-to-gel or gel-to-sol transition upon an increase in temperature.[40-42] The formation of the gels takes place via physical crosslinking between the copolymers.[42] Physical crosslinks are not permanent bonds and can be formed and removed with changes in temperature. When the physical crosslinks are formed, the water is entrapped within the polymer matrix, forming a hydrogel. The phase transition can be adjusted by changing different parameters such as the composition and the molecular weight of the copolymer. The sol-to-gel transition is particularly attractive for applications because the drug can be mixed with the aqueous copolymer solutions at low temperatures (at about 4 °C) and be injected into the body, where the higher body temperature would lead to the formation of a gel depot for the sustained release of the drug via diffusion or erosion of the copolymer gel. Thermogelling copolymers have different molecular architectures such as diblocks, triblocks, graft copolymers and star copolymers. These different architectures lead to the formation of different types of nano-structures in the aqueous solutions and consequently lead to different gelation mechanisms.

The development of many biodegradable thermogelling copolymers has been progressing rapidly over the past decade.[42] These materials can be implanted in the human body by injection, having potential applications in the areas of sustained drug delivery, gene delivery and tissue engineering. Biocompatible thermogelling poly(ethylene glycol)-*block*-poly(propylene glycol)-*block*-poly(ethylene glycol) (PEG-PPG-PEG) triblock copolymers (commonly known as Pluronics) have been widely investigated for controlled drug delivery,[43,44] wound covering,[45] and chemosensitizing for cancer therapy.[46] It has several drawbacks such as non-biodegradability, burst effect of the release of bioactive agents, requirement of high weight percentage for gelation to occur and poor gel stability *in vivo*.[47,48] In order to introduce biodegradable components in the polymer backbone, a variety of components such as PLGA, PDLLA, PCL, poly(organophosphazene), poly(propylene fumarate) (PPF), and poly(propylene phosphate) have been introduced into the thermoresponsive copolymers.[49-55] However, most of these copolymers require a high concentration before the thermogelling effect can be observed. At present, studies of thermogelling copolymers are still at its developmental research stage. Presently, OncoGel^{TM} is the only example of a commercially viable thermogelling copolymer/drug formulation.[42] Clinical trials are currently underway for the use of this product in a minimally invasive procedure for cancer treatment.

2.3. Smart Biomaterials for Tissue Engineering

Smart biosurfaces have been developed for cell culture. By using a cell culture substrate that is surface-modified with a thermally responsive polymer, the surface properties of the substrate can be changed by changing the temperature of the environment. PNIPAAm is popularly used as a cell substrate modifier due to its thermoresponsive properties.[56] At cell culture temperature above the LCST, the surface is hydrophobic and cells/tissues are attached to the substrate. When the temperature is lowered below the LCST, the surface becomes

hydrophilic and the cells/tissues are detached from the surface. This mild technique of cell detachment preserves cell-cell and cell-extracellular matrix (ECM) interactions, unlike the typical approach of using proteases such as trypsin, to detach cells.[57-59] In 1990, this novel approach for cell culture harvesting, known as cell sheet engineering, was first reported by Okano's group.[60] Since then, this unique change in the physical property of surfaces has been exploited by researchers in the fabrication of thermally responsive surfaces for cell sheet engineering.[61-70] Various improvements have been made since the fabrication of the first thermoresponsive substrate for cell culture. It was found that the rate of cell sheet detachment could be accelerated if porous cell culture membranes grafted with PNIPAAm were used as cell culture substrates.[71] Further enhancement of cell sheet detachment was then reported by co-grafting PEG to the PNIPAAm grafted porous cell culture membrane.[72] Applications of cell sheet engineering have been gaining popularity in clinical settings. In 2004, the use of autologous oral mucosal epithelial cells as a source of cells for the reconstruction of the corneal surface was reported. The cells were culture and harvested from temperature-sensitive cell culture substrates to preserve the integrity of the cells. Besides this example, a variety of cell types including epidermal keratinocytes,[74] vascular endothelial cells,[75] renal epithelial cells,[76,77] periodontal ligaments,[78,79] and cardiomyocytes[80,81] have been cultured and harvested from these thermally responsive surfaces. This trypsin-free cell harvesting approach preserves the growth factor receptors, ion channels, and cell-to-cell junction proteins. Layers of cell sheets can be attached onto host tissue due to the retention of the ECM. Using this approach, organ repair can be successfully carried out using a procedure that is similar to the repair of blankets by patchwork. As the cell sheet technology progressed, reports of the construction of artificial organ-like structures from these tissue-engineered cell sheets have emerged. The fabrication of a myocardial chamber that can pump at significant pressures and provide independent cardiac

support has recently been reported.[82,83] These man-made structures were found to be able to produce their own independent graft pressures after replacement of the host abdominal aorta.[84] These structures work almost like the native myocardium, generating spontaneous electrical activity which induces graft pressures that are independent of the host blood pressure. In addition, long surviving artificial liver systems have been engineered with this technology.[85] Compared to current technology that fabricates tissue systems that lasts only 2 to 3 weeks, the system engineered by cell sheet technology persists for more than 200 days. The artificial system possesses some functions like the native liver. It is able to absorb and metabolize circulating compounds as well as respond to proliferative stimuli. In addition, 3-D miniature liver systems with greater tissue volumes could also be created by stacking layers of hepatic tissue sheets within the vascular enclosure.

Regenerative therapies can be achieved by a combination of biomaterials and living cells. The use of the non enzymatic tissue detachment technology, through the use of a temperature responsive cell culture surface, can be exploited for the regeneration of a variety of tissues. The application of cell sheet engineering opens new avenues in the area of regenerative medicine and for applications in tissue engineering.

2.4. References

1. Ratner, B.D.; Hoffman, A.S.; Schoen, F.J.; Lemons, J.E. (eds). *Biomaterials science: An introduction to materials in medicine*, Elsevier, Amsterdam, 2004.
2. Gil, E. S.; Hudson, S. A. *Progress in Polymer Science* **2004**, 29, (12), 1173-1222.
3. Qiu, Y.; Park, K. *Advanced Drug Delivery Reviews* **2001**, 53, (3), 321-339.
4. Anderson, D. G.; Burdick, J. A.; Langer, R. *Science* **2004**, 305, 1923-1924.
5. Hoffman, A. S.; Stayton, P. S.; Bulmus, V.; Chen, G. H.; Chen, J. P.; Cheung, C.; Chilkoti, A.; Ding, Z. L.; Dong, L. C.; Fong, R.; Lackey, C. A.; Long, C. J.; Miura, M.; Morris, J. E.; Murthy, N.; Nabeshima, Y.; Park, T. G.; Press, O. W.; Shimoboji, T.; Shoemaker, S.; Yang, H. J.; Monji, N.; Nowinski, R. C.; Cole, C. A.; Priest, J. H.; Harris, J. M.; Nakamae, K.; Nishino, T.; Miyata, T. *Journal of Biomedical Materials Research* **2000**, 52, (4), 577-586.
6. Roseman, T. J.; Yalkowsky, S. H. *Controlled release polymeric formulations,* ACS Symposium Series 33, American Chemical Society, Washington DC, 33-52, **1976**.
7. Loh, X. J.; Li, J. *Expert Opinion on Therapeutic Patents* **2007**, 17, (8), 965-977.
8. Hirokawa, Y.; Tanaka, T. *Journal of Chemical Physics* **1984**, 81, (12), 6379-6380.
9. Amiya, T.; Hirokawa, Y.; Hirose, Y.; Li, Y.; Tanaka, T. *Journal of Chemical Physics* **1987**, 86, (4), 2375-2379.
10. Chen, G. H.; Hoffman, A. S. *Nature* **1995**, 373, (6509), 49-52.
11. Tanaka, T.; Nishio, I.; Sun, S. T.; Uenonishio, S. *Science* **1982**, 218, (4571), 467-469.
12. Osada, Y.; Okuzaki, H.; Hori, H. *Nature* **1992**, 355, (6357), 242-244.
13. Tanaka, T.; Fillmore, D.; Sun, S. T.; Nishio, I.; Swislow, G.; Shah, A. *Physical Review Letters* **1980**, 45, (20), 1636-1639.
14. Irie, M. *Advances in Polymer Science* **1993**, 110, 49-65.

15. Suzuki, A.; Tanaka, T. *Nature* **1990**, 346, (6282), 345-347.

16. Szabo, D.; Szeghy, G.; Zrinyi, M. *Macromolecules* **1998**, 31, (19), 6541-6548.

17. Dissemond, J.; Witthoff, M.; Brauns, T. C.; Haberer, D.; Goos, M. *Hautarzt* **2003**, 54, (10), 959-965.

18. Vaupel, P.; Kallinowski, F.; Okunieff, P. *Cancer Research* **1989**, 49, (23), 6449-6465.

19. Rofstad, E. K.; Mathiesen, B.; Kindem, K.; Galappathi, K. *Cancer Research* **2006**, 66, (13), 6699-6707.

20. Duncan, R. *Nature Reviews Drug Discovery* **2003**, 2, (5), 347-360.

21. Storrie, H.; Mooney, D. J. *Advanced Drug Delivery Reviews* **2006**, 58, (4), 500-514.

22. Ringsdorf, H.; Venzmer, J.; Winnik, F. M. *Angewandte Chemie-International Edition in English* **1991**, 30, (3), 315-318.

23. Kusonwiriyawong, C.; van de Wetering, P.; Hubbell, J. A.; Merkle, H. P.; Walter, E. *European Journal of Pharmaceutics and Biopharmaceutics* **2003**, 56, (2), 237-246.

24. Motokawa, R.; Morishita, K.; Koizumi, S.; Nakahira, T.; Annaka, M. *Macromolecules* **2005**, 38, (13), 5748-5760.

25. Kim, Y. C.; Kil, D. S.; Kim, J. C. *Journal of Applied Polymer Science* **2006**, 101, (3), 1833-1841.

26. Wei, H.; Zhang, X. Z.; Cheng, C.; Cheng, S. X.; Zhuo, R. X. *Biomaterials* **2007**, 28, (1), 99-107.

27. Li, Y. Y.; Zhang, X. Z.; Cheng, H.; Kim, G. C.; Cheng, S. X.; Zhuo, R. X. *Biomacromolecules* **2006**, 7, (11), 2956-2960.

28. Wei, H.; Zhang, X. Z.; Cheng, H.; Chen, W. Q.; Cheng, S. X.; Zhuo, R. X. *J. Controlled Release* **2006**, 116, (3), 266-274.

29. Li, Y. Y.; Zhang, X. Z.; Kim, G. C.; Cheng, H.; Cheng, S. X.; Zhuo, R. X. *Small* **2006**, 2, (7), 917-923.

30. Kohori, F.; Sakai, K.; Aoyagi, T.; Yokoyama, M.; Sakurai, Y.; Okano, T. *J. Controlled Release* **1998**, 55, (1), 87-98.

31. Liu, S. Q.; Tong, Y. W.; Yang, Y. Y. *Biomaterials* **2005**, 26, (24), 5064-5074.

32. Liu, S. Q.; Tong, Y. W.; Yang, Y. Y. *Molecular Biosystems* **2005**, 1, (2), 158-165.

33. Nakayama, M.; Okano, T.; Miyazaki, T.; Kohori, F.; Sakai, K.; Yokoyama, M. *J. Controlled Release* **2006**, 115, (1), 46-56.

34. Li, Y. Y.; Zhang, X. Z.; Cheng, H.; Zhu, J. L.; Li, U. N.; Cheng, S. X.; Zhuo, R. X. *Nanotechnology* **2007**, 18, (50), 8.

35. Nauck, M. A.; Kleine, N.; Orskov, C.; Holst, J. J.; Willms, B.; Creutzfeldt, W. *Diabetologia* **1993**, 36, (8), 741-744.

36. Tschop, M.; Weyer, C.; Tataranni, P. A.; Devanarayan, V.; Ravussin, E.; Heiman, M. L. *Diabetes* **2001**, 50, (4), 707-709.

37. Reubi, J. C. *Endocrine Reviews* **2003**, 24, (4), 389-427.

38. Zasloff, M. *Nature* **2002**, 415, (6870), 389-395.

39. Takeuchi, H.; Yamamoto, H.; Kawashima, Y. *Advanced Drug Delivery Reviews* **2001**, 47, (1), 39-54.

40. Jeong, B.; Kim, S. W.; Bae, Y. H. *Advanced Drug Delivery Reviews* **2002**, 54, (1), 37-51.

41. Jeong, B.; Bae, Y. H.; Lee, D. S.; Kim, S. W. *Nature* **1997**, 388, (6645), 860-862.

42. Loh, X. J.; Li, J. *Expert Opinion on Therapeutic Patents* **2007**, 17, (8), 965-977.

43. Yokoyama, M. *Crit. Rev. Ther. Drug Carrier Systems* **1992**, *9*, 213-248.

44. Gilbert, J. C.; Hadgraft, J.; Bye, A.; Brookes, L. *Int. J. Pharm.* **1986**, *32*, 223-228.

45. Nalbandian, R. M.; Henry, R. L.; Wilks, H. S. *J. Biomed. Mater. Res.* **1972**, *6*, 583-590.

46. Exner, A. A.; Krupka, T. Y.; Scherrer, K.; Teets, J. M. *J. Control Release* **2005**, *106*, 188-197.

47. Esposito, E.; Carotta, Y.; Scabbia, A.; Trombelli, L.; D'Antona, P.; Menegatti, E.; Nastruzzi, C. *Int. J. Pharm.* **1996**, *142*, 9-23.

48. Katakam, M.; Ravis, W. R.; Golden, D. L.; Banga, A. K. *Int. J. Pharm.* **1997**, *152*, 53-58.

49. Jeong, B.; Bae, Y. H.; Kim, S.W. *Macromolecules* **1999**, *32*, 7064-7069.

50. Joo, M. K.; Sohn, Y. S.; Jeong, B. *Macromolecules* **2007**, 40, (14), 5111-5115.

51. Hwang, M. J.; Suh, J. M.; Bae, Y. H.; Kim, S.W.; Jeong, B. *Biomacromolecules* **2005**, *6*, 885-890.

52. Bae, S. J.; Suh, J. M.; Sohn, Y. S.; Bae, Y. H.; Kim, S.W.; Jeong, B. *Macromolecules* **2005**, *38*, 5260-5265.

53. Lee, B. H.; Lee, Y. M.; Sohn, Y. S.; Song, S. C. *Macromolecules* **2002**, 35, (10), 3876-3879.

54. Behravesh, E.; Shung, A. K.; Jo, S.; Mikos, A. G. *Biomacromolecules* **2002**, *3*, 153-158.

55. Wang, J.; Sun, D. D. N.; Shin-ya, Y.; Leong, K. W. *Macromolecules* **2004**, 37, (2), 670-672.

56. Xia, Y.; Yin, X. C.; Burke, N. A. D.; Stover, H. D. H. *Macromolecules* **2005**, 38, (14), 5937-5943.

57. Masuda, S.; Shimizu, T.; Yamato, M.; Okano, T. *Advanced Drug Delivery Reviews* **2008**, 60, (2), 277-285.

58. Yamato, M.; Akiyama, Y.; Kobayashi, J.; Yang, J.; Kikuchi, A.; Okano, T. *Progress in Polymer Science* **2007**, 32, (8-9), 1123-1133.

59. Matsuda, N.; Shimizu, T.; Yamato, M.; Okano, T. *Advanced Materials* **2007**, 19, (20), 3089-3099.

60. Yamada, N.; Okano, T.; Sakai, H.; Karikusa, F.; Sawasaki, Y.; Sakurai, Y. *Makromolekulare Chemie-Rapid Communications* **1990**, 11, (11), 571-576.

61. Akiyama, Y.; Kikuchi, A.; Yamato, M.; Okano, T. *Langmuir* **2004**, 20, (13), 5506-5511.

62. Hirose, M.; Kwon, O. H.; Yamato, M.; Kikuchi, A.; Okano, T. *Biomacromolecules* **2000**, 1, (3), 377-381.

63. Okano, T.; Yamada, N.; Okuhara, M.; Sakai, H.; Sakurai, Y. *Biomaterials* **1995**, 16, (4), 297-303.

64. Okano, T.; Yamada, N.; Sakai, H.; Sakurai, Y. *Journal of Biomedical Materials Research* **1993**, 27, (10), 1243-1251.

65. Yamato, M.; Utsumi, M.; Kushida, A.; Konno, C.; Kikuchi, A.; Okano, T. *Tissue Engineering* **2001**, 7, (4), 473-480.

66. Chen, G. P.; Imanishi, Y.; Ito, Y. *Journal of Biomedical Materials Research* **1998**, 42, (1), 38-44.

67. Chen, G. P.; Ito, Y.; Imanishi, Y. *Biotechnology and Bioengineering* **1997**, 53, (3), 339-344.

68. Ito, Y.; Chen, G. P.; Guan, Y. Q.; Imanishi, Y. *Langmuir* **1997**, 13, (10), 2756-2759.

69. Liu, H. C.; Ito, Y. *Lab on a Chip* **2002**, 2, (3), 175-178.

70. Liu, H. C.; Ito, Y. *Journal of Biomedical Materials Research Part A* **2003**, 67A, (4), 1424-1429.

71. Kwon, O. H.; Kikuchi, A.; Yamato, M.; Sakurai, Y.; Okano, T. *Journal of Biomedical Materials Research* **2000**, 50, (1), 82-89.

72. Kwon, O. H.; Kikuchi, A.; Yamato, M.; Okano, T. *Biomaterials* **2003**, 24, (7), 1223-1232.

73. Nishida, K.; Yamato, M.; Hayashida, Y.; Watanabe, K.; Yamamoto, K.; Adachi, E.; Nagai, S.; Kikuchi, A.; Maeda, N.; Watanabe, H.; Okano, T.; Tano, Y. *New England Journal of Medicine* **2004**, 351, (12), 1187-1196.

74. Yamato, M.; Utsumi, M.; Kushida, A.; Konno, C.; Kikuchi, A.; Okano, T. *Tissue Engineering* **2001**, 7, (4), 473-480.

75. Yamato, M.; Okuhara, M.; Karikusa, F.; Kikuchi, A.; Sakurai, Y.; Okano, T. *Journal of Biomedical Materials Research* **1999**, 44, (1), 44-52.

76. Kushida, A.; Yamato, M.; Isoi, Y.; Kikuchi, A.; Okano, T. *Eur Cell Mater* **2005**, 10, 23–30

77. Kushida, A.; Yamato, M.; Kikuchi, A.; Okano, T. *Journal of Biomedical Materials Research* **2001**, 54, (1), 37-46.

78. Akizuki, T.; Oda, S.; Komaki, M.; Tsuchioka, H.; Kawakatsu, N.; Kikuchi, A.; Yamato, M.; Okano, T.; Ishikawa, I. *Journal of Periodontal Research* **2005**, 40, (3), 245-251.

79. Hasegawa, M.; Yamato, M.; Kikuchi, A.; Okano, T.; Ishikawa, I. *Tissue Engineering* **2005**, 11, (3-4), 469-478.

80. Shimizu, T.; Yamato, M.; Akutsu, T.; Shibata, T.; Isoi, Y.; Kikuchi, A.; Umezu, M.; Okano, T. *Journal of Biomedical Materials Research* **2002**, 60, (1), 110-117.

81. Shimizu, T.; Yamoto, M.; Kikuchi, A.; Okano, T. *Tissue Engineering* **2001**, 7, (2), 141-151.

82. Laflamme, M. A.; Murry, C. E. *Nature Biotechnology* **2005**, 23, (7), 845-856.

83. Zandonella, C. *Nature* **2003**, 421, (6926), 884–6.

84. Sekine, H.; Shimizu, T.; Yang, J.; Kobayashi, E.; Okano, T. *Circulation* **2006**, 114, I87–93.

85. Ohashi, K.; Yokoyama, T.; Yamato, M.; Kuge, H.; Kanehiro, H.; Tsutsumi, M.; Amanuma, T.; Iwata, H.; Yang, J.; Okano, T.; Nakajima, Y. *Nature Medicine* **2007**, 13, (7), 880-885.

CHAPTER THREE

SYNTHESIS AND CHARACTERIZATION OF MULTIBLOCK BIODEGRADABLE THERMOGELLING COPOLYMERS COMPRISING POLY(ETHYLENE GLYCOL), POLY(PROPYLENE GLYCOL) AND POLY[(R)-3-HYDROXYBUTYRATE]

3.1. Introduction

The synthesis of biodegradable thermogelling polymers have attracted much attention because of their potential applications for drug delivery and tissue engineering.[1-6] Bioactive agents can be incorporated in the sol state at low temperatures. This formulation can be injected into the body where the higher body temperature would lead to the formation of a gel depot. This depot can be used for the controlled release of the bioactive agents. Biodegradable linkages introduced into the polymer backbone would facilitate the degradation of the copolymer into smaller fragments and subsequent removal of the polymer from the body.

As an example of thermogelling polymers, the triblock copolymers of poly(ethylene glycol)-poly(propylene glycol)-poly(ethylene glycol) (PEG-PPG-PEG) have been widely investigated for controlled drug delivery,[6,7] wound covering,[8] and chemosensitizing for cancer therapy.[9] PEG and PPG are also approved for use as food contact materials by the U.S. Food and Drug Administration Department. However, they generally have a high critical gelation concentration (CGC) (15 – 20 wt % or above), exhibiting poor resilience as well as having the burst effect of the release of bioactive agents. These shortcomings have made this system unsuitable for many biomedical applications.[10-11] Moreover, PEG-PPG-PEG triblock copolymers are non-biodegradable and have been reported to induce hyperlipidemia and increase the plasma level of cholesterol in rabbits and rats, suggesting that its use in the human body may not be an attractive option.[12-14]

Attempts have been made to lower the CGCs of PEG-PPG-PEG triblock copolymers. By grafting PEG-PPG-PEG triblocks to poly(acrylic acid), polymers having very low CGCs (0.1 wt%) have been synthesized.[15-18] However, these polymers are non-biodegradable and the excretion from the body could be difficult. High molecular weight multiblock PEG-PPG-PEG triblock copolymers with a short junction linkages have been synthesized and found to exhibit

lower CGCs than PEG-PPG-PEG triblock copolymers.[19-20] Cohn *et al.* have synthesized reverse thermogelling multiblock copolymers based on PEG, PPG and PCL.[21] These biodegradable copolymers exhibited CGCs of 10 wt%. Interestingly, this work showed that the incorporation of oligo-caprolactone segments lowered the CGCs of the copolymers as compared with the PPG-PEG multiblock copolymers. The viscosities of the gels were also lowered compared with the PPG-PEG multiblock copolymers. On the other hand, PEG-PPG-PEG analogs were developed where the middle PPG block was replaced by a biodegradable polyester such as poly(ε-caprolactone) or poly(L-lactide), which are of great significance in biomedical applications because of their biodegradability. However, their CGCs are at a similar range of PEG-PPG-PEG triblock copolymers.[22]

Poly[(R)-3-hydroxybutyrate] (PHB) is a natural biodegradable polyester, which is highly crystalline and hydrophobic, showing a greater hydrophobicity than either poly(lactic acid) or poly(ε-caprolactone).[23] Herein it is hypothesized that the incorporation of PHB segments into a PEG-PPG block copolymer would allow the formation of extra physical crosslinking in the hydrogel, increasing its resilience. Additionally, PHB segments would provide the biodegradable segments in the polymer backbone. In this chapter, a series of novel thermogelling high molecular weight amphiphilic multiblock poly(ether ester urethane)s consisting of PEG, PPG, and PHB blocks was designed. This simple synthetic method produces thermogelling copolymers with very low CGCs and tunable properties, which may be potentially applied as an *in-situ* forming biodegradable gel depot suitable for sustained drug delivery.

3.2. Experimental Section

3.2.1. Materials

Natural source poly[(*R*)-3-hydroxybutyrate] (PHB) was supplied by Aldrich, and purified by dissolving in chloroform followed by filtration and subsequent precipitation in hexane before use. The M_n and M_w of the purified PHB were 8.7 x 10^4 and 2.3 x 10^5, respectively. Poly(ethylene glycol) (PEG) and poly(propylene glycol) (PPG) with M_n of ca. 2000 was purchased from Aldrich. Purification of the PEG was performed by dissolving in dichloromethane followed by precipitation in diethyl ether and vacuum dried before use. Purification of PPG was performed by washing in hexane three times and vacuum dried before use. The M_n and M_w of PEG were found to be 1890 and 2060, respectively. The M_n and M_w of PPG were found to be 2180 and 2290, respectively. Bis(2-methoxyethyl) ether (diglyme, 99 %), ethylene glycol (99 %), dibutyltin dilaurate (95 %) 1,6-hexamethylene diisocyanate (HDI) (98 %), methanol, diethyl ether, 1,2-dichloroethane (99.8 %) and 1,6-diphenyl-1,3,5-hexatriene (DPH) were purchased from Aldrich. Diglyme was dried with molecular sieves, and 1,2-dichloroethane was distilled over CaH_2 before use. PEG-PPG-PEG triblock copolymer with a chain composition of $EG_{100}PG_{65}EG_{100}$ (also known as Pluronic F127) was purchased from Aldrich and used as received.

3.2.2. Synthesis of Poly(PEG/PPG/PHB urethane)s

Telechelic hydroxylated PHB (PHB-diol) prepolymers with various molecular weight were prepared by transesterification between the natural source PHB and ethylene glycol using dibutyltin dilaurate in diglyme as reported previously.[24-26] The yields were about 80 %. Poly(PEG/PPG/PHB urethane)s were synthesized from PHB-diol, PEG and PPG with molar ratios of PEG/PPG fixed at 2:1 and PHB content ranging from 5 to 20 mol % (calculated from the M_n of PHB-diol) using HDI as a coupling reagent. The amount of HDI added was equivalent

to the reactive hydroxyl groups in the solution. Typically, 0.064 g of PHB-diol (M_n = 1070, 6.0 x 10^{-5} mol), 1.44 g of PEG (M_n = 1890, 7.6 x 10^{-4} mol) and 0.82 g of PPG (M_n = 2180, 3.8 x 10^{-4} mol) were dried in a 250-ml two-neck flask at 50 °C under high vacuum overnight. Then, 20 ml of anhydrous 1,2-dichloroethane was added to the flask and any trace of water in the system was removed through azeotropic distillation with only 1 ml of 1,2-dichloroethane being left in the flask. When the flask was cooled down to 75 °C, 0.20 g of HDI (1.2 x 10^{-3} mol) and two drops of dibutyltin dilaurate (~8 x 10^{-3} g) were added sequentially. The reaction mixture was stirred at 75 °C under a nitrogen atmosphere for 48 hrs. The resultant copolymer was precipitated from diethyl ether, and further purified by redissolving into 1,2-dichloroethane followed by precipitation in a mixture of methanol and diethyl ether to remove remaining dibutyltin dilaurate. A series of poly(PEG/PPG/PHB urethane)s with different compositions of PHB were prepared, and their number-average molecular weight and polydispersity values are given in Table 1. The yield was 80% and above after isolation and purification.

^{1}H NMR ($CDCl_3$) of poly(PEG/PPG/PHB urethane)s EPH2: δ (ppm) 1.14 (-O(C***H*****$_3$**)CH CH_2O-), 1.26 (-O(C***H*****$_3$**)$CHCH_2CO$-), 1.32 (-$OOCNHCH_2CH_2C$***H*****$_2$**C***H*****$_2$**CH_2CH_2NHCOO-), 1.48 (-$OOCNHCH_2C$***H*****$_2$**CH_2CH_2C***H*****$_2$**CH_2NHCOO-), 2.44-2.63 (-$O(CH_3)CHC$***H*****$_2$**CO-), 3.13 ($OOCNH$ C***H*****$_2$**$CH_2CH_2CH_2CH_2C$***H*****$_2$**$NHCOO$-), 3.41 (-$O(CH_3)C$***H***CH_2O-), 3.46 (-$O(CH_3)CHC$***H*****$_2$**O-), 3.64 (-OC***H*****$_2$**C***H*****$_2$**O-), 4.20 (-$OOCN$***H***$CH_2CH_2CH_2CH_2CH_2CH_2N$***H***$COO$-), 5.21-5.29 (-$O(CH_3)C$***H*** CH_2CO-). ^{13}C NMR of EPH2 ($CDCl_3$) of poly(PEG/PPG/PHB urethane)s: δ (ppm) 17.77 ($O($***C***$H_3)CHCH_2O$-), 20.14 (-$O($***C***$H_3)CHCH_2CO$-), 26.69 (-$OOCNHCH_2CH_2$***C***H_2***C***$H_2CH_2CH_2$ $NHCOO$-), 30.26 (-$OOCNHCH_2$***C***$H_2CH_2CH_2CH_2$***C***H_2CH_2NHCOO-), 41.20 (-$O(CH_3)CH$***C***H_2CO-), 64.18 (-$OOCNH$***C***$H_2CH_2CH_2CH_2CH_2$***C***H_2NHCOO-), 67.99 (-$O(CH_3)$***C***HCH_2CO-), 70.94 (-O***C***H_2***C***H_2O-), 73.56 (-$O(CH_3)CH$***C***H_2O-), 75.72 (-$O(CH_3)$***C***HCH_2O-),

156.82 (-OO***C***NHCH$_2$CH$_2$CH$_2$CH$_2$CH$_2$CH$_2$NH***C***OO-), 169.98 (-O(CH$_3$)CHCH$_2$***C***O-).

3.2.3. Polymer Characterization

Gel permeation chromatography (GPC). GPC analysis was carried out with a Shimadzu SCL-10A and LC-8A system equipped with two Phenogel 5μ 50 and 1000 Å columns (size: 300 × 4.6 mm) in series and a Shimadzu RID-10A refractive index detector. THF was used as eluent at a flow rate of 0.30 ml/min at 40 °C. Monodispersed poly(ethylene glycol) standards were used to obtain a calibration curve.

Nuclear magnetic resonance (NMR) measurements. The ^{1}H NMR (400 MHz) and ^{13}C NMR (100 MHz) spectra were recorded on a Bruker AV-400 NMR spectrometer at room temperature. The ^{1}H NMR measurements were carried out with an acquisition time of 3.2 s, a pulse repetition time of 2.0 s, a 30° pulse width, 5208 Hz spectral width, and 32K data points. Chemical shift was referred to the solvent peaks (δ = 7.3 ppm for $CHCl_3$). Fourier transform infrared (FTIR) spectra of the polymer films coated on CaF_2 plate were recorded on a Bio-Rad 165 FT-IR spectrophotometer; 64 scans were signal-averaged with a resolution of 2 cm^{-1} at room temperature.

Thermal Analysis. Thermogravimetric analyses (TGA) were carried out on a TA Instruments SDT 2960. Samples were heated at 20 °C min^{-1} from room temperature to 800 °C in a dynamic nitrogen atmosphere (flow rate = 70 ml min^{-1}).

Critical Micellization Concentration (CMC) Determination. The CMC values were determined by using the dye solubilization method.[27,28] The hydrophobic dye 1,6-diphenyl-1,3,5-hexatriene (DPH) was dissolved in methanol with a concentration of 0.6 mM. 20 μL of this solution was mixed with 2.0 mL of copolymer aqueous solution with concentrations ranging

from 0.0001 to 0.5 wt % and equilibrated overnight at 4 ^{o}C. A UV-Vis spectrophotometer was used to obtain the UV-Vis spectra in the range of 330-430 nm at 25 ^{o}C. The CMC value was determined by the plot of the difference in absorbance at 378 nm and at 400 nm ($A_{378} - A_{400}$) versus logarithmic concentration.

Sol-Gel Transition. The sol-gel transition was determined by a test tube inverting method with temperature increments of 2 °C per step.[22a,29] Each sample of a given concentration was prepared by dissolving the polymer in distilled water in a 2-mL vial. After equilibration at 4 ^{o}C for 24 h, the vials containing samples were immersed in a water bath at a constant designated temperature for 15 min. The gelation temperature was characterized by the formation of a firm gel that remained intact when the tube was inverted by 180^{o}.[30]

Viscosity Measurements. Viscosities of the hydrogels were measured at 25 °C using a Brookfield HADV-III+ digital viscometer coupled to a temperature-controlling unit. The small sample adapters SSA 15/7R was used. The revolution rate of the spindle was set at 20 cycles min^{-1} and shear rate was set at 9.6 s^{-1}.

3.3. Results and Discussion

3.3.1. Synthesis and Characterization of Poly(PEG/PPG/PHB urethane)s.

The synthesis and biodegradation behavior of amphiphilic multiblock poly(ether ester urethane)s consisting of PEG and PHB blocks were previously reported.[24-26] These water-insoluble copolymers could not undergo a sol-gel transition and were non-thermosensitive. However, in this study, water-soluble and thermosensitive poly(PEG/PPG/PHB urethane)s were synthesized, and for the first time PHB has been incorporated into a thermogelling copolymer, to enhance the gel properties as well as to make the copolymers biodegradable. Telechelic hydroxylated PHB (PHB-diol) with lower molecular weight were obtained through transesterification between high-molecular-weight natural source PHB and ethylene glycol using

dibutyltin dilaurate as catalyst.[24] The transesterification reaction was allowed to proceed for a few hours to overnight to produce PHB-diols with M_n of 1070, and 2800, respectively, as determined by GPC.

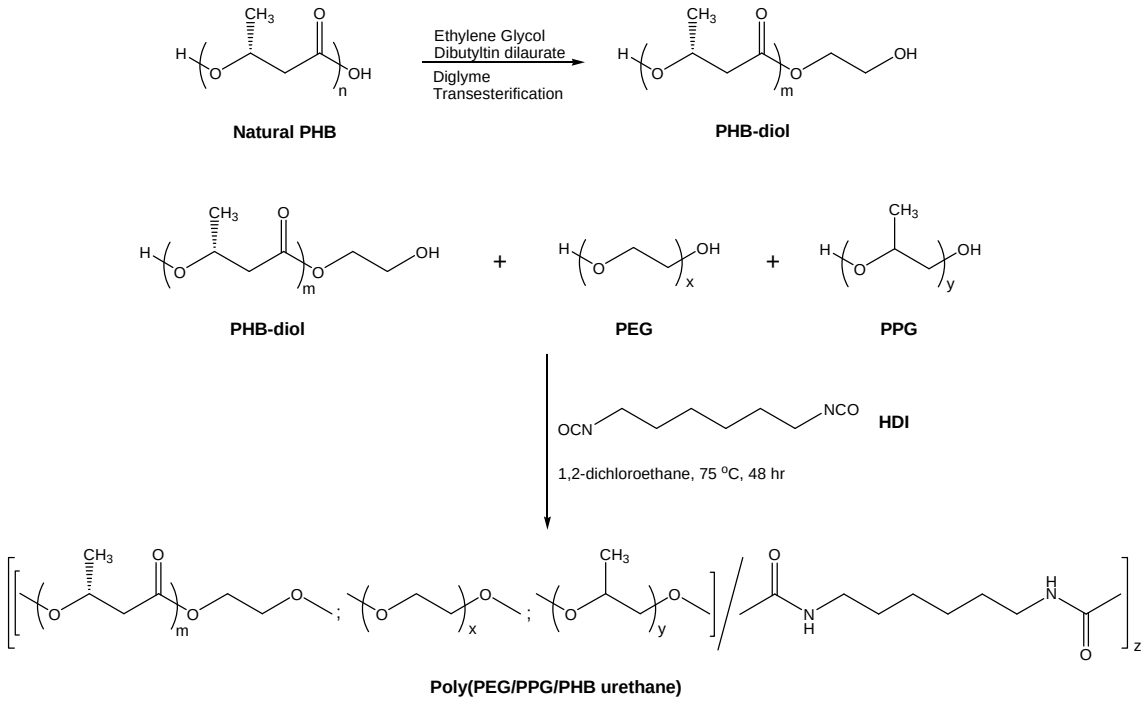

Scheme 3.1. Synthesis of PHB-diol and poly(PEG/PPG/PHB urethane)s

The reaction of hydroxyl groups of PHB-diol, PEG and PPG with isocyanate of 1,6-hexamethlyene diisocyanate (HDI) in the presence of dibutyltin dilaurate led to formation of poly(PEG/PPG/PHB urethane)s. The procedures for the synthesis of PHB-diol and poly(PEG/PPG/PHB urethane)s are presented in Scheme 3.1. Owing to the moisture sensitive nature, any trace of water in the system was removed through azeotropic distillation, and the reaction was carried out in dried 1,2-dichloroethane under a nitrogen atmosphere. The target poly(PEG/PPG/PHB urethane)s were isolated and purified from the reaction mixture by repeated precipitation from a mixture of methanol and diethyl ether.

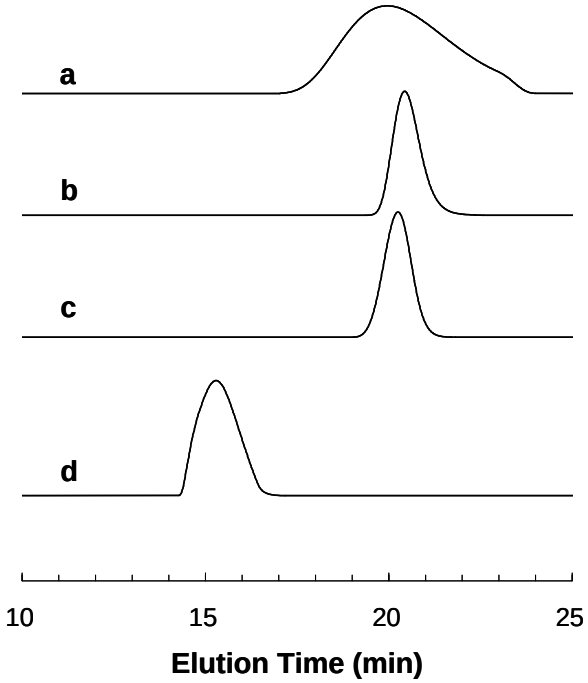

Figure 3.1. GPC diagrams of EPH2 and its PHB, PEG and PPG precursors: (a) PHB-diol (M_n 1080); (b) PEG (M_n 1890); (c) PPG (M_n 2180); and (d) EPH2 (M_w 62.8 × 10^3, M_n 45.5 × 10^3, M_w/M_n 1.38).

A series of random multiblock poly(PEG/PPG/PHB urethane)s with different amounts of PHB incorporated were synthesized, and their molecular weights and molecular weight distributions were determined by GPC (Table 3.1). A typical GPC chromatograph for one of the poly(PEG/PPG/PHB urethane)s together with its corresponding precursors is shown in Figure 3.1. The observation of unimodal peak in GPC chromatograph of the purified poly(PEG/PPG/PHB urethane) with non-overlapping nature with those of corresponding precursors indicates that a complete reaction took place with no unreacted precursor remained.[24-26] All the poly(PEG/PPG/PHB urethane)s synthesized had narrow molecular weight distribution and high molecular weight, with polydispersity ranging from 1.16 to 1.56 and M_n from 3.00 × 10^4 to 5.06 × 10^4. The results are tabulated in Table 3.1.

The chemical structure of poly(PEG/PPG/PHB urethane)s was verified by ^{1}H NMR and ^{13}C NMR spectroscopy (Figure 3.2a and b). Figure 3.2a shows the ^{1}H NMR spectrum of EPH2 in $CDCl_3$, in which all proton signals belonging to both PHB, PEG and PPG segments are confirmed. Signals corresponding to methylene protons in repeated units of PEG segments are observed at 3.64 ppm, the signals at 5.25 ppm are assigned to methine protons in the repeated unit of PHB segments,[24-26] the signals at 1.14 ppm are assigned to the methyl protons of PPG. As the content of HDI among the starting materials is below 1 wt%, the compositions of the poly(PEG/PPG/PHB urethane)s could be determined from the integration ratio of resonances at 1.14, 3.64 and 5.25 ppm within the limits of ^{1}H NMR precision, and the results are shown in Table 3.1.

The ^{13}C NMR was used to ascertain the chemical composition of the poly(PEG/PPG/PHB urethane)s. The peak assignments of the copolymers were performed by comparison with the ^{13}C NMR spectra of the precursors. Figure 3.2b shows the ^{13}C NMR spectra of EPH2 in $CDCl_3$. Briefly, peaks at 17.77 (methyl C), 73.56 (methylene C) and 75.72 ppm (methine C) are assigned to the PPG moiety. A peak at 70.94 ppm is assigned to the methylene C of the PEG segment. Peaks at 20.14 (methyl C), 41.20 (methylene C), 67.99 (methine C) and 169.98 ppm (carbonyl C) are attributed to the PHB segment. In addition, peaks due to the HDI junction unit could be observed in the spectra (26.69, 30.26, 64.18 and 156.82 ppm).

A ^{13}C NMR spectrum of hexamethylene diisocyanate was obtained and the carbonyl carbon peak was observed at 122.85 ppm. After the polymerization reaction, the ^{13}C peak of the carbonyl carbon of the newly formed urethane linkage was observed at 156.82 ppm. This shift was attributed to the attachment of the hydroxyl groups to the isocyanate functional groups in the formation of the urethane linkage (-NCO- $\rightarrow$ -NHCOO-). This observation, together with the

concomitant increase in the molecular weight of the copolymers indicates that the polycondensation reaction was successful.

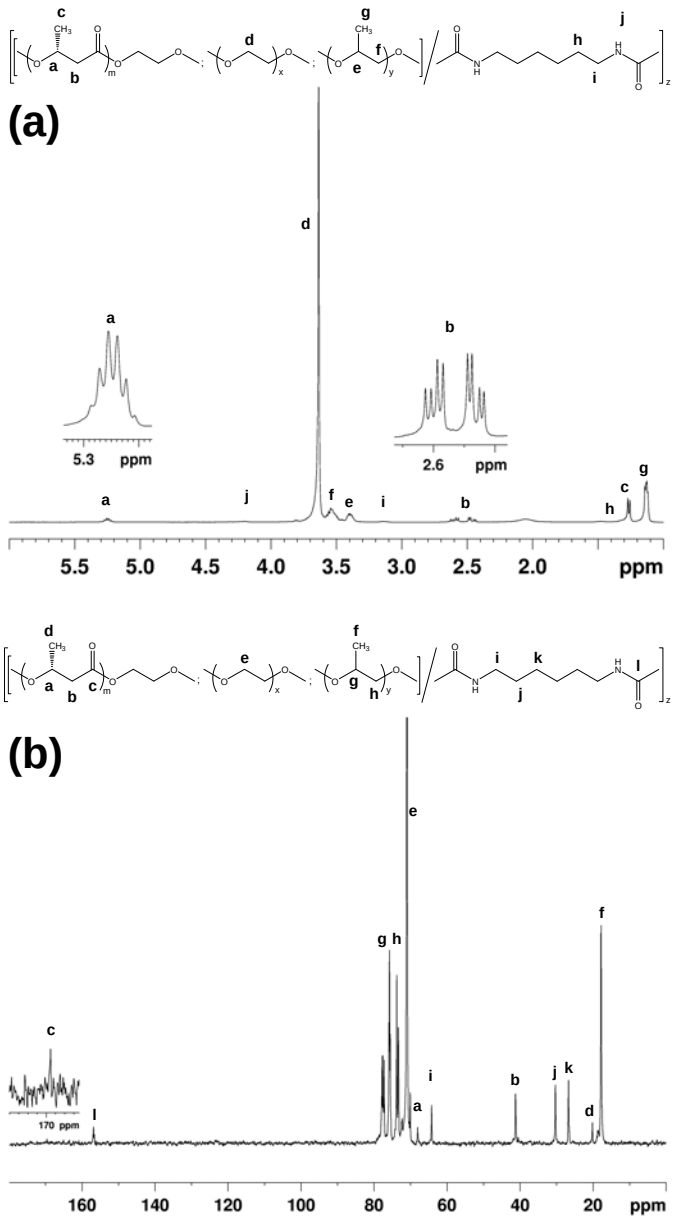

Figure 3.2. (a) 400 MHz ^{1}H NMR and (b) 100 MHz ^{13}C NMR spectra of EPH2 in $CDCl_3$**.**

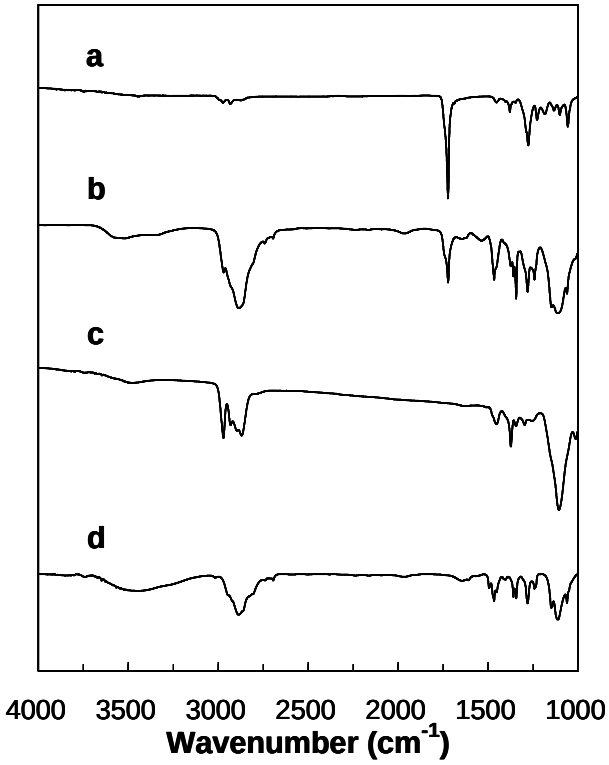

Figure 3.3. FTIR spectra of EPH2 and its PHB, PEG and PPG precursors: (a) PHB-diol (M_n 1080); (b) EPH2; (c) PPG (M_n 2180); and (d) PEG (M_n 1890).

FTIR is useful in the characterization of the functional groups present in the polymer. As a typical example, Figure 3.3 shows FTIR spectra of EPH2 and its PEG, PPG and PHB precursors. For PPG (Figure 3.3c) and PEG (Figure 3.3d), the characteristic C-O-C stretching vibration of the repeated -OCH_2CH_2- units is observed at 1102 cm^{-1}. An intensive carbonyl stretching band at 1723 cm^{-1} characterizes the FTIR spectrum of pure PHB-diol as shown in Figure 3.3a. It is clearly seen that in Figure 3.3b, all the characteristic absorptions for PHB-diol, PEG and PPG appear in the spectrum of EPH2, which confirms the presence of the three segments in the poly(PEG/PPG/PHB urethane)s. Furthermore, it can be seen in the profile of EPH2 that the peak ascribed to the -NCO- stretching was not observed in the region around 2200 cm^{-1}. This provides evidence that the isocyanate groups of the junction units have been reacted

and is not present in the polymer product. These observations, together with the afore-mentioned evidences (GPC and NMR results) provide a solid justification for the successful synthesis of the multiblock copolymers.

3.3.2. Thermal Properties.

The thermal stability of poly(PEG/PPG/PHB urethane)s was evaluated using thermogravimetric analysis (TGA). Figure 3.4 shows the TGA scan results for EPH2 compared with its PHB, PEG and PPG precursors. The degradation of pure PHB-diol starts at 218 °C and completes at 295 °C (Figure 3.4a), PPG starts to degrade at 350 °C (Figure 3.4c) while that of pure PEG starts at 400 °C (Figure 3.4b), at which pure PHB-diol has completed the degradation. EPH2 undergoes a three-step thermal degradation with the first step occurring between 227 and 303 °C and the second and third steps between 350 and 433 °C (Figure 3.4d). In comparison with the TGA curves of pure PHB-diol and pure PEG, the first weight loss step is attributed to the

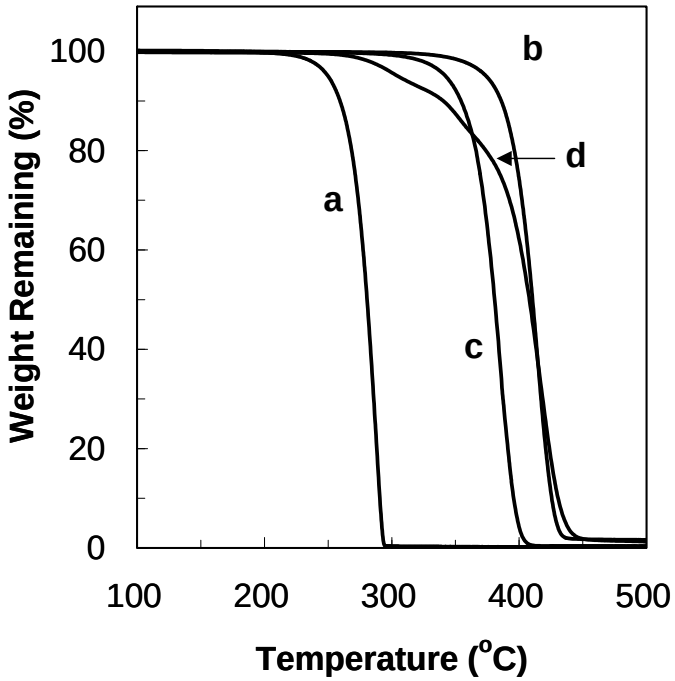

Figure 3.4. TGA curves of EPH2 and its PHB, PEG and PPG precursors: (a) PHB-diol (M_n 1080); (b) PEG (M_n 1890); (c) PPG (M_n 2180); and (d) EPH2.

decomposition of PHB segment and the second and third weight loss step to the decomposition of both the PEG and PPG segments. However, the second and third weight loss steps are too close for the accurate determination of the compositions of PPG and PEG separately. Therefore, only the PHB content of EPH2 could be determined from the degradation profile. Similar weight loss curves were also observed for other poly(PEG/PPG/PHB urethane)s. The PHB contents estimated from TGA results are in good agreement with those calculated from ^{1}H NMR.

3.3.3. Micelle Properties.

Among the six poly(PEG/PPG/PHB urethane)s, only EPH1, EPH2, EPH3 and EPH5 were soluble in water. The CMC determination was carried out for these four copolymers. This experiment was conducted by varying the aqueous polymer concentration in the range of 0.0001 to 0.5 wt %, while keeping the concentration of DPH constant. DPH shows a higher absorption coefficient in a hydrophobic environment than in water. Thus, with increasing polymer concentration, the absorbances at 344, 358 and 378 nm increased (Figure 3.5a). The point where the absorbance suddenly increases corresponds to the concentration at which micelles are formed. When the micelle is formed, DPH partitions preferentially into the hydrophobic core formed in the aqueous solution.[22a,27-29] The CMC was determined by extrapolating the absorbance at 378 nm minus the absorbance at 400 nm ($A_{378} - A_{400}$) versus logarithmic concentration (Figure 3.5b). The CMC values for the water-soluble copolymers are tabulated in Table 3.1 and are in the range of 5.16×10^{-4} to 9.79×10^{-4} g.mL^{-1}. Comparing the copolymers of similar molecular weights, the CMC values are much lower than that reported by Ahn *et al.* for a series of multiblock PEG-PPG-PEG copolymers,[19] showing that the incorporation of PHB greatly increases the hydrophobicity of the copolymers, resulting in a decrease in the CMC values.

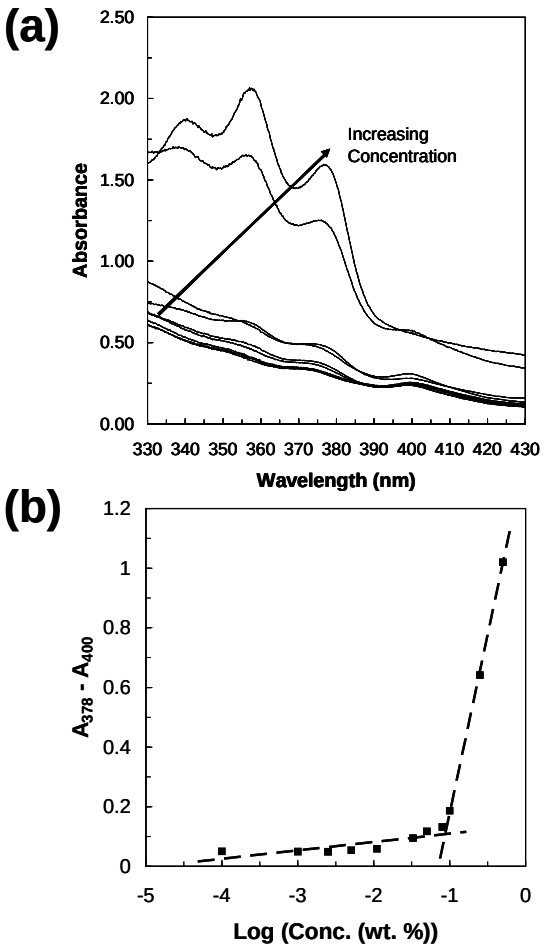

Figure 3.5. a) UV-vis spectra changes of DPH with increasing EPH2 copolymer concentration in water at 25 °C. DPH concentration was fixed at 6 mM and the polymer concentration varied between 0.0001 and 0.5 wt %. The increase in the absorbance band at 378 nm indicates the formation of a hydrophobic environment in water. b) CMC determination by extrapolation of the difference in absorbance at 378 nm and 400 nm.

The ^{13}C NMR was used to investigate the effect of solvent on the micelle structure.[29,31-34] $CDCl_3$ is a good nonselective solvent for PHB, PEG and PPG while water is a good selective solvent for PEG but poor for PPG and PHB. As shown in Figure 3.6, in $CDCl_3$, the peaks due to the PHB, PEG and PPG were sharp and well defined. In D_2O, PEG is shown as a sharp peak but the PHB and the PPG peaks are collapsed and broadened. This shows that the molecular motion of PHB and PPG is slow in water, indicating a hydrophobic core structure made up of PHB and PPG with PEG as the outer corona structure, confirming the core-corona structure of the

micelle. [31-33] However, in the light of the multiblock architecture of the copolymers, it is not reasonable to expect that the simple micelles of an ABA-type amphiphilic polymer be formed. Instead, it would be more plausible to consider an associated micelle model in the consideration of the above results. An associated micelle structure could be formed by the network-like packing of the polymer chains, as illustrated in Figure 3.7.

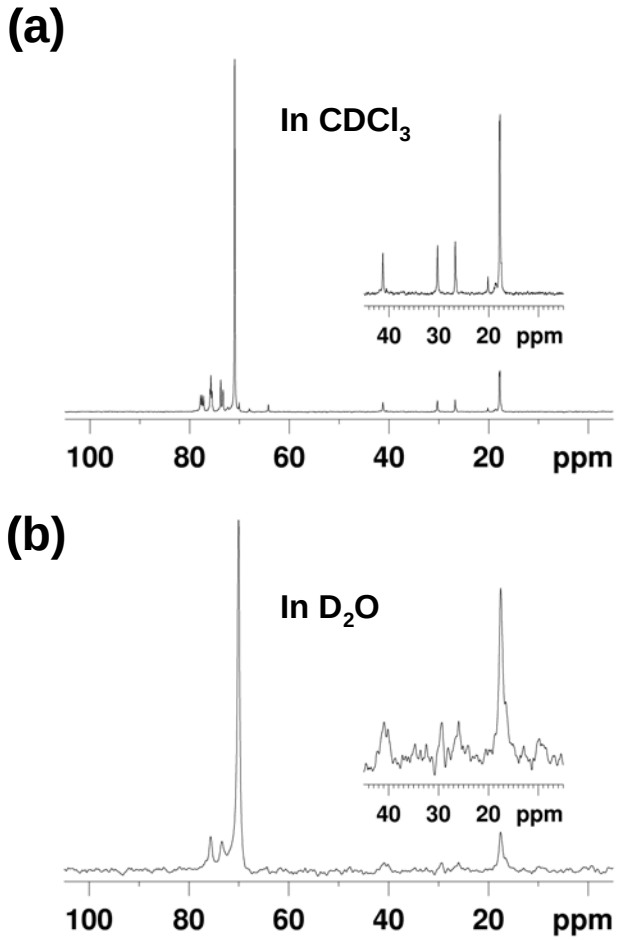

Figure 3.6. ^{13}C NMR spectra of EPH2 (5 wt %) in (a) $CDCl_3$ and (b) D_2O at 25 °C.

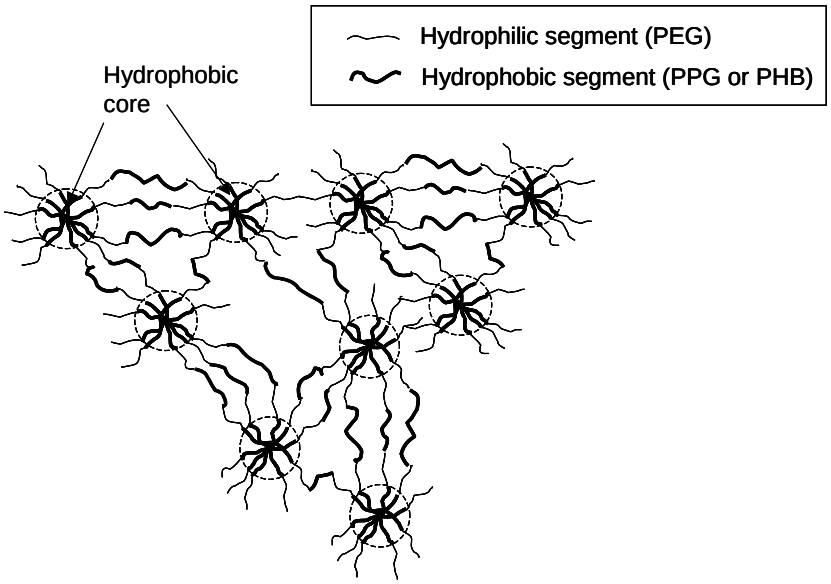

Figure 3.7. Associated micelle model showing the network-like packing of the polymer chains.

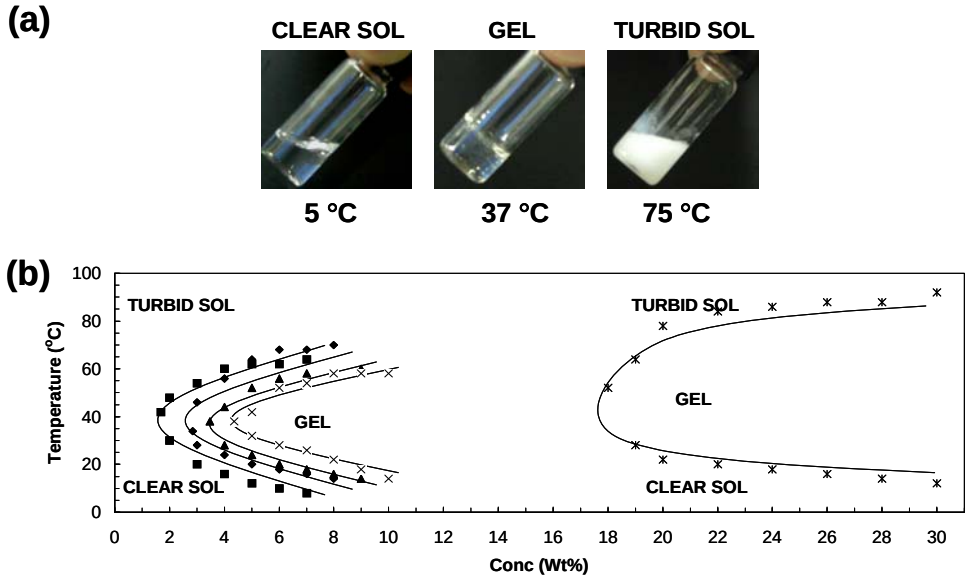

Figure 3.8. (a) Graphics showing the gel transition of poly(PHB/PEG/PEG urethanes) (EPH2: 5 wt % in H_2O) with increasing temperature. The transition from a clear sol to a gel to a turbid sol is observed in the graphics. (b) Sol-gel phase diagrams of poly(PEG/PPG/PHB urethanes) in aqueous solutions in comparison with $EG_{100}PG_{65}EG_{100}$ triblock polymer (▲, EPH1; ■,EPH2; ♦, EPH3; ×, EPH5; ∗, $EG_{100}PG_{65}EG_{100}$).

3.3.4. Thermo-reversible Sol-Gel Transition of the Copolymers.

The phase diagrams of the poly(ester urethane)s in aqueous solutions were determined by the test tube inverting method.[22a,29] The results are shown in Figure 3.8. Three regions can be identified from the diagram, the lower soluble region, gel region and the upper soluble region. As the temperature increased monotonically from 4 to 80 °C, the aqueous polymer solution underwent a sol-gel-sol transition. It is noted that the reverse transition also took place upon cooling from 80 to 4 °C. The critical gelation concentration (CGC) is defined as the minimum copolymer concentration in aqueous solution at which the gelation behavior could be observed. The CGCs of the copolymers in this work were found to be between 2 and 5 wt %. These values are much lower than that reported for many thermogelling copolymers.[19-22,28-30,32,35] Examining the gelation properties of the EPH series of copolymers, it appears that the incorporation of a small amount of PHB led to a decrease in CGC (EPH1 $\rightarrow$ EPH2). However, upon further addition of PHB, the CGC increased (EPH2 $\rightarrow$ EPH3).

The changes of the molecular environment occurring during the sol-gel transition of a 5 wt % EPH2 solution in D_2O was monitored by ^{13}C NMR technique at different temperatures (Figure 3.9). At low temperatures where the copolymer was a solution, the peaks ascribed to the PEG, PPG, and PHB segments were sharp and well defined because the segments interacted freely with the solvent molecules in the solution. At higher temperatures where the copolymer formed a hydrogel, the peaks were collapsed and broadened as compared with those observed at low temperatures. The phenomena can be attributed to the lower dynamic motion of the copolymer segments in the gel state.[22a,28,29,31-33,36] Due to the network-like packing of the multiblock polymer chains, the motion of all the components in the copolymer became restricted to a certain extent. Upon further increase in the temperature to 75 °C, the turbid sol state was

obtained, and the PEG, PPG, and PHB peaks were consequently seen as sharp and well defined again, which indicates that there was an increase in molecular motion of the PEG, PPG, and PHB blocks, possibly due to phase mixing between the blocks. Additionally, this reflects the disruption of the core-corona structure and an exposure of the hydrophobic core to the aqueous environment.[31-36] It has been reported that PEG dissolved in aqueous solution becomes dehydrated at higher temperatures.[37] Furthermore, the hydrodynamic radius of PEG in water decreases with an increase in temperature.[38] PPG has also been reported to be less soluble in water at elevated temperatures.[39] As the copolymer was made up of more than 60 wt% of PEG, it is reasonable to expect that any change in the properties of PEG segments would significantly affect the properties of the copolymer. At the turbid sol state, there could be significant dehydration of the PEG segments, leading to a phase separation between the polymer and water. The decrease of the hydrodynamic radius of the copolymer was largely influenced by the dehydration of PEG. This brough the different segment blocks closer together, resulting in a collapse in the copolymer structure. There could then be possible phase mixing between the segments. PEG has been demonstrated to be a solvent for PHB at elevated temperatures.[40] Thus, it was possible that the PEG, PPG and PHB segments form a homogenous mixture which was phase separated from the aqueous solution. Upon phase separation, the core-corona structure was disrupted and consequently, the hydrophobic core was exposed to the aqueous environment.[32] Overall, the ^{13}C NMR technique has offered important insights on the packing mechanism at the molecular level for the gel-sol transition process.

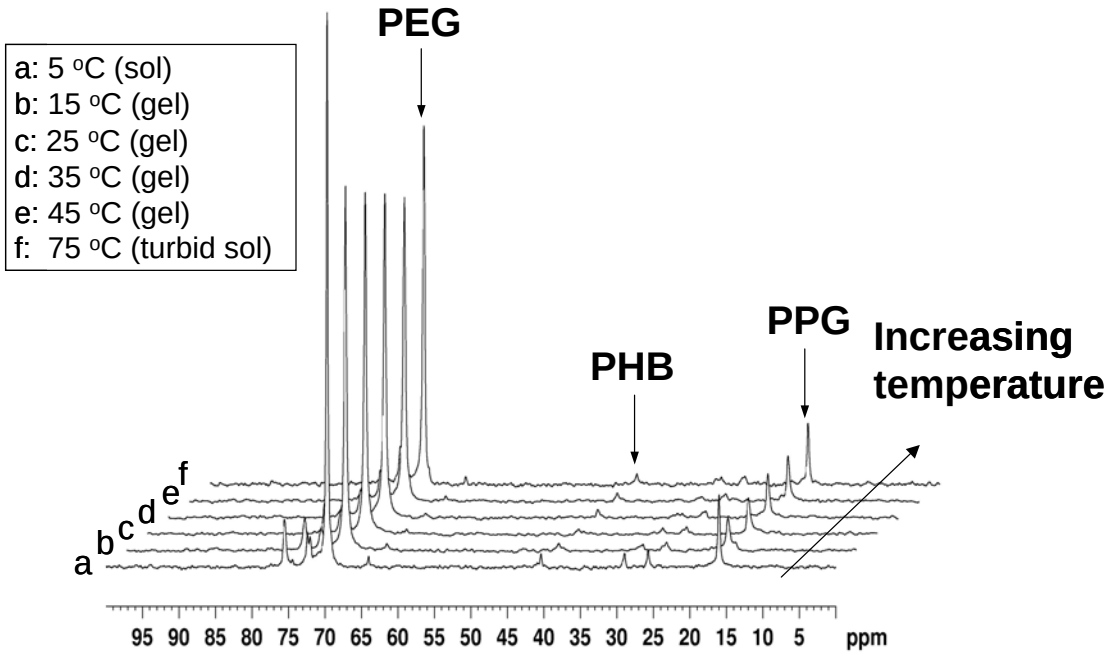

Figure 3.9. ^{13}C NMR of EPH2 in D_2O (5 wt %) at different temperatures.

The viscosities of the hydrogels were studied as a function of temperature. In general, the transition temperature corresponded well with the transition temperature determined using the test tube inverting method. The viscosity of the gels at 5 °C was between 50 to 200 cP, corresponding to a fluidic sol state. Figure 3.10 shows that as the concentration of EPH2 in aqueous solution increased, the viscosity of the gel increased. It is interesting to note that at the critical gelation concentration of EPH2 (2 wt %), the hydrogel displayed a higher maximum viscosity (43,000 cP) than a hydrogel containing 20 wt % $EG_{100}PG_{65}EG_{100}$ triblock polymer gel (33,000 cP). The result clearly shows that the gels of this work are more viscous than that of the PEG-PPG-PEG triblock copolymer gel. Above 3 wt %, the EPH2 gels attained a maximum viscosity of more than 55000 cP.

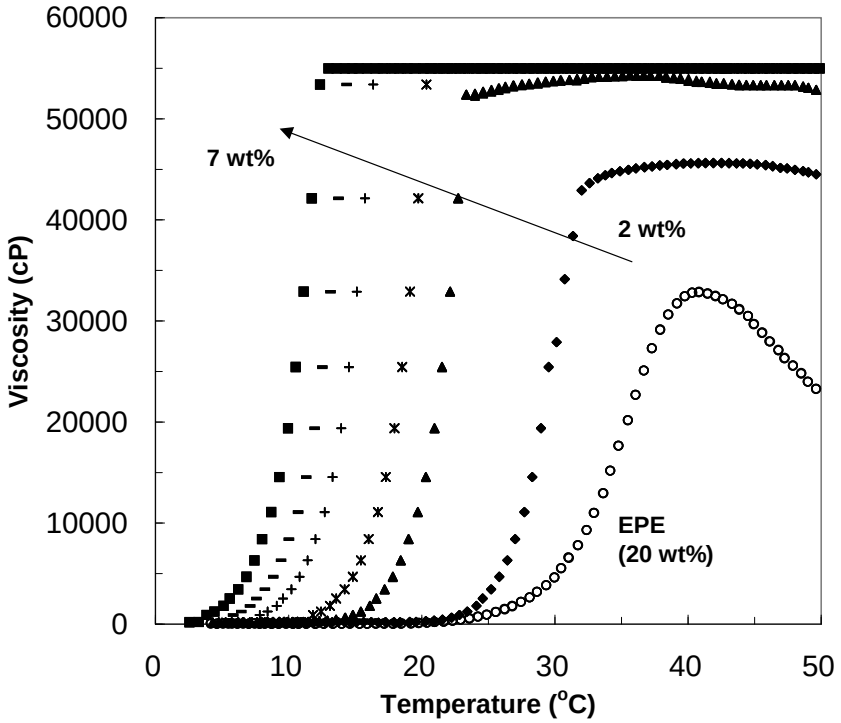

Figure 3.10. Viscosity as a function of temperature for EPH2 in aqueous solution at different concentrations (♦, 2 wt %; ▲, 3 wt %; ∗, 4 wt %; +, 5 wt %; –, 6 wt %; ■, 7 wt %) in comparison with $EG_{100}PG_{65}EG_{100}$ triblock copolymer (○, 20 wt %) at the shear rate of 9.6 s^{-1}.

3.3.5. Proposed Sol-Gel Transition Mechanism.

From the collated results of the micellar and gelation studies, a sol-gel transition mechanism for the multiblock copolymer system can be proposed as follows. The amphiphilic block copolymers form associated micelles at concentrations in the region of 0.1 wt %. These micelles comprise the hydrophobic PPG and PHB core and the hydrophilic PEG corona that interacts with the water molecules. Upon increasing the concentration up to above 2 wt %, the thermoresponsive copolymers exist as a solution at low temperatures, but undergo a reversible phase transition from a clear solution to a clear gel, and further to a turbid sol upon increase in temperature from 4 to 80 °C. From a solution state at low temperatures, a monotonic increase in temperature causes the PEG segments to become slightly dehydrated.[37] PPG segments also

become less soluble in water with increasing temperatures.[39] These changes provide the driving forces for the micellar aggregation when the hydrophobicity and hydrophilicity of the system achieves a balanced state. The PEG corona would self-associate instead of interacting with the neighboring water molecules, forming micelle aggregates.[38] As the micelle aggregates form a close packed structure, a gel state is observed. Further increase in temperature leads to a significant dehydration and the eventual collapse of the PEG corona.[38] Phase mixing of PEG, PPG, and PHB segments takes place due to the favourable interactions between the polymer segments of different blocks. The phase separation of the polymeric components from the aqueous solution results in the disruption of the core-corona structure and exposes the hydrophobic core to the aqueous environment.[31,36] This leads to the formation of a fluidic turbid sol at high temperatures.

These multiblock copolymer gels possess lower CMCs and CGCs than the widely studied thermogelling copolymers with the triblock chain architecture. This could be in part due to the increased association of the micelles brought about by the multiple segments that link the micelles together in a network-like structure. These segmental links facilitate the micellar aggregation process by reducing the degree of freedom possessed by the individual micelles. Cohn *et al*. developed a series of PEG/PPG/PCL multiblock copolymers which showed higher CGCs as compared with PEG/PPG multiblock copolymers.[21] This was attributed to the spatial effect of the caprolactone segments, which affects the packing of the polymer chains. In this work, the CGC value of the copolymer is very sensitive to the amount of PHB incorporated into the copolymers. Comparing EPH1 and EPH2, both having very low PHB levels, the effect of the spatial hindrances due to the PHB segments were superseded by the strong hydrophobic interaction between the PHB segments. However, a further increase in the PHB content increased the CGC of the copolymer (EPH3), reflecting the spatial effect of the PHB segment on

the packing of the polymer chains (Figure 3.8). Comparing the CGC values of EPH3 and EPH5 (3 wt % and 6 wt %, respectively), the copolymers having similar PHB content but different PHB block lengths, it appears that longer PHB segments would lead to a greater spatial hindrance and thus lead to a higher CGC value. This shows that the block length and the content of PHB incorporated into the copolymer could be utilized as parameters in the control of the properties of the thermogelling copolymers.

3.4. Conclusions

Potentially biodegradable and biocompatible poly(PEG/PPG/PHB urethanes), with PEG and PPG molar ratios fixed at 2:1 and various amounts of PHB, have been successfully synthesized using HDI as a coupling agent. Their chemical structure and molecular characteristics were studied with GPC, ^{1}H NMR, ^{13}C NMR and FTIR, which confirmed the architecture of the random multiblock poly(PEG/PPG/PHB urethanes). The GPC results indicated that the synthesized poly(PEG/PPG/PHB urethanes) had high molecular weights with relatively narrow molecular weight distributions. The contents of PHB segments in the copolymers calculated from ^{1}H NMR ranged from 2.1 to 12.7 wt %. It was found that the incorporation of 11.4 wt % of PHB and above rendered the poly(PEG/PPG/PHB urethanes) insoluble in water. The thermal stability of the poly(PEG/PPG/PHB urethanes) was studied by TGA, and three separate thermal degradation steps corresponding to PHB, PPG, and PEG segments were observed, from which the PHB contents were calculated. The results were in good agreement with those from the ^{1}H NMR measurements. The poly(PEG/PPG/PHB urethanes) presented better thermal stability than the PHB precursors. The CMC values of the water-soluble copolymers were determined by the dye solubilization method. The CMC values of the copolymers in this work ranged from 5.16×10^{-4} to 9.79×10^{-4} g mL^{-1}. On the basis of the dye solubilization and ^{13}C NMR experiments, the micelles are concluded to have a hydrophobic

core made up of PHB and PPG segments and an outer hydrophilic corona of PEG segments. The sol-gel transitions of the aqueous copolymers were studied, and phase diagrams showing the various sol and gel regions as a function of temperature and concentration of the solution was generated. The critical gelation concentration of the copolymers in this work ranged from 2 – 5 wt %. From the ^{13}C NMR spectra of the copolymers at various temperatures, the sol-gel transition can be elucidated at a molecular level. The viscosities of the EPH2 gel at various concentrations were studied and were found to be much higher than the gel formed by the $EG_{100}PG_{65}EG_{100}$ triblock copolymer (20 wt %). From the collated experimental results of the micellar and gelation studies as well as consideration of the multiblock architecture of the copolymers, an associated micelle packing mechanism for the sol-gel transition for the copolymers at increasing temperatures can be proposed.

Table 3.1. Molecular Characteristics of Poly(PEG/PPG/PHB urethane)s

Copolymer[a]	M_n of PHB used[b] (g mol^{-1})	Feed ratio (wt %)			Composition in copolymer (wt %)[c]			Copolymer characteristics		
		PHB	PEG	PPG	PHB	PEG	PPG	M_n[b] ($\times 10^3$)	M_w/M_n[b]	cmc[d] (g/mL)
EPH1	1070	2.8	61.7	35.5	2.1	64.0	33.9	50.6	1.56	9.79 x 10^{-4}
EPH2	1070	5.6	59.9	34.5	5.1	57.0	37.9	45.5	1.38	8.69 x 10^{-4}
EPH3	1070	8.7	58.0	33.4	8.1	56.3	35.7	42.5	1.37	5.16 x 10^{-4}
EPH4	1070	11.8	55.9	32.2	11.4	61.6	27.0	37.8	1.16	-[e]
EPH5	2800	6.9	59.1	34.0	7.1	63.3	29.7	39.2	1.18	8.88 x 10^{-4}
EPH6	2800	13.6	54.8	31.6	12.7	59.0	28.3	30.0	1.20	-[e]

[a] Poly(PEG/PPG/PHB urethane)s are denoted EPH, E for P**E**G, P for P**P**G and H for P**H**B. The M_n of PEG and PPG used for the copolymer synthesis was 1890 and 2180 g mol^{-1}, respectively. [b] Determined by GPC. [c] Calculated from ^{1}H NMR results. [d] Critical micellization concentration (cmc) in water determined by the dye solubilization technique at 25 °C. [e] Copolymers not water-soluble.

3.5. References

1. Huang, K.; Lee, B. P.; Ingram, D. R.; Messersmith, P. B.; *Biomacromolecules* **2002,** *3*, 397-406.
2. Daga, A.; Muraglia, A.; Quarto, R.; Cancedda, R.; Corte, G. *Gene Ther.* **2002**, *9*, 915-921.
3. Packhaeuser, C. B.; Schnieders, J.; Oster, C. G.; Kissel, T. *Eur. J. Pharm. Biopharm.* **2004**, *58*, 445-455.
4. Heller, J.; Barr, J.; Ng, S. Y.; Shen, H. R.; Abdellaoui, S.; Gurny, R.; Castioni, N. V.; Loup, P. J.; Baehni, P.; Mombelli, A. *Biomaterials* **1999**, *23*, 4397-4404.
5. Hill-West, J. L.; Chowdhury, S. M.; Slepian, M. J.; Hubbell, J. A. *Proc. Natl. Acad. Sci. U.S.A.* **1994**, *91*, 5967-5971.
6. Yokoyama, M. *Crit. Rev. Ther. Drug Carrier Systems* **1992**, *9*, 213-248.
7. Gilbert, J. C.; Hadgraft, J.; Bye, A.; Brookes, L. *Int. J. Pharm.* **1986**, *32*, 223-228.
8. Nalbandian, R. M.; Henry, R. L.; Wilks, H. S. *J. Biomed. Mater. Res.* **1972**, *6*, 583-590.
9. Exner, A. A.; Krupka, T. Y.; Scherrer, K.; Teets, J. M. *J. Control Release* **2005**, *106*, 188-197.
10. Esposito, E.; Carotta, Y.; Scabbia, A.; Trombelli, L.; D'Antona, P.; Menegatti, E.; Nastruzzi, C. *Int. J. Pharm.* **1996**, *142*, 9-23.
11. Katakam, M.; Ravis, W. R.; Golden, D. L.; Banga, A. K. *Int. J. Pharm.* **1997**, *152*, 53-58.
12. Blonder, J. M.; Baird, L.; Fulfs, J.; Rosenthal, G. J. *Life Sci.* **1999**, *65*, 261-266.
13. Wout, Z. G. M.; Pec, E. A.; Maggiore, J. A.; Williams, R. H.; Palicharla, P.; Johnston, T.P. *J. Parenteral Sci. &Tech.* **1992**, *46*, 192-200.
14. Palmer, W. K.; Emeson, E. E.; Johnston, T. P. *Atherosclerosis* **1998**, *136*, 115-123.

15. Ho, A. K.; Bromberg, L.; Huibers, P. D. T.; O'Connor, A. J.; Perera, J. M.; Stevens, G. W.; Hatton, T. A. *Langmuir* **2002**, *18*, 3005-3013.

16. Cleary, J.; Bromberg, L.; Magner. E. *Langmuir* **2002**, *19*, 9162-9172.

17. Bromberg. L. *Ind. Eng. Chem. Res.* **1998**, *37*, 4267-4274.

18. Bromberg. L. *J. Phys. Chem. B.* **1998**, 102, 10736-10744.

19. Ahn, J. S.; Suh, J. M.; Lee, M.; Jeong, B. *Polym. Int*. **2005**, *54*, 842-847.

20. Cohn, D.; Sosnik, A.; Levy. A. *Biomaterials* **2003**, *24*, 3707-3714.

21. Cohn, D.; Sosnik, A. *Biomaterials* **2005**, *26*, 349-357.

22. (a) Hwang, M. J.; Suh, J. M.; Bae, Y. H.; Kim, S.W.; Jeong, B. *Biomacromolecules* **2005**, *6*, 885-890. (b) Jeong, B.; Bae, Y. H.; Kim, S. W. *J. Controlled Release* **2000**, *63*, 155-163. (c) Jeong, B., Bae, Y. H.; Lee, D. S.; Kim, S. W. *Nature* **1997**, *388*. 860-862.

23. (a) Li, J.; Li, X.; Ni, X. P.; Leong, K. W. *Macromolecules* **2003**, *36*, 2661-2667. (b) Li, J.; Ni, X. P.; Li, X.; Tan, N. K.; Lim, C. T.; Ramakrishna, S; Leong, K. W. *Langmuir* **2005**, *21*, 8681-8685. (c) Li, X.; Mya, K. Y.; Ni, X. P.; He, C.; Leong, K. W.; Li, J. *J. Phys. Chem. B* **2006**, *110*, 5920-5926.

24. Li, X.; Loh, X. J; Wang, K.; He, C.; Li, J. *Biomacromolecules* **2005**, *6*, 2740-2747.

25. Loh, X. J.; Tan, K. K.; Li, X.; Li, J. *Biomaterials* **2006**, 27, 1841-1850.

26. Loh, X. J.; Wang, X.; Li, H.; Li, X.; Li, J. *Materials Science and Engineering C.* **2007**, *27*, 267-273.

27. Alexandridis, P.; Holzwarth, J. F.; Hatton, T. A. *Macromolecules* **1994**, *27*, 2414-2425.

28. Bae, S. J.; Suh, J. M.; Sohn, Y. S.; Bae, Y. H.; Kim, S.W.; Jeong, B. *Macromolecules* **2005**, *38*, 5260-5265.

29. Jeong, B.; Bae, Y. H.; Kim, S.W. *Macromolecules* **1999**, *32*, 7064-7069.

30. Behravesh, E.; Shung, A. K.; Jo, S.; Mikos, A. G. *Biomacromolecules* **2002**, *3*, 153-158.

31. Jeong, B.; Bae, Y. H.; Kim, S.W. *Colloids and Surfaces B: Biointerfaces* **1999**, *16*, 185-193.

32. Jeong, B.; Windisch, Jr., C. F.; Park, M. J.; Sohn, M. J.; Gutowska, A.; Char, K. *J. Phys. Chem. B* **2003**, 107, 10032-10039.

33. Lee, B. H.; Lee, Y. M.; Sohn, Y. S.; Song, S. C. *Macromolecules* **2002**, 35, 3876-3879.

34. Durand, A.; Hourdet, D.; Lafuma, F. *J. Phys. Chem. B* **2000**, 104, 9371-9377.

35. Booth, C.; Attwood, D. *Macromol. Rapid. Comm.* **2000**, *21*, 501-527.

36. Jeong, B.; Kibbey, M. R.; Birnbaum, J. C.; Won, Y. Y.; Gutowska, A. *Macromolecules* **2000**, 33, 8317-8322.

37. Harris, J. M. *Poly(ethylene glycol) Chemistry;* Plenum Press: New York, **1993**; pp 263-268.

38. Jeong, B. Ph.D. Thesis, University of Utah, 1999.

39. Yu, M.; Nishiumi, H.; Arons, J. S. *Fluid Phase Equilibria* **1993**, 83, 357-364.

40. Ravenelle, F.; Marchessault, R. H. *Biomacromolecules* **2002**, *3*, 1057-1064.

CHAPTER FOUR

SELF-ASSEMBLY BEHAVIOR OF MULTIBLOCK BIODEGRADABLE THERMOGELLING COPOLYMERS COMPRISING POLY(ETHYLENE GLYCOL), POLY(PROPYLENE GLYCOL) AND POLY[(R)-3-HYDROXYBUTYRATE]

4.1. Introduction

Thermogelling copolymers can be applied in areas such as, sustained drug delivery, gene delivery and tissue engineering.[1-7] Currently, poly(ethylene glycol)-block-poly(propylene glycol)-block- poly(ethylene glycol) (PEG-PPG-PEG) triblock copolymers (commonly known as Pluronics) are the most widely used thermogelling copolymers. They have been used for controlled drug delivery, wound covering, and chemosensitizing for cancer therapy.[8-10] However, it is not biodegradable. Other disadvantages of Pluronics include, burst release of bioactive agents encapsulated within the gel, as well as, poor gel stability in vivo.[11-12] Generally, biodegradability is an issue that practitioners consider when using these thermogelling copolymers in biomedical systems. In an ideal scenario, the gel should be completely removed from the body after its period of application. The size of the polymer can be reduced by hydrolysis and the polymer fragments can then be excreted from the body. Biodegradability can be introduced into copolymers by incorporating hydrolysable segments, such as poly(ε-caprolactone) (PCL) or poly(lactic acid) in the copolymer. There have been many reports of biodegradable thermogelling copolymers in recent literature.[13-22] Extensive reviews on thermogelling copolymers have recently been published.[7,23]

The synthesis and characterization of thermogelling poly(ester urethane)s comprising PEG, PPG and PHB was described in Chapter 3. In this chapter, the self assembly behavior of the copolymers at different concentrations and at different temperatures is investigated. The thermodynamics of the micellization process was studied based on the change in the critical micelle concentration (CMC) of the copolymer solution at different temperatures. The analysis of the gelation process based on ^{1}H and ^{13}C NMR spectroscopic studies carried out at various temperatures to gain a better understanding of the phase transition process from soluble state to gel state.

4.2. Experimental Section

4.2.1. Materials

The copolymers used in this study were the poly(PEG/PPG/PHB urethane)s, EPH1, EPH2 and EPH3, synthesized in Chapter 3. The hydrophobic dye probe, 1,6-diphenyl-1,3,5-hexatriene (DPH) was purchased from Aldrich.

4.2.2. Micelle Characterization

Nuclear magnetic resonance (NMR) measurements. The ^{1}H NMR (400 MHz) and ^{13}C NMR (100 MHz) spectra were recorded on a Bruker AV-400 NMR spectrometer at room temperature. The ^{1}H NMR measurements were carried out with an acquisition time of 3.2 s, a pulse repetition time of 2.0 s, a 30° pulse width, 5208 Hz spectral width, and 32K data points. Chemical shift was referred to the solvent peak (δ = 7.3 ppm for $CHCl_3$). Sodium 3-trimethylsilylpropanesulfonate was used as the internal standard for the measurements conducted in D_2O.

CMC Determination. The CMC values were determined by using the dye solubilization method at 15, 25, 35 and 45 ^{o}C.[22] The hydrophobic dye 1,6-diphenyl-1,3,5-hexatriene (DPH) was dissolved in methanol with a concentration of 0.6 mM. 20 μL of this solution was mixed with 2.0 mL of copolymer aqueous solution with concentrations ranging from 0.0001 to 0.5 wt % and equilibrated overnight at 4 ^{o}C. A UV-Vis spectrophotometer was used to obtain the UV-Vis spectra in the range of 330-430 nm at 15 ^{o}C, 25 ^{o}C, 35 ^{o}C and 45 ^{o}C. The CMC value was determined by the plot of the difference in absorbance at 378 nm and at 400 nm ($A_{378} - A_{400}$) versus logarithmic concentration. Experiments were carried out in triplicates.

Atomic Force Microscopy. A Digital Instruments MultiMode atomic force microscope with a Nanoscope IV controller in tapping mode was employed to image the gel samples. Gel samples were prepared from 5 wt% copolymer solution and were incubated at 37 ^{o}C for 3 hours

prior to the experiment. Briefly, silicon disks were soaked in 50% acetone for a minimum of 2 h and rinsed with distilled water. When the silicon disk was completely dried, a thin layer of the gel was coated onto the disks. The gel was further flattened by pressing a glass coverslip over the silicon disk and the sample was imaged immediately. All the atomic force microscopy (AFM) images were obtained with a scan rate of 1 Hz over a selected area of 10 μm x 10 μm. Image analysis was performed using Nanoscope software after removal of the background slope by flattening the images.

4.3 Results and Discussion

4.3.1. Micelle Properties

The micelle properties of the poly(PEG/PPG/PHB urethane)s were studied. The CMC determination was carried out for these copolymers at 15, 25, 35 and 45 ^{o}C. This experiment was conducted by varying the aqueous polymer concentration in the range of 0.0001 to 0.5 wt %, while keeping the concentration of DPH constant. DPH shows a higher absorption coefficient in a hydrophobic environment than in water. Thus, with increasing polymer concentration, the absorbances at 344, 358 and 378 nm increased. The point where the absorbance suddenly increases corresponds to the concentration at which micelles are formed. When the micelle is formed, DPH partitions preferentially into the hydrophobic core formed in the aqueous solution.[13-14,16] The CMC was determined by extrapolating the absorbance at 378 nm minus the absorbance at 400 nm ($A_{378} - A_{400}$) versus logarithmic concentration. The CMC values for the water-soluble copolymers at the different temperatures are tabulated in Table 4.1.

Assuming a closed association of unimers into micelles, thermodynamic functions such as the molar standard enthalpy, $\Delta H°$, and the entropy, $\Delta S°$, and free energy, $\Delta G°$, for micelle

formation can be extracted from the studies of the CMC dependence on temperature.[24] The free energy of micellization ΔG°, can be calculated by

$$\Delta G° = RT \ln(X_{cmc}) \quad (4.1)$$

where R is the gas law constant, T is the temperature in K and X_{cmc} is the CMC in mole fractions at temperature T. The values of ΔG° are negative, indicating the spontaneity of the micellization process. These values are temperature-dependent, becoming more negative at higher temperatures. Further, the values of the standard enthalpy of micellization, ΔH°, and the standard entropy of micellization, ΔS°, can be extracted from the Arrhenius plot of $\ln(X_{cmc})$ versus 1 / T.

$$\Delta H° = R(d \ln X_{cmc} / d\, T^{-1}) \quad (4.2)$$

$$\Delta S° = (\Delta H° - \Delta G°) / T \quad (4.3)$$

Figure 4.1 shows the plot of $\ln X_{cmc}$ *versus* T^{-1}. ΔH° was derived from the slope of the linear plot. In all the solutions studied, enthalpy of micellization was shown to be an endothermic process, similar to aqueous solutions of PEG-PPG-PEG triblock copolymers.[24] The enthalpy values became less positive with increasing PHB content, very similar to the previously reported thermogelling poly(PEG/PPG/PLA urethane)s.[22] On the other hand, the micellization process is entropy-driven, with the value becoming less positive with increasing PHB content. Thus, when the micelles form, ordered water molecules are expelled from the polymer chains, leading to an increase in the entropy.[15] When the PHB content is higher, the association of the polymer chains is greater due to the highly hydrophobic nature of the PHB segments and therefore there is a higher enthalpy gain. However, this leads to a lower extent of interaction with the water molecules and a corresponding decrease in the entropy when the copolymer chains self-assemble into micelles.

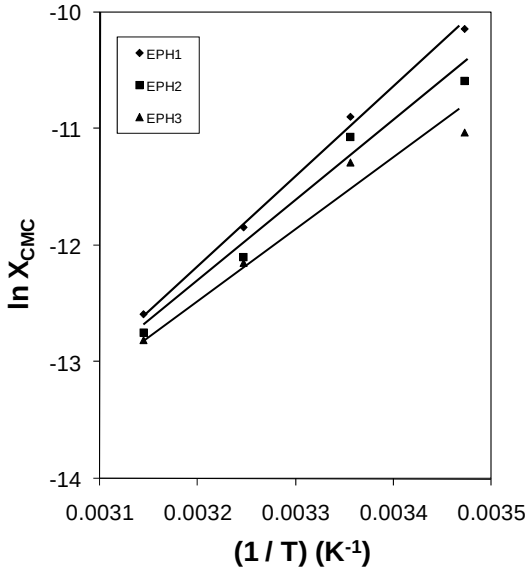

Figure 4.1. Plot of ln X_{CMC} against (1/T) for the determination of $\Delta H_{micellization}$ of the EPH series of copolymers.

Table 4.1. Thermodynamic parameters of the micellization process of poly(PEG/PPG/PHB urethane)s

Copolymer	Temperature (^{o}C)	cmc x 10^4 (g/mL)	ΔG (kJ/mole)	ΔS (kJ/mole/K)	ΔH (kJ/mole)
EPH1	15	19.9 ± 3.1	-23.0 ± 0.3	0.300 ± 0.001	
	25	9.4 ± 2.2	-24.7 ± 0.5	0.295 ± 0.002	63.7 ± 13.6
	35	3.7 ± 1.1	-26.9 ± 0.7	0.293 ± 0.002	
	45	1.7 ± 0.5	-28.9 ± 0.7	0.289 ± 0.002	
EPH2	15	11.5 ± 0.8	-24.0 ± 0.1	0.282 ± 0.001	
	25	7.1 ± 1.5	-25.1 ± 0.5	0.277 ± 0.002	57.2 ± 3.4
	35	2.6 ± 0.7	-27.5 ± 0.6	0.275 ± 0.002	
	45	1.3 ± 0.2	-28.9 ± 0.3	0.271 ± 0.001	
EPH3	15	6.9 ± 0.8	-25.0 ± 0.3	0.251 ± 0.001	
	25	5.3 ± 1.3	-25.6 ± 0.5	0.244 ± 0.002	47.1 ± 5.2
	35	2.3 ± 0.9	-27.6 ± 0.9	0.243 ± 0.003	
	45	1.2 ± 0.2	-29.1 ± 0.5	0.240 ± 0.002	

4.3.2. Variable Temperature ^{1}H NMR Studies of the Thermogelling Copolymer Solution.

The poly(PEG/PPG/PHB urethane)s are water soluble and the aqueous copolymer solutions showed thermogelling properties. At low temperatures of around 5 to 15 ^oC, the solution has low viscosity and appears clear. Gelation of the solution occurs at about 20 ^oC and a clear gel is obtained up to about 50 ^oC. Above 50 ^oC, the gel structure collapses and a turbid solution is obtained. The ^{1}H NMR spectrum of the copolymer solution (EPH1) at 5 wt% in D_2O were recorded at different temperatures. The peak widths corresponding to specific functional of the copolymers were measured. For PPG, the peak width measurements were done on the peak corresponding to the methyl group of the polymer segment. For PEG, the peak width measurements were done on the peak corresponding to the methylene groups of the polymer segment. Due to the low PHB content and subsequently low signal-to-noise ratio of the peaks, reliable information regarding the change in the peak width of the functional groups of the PHB segments could not be obtained. However, the peak shape changes of the PEG, PPG and PHB segments are presented in Figure 4.2. The solution changes from a liquid state to a gel state to a turbid solution as the temperature was raised from 5 ^oC to 65 ^oC. For the PEG protons, there is minimal shift in the peak position from 5 to 45 ^oC (Figure 4.2a). Ma *et al.* have presented a detailed ^{1}H NMR spectroscopy study on the PEG-PPG-PEG triblock copolymers in D_2O.[26] Their work focused on the micellization process of the triblock copolymers with a small section on the gelation of the polymers. This observation is similar to Ma's observation of the PEG segments for a PEG-PPG-PEG triblock copolymer at high concentrations in D_2O. The peak width at half height remained fairly constant until above 45 ^oC, where phase transition occurs. The phase transition led to an increase in the peak width at half height for the PEG protons. As for the PPG segment, at low temperatures, two doublets corresponding to the methyl and methylene groups of the PPG segment are observed (Figures 4.2b and 4.2c). As the temperature is increased, the

peaks broaden. Specifically, for the PPG methyl peak, there is an upfield shift in the methyl peak signal which signals increasing hydrophobicity at higher temperatures.[26] There is a sudden increase in the peak width at half height between 15 ^{o}C to 25 ^{o}C upon gelation. This is similar to the observation made by Nivaggioli *et al.*[25] At above 45 ^{o}C, phase separation occurs and the peak width at half height increases again. The change in the peak width of both peaks of PEG and PPG segments in ^{1}H NMR is reflected in Figure 4.3. For the PHB segments, the peak corresponding to the –CH_2– group appears very different from the typical "doublet of doublet" peaks observed with the spectra in $CDCl_3$. This peak shifts upfield and broadened as the temperature was raised. As for the –CH– group, at low temperatures, a multiplet was discernable. As the temperature was increased, the peaks broaden and the fine features of the peak disappear.

4.3.3. Variable Temperature ^{13}C NMR Studies of the Thermogelling Copolymer Solution

The evidence shown by the ^{13}C NMR spectrum is slightly different from the ^{1}H NMR spectrum. The changes in the ^{13}C NMR spectrum of EPH1 in D_2O at different temperatures are shown in Figure 4.4. A downfield shift was observed for both the methylene groups of PEG and the methyl group of PPG. For the change in the shape of the PPG peak, the observations were similar to that made by Yu *et al*.[27] The change in the peak width of the PEG and PPG segments are shown in Figure 4.5. Both the PEG and PPG polymer segments display almost the same trend. The peak width increases from 15 ^{o}C to 25 ^{o}C, indicating reduced polymer segment motion in the solution. This corresponds to the temperature at which gelation of the copolymer solution occurs. This is similar to the observations made by Yu *et al.*[27] The peak width of the polymer segments decreases only between 55 and 65 ^{o}C when the phase separation of the copolymer occurs. It is also interesting to note that the phase separation leads to a broadening of the peaks in the ^{1}H NMR spectrum and a narrowing of peaks in the ^{13}C NMR spectrum.

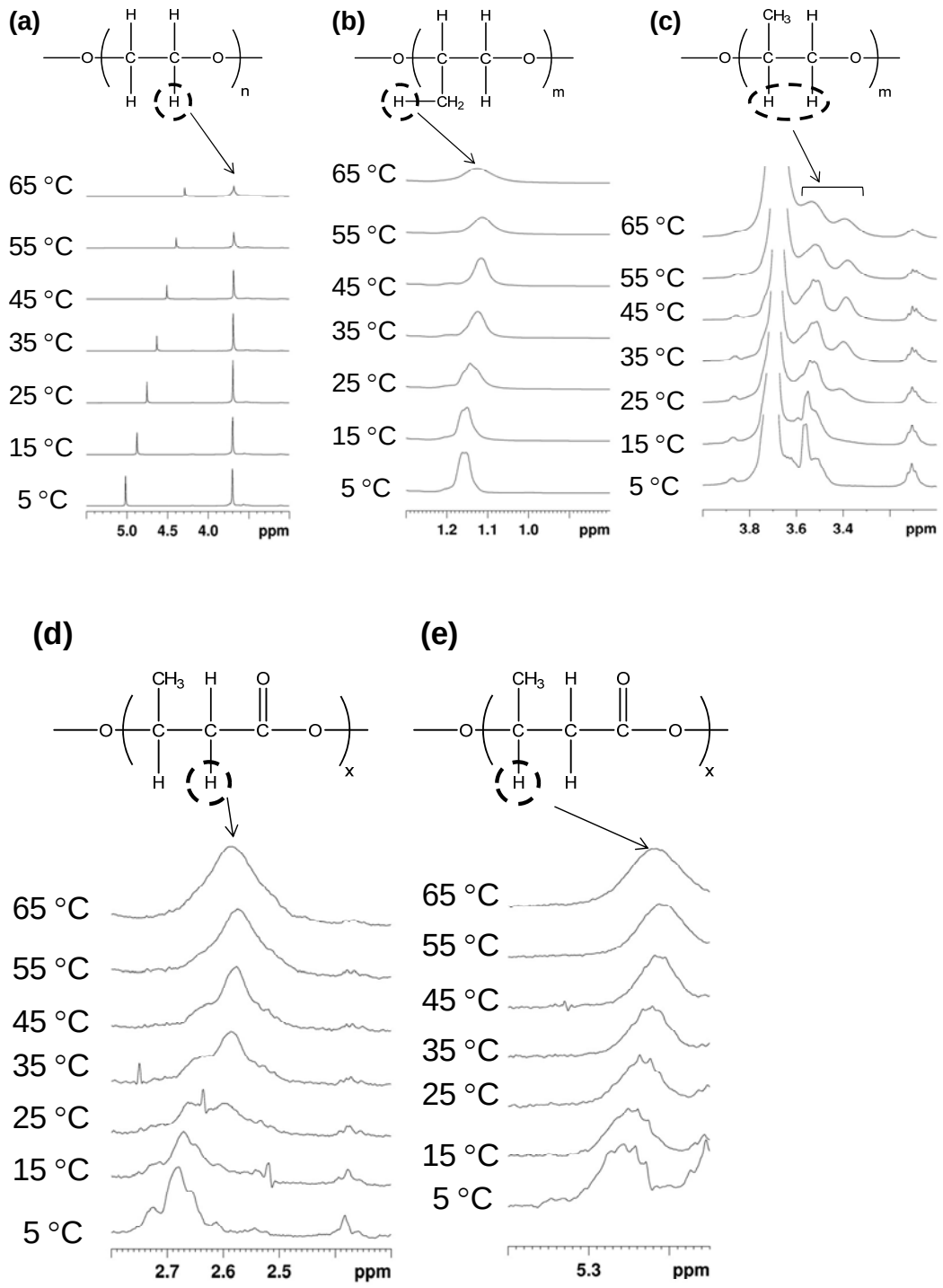

Figure 4.2. ^{1}H NMR spectrum of specific segments of (a) PEG, (b, c) PPG, (d, e) PHB of the poly(PEG/PPG/PHB urethane) copolymer (5 wt%), EPH1, in D_2O at different temperatures.

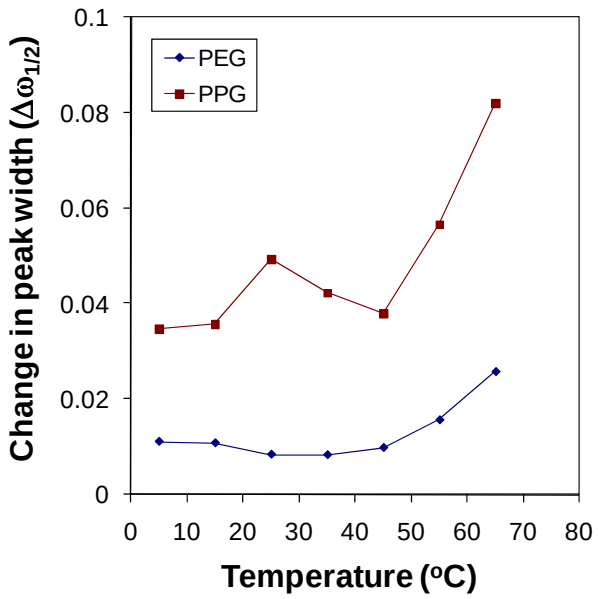

Figure 4.3. Change in the peak width of the ^{1}H NMR peaks corresponding to the $–CH_3$ group of PPG and the $–CH_2–$ group of PEG. [Poly(PEG/PPG/PHB urethane) copolymer (5 wt%), EPH1, in D_2O at different temperatures].

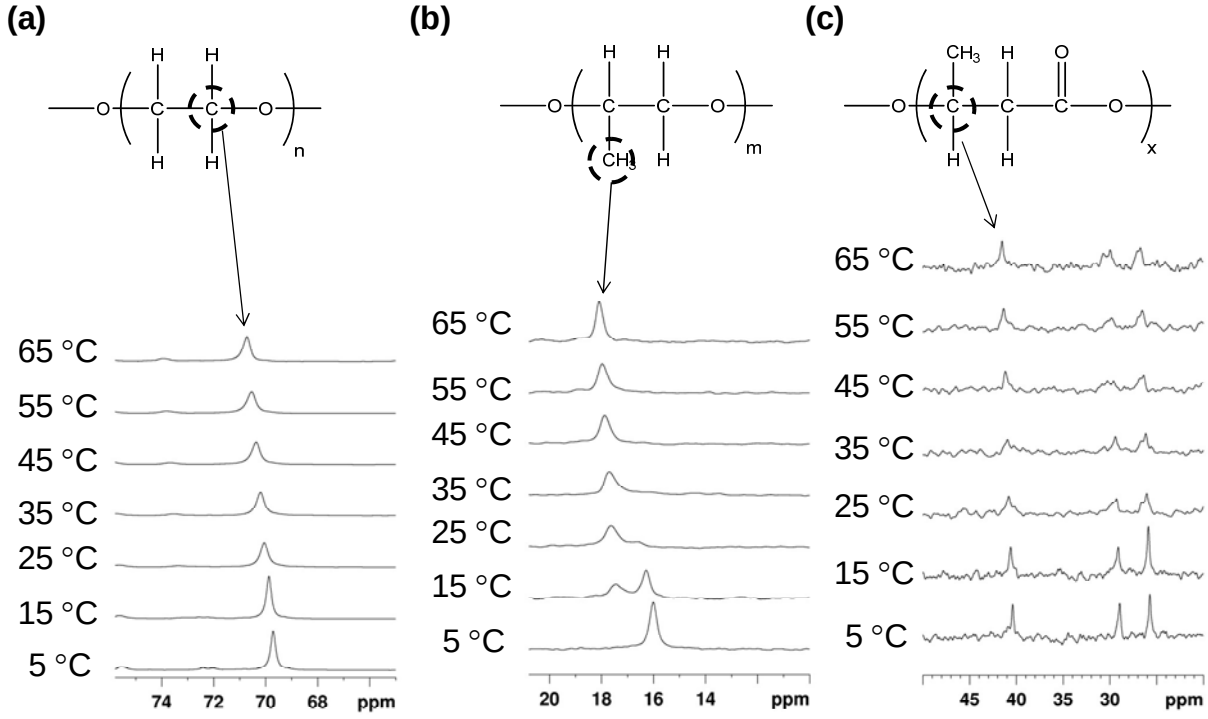

Figure 4.4. ^{13}C NMR spectrum of specific segments of (a) PEG, (b) PPG, (c) PHB of the poly(PEG/PPG/PHB urethane) copolymer (5 wt%), EPH1, in D_2O at different temperatures.

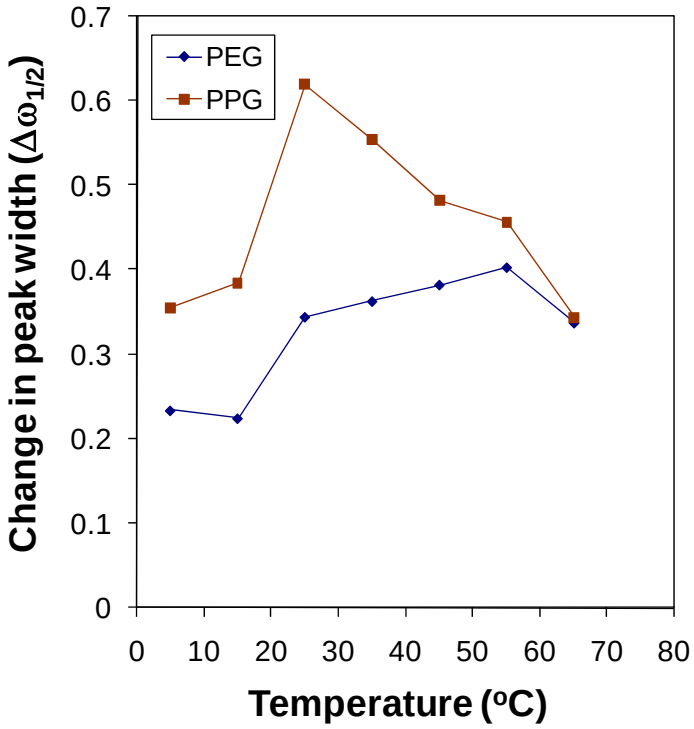

Figure 4.5. Change in the peak width of the ^{13}C NMR peaks corresponding to the $–CH_3$ group of PPG and the $–CH_2–$ group of PEG. [Poly(PEG/PPG/PHB urethane) copolymer (5 wt%), EPH1, in D_2O at different temperatures].

4.3.4. Understanding the NMR results.

From both the ^{1}H and ^{13}C NMR spectrum, the gelation of the copolymer solution leads to a broadening of the peaks. This clearly shows that the movement of the polymer segments is retarded by the gelation process. This is consistent with the observation that the diffusive motion is slowed down in the gel regime of aqueous PEG-PPG-PEG copolymer solutions.[28] However, the difference between this copolymer gel and the conventional Pluronics gel is that the former phase separates at a lower temperature. This allows the study of the change in the molecular motion occurring at the phase transition. During the phase separation stage (clear gel to turbid sol stage), a major difference between the ^{1}H and the ^{13}C NMR spectra is observed. The ^{1}H NMR spectra of both the PEG and PPG segments show a peak broadening, indicating reduced molecular motion. The ^{13}C NMR of both the PEG and PPG segments shows peak narrowing,

indicating increased motion. Before phase separation, there is greater proportion of polymer-water interactions than polymer-polymer interactions. After phase separation, there is greater proportion of polymer-polymer interactions than polymer-water interactions. The ^{1}H NMR profile is greatly influenced by the extent of the polymer-water interactions. The interaction between the water molecules and the polymer segments, such as the PEG segment, takes place via the hydrogen bonding interaction between the proton of the polymer segment and the water molecule.[25,29] Upon the dehydration of the PEG and PPG segments, the polymer-water interactions are reduced leading to reduced molecular motion of the protons on the copolymer segments. On the other hand, the ^{13}C NMR profile is influenced more significantly by the extent of the polymer-polymer interactions than polymer-water interactions. The carbon atoms of the polymer segment do not interact or are indirectly affected by the surrounding water molecules. Therefore, the molecular motion of these atoms would be less sensitive to changes in the external water environment. Instead, it will be more affected by the phase separation process, leading to increased polymer-polymer interactions. When phase separation occurs, the collapse of the polymer chains lead to possible phase blending between the polymer segments. PEG and PPG are known to be compatible polymers.[30,31] Furthermore, at higher temperatures, the vibrational, rotational and translational motion of the polymer segments increases, the ^{13}C NMR spectra thus shows a narrowing of the peak width. The self diffusion of the PEG-PPG-PEG triblock copolymer has been reported to show greater self diffusion coefficients at temperatures higher than 50 ^{o}C.[30] When the copolymer chains are dehydrated, the copolymer molecules become more flexible as the solution becomes a mixture resembling a polymer melt containing water.[30]

4.3.5. AFM Microscopy Observation of the Thermogelling Copolymers.

The surface of the thermogelling copolymers were observed using AFM. The images are shown in Figure 4.6. The images show that the gels were assembled from micron-sized entities.

It is very likely that these entities are made of micelle clusters. The gelation process of Pluronics F127 in water had been suggested to take place via close packing of micellar spheres.[27] Here, the formation of micelle clusters are likely to be from the self assembly of micelle spheres. When there is a sufficiently high concentration of the micelle clusters assembling together, a supramolecular water retaining gel structure is formed. From the micrographs, it can be seen that as the PHB content increases, the micelle clusters become larger in size. Wanka *et al.* have previously reported that for a PEG-PPG-PEG copolymer with the same PPG block length but decreasing PEG block length, the cubic phase, followed by the hexagonal phase disappears.[29] In the AFM micrographs of the gels, EPH1 shows a nearly worm-like structure made of spherical particles. The surface structure of this gel appears to be on the boundary of the cubic and the hexagonal phase. EPH2 shows a better defined worm-like structure. Interestingly, an AFM image of the Pluronics F127 copolymer (1 wt%) coated on untreated silicon substrate shows very similar morphology to the AFM image of EPH2 gel.[32] EPH3 shows a nearly lamellar structure. From the critical gelation concentration studies reported previously, it was found that the critical gelation concentration is the highest for EPH3, followed by EPH1, followed by EPH2. From here, it appears that the worm-like hexagonal packing gives the most efficient packing for the gels, leading to the lowest critical gelation concentration.

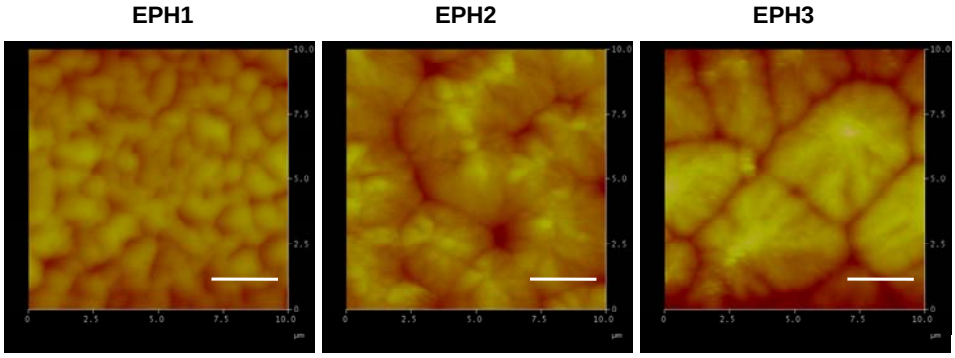

Figure 4.6. Atomic force microscopy images of the surface of the poly(PEG/PPG/PHB urethane) copolymer gels. (Scale bar corresponds to 2.5 μm)

4.4. Conclusions

The thermodynamics of micellization of multiblock poly(ester urethane)s having poly[(*R*)-3-hydroxybutyrate] (PHB), poly(ethylene glycol) (PEG), and poly(propylene glycol) (PPG) segments was studied. Micelle formation was found to be entropy-driven. The gelation of the thermogelling copolymers were studied by variable temperature ^{1}H and ^{13}C NMR. Macroscopic observations of the gelation process were related to the NMR results. Using AFM, micron-sized entities which could possibly be micelle clusters were observed. Further, it appears that the formation of the gel is due to the aggregation of micelle clusters. A higher content of PHB increased the size of the micelle cluster.

4.5. References

1. Huang, K.; Lee, B. P.; Ingram, D. R.; Messersmith, P. B. *Biomacromolecules* **2002**, *3*, 397-406.
2. Daga, A.; Muraglia, A.; Quarto, R.; Cancedda, R.; Corte, G. *Gene Ther.* **2002**, *9*, 915-921.
3. Packhaeuser, C. B.; Schnieders, J.; Oster, C. G.; Kissel, T. *Eur. J. Pharm. Biopharm.* **2004**, *58*, 445-455.
4. Heller, J.; Barr, J.; Ng, S. Y.; Shen, H. R.; Abdellaoui, S.; Gurny, R.; Castioni, N. V.; Loup, P. J.; Baehni, P.; Mombelli, A. *Biomaterials* **1999**, *23*, 4397-4404.
5. Hill-West, J. L.; Chowdhury, S. M.; Slepian, M. J.; Hubbell, J. A. *Proc. Natl. Acad. Sci. U.S.A.* **1994**, *91*, 5967-5971.
6. Yokoyama, M. *Crit. Rev. Ther. Drug Carrier Syst.* **1992**, *9*, 213-248.
7. Loh, X. J.; Li, J. *Expert Opin. Ther. Pat.* **2007**, *17*, 965-977.

8. Gilbert, J. C.; Hadgraft, J.; Bye, A.; Brookes, L. *Int. J. Pharm.* **1986**, *32*, 223-228.

9. Nalbandian, R. M.; Henry, R. L.; Wilks, H. S. *J. Biomed. Mater. Res.* **1972**, *6*, 583-590.

10. Exner, A. A.; Krupka, T. Y.; Scherrer, K.; Teets, J. M. *J. Controlled Release* **2005**, *106*, 188-197.

11. Esposito, E.; Carotta, Y.; Scabbia, A.; Trombelli, L.; D'Antona, P.; Menegatti, E.; Nastruzzi, C. *Int. J. Pharm.* **1996**, *142*, 9-23.

12. Katakam, M.; Ravis, W. R.; Golden, D. L.; Banga, A. K. *Int. J. Pharm.* **1997**, *152*, 53-58.

13. Bae, S. J.; Suh, J. M.; Sohn, Y. S.; Bae, Y. H.; Kim, S. W.; Jeong, B. *Macromolecules* **2005,** *38*, 5260-5265 .

14. Hwang, M. J.; Suh, J. M.; Bae, Y. H.; Kim, S. W.; Jeong, B. *Biomacromolecules* **2005,** *6*, 885-890.

15. Jeong, B.; Bae, Y. H.; Kim, S. W. *Colloids and Surfaces B-Biointerfaces* **1999,** *16*, 185-193.

16. Jeong, B.; Bae, Y. H.; Kim, S. W. *Macromolecules* **1999,** *32*, 7064-7069 .

17. Jeong, B.; Bae, Y. H.; Lee, D. S.; Kim, S. W. *Nature* **1997,** *388*, 860-862.

18. Jeong, B.; Kibbey, M. R.; Birnbaum, J. C.; Won, Y. Y.; Gutowska, A. *Macromolecules* **2000,** *33*, 8317-8322 .

19. Joo, M. K.; Sohn, Y. S.; Jeong, B. *Macromolecules* **2007,** *40*, 5111-5115 .

20. Loh, X. J.; Goh, S. H.; Li, J. *Biomacromolecules* **2007,** *8*, 585-593.

21. Loh, X. J.; Goh, S. H.; Li, J. *Biomaterials* **2007,** *28*, 4113-4123.

22. Loh, X. J.; Tan, Y. X.; Li, Z.; Teo, L. S.; Goh, S. H.; Li, J. *Biomaterials* **2008,** *29*, 2164-2172.

23. He, C.; Kim, S. W.; Lee, D. S. *J. Controlled Release* **2008,** *127*, 189-207.

24. Alexandridis, P.; Holzwarth, J. F.; Hatton, T. A. *Macromolecules* **1994**, *27*, 2414-2425.

25. Nivaggioli, T.; Tsao, B.; Alexandridis, P.; Hatton, T. A. *Langmuir* **1995**, *11*, 119-126.

26. Ma, J.; Guo, C.; Tang, Y.; Liu, H. *Langmuir* **2007**, *23*, 9596-9605.

27. Yu, G.-E.; Deng, Y.; Dalton, S.; Wang, Q.-G.; Attwood, D.; Price, C.; Booth, C. *J. Chem. Soc. Fadaday Trans.* **1992**, *88*, 2537-2544.

28. Walderhaug, H.; Nystrom, B. *Journal of Physical Chemistry B* **1997,** 101, 1524-1528.

29. Wanka, G.; Hoffmann, H.; Ulbricht, W. *Macromolecules* **1994**, *27*, 4145-4159.

30. Fleischer, G.; Bloss, P.; Hergeth, W. D. *Colloid and Polymer Science* **1993**, *271*, 217-222.

31. Morales, E.; Salmeron, M.; Acosta J. L. *J. Polym. Sci. Part. B, Polym. Phys.* **1996**, 34, 2715-2721.

32. Wu, C. H.; Liu, T. B.; White, H.; Chu, B. *Langmuir* **2000**, *16*, 656-661.

CHAPTER FIVE

HYDROLYTIC DEGRADATION, DRUG RELEASE AND CYTO-COMPATIBILITY OF MULTIBLOCK BIODEGRADABLE THERMOGELLING COPOLYMERS COMPRISING POLY(ETHYLENE GLYCOL), POLY(PROPYLENE GLYCOL) AND POLY[(R)-3-HYDROXYBUTYRATE]

5.1. Introduction

In the rapidly developing field of biotechnology, thermogelling polymers have exhibited interesting properties that have made them potential candidates for drug delivery and tissue engineering applications.[1-6] The synthesis and characterization of thermogelling poly(ester urethane)s comprising PEG, PPG and PHB was described in Chapter 3.

PHB is a natural biodegradable and biocompatible polyester which degrades to D-3-hydroxybutyrate, a natural non-toxic human blood plasma component.[7,8] On the other hand, the PEG-PPG-PEG triblock copolymer is an FDA-approved biocompatible polyether.[9,10] The biostability of polyurethane-based medical implants and the toxicity of the degradation products are important considerations when assessing polymers for biomedical applications.[11] Chain scission of poly(ester urethane)s could either occur at the urethane linkage or the ester linkage, with the ester linkage being the primary site of hydrolysis in poly(ester urethane)s.[12,13]

The degradation of such thermogelling copolymers must be distinguished from the conventional degradation of typical crosslinked hydrogels. In a crosslinked polymer gel, the chemical bond of the crosslinking agent or polymer backbone must be broken before erosion of the polymer fragments can take place.[14-16] The rate of degradation of the conventional crosslinked gel can be controlled by the quantity and nature of the crosslinking agent or degradability of the polymer backbone. In a thermogelling copolymer, the formation of the hydrogel results from the physical packing of the polymeric segments in solution. Surface erosion is expected to occur with aqueous dissolution of the exposed polymer chains. Degradation of the polymer chains is expected to take place at a much later time period after further exposure to the aqueous environment, thus the degradation behavior is expected to be markedly different from that of conventional hydrogels.

Currently, there have been limited studies of the degradation process of a thermogelling polymer. Jeong *et al.* studied the degradation of the PEG-PLGA-PEG triblock hydrogel, while Shim *et al.* studied the biodegradability of a sulfonamide-modified poly(ε-caprolactone-co-lactide)-poly(ethylene glycol)- poly(ε-caprolactone-co-lactide).[17,18] Based on these studies, it can be hypothesized that the degradation of the thermogelling polymer may involve three basic phases comprising an *incubation* period, a *gel erosion* period, and a *chain scission* period. The objective of this study is to provide a detailed study of the hydrolytic degradation of these thermogelling polymers.

Besides its biodegradability, thermogelling polymers are interesting from the viewpoint of sustained drug release. PEG-PPG-PEG triblock copolymers have been thoroughly studied for sustained drug delivery, wound covering and chemosensensitizing for cancer therapy.[19-21] A high concentration of the polymer is often incorporated into the thermogelling formulations (above 15 wt%). These formulations exhibit poor resilience as well as having the burst effect of the release of bioactive agents. These shortcomings have made this system unsuitable for many biomedical applications.[22,23] Moreover, PEG-PPG-PEG triblock copolymers are non-biodegradable and have been reported to induce hyperlipidemia in rabbits and rats, suggesting that its use in the human body may not be an attractive option. [24,25] In contrast, this series of thermogelling poly(ester urethane)s require an extremely low concentration of polymer in a formulation to form a gel from a thermogelling solution.

In this chapter, the hydrolytic degradation, drug release and cytocompatibility behaviors of poly(PEG/PPG/PHB urethane)s are presented. This study is relevant to the potential applications of the material as well as to assess the possibility of using this polymer as a biomaterial.

5.2. Experimental Section

5.2.1. Materials

The copolymers used in this study were the poly(PEG/PPG/PHB urethane)s, EPH1, EPH2 and EPH3, synthesized in Chapter 3.

5.2.2. Erosion Study of Poly(PEG/PPG/PHB urethane) Thermogels

The erosion mass loss of the polymer gels after degradation was evaluated with mass loss (%), which was defined by Eq. (5.1):

$$\text{Mass Loss (\%)} = [1-(W_t / W_0)] \times 100\% \quad (5.1)$$

where W_0 and W_t were the initial weight and the weight of the polymer dissolved in the polymer solution at time t, respectively. W_t was obtained after drying the samples at 50 °C under vacuum for 1 week.

5.2.3. Hydrolytic Degradation Study of Poly(PEG/PPG/PHB urethane) Thermogels

Aqueous solutions comprising 5 wt% copolymer were mixed and left to equilibrate overnight at 4 ^{o}C. Polymer solution (1 mL) was injected into a porous cellulose cassette (pore size: ~100μm), left to equilibrate at 37 ^{o}C to form a polymer slab (10 mm x 25 mm x 4 mm) and placed in 25 mL of phosphate buffer release solution (pH = 7.4). The pH 7.4 buffer solution contained 8.0 g of NaCl, 0.2 g of KCl, 1.44 g of Na_2HPO_4, and 0.24 g of $K_2H_2PO_4$ in 1 litre of solution. Fresh batches of release solutions were replaced at various time intervals. Experiments were done in triplicate. The resultant solutions were lyophilized and lyophilized samples were weighed and the weights were recorded as W_1. In order to determine the weight attributed to the salt content, 'blank' samples containing only 25 ml of phosphate buffer release solution were lyophilized and the residue was weighed to obtain the weight of the dry salt per 25 ml of buffer solution, W_o. The dry weight of the polymer eroded into the solution was obtained by the difference between W_1 and W_o. The pH 7.4 degradation process was studied over a period of 6

months and the samples were removed at predetermined time intervals. The water-soluble products in the buffer solution were extracted from the buffer using chloroform. For the fraction obtained in the organic phase, chloroform was removed by evaporation and dried in vacuo at 50 °C for 1 week. For the fraction obtained in the aqueous phase, the solution was removed by lyophilization and the salt residue was dried in vacuo at 50 °C for 1 week and kept for further analysis.

5.2.4. Characterization of Degraded Samples

Gel permeation chromatography (GPC). Molecular weight of determination of the samples were performed by GPC using a Shimadzu SCL-10A and LC-8A system equipped with two Phenogel 5μ 50 and 1000 Å columns (size: 300 × 4.6 mm) in series and a Shimadzu RID-10A refractive index detector. THF was used as eluent at a flow rate of 0.20 $mL.min^{-1}$ at 45 °C. Monodispersed poly(ethylene glycol) standards were used to obtain a calibration curve.

Nuclear magnetic resonance (NMR) measurements. ^1H NMR spectra were recorded on a Bruker AV-400 NMR spectrometer at 400 MHz at room temperature. Chemical shift was referred to the solvent peak ($\delta = 7.3$ for $CHCl_3$).

MALDI-TOF mass spectrometry. MALDI-TOF was performed on a Bruker (Karlsruhe, Germany) Autoflex MALDI Tandem TOF/TOF mass spectrometer. Dithranol or trans-2-[3—tert-butylphenyl)-2-methyl-2-propenylidene] malononitrile was used as the matrix and silver trifluoromethanesulfonate as the ion source.

Fourier transform infrared spectroscopy (FTIR). FTIR spectra of the polymer films were recorded on a Bio-Rad 165 FT-IR spectrophotometer; 64 scans were signal-averaged with a resolution of 2 cm^{-1} at room temperature.

Thermal analysis. Thermogravimetric analyses (TGA) were made using a TA Instruments SDT 2960. Samples were heated at 20 °C min^{-1} from room temperature to 800 °C in a dynamic nitrogen atmosphere (flow rate = 70 mL min^{-1}).

Field emission scanning electronic microscopy (SEM). SEM images were obtained at acceleration voltage of 5 kV on a JSM-6700F microscope (JEOL, Japan). The samples were sputter-coated with a thin layer of gold for 15 s to make the sample conductive before testing.

5.2.5. Protein Release Study of Poly(PEG/PPG/PHB urethane) Thermogels

Aqueous solutions comprising 5 wt% copolymer were mixed and left to equilibrate overnight at 4 ^{o}C. Appropriate amounts of BSA were loaded to make the concentration of BSA in the polymer solution 5 mg.mL^{-1}. For comparison, 30 wt% of $EG_{100}PG_{65}EG_{100}$ triblock copolymer in aqueous solutions was prepared. The concentration of BSA in these solutions was also 5 mg.mL^{-1}. Polymer solution (1 mL) was injected into a porous cellulose cassette (pore size: ~100μm), left to equilibrate at 37 ^{o}C and placed in 25 mL of phosphate buffer release solutions. Fresh batches of release solutions were replaced at various time intervals. Experiments were done in triplicate. The resultant solutions were lyophilized and lyophilized samples were kept at –80 ^{o}C for further analysis. The BSA content was determined using the Pierce BCA Protein Assay. Quantitation of BSA was based on a calibration curve, obtained using the BSA standards provided, in the range of 20 μg – 2000 μg.mL^{-1}.

5.2.6. Cell Culture

Cell Cultivation. L929 mouse fibroblasts were obtained from American Type Culture Collection (ATCC) and cultivated in Dulbecco's Minimum Essential Medium (DMEM) containing 10% fetal bovine serum (FBS) and 1% penicillin / streptomicin. Cells grow as a monolayer and were passaged upon confluence using trypsin (0.5% w/v in PBS). L929 cells were harvested from culture by incubating in trypsin solution for 15 min. The cells were

centrifuged and the supernatent was discarded. 3 mL of serum-supplemented DMEM was added to neutralize any residual trypsin. The cells were resuspended in serum-supplemented DMEM at a concentration of 2 x 10^4 cells / mL. Cells were cultivated at 37 ^oC and 5% CO_2.

Cell Growth on Gel Surface. The copolymers (5 wt%) and F127 copolymers (20 wt%) were dissolved in DMEM. At 5 wt%, all the copolymers formed thermogelling formulations. All copolymer solutions were sterilized by filtration with a 0.45 μm filter before tests. 0.5 mL of the polymer solution was transferred to each well in a 24-well cell culture plate and allowed to incubate at 37 ^oC for 1 hr. 0.5 mL of the suspended cell solution was added to each well (10^4 cells / well). The cell culture plate was allowed to incubate for 3 days. Cells were observed using an inverted microscope (Olympus) (magnification = 200X) at time intervals of 1, 2 and 3 days.

Cytotoxicity Study of Copolymer. The biocompatibility of the copolymers and F127 copolymers was evaluated by 3-(4, 5-dimethylthiazol-2-yl)-2,5-diphenyl tetrazolium bromide (MTT) assay in a 96-well cell culture plate. All copolymer solutions were sterilized by filtration with a 0.45 μm filter before tests. The copolymers and F127 copolymers were dissolved in DMEM (maximum concentration: 100 mg / mL). Cells were seeded at a density of 3 x 10^3 cells / well. Phenol was used as a cytotoxic control. Cells not exposed to any biomaterials were used as a positive control. The plates were incubated at 37 ^oC in a humidified 5% CO_2 atmosphere. After 3 days, 10 mL of MTT solution (5 mg / mL) were added to each well. After 4 h of incubation at 37 ^oC, the MTT solution was removed and the insoluble formazan crystals that formed were dissolved in 100 mL of dimethylsulfoxide (DMSO). The absorbance of the formazan product was measured at 570 nm using a spectrophotometer (TECAN SpectrofluorPlus).

Extraction of Leachable Products from Gel. 1 mL of polymer gels were placed in a cellulose bag and kept in 50 mL of buffer solution at 37 ^oC in a shaking water bath at 50 rpm. 2 mL of the gel extracts were collected at various time intervals of 1, 3, 7, 14 and 30 days. The

solutions were lyophilized and an equivalent amount of DMEM solution was added to re-dissolve the residue. All copolymer solutions were sterilized by filtration with a 0.45 μm filter before tests.

Cytotoxicity of Leachable Products from Gel. The biocompatibility of leachable gel products of the copolymers and F127 copolymers were evaluated by MTT assay. Cells were seeded at a density of 3 x 10^3 cells / well. 100 mL of the extract solution in DMEM was added to each well. Phenol was used as a cytotoxic control. Cells not exposed to any biomaterials were used as a positive control. The plates were incubated at 37 ^oC in a humidified 5% CO_2 atmosphere. After 3 days, 10 mL of 3-(4, 5-dimethylthiazol-2-yl)-2,5-diphenyl tetrazolium bromide (MTT) solution were added to each well. After 4 h of incubation at 37 ^oC, the solutions in the wells were removed and the insoluble formazan crystals that formed were dissolved in 100 mL of dimethylsulfoxide (DMSO). The absorbance of the formazan product was measured at 570 nm using a spectrophotometer (TECAN SpectrofluorPlus).

5.3. Results and Discussion

5.3.1. Experimental Setup

The hydrogel samples were enclosed in a porous cellulose cassette and immersed in a large excess of phosphate buffer solution to minimize any pH variations during the experiments. The buffer solutions were replaced with fresh ones at regular time intervals in an attempt to simulate the dynamic flow of fluids in the body. The hydrolytic degradation experiments were carried out at pH 7.4 and 37 °C to simulate physiological conditions. The water bath was set in motion at 50 rpm to account for bodily movements upon injection of the gel depot. At various time points, the gel residues and buffer solutions were collected and lyophilized. The contents in the buffer solutions were divided into two parts: the part that could be extracted by chloroform (mainly copolymer with long chains) and the part that remained in the aqueous buffer solution

phase (mainly salts and low-molecular weight final degradation products). A similar setup was used for the protein release study with protein-loaded hydrogels.

5.3.2. Erosion of the Gels and Chain Scission of the Copolymer

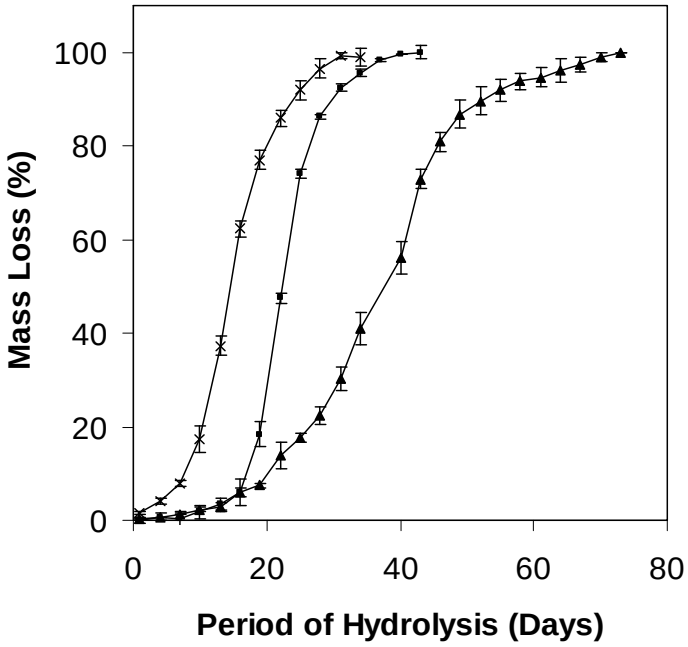

Figure 5.1. Mass loss (%) of the poly(PEG/PPG/PHB urethane) gels (5 wt%) after incubation at 37 ^{o}C (▲: EPH1, ■: EPH2, x: EPH3).

The hydrolytic degradation process was accompanied by the mass loss of the hydrogels, as shown in Figure 5.1. For all the gels, an incubation period (period during which there was little mass loss) was observed. The incubation period of the gels increased with decreasing PHB content. The length of the incubation time is as follows: EPH1 > EPH2 > EPH3. The incubation period was followed by a period of steady mass loss. At the end of the erosion process, the rate of mass loss was observed to have decreased and a plateau feature was observed at the terminating end of the erosion profile. Polymer gel erosion can be controlled by the composition of the polymer. With decreasing PHB content, the time required to completely erode the gel increased. EPH3 erodes completely after 30 days, EPH2 after 40 days and EPH1 after 70 days.

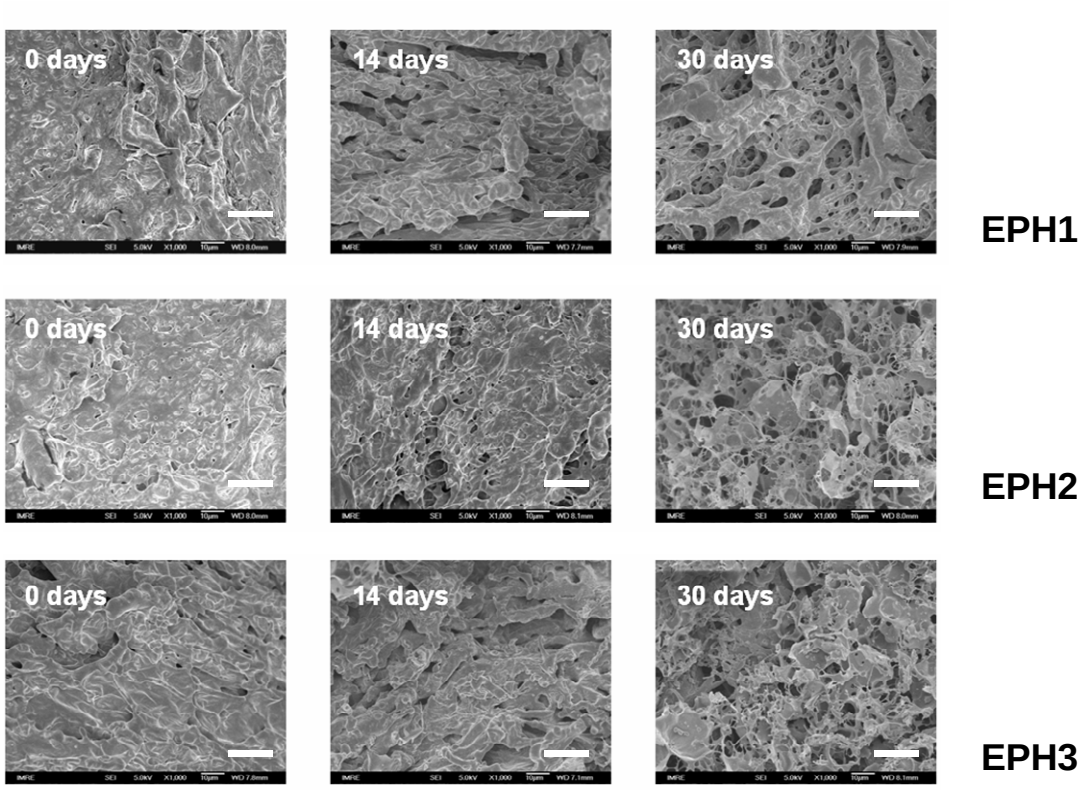

Figure 5.2. SEM micrographs of gel residue after various periods of degradation at pH 7.4. Scale bars corresponds to 20 μm.

Visual examinations of the remaining hydrogel samples were carried out using SEM in order to observe changes in the surface structure of the gel. The micrographs are shown in Figure 5.2 for EPH1, EPH2 and EPH3 at time intervals of 0 days, 14 days and 30 days. The surface of the gel residue before erosion was devoid of pores and packing of the lyophilized gel appeared to be compact. After 14 days of erosion, structural deterioration of the gel was observed and pores (ca. 5-10 μm) developed on the surface of the films. After 30 days of erosion, the pores became more numerous and an enlargement of the pores was observed.

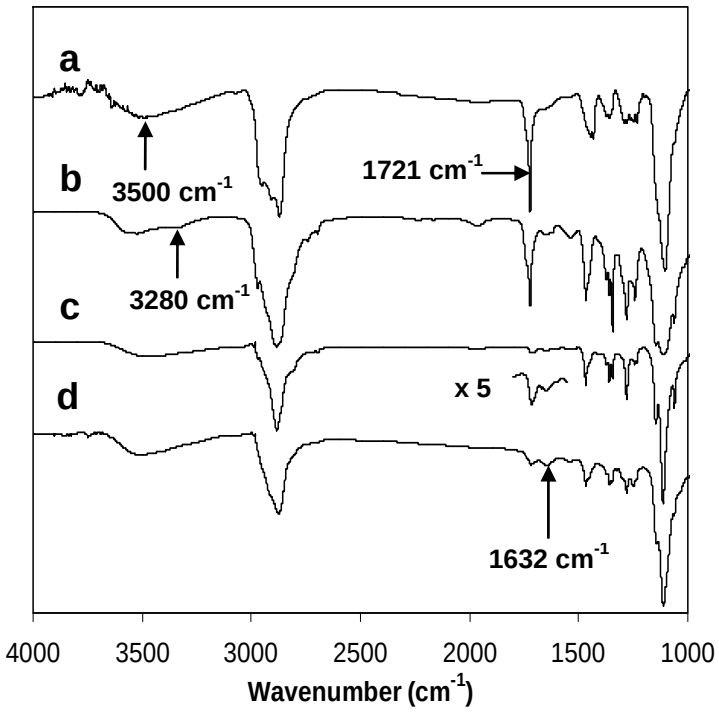

Figure 5.3. FTIR spectra of the EPH2 samples after different periods of degradation at pH 7.4. a) Original EPH2 sample, b) Gel residue after 1 month of degradation, c) Water-soluble fraction after 1 month of degradation, d) Water-soluble fraction after 6 months of degradation.

FTIR was used to probe the molecular changes occurring in the polymer segments after various periods of degradation (Figure 5.3). In the original un-degraded sample, the PHB ester peak corresponding to 1721 cm^{-1} can be observed, along with a small peak at 1660 cm^{-1} which corresponds to the –C=O stretch of the urethane peak.[26,27] The gel residue obtained after one month of hydrolysis showed a broadening as well as a shift of the peak to 1632 cm^{-1} (attributed to the –C=O carboxylic stretching) and a concomitant decrease in the height of the 1721 cm^{-1} ester peak was observed.[27] The water-soluble fraction of the hydrolysis products after 1 month show that the ratio of the peak height at 1721 cm^{-1} to the peak height at 1632 cm^{-1} greatly decreased. This confirms that the ester bonds were hydrolysed to the carboxylic acid groups. After 6 months of hydrolysis, the ratio of the peak height at 1721 cm^{-1} to the peak height at 1632 cm^{-1} decreased even further implying further scission of the PHB segments in the water-soluble

fraction after 6 months of hydrolysis. When the PHB segment hydrolyses to form 3-hydroxybutyric acid, the number of hydroxyl and carboxylic acid groups increases. In figures 5.3b, 5.3c and 5.3d, two peaks are observed in the –OH stretching region. The 3500 cm^{-1} peak corresponds to the –OH stretch of the hydroxyl moiety while the peak observed at between 3250 and 3300 cm^{-1} corresponds to the –OH stretch of the carboxylic acid moiety. It can be observed that the peak corresponding to the –OH stretch of the carboxylic acid moiety is absent in the FTIR spectrum of the original un-degraded polymer sample.

5.3.3. Characterization the Fraction Obtained From Organic Phase

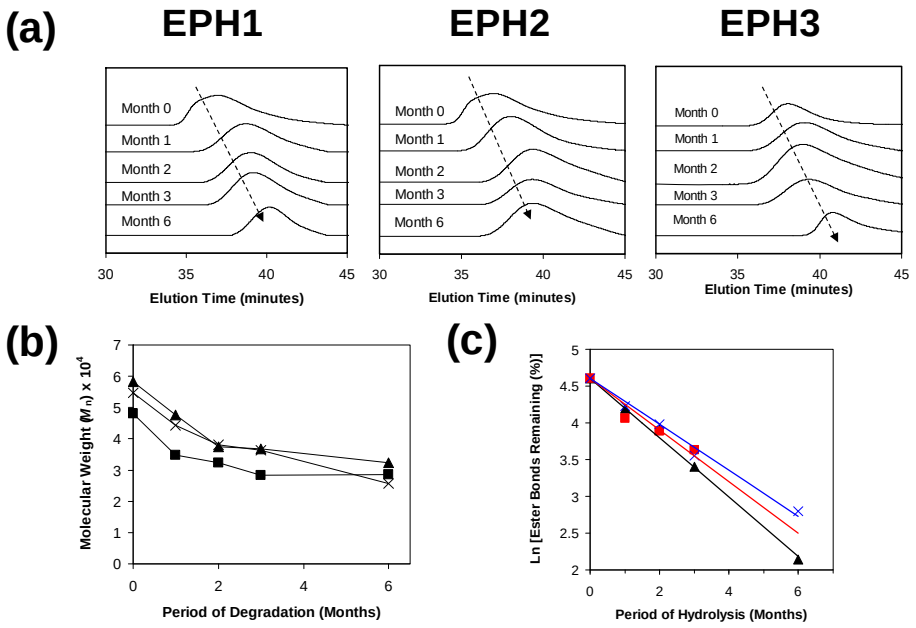

Figure 5.4. (a) GPC profile of the water-soluble fraction of the polymers at various time intervals at pH 7.4.; (b) Changes in molecular weight of the polymers after 6 months of degradation at pH 7.4 (▲: EPH1, ■: EPH2, x: EPH3); (c) Plot of the natural logarithm of the fractional ester bonds remaining versus degradation time of the polymers after various periods of degradation at pH 7.4 (▲: EPH1, ■: EPH2, x: EPH3).

At various time points during the hydrolytic degradation experiments, the buffer solutions containing degradation products were extracted by chloroform. It can be hypothesized that the chloroform extracts mainly contained the copolymer degradation products which still have large molecular weight. The very short fragments such as 3-hydroxybutyric acid or its

oligomers tend to remain in the buffer solution. The molecular weight of the copolymers in the chloroform extracts were measured by GPC. The GPC profiles of the copolymers were unimodal, as shown in Figure 5.4a. The molecular weight of the copolymer samples decreased quite sharply until the first two months of hydrolysis, as shown in Figure 5.4b. Throughout the period of 6 months of hydrolytic degradation, the molecular weight of the polymer chains continuously decreased, reducing to a final value of just slightly more than half their original molecular weight. The results are consistent with those of the FTIR spectra presented in the previous section which show that hydrolytic degradation was continuous from 1 to 6 months. In addition to the molecular weight information, the PHB content of the copolymer degradation products were determined by ^{1}H NMR and TGA, and the results are listed in Table 5.1. The PHB content of the polymer chains decreased as the hydrolysis proceeded, indicating that a significant amount of water-soluble products containing PHB leached into the buffer solution during hydrolysis. The mode of chain scission was determined by the method of Shih.[28,29] The number of ester bonds in the polymer chains were calculated based on Eq. (5.2),

$$\text{Number of ester bonds} = \frac{\text{Weight fraction of PHB segments x } M_n \text{ (polymer chain)}}{\text{Molar mass of 1 repeating HB unit}} \qquad (5.2)$$

The fractional ester bonds (%) were calculated based on Eq. (5.3),

$$Es = \frac{\text{Number of ester bonds at time t}}{\text{Initial number of ester bonds}} \text{ x } 100\% \qquad (5.3)$$

Where Es refers to the fractional ester bonds (%) remaining at time t. The rate of decrease of the ester bonds will follow a pseudo-first order kinetics[28,29] as described by Eq. (5.4),

$$-d[Es] / dt = k\, Es \qquad (5.4)$$

Where k is the pseudo-first order rate constant.

The extent of cleavage of ester bonds was found dependant on the total number of ester bonds in the polymer chain and the rate of decrease of the ester bonds followed pseudo-first

order kinetics, giving linear natural logarithm plots (Figure 5.4c). Chain scission of the ester bonds occurred at a faster rate with decreasing PHB content. The values of the rate constant k obtained were as follows: EPH1 (-0.40 $month^{-1}$), EPH2 (-0.35 $month^{-1}$) and EPH1 (-0.31 $month^{-1}$). In a study of the hydrolysis process of D,L-lactic acid oligomers, Schliecker *et al.* reported that the rate of decrease of the number of ester bonds follows Eq. (5.4). He proposed a random chain scission of the D,L-lactic acid oligomers.[30] Similarly, degradation of the polymer chains in this study can be expected to occur via the random hydrolytic ester cleavage along the PHB segments, which accounted for the decrease in the molecular weight of the polymers in the degradation process at pH 7.4. The decreasing k values show that with increasing hydrophobicity of the polymers (due to the increasing PHB content), the rate of degradation of the polymers decrease. The rate of degradation of this series of thermogelling poly(ester urethane)s can be tuned by an adjustment of the composition of the polymers.

5.3.4. Characterization the Fraction Obtained From Aqueous Phase

After chloroform extraction, short fragments of the degradation products such as 3-hydroxybutyric acid or its oligomers and some PEG-PPG fragments may still remain in the buffer solution together with the salts. This part of the degradation products was characterized using NMR and MALDI-TOF spectroscopy. The ^{1}H NMR spectrum of the degradation products of EPH2, obtained after 6 months of hydrolysis, is shown in Figure 5.5. The products were identified to be 3-hydroxybutyric acid, PEG and PPG segment blocks. The PEG and PPG peaks did not display any shifts in the peak position and indicates that the chain scission did not occur at the polyether segments. The MALDI-TOF spectrum of the degradation products is shown in Figure 5.6. The m/z values of the peaks correspond to the monomers up to pentamers of 3-hydroxybutyric acid. In general, for each fragment, 3 different peaks can be identified,

corresponding to the molecules with no sodium ions, 1 sodium ion, and 2 sodium ions, respectively.

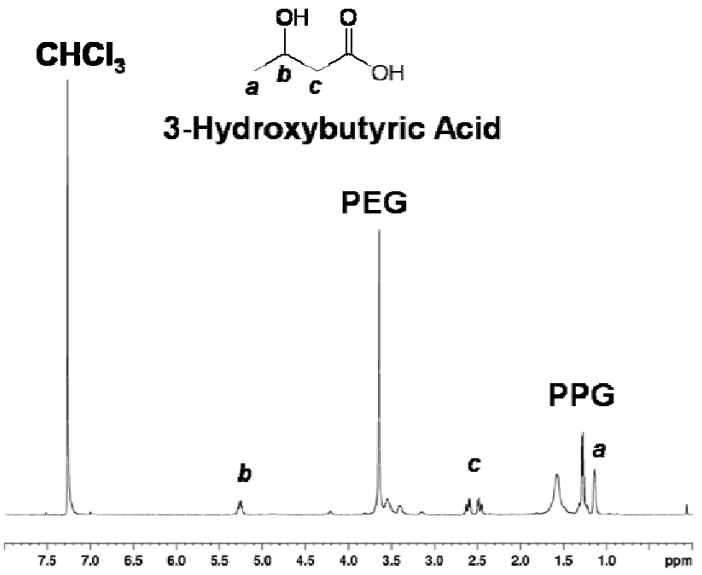

Figure 5.5. ^{1}H NMR spectrum of degradation products of EPH2 after 6 months of hydrolysis.

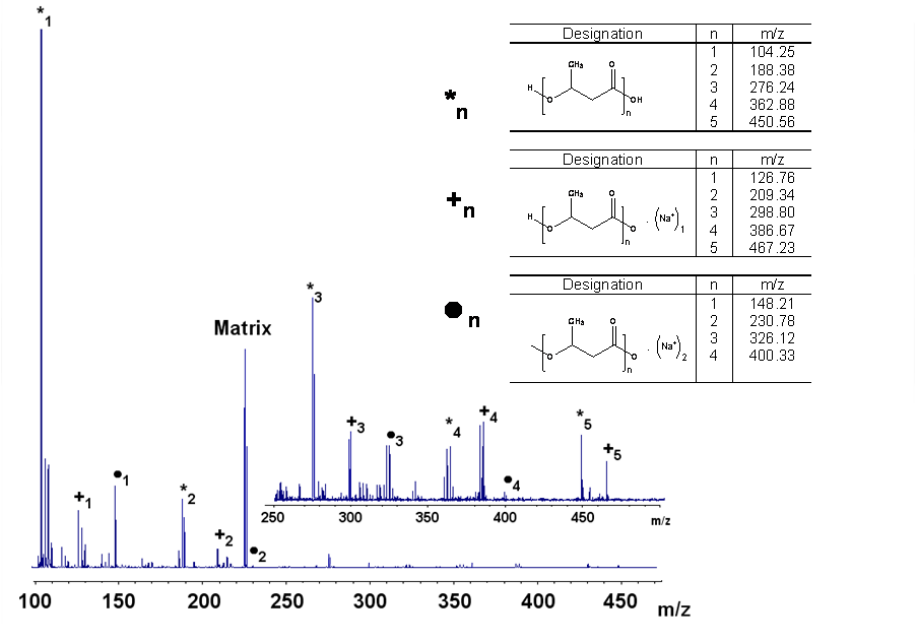

Figure 5.6. Characteristic matrix-assisted laser desorption ionization spectra of the water-soluble fraction EPH2 samples after 6 months of degradation at pH 7.4.

Table 5.1. Molecular weight and composition of the poly(PEG/PPG/PHB urethane) gels before and after degradation at pH 7.4

Sample	EPH1[a]				EPH2[a]				EPH3[a]			
Months	M_n[b]	PDI[c]	PHB (wt%)		M_n[b]	PDI[c]	PHB (wt%)		M_n[b]	PDI[c]	PHB (wt%)	
			NMR[d]	TGA[e]			NMR[d]	TGA[e]			NMR[d]	TGA[e]
0	58200	1.36	2.12	2.49	48100	1.27	5.11	5.71	54700	1.13	8.07	7.24
1	47600	1.15	2.11	2.01	34700	1.27	5.88	4.59	44300	1.12	8.02	6.11
2	37500	1.28	1.94	1.92	32400	1.30	5.38	4.11	38000	1.26	6.50	5.59
3	36700	1.23	0.95	1.19	28400	1.28	3.67	3.63	36300	1.31	3.40	3.81
6	32400	1.14	0.42	0.38	28500	1.31	3.14	2.58	25700	1.36	2.99	2.53

[a] Poly(PEG/PPG/PHB urethane)s are denoted EPH, E for P**E**G, P for P**P**G and H for P**H**B. The M_n of PEG and PPG used for the copolymer synthesis was 1890 and 2180 g mol^{-1}, respectively.

[b]As determined from GPC.

[c]PDI: Poly dispersity index.

[d]Calculated from ^{1}H NMR results.

[e]Calculated from TGA results.

5.3.5. Hydrolytic Degradation of Poly(PEG/PPG/PHB urethane)s

Thermogelling copolymers have high water content and behave differently from conventional crosslinked hydrogels. Chemically crosslinked hydrogels require degradation of the crosslinks before polymer erosion can be observed. Thermogelling copolymers behave differently. Due to its physical crosslinks, these polymer gels could either undergo gel erosion with or without degradation of the polymer chains. The initial stage of the hydrolytic degradation of the gel is characterized by an erosion of the gel material into the buffer solution. The erosion process can be broken down into 3 sub-stages. The first sub-stage is the incubation period. Anseth *et al.* calculated that the length of incubation time increases with an increase in the extent of crosslinking in a hydrogel.[14] In this system, a lower PHB content increases the efficiency of the gel packing and increases the effective physical crosslinks in the gel, thereby prolonging the incubation period. Similar observations have been made in a study of chemically crosslinked hydrogels based on poly(vinyl alcohol) macromers.[15] This has been attributed to a "high degree of inter-connectivity" present in the chemically crosslinked hydrogels. In this case, the enhanced interactions between the hydrophobic segments hold the polymer chains together in the polymer gel for a certain period of time. The tight compact packing can be seen in the SEM micrographs of the polymer gels before the hydrolysis. Upon equilibration with the buffer system, the gel surface slowly dissolved. The onset of the dissolution depends on the composition of the copolymer. With increasing PHB content, the dissolution process of the polymer gel begins earlier. This phenomenon can be understood by relating the gelation process to a micelle packing process. Previously in Chapter 3, it was postulated that the polymer micelles of this work are of an associated micelle nature. At higher temperatures, an aggregation of the micelles results in the formation of a gel state. An increase in the PHB content in the polymer gels could lead to a disruption on the micelle packing which would further disturb the packing of the gel. Adept use

of this knowledge allows control of the onset of dissolution by the variation of the PHB content in the copolymer. Sub-stage 2 is characterized by a period of constant mass loss. This happens when the physical crosslinks have been broken, allowing a constant dissolution of the polymer gel. From the GPC profiles, a rapid decrease in the molecular weight of the polymer was observed in the first month of degradation. This leads to the formation of polymer chains which are much more soluble in the buffer solution than the original polymer sample, consequently, the erosion of the gel takes place at a faster rate. Sub-stage 3 shows that there is little mass loss towards the end of the erosion process. This feature of the erosion profile was not predicted by the theoretical studies of the erosion of hydrogels.[14-16] This strongly suggests that the erosion of the polymer gel is dependent on the volume of the gel depot. When the volume of the gel is small, there appears to be a lower driving force for erosion to occur. From the combined GPC and FTIR results, it appears that erosion of the polymer gel occurs in parallel with the chain scission of the polymer chains. The molecular weight of the polymer chains decreased greatly in the initial stages of the hydrolytic degradation process via a random chain scission occurring at the ester linkages of the PHB segments.

5.3.6. Protein Release of Poly(PEG/PPG/PHB urethane)s

The in-vitro release kinetics of the model protein BSA released from the copolymer hydrogels was studied and compared with EG_{100}-PG_{65}-EG_{100} triblock copolymer hydrogel (Figure 5.7). The EG_{100}-PG_{65}-EG_{100} triblock copolymer hydrogel released its entire content of BSA within 4 hours but the gels formed by the new thermogelling copolymers were able to achieve a sustained release of up to 80 days.

The release profile of all the polymers can be fitted to the following equation (Eq. 5.5) for protein release from a gel slab in the range of $M_t/M_\infty \leq 0.6$:[31,32]

$$M_t/M_\infty = k.t^n \qquad (5.5)$$

where M_t and M_∞ are the mass of protein released at time t and infinite time, respectively; k, a characteristic exponent of the mode of transport of the protein. The values of n and k were calculated from the slopes and intercepts, respectively, of the plot of log (M_t/M_∞) versus log(t) and tabluated in table 5.2. For Fickian diffusional release, in which the rate of diffusion of the protein is rate limiting, n = 0.5, while values of n between 0.5 to 1 indicate the anomalous (non-Fickian) transport.[31]

The collective diffusional coefficients of the gels, D_0, were determined from the gradient of the plot of the initial release rate versus the square root of time, using the following equation (Eq. 5.6), within the same range of $M_t/M_\infty \leq 0.6$:

$$M_t/M_\infty = 4/l \times (D_0 \times t/\pi)^{1/2} \qquad (5.6)$$

where l = 0.4 cm, the thickness of the gel. The protein release profile can be divided into 2 stages, the diffusion-controlled stage and the combined erosion/diffusion-controlled stage. The initial release profile is defined by the Fickian diffusion for the first 60% of the release process, followed by a linear release of the protein with respect to time. Sustained release profiles of the gels with the same polymer concentration were compared. The polymer with the highest PHB content (EPH3) formed a gel with the fastest sustained release characteristics. The period of sustained release (15 to 40 days) can be controlled by adjustment of the concentration of the polymer EPH2 in the thermogelling solution from 3 to 5 wt%. When an extended sustained release is desired, the thermogelling solution can be made more concentrated, leading to greater packing in the gel structure.

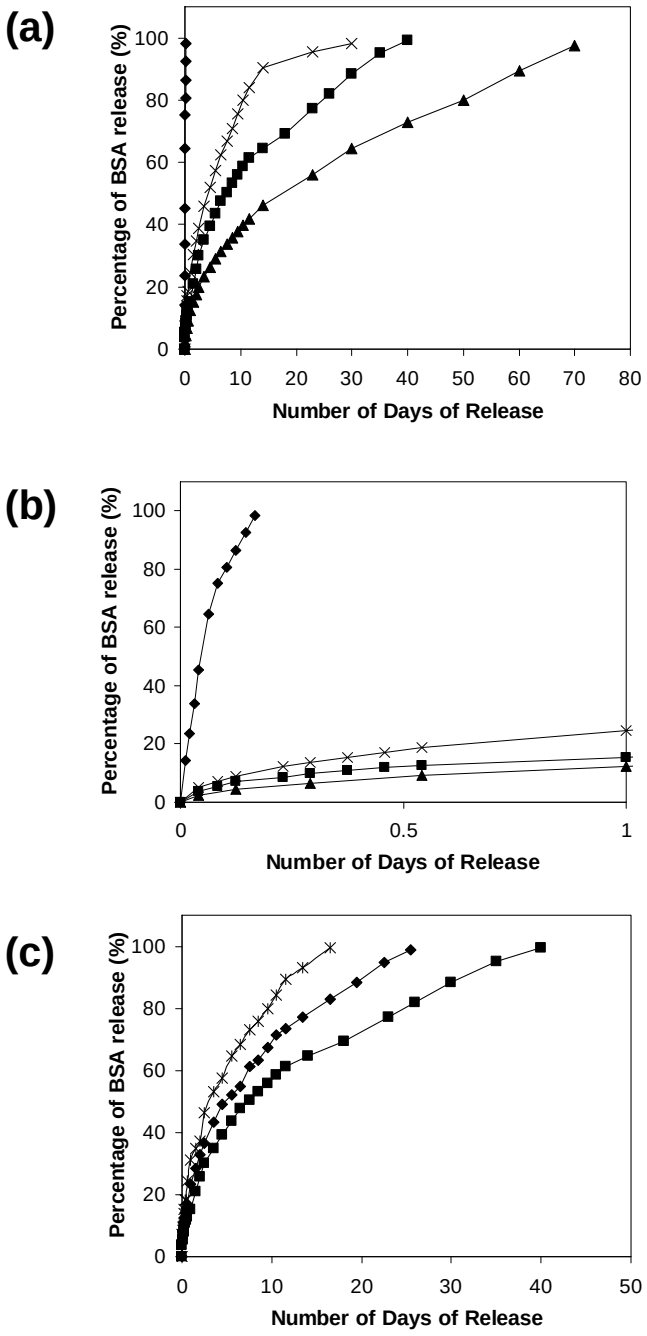

Figure 5.7. (a) Protein release profile of poly(ester urethane)s of different composition [▲: EPH1, ■: EPH2, x: EPH3, ♦: EG_{100}-PG_{65}-EG_{100} triblock copolymer (30 wt%)]; (b) Expanded protein release profile of up to 1 day of poly(ester urethane)s of different composition [▲: EPH1, ■: EPH2, x: EPH3, ♦: EG_{100}-PG_{65}-EG_{100} triblock copolymer (30 wt%)]; (c) Protein release profile of EPH2 of different concentrations in a thermogelling formulation (x: 3 wt% ♦: 4 wt% ■: 5 wt%). (Samples were measured in triplicate and the standard deviation for all the data points were ± 5%)

Table 5.2. Release characteristics of BSA from the different formulations

Formulation[a]	n	k / day $^{-1/2}$	D_o x 10^7 / cm.s^{-1}
EPH1 (5%)	0.491	0.122	0.054
EPH2 (5%)	0.500	0.183	0.121
EPH3 (5%)	0.502	0.246	0.220
EPH2 (3%)	0.475	0.283	0.291
EPH2 (4%)	0.493	0.227	0.187
EPH2 (5%)	0.500	0.183	0.121

[a]Formulations are denoted as EPH*x* (*y*%), *x* refers to the sample code as used in Chapter 3 and *y* refers to the percentage of copolymer incorporated into the gel.

For all protein release kinetics calculations, data set in the range of $M_t/M_\infty \leq 0.6$ was used.

Value of n was calculated by the following equation: $\log (M_t/M_\infty) = n \log t + \log k$

Value of *k* was calculated by the following equation: $M_t/M_\infty = k.t^{1/2}$

Value of D_o was calculated by the following equation: $M_t/M_\infty = 4/l \times (D_o \times t/\pi)^{1/2}$

This demonstration is consistant with other reported drug release studies.[33-34] This study also shows that the entire protein content loaded in the gel can be released during the course of the drug release study. This is a distinct advantage from other gel systems which are unable to achieve complete release of the loaded drug.[34-36]

5.3.7. Correlation Between Polymer Gel Erosion and Protein Release

The polymer gel erosion profile can be corelated with the protein release profile. Erosion sub-stage 1 (period of no mass loss) coincides with the diffusional controlled release of the protein. At the initial stages of the release experiment, the gel exists as a tightly packed structure. Protein appears to be only released via the diffusion through water-rich regions of the gel structure. Diffusivity of a solute through physically crosslinked hydrogels decreases with an increase in the crosslinking density and with a decrease of the volume fraction of solvent within the hydrogel.[37] Increasing the concentration of the poly(ester urethane)s in the thermogelling

formulation reduced the proportion of the solvent-rich regions, leading to a decrease in the diffusional coefficient of BSA as observed. The effect of the composition of the poly(ester urethane)s was studied in relation to the sustained protein release. It can be observed that the diffusivity of the protein increased with increased PHB content. Cohn *et al.* reported that for a multiblock PEG, PPG and PCL copolymer, the inclusion of PCL induces possible spatial hindrances in the gel structure.[38] The presence of PHB segments could have reduced the packing efficiency of the polymer chains and reduced the amount of effective physical crosslinking in the gel structure. As such, gels made from the poly(ester urethane)s with the highest PHB content gave the shortest release period in these experiments. The diffusion coefficients reported in this study can be compared with the calculated diffusion coefficient of BSA of 9.35×10^{-7} cm^2/s in an infinite solution at 37 ^oC.[37] It can be seen that the all the gels of different compositions and different concentrations reduced the diffusion coefficient markedly. The values show that the presence of the polymer chains in the gel structure could have caused an obstruction effect to the free diffusion of the BSA protein molecule.

After some time, erosion of the polymer gel structure follows. During the linear polymer erosion phase (sub-stage 2), a linear release of the protein with respect to time was observed (compare Figures 5.1 and 5.7a). The release of the protein is dominated by the erosion of the polymer gel leading to a linear profile in the release of the protein. The rate of release of the protein is affected by the concentration of the poly(ester urethane)s in the formulation and the PHB composition of the poly(ester urethane)s. This example further illustrates that the packing of the gel structure is an important factor in the determination of the release rate of the protein. Hennink *et al.* performed Monte Carlo simulations which showed that higher crosslink density in a gel led to a slower rate of release.[39] These experimental results showed that better packing tends to result in greater resistance against erosion and manifests itself as a longer lasting

sustained release profile. The rates of release of the protein decrease as follows: EPH3 > EPH2 > EPH1. For the formulations with different concentrations, the rates of release of the protein decrease as follows, 3 wt% > 4 wt% > 5 wt%.

5.3.8. *In vitro* Cytotoxicity Study

The cytotoxicity of the polymers was tested at various concentrations ranging from 3.125 mg/mL to 100 mg/mL using the mouse fibroblast L929 cells. Quantification of the cytotoxic response was done using the MTT assay (Figure 5.8). In general, the polymers do not show significant toxicity. It is important to note that at concentrations above 12.5 mg/mL, the solution becomes viscous or even in a gel state. It means that even when the cells are in the interior of the gel, they remain viable. These results show that potentially, these cells can be encapsulated for 3D-cell growth.

The cytotoxicity of the leachable products from the copolymer gel was evaluated by incubating the gel in the cell culture medium over a period of 30 days at 37 ^{o}C. The aim of this experiment is to simulate the actual usage conditions when the gel is injected. Quantification of the cytotoxic response was done using the MTT assay (Figure 5.9). Aqueous extracts of the copolymer gel do not show significant cytotoxicity against L929 cells, regardless of the incubation length. The use of dibutyltin dilaurate as a catalyst raises a safety concern, particularly when it is a known cytotoxic chemical. In the cytotoxicity test of this chemical, it was observed that below a concentration of 1ppm, this chemical does not elicit a cytotoxic response against the L929 mouse fibroblast cells. In this work, the tin content in the copolymer was found to be below 1 ppm by UV absorption studies of the copolymer dissolved in chloroform as well as NMR. From the MTT assay results of the leachable extracts of the copolymer gels and the determined tin content in the copolymer, the gels are expected to be safe for biomedical applications.

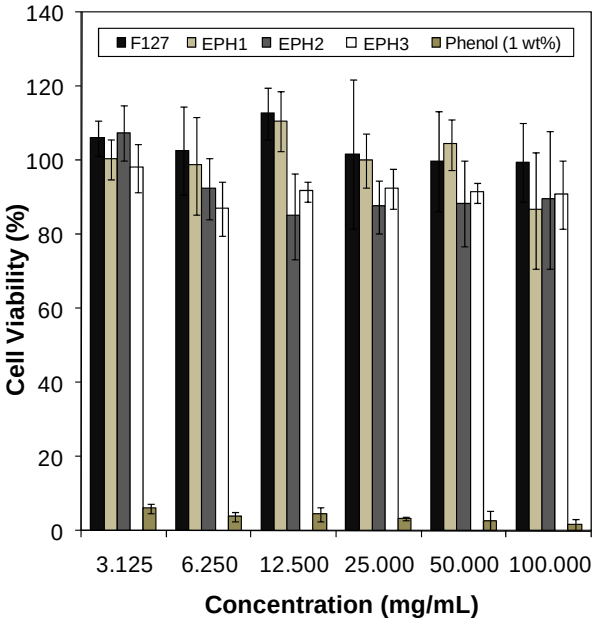

Figure 5.8. Cell viability plot of various concentrations of poly(PEG/PPG/PHB urethane)s incubated with mouse fibroblast L929 cells for 3 days.

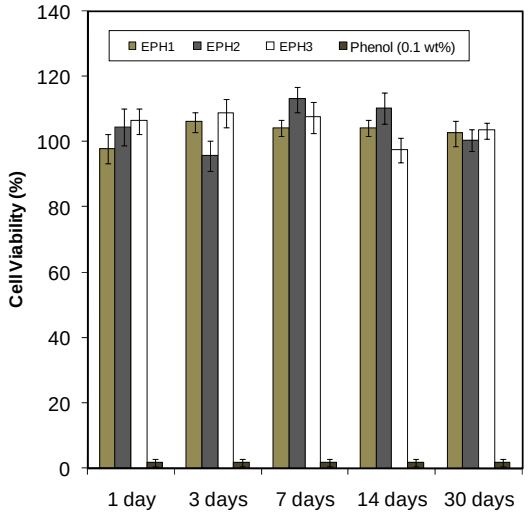

Figure 5.9. Cell viability plot of the leachable products of poly(PEG/PPG/PHB urethane) gels obtained after different days.

5.3.9. Cell Growth on Gel Surface.

The cell growth on the gel surfaces was tested. On the Pluronics F127 (20 wt%) gel surface, the cells did not attach well to the surface. The almost smooth morphology observed in

the micrograph was due to the difficulty in capturing the image of the floating cells (Figure 5.10a). This is similar to the observation made previously.[40] That study showed faint images of the cells. At a concentration of 15 wt%, the solution was viscous but not in a gel state (Figure 5.10b). In this state, some of the cells were observed to be attached and some were observed to be rounded. At even lower concentrations, the extent of attachment of the cells increased (Figure 5.10c-g). The number of attached cells was observed to be higher as the concentration of Pluronics F127 became lower. These results indicate the excellent biocompatibility of Pluronics F127. Fibroblast cell growth on the surface of the poly(PEG/PPG/PHB urethane) gels appear to be more promising (Figure 5.11). After 24 hours of incubation, the typical spindle-like fibroblast morphology was observed (Figure 5.11a-c). The cells were incubated for up to 72 hours. For the copolymer gels, the cell numbers were found to increase up to 72 hours (Figure 5.11g-i). Moreover, the cells maintained a healthy morphology. However, for the Pluronics F127 gel, the cell growth was suppressed at longer time periods. It has been previously reported that the cell growth on hydrophilic surfaces is not favourable and such a surface would inhibit the growth of cells.[41] On the other hand, PHB has been reported to be compatible to cells such as osteoblastic, epithelial cell and ovine chondrocytes. [42-43] Recently, it was shown that excellent fibroblastic proliferation occurs in the presence of PNIPAAm-PHB-PNIPAAm block copolymers in solution.[44] In addition, these triblock copolymers were compatible with human mesenchymal stem cells and mouse embryonic stem cells.[45-46] Therefore, the incorporation of the PHB segment to the PEG and PPG segments, greatly enhances the cell adhesion capability of the copolymer gel.

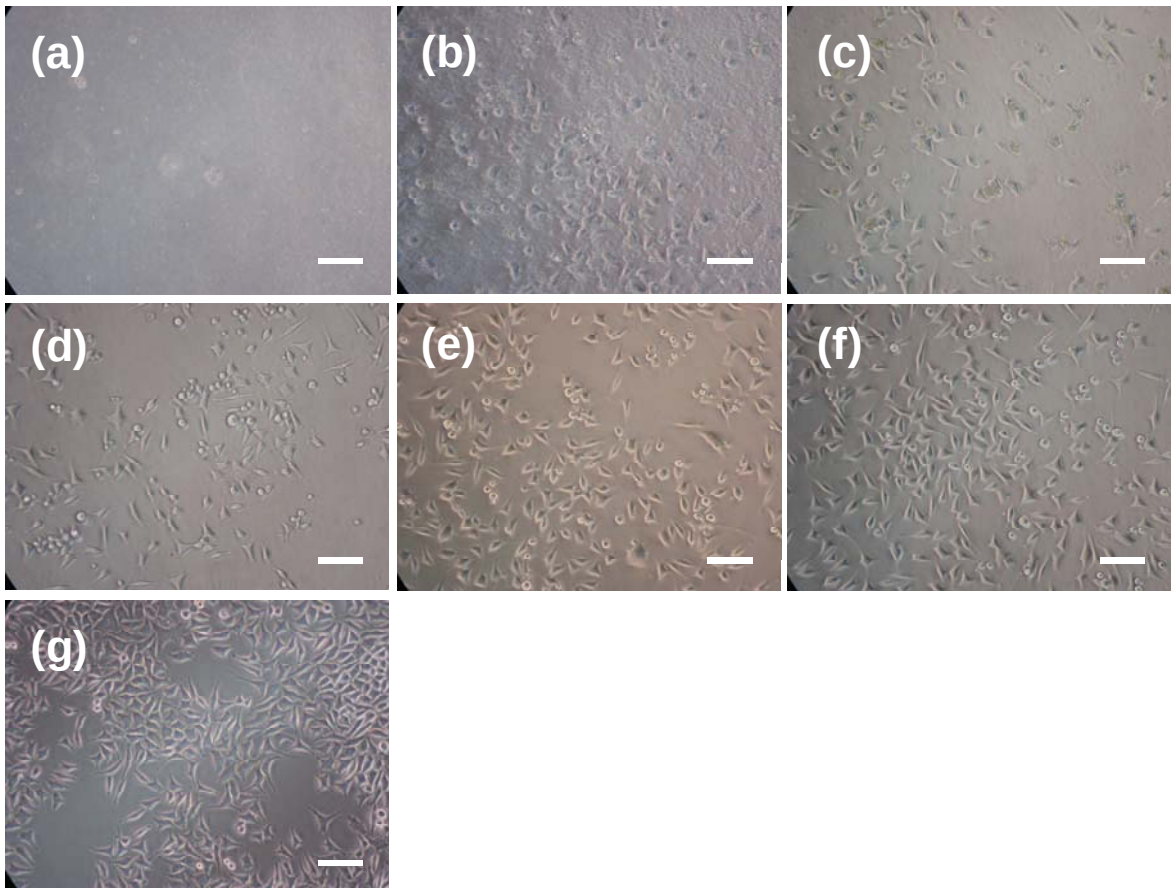

Figure 5.10. Phase contrast micrographs of L929 cells cultured on Pluronics F127 at different concentrations (a) 20 wt% (gel state), (b) 15 wt%, (c) 10 wt%, (d) 5 wt%, (e) 2.5 wt%, (f) 1.25 wt%, (g) polystyrene tissue culture dish. Scale bar corresponds to 100 μm

The incorporation of PHB into the copolymers could have increased the hydrophobicity of the copolymer gel surface compared with Pluronics F127 gel. Both Pluronics F127 and the poly(PEG/PPG/PHB urethane) copolymers are non-toxic to cells. However, this is not sufficient for good cell adhesion. This study shows that the surface properties of the gels are crucial requirements for the favorable adhesion of cells onto the gels. This is an important finding which has possible implications in the design of materials for tissue engineering and the engineering of biomaterials for *in vivo* applications.

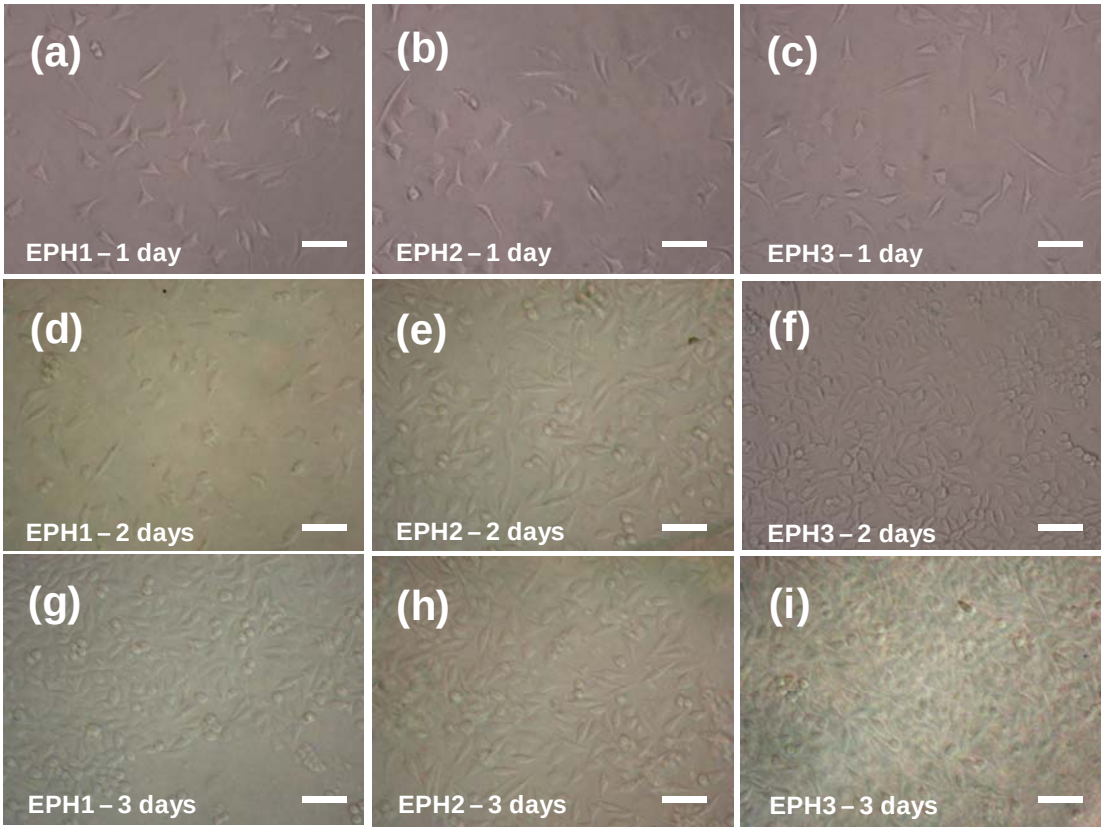

Figure 5.11. Phase contrast micrographs of L929 cells cultured on poly(PEG/PPG/PHB urethane) gel surface at different periods of incubation. Scale bar corresponds to 100 μm

5.4. Conclusions

The hydrolytic degradation and protein release characteristics of a series of new thermogelling poly(ether ester urethane)s consisting of PEG, PPG, and PHB were investigated. The correlation between the protein release of the hydrogels and the hydrolytic degradation was studied for the first time for such a thermogelling copolymer system. The hydrolytic degradation process is characterized by an initial incubation period followed by the erosion of the polymer gel and the random scission via the ester bonds of the PHB segments of the polymer chains in buffer solution. The rate of chain scission can be controlled by an adjustment of the composition of the copolymer. In the protein release studies, the gels released the entire loaded content of the model protein. The initial stage of the drug release was diffusion controlled, the later stage was

erosion controlled. Tunable rate of release of the protein by the formulation was demonstrated. Cytotoxicity studies performed on the copolymer or the extracts of the copolymer gel indicate good cell compatibility. Excellent cell attachment was observed on the surface of the gel. The results are significantly better than on the commercially available PEG-PPG-PEG triblock copolymer. These studies indicate a potential for the copolymer gel to be used for tissue engineering applications or for 3D cell culture.

5.5. References

1. Huang, K.; Lee, B. P.; Ingram, D. R.; Messersmith, P. B. *Biomacromolecules* **2002**, *3*, 397-406.
2. Daga, A.; Muraglia, A.; Quarto, R.; Cancedda, R.; Corte, G. *Gene Ther.* **2002**, *9*, 915-921.
3. Packhaeuser, C. B.; Schnieders, J.; Oster, C. G.; Kissel, T. *Eur. J. Pharm. Biopharm.* **2004**, *58*, 445-455.
4. Heller, J.; Barr, J.; Ng, S. Y.; Shen, H. R.; Abdellaoui, S.; Gurny, R.; Castioni, N. V.; Loup, P. J.; Baehni, P.; Mombelli, A. *Biomaterials* **1999**, *23*, 4397-4404.
5. Hill-West, J. L.; Chowdhury, S. M.; Slepian, M. J.; Hubbell, J. A. *Proc. Natl. Acad. Sci. U.S.A.* **1994**, *91*, 5967-5971.
6. Yokoyama, M. *Crit. Rev. Ther. Drug Carrier Syst.* **1992**, *9*, 213-248.
7. Doi, Y. *Microbial polyester.* New York: VCH, 1990
8. Reusch, R. N. *Can. J. Microbiol.* **1995**, 41, 50-54.
9. Lee, S. H.; Kim, S. H.; Kim, Y. H.; Han, Y. K. *Macromolecular Research* **2002,** 10, (2), 85-90.
10. Xiong, X. Y.; Tam, K. C.; Gan, L. H. *Macromolecules* **2003,** 36, (26), 9979-9985.

11. Lelah, M. D.; Cooper, S. L. *Polyurethanes in Medicine.* Boca Raton, Florida: CRC Press, 1986

12. Schoonover, J. R.; Thompson, D. G.; Osborn, J. C.; Orler, E. B.; Wrobleski, D. A.; Marsh, A. L.; Wang, H. C.; Palmer, R. A. *Polymer Degradation and Stability* **2001,** 74, (1), 87-96.

13. Brown, D. W.; Lowry, R. E.; Smith, L. E. *Macromolecules* **1980,** 13, (2), 248-252.

14. Anseth, K. S.; Metters, A. T.; Bryant, S. J.; Martens, P. J.; Elisseeff, J. H.; Bowman C. N. *J. Controlled Release* **2002,** 78, (1-3), 199-209.

15. Martens, P. J.; Bowman, C. N.; Anseth, K. S. *Polymer* **2004,** 45, (10), 3377-3387.

16. Metters, A. T.; Anseth, K. S.; Bowman, C. N. *Polymer* **2000,** 41, (11), 3993-4004.

17. Jeong, B.; Bae, Y. H.; Kim, S. W. *Journal of Biomedical Materials Research* **2000,** 50, (2), 171-177.

18. Shim, W. S.; Kim, J. H.; Park, H.; Kim, K.; Kwon, I. C.; Lee, D. S. *Biomaterials* **2006,** 27, (30), 5178-5185.

19. Gilbert, J. C.; Washington, C.; Davies, M. C.; Hadgraft, J. *Int. J. Pharm.* **1987,** 40, (1-2), 93-99.

20. Nalbandian, R. M.; Henry, R. L.; Wilks, H. S. *J. Biomed. Mater. Res.* **1972**, *6*, 583-590.

21. Exner, A. A.; Krupka, T. Y.; Scherrer, K.; Teets, J. M. *J. Controlled Release* **2005**, *106*, 188-197.

22. Esposito, E.; Carotta, Y.; Scabbia, A.; Trombelli, L.; D'Antona, P.; Menegatti, E.; Nastruzzi, C. *Int. J. Pharm.* **1996**, *142*, 9-23.

23. Katakam, M.; Ravis, W. R.; Golden, D. L.; Banga, A. K. *Int. J. Pharm.* **1997**, *152*, 53-58.

24. Blonder, J. M.; Baird, L.; Fulfs, J. C.; Rosenthal, G. J. *Life Sciences* **1999**, 65, (21), PL261-PL266.

25. Palmer, W. K.; Emeson, E. E.; Johnston, T. P. *Atherosclerosis* **1998,** 136, (1), 115-123.

26. Li, X.; Loh, X. J.; Wang, K.; He, C. B.; Li, J. *Biomacromolecules* **2005,** 6, (5), 2740-2747.

27. Loh, X. J.; Tan, K. K.; Li, X.; Li, J. *Biomaterials* **2006,** 27, (9), 1841-1850.

28. Shih, C. *J. Controlled Release* **1995,** 34, (1), 9-15.

29. Shih, C. *Pharmaceutical Research* **1995,** 12, (12), 2036-2040.

30. Schliecker, G.; Schmidt, C.; Fuchs, S.; Kissel, T. *Biomaterials* **2003,** 24, (21), 3835-3844.

31. Loh, X. J.; Deen, G. R.; Gan, Y. Y.; Gan, L. H. *Journal of Applied Polymer Science* **2001,** 80, (2), 268-273.

32. Lee, W. F.; Hsu, C. H. *Journal of Applied Polymer Science* **1998,** 69, (9), 1793-1803.

33. Jeong, B.; Bae, Y. H.; Kim, S. W. *J. Controlled Release* **2000,** 63, (1-2), 155-163.

34. Jeong, B.; Bae, Y. H.; Lee, D. S.; Kim, S. W. *Nature* **1997,** 388, (6645), 860-862.

35. Bhattarai, N.; Ramay, H. R.; Gunn, J.; Matsen, F. A.; Zhang, M. Q. *J. Controlled Release* **2005,** 103, (3), 609-624.

36. Chen, S. B.; Pieper, R.; Webster, D. C.; Singh, J. *Int. J. Pharm.* **2005,** 288, (2), 207-218.

37. Liang, S. M.; Xu, J.; Weng, L. H.; Dai, H. J.; Zhang, X. L.; Zhang, L. N. *J. Controlled Release* **2006,** 115, (2), 189-196.

38. Sosnik, A.; Cohn, D. *Biomaterials* **2005,** 26, (4), 349-357.

39. Vlugt-Wensink, K. D. F.; Vlugt, T. J. H.; Jiskoot, W.; Crommelin, D. J. A.; Verrijk, R.; Hennink, W. E. *J. Controlled Release* **2006,** 111, (1-2), 117-127.

40. Higuchi, A.; Yamamoto, T.; Sugiyama, K.; Hayashi, S.; Tak, T. M.; Nakagawa, T. *Biomacromolecules* **2005,** *6*, 691-696.

41. Higuchi, A.; Tamiya, S.; Tsubomura, T.; Katoh, A.; Cho, C. S.; Akaike, T.; Hara, M. *J. Biomater. Sci., Polym. Ed.* **2000**, *11*, 149-168.

42. Nebe, B.; Forster, C.; Pommerenke, H.; Fulda, G.; Behrend, D.; Bernewski, U.; Schmitz, K. P.; Rychly, J. *Biomaterials* **2001**, *22*, 2425–2434.

43. Rivard, C. H.; Chaput, C.; Rhalmi, S.; Selmani, A. *Ann. Chir.* **1996**, *50*, 651–658.

44. Loh, X. J.; Zhang, Z. X.; Wu, Y. L.; Lee, T. S.; Li, J. *Macromolecules* **2009,** 42, 194-202.

45. Loh, X. J.; Cheong, W. C. D.; Li, J.; Ito, Y. *Soft Matter* **2009,** 5, 2937-2946.

46. Loh, X. J.; Gong, J.; Sakuragi, M.; Kitajima, T.; Liu, M.; Li, J.; Ito, Y. *Macromolecular Bioscience* **2009,** DOI: 10.1002/mabi.200900081

CHAPTER SIX

SYNTHESIS AND CHARACTERIZATION OF BIODEGRADABLE THERMORESPONSIVE TRIBLOCK COPOLYMERS BASED ON POLY[(*R*)-3-HYDROXYBUTYRATE] AND POLY(*N*-ISOPROPYLACRYLAMIDE)

6.1. Introduction

Amphiphilic block copolymers have the ability to self-assemble into micelles in the aqueous medium, and have been extensively investigated for their potential application in the nanomedicine and biomedical fields.[1-3] Micelles can be used as cleaning agents to extract pollutants from wastewater,[4] as template and structure control agents for materials synthesis,[5] as nano-bioreactors in biotransformation processes,[6] or as phase transfer catalysts.[7] The micelles have a hydrophobic core and hydrophilic corona which interacts with the external aqueous environment. These micelles can aid in the aqueous solubilization of hydrophobic compounds and can act as 'nano-containers' of these compounds. As an example, micelles containing a hydrophobic drug can be injected into the human body. At the onset of injection, it is important that the micelles remain stable and not rupture under the sudden high dilution. Thus, having micelles with a low critical micelle concentration is critical to its application.

Poly[(*R*)-3-hydroxybutyrate] (PHB) belongs to a class of biologically synthesized polyesters known as poly[(*R*)-3-hydroxyalkanoate]s.[8-13] PHB has been extracted from genetically modified plants.[14] PHB is a thermoplastic polyester, with mechanical properties close to those of isotactic polypropylene, which can be extruded, molded, and spun using conventional processing equipment. Rising oil prices has seen the increasing popularity of the PHB compared with conventional commodity plastics. Due to its degradable nature, PHB is considered to be an environmentally friendly plastic when compared to its non-degradable counterparts such as polystyrene or polyethylene. These attractive properties have led to the use of PHB as materials in areas such as packaging. PHB degrades to D-3-hydroxybutyrate which is a natural constituent of human blood.[15] As a result of this advantageous property, PHB may be suitable for a variety of biomedical applications, such as uses as drug carriers and tissue engineering scaffolds. Due to its inherent hydrophobicity, PHB is rarely used in applications requiring good water solubility,

such as polymeric micelles and gels. In 2003, the synthesis of the first water-soluble PHB-based triblock copolymer was reported.[3] These poly(ethylene oxide)-poly[(*R*)-3-hydroxybutyrate]-poly(ethylene oxide) (PEO-PHB-PEO) copolymers formed micelles which possess very good stability under high dilution conditions. More recently, the first thermogelling copolymer based on PHB was reported.[16-18] The advantage gained from using PHB in this case was that these PHB-based copolymers required very low concentrations in solution to exhibit the thermogelling behavior. This reduces the amount of polymer required in preparing an injectable formulation for drug release applications.[17]

Recently, thermo-sensitive micelles derived from poly(N-isopropylacrylamide) (PNIPAAm) have been reported.[19-24] PNIPAAm exhibits a lower critical solution temperature (LCST) of 32 to 33 °C, being hydrophilic at low temperatures and precipitating above the critical phase transition temperature. Block copolymers comprising a hydrophobic segment such as poly(methyl methacrylate) (PMMA), poly(10-undecenoic acid) and poly(oleic acid) and hydrophilic PNIPAAm segments have been reported.[21-24] However, these thermoresponsive micelles are non-degradable, raising questions on the elimination of the micelles from the body after its use. The thermoresponsive poly(N-isopropylacrylamide-*co*-N,N-dimethylacrylamide) (PNIPAAm–PDMAAm) segments have been copolymerized with hydrophobic biodegradable segments such as poly(DL-lactic acid) (PDLLA), poly(lactic-co-glycolic acid) (PLGA), or PCL.[25-28] Biotinylated poly(N-isopropylacrylamide-*co*-N-(3-dimethylamino propyl)methacrylamide) have been copolymerized with PCL for cell tracking and drug delivery applications.[29] It was demonstrated that these micelles have a slow rate of drug release at temperatures below the critical phase transition temperature but rapidly release encapsulated drug upon heating to above the critical phase transition temperature. Triblock copolymers of PNIPAAm-PCL-PNIPAAm and PCL-PNIPAAm-PCL have been synthesized.[30,31] These

copolymers show very low critical micellization concentrations in the range of 4-40 mg/L. The micelles obtained in both cases showed a spherical morphology seen on TEM micrographs. Incorporation of the hydrophobic PCL segment does not appear to significantly lower the LCST of the copolymer. The synthesis of diblock copolymers of PNIPAAm and PDLLA were reported.[32] These diblock copolymers formed micelles in water. It was found that when the length of the PDLLA segment is too long, precipitates were obtained instead of micelles.

In this chapter, the synthesis of a new series of biodegradable thermoresponsive PNIPAAm-PHB-PNIPAAm triblock copolymers by atom transfer radical polymerization (ATRP) is reported. Prior literature survey did not reveal any precedent reports on the synthesis and characterization of these copolymers. These triblock copolymers are expected to form thermoresponsive micelles which would be very stable under high dilution concentrations in the aqueous environment. These micelles can be made to release the contents held in the core upon exposure to thermal stimulus, potentially allowing for thermally triggered drug release. In order to form micelles, the central PHB block must not be too long, otherwise, this would lead to water-insoluble block copolymers. During the design of the copolymers, the length of PNIPAAm blocks on either side of the PHB block was restricted to a molecular weight of less than 20,000 g/mol, so as to allow the final degraded fragment to be easily excreted from the body via renal filtration. The renal excretion of PEG from the body system has been investigated.[33-35] For PEG with molecular weight lower than 30,000 g/mol, the elimination of the polymer was determined by molecular size and was removed from the body fairly rapidly. However, when the molecular weight of PEG was greater than 30,000 g/mol, the polymers were excreted much more slowly by renal filtration. Based on the biodegradability and biocompatibility of the copolymers, these materials are excellent candidates for the encapsulation and delivery of hydrophobic drugs to the human body

6.2. Experimental Section

6.2.1. Materials.

Natural source poly[(*R*)-3-hydroxybutyrate] (PHB) was purchased from Aldrich. The PHB sample was purified by dissolving in chloroform followed by filtration and precipitation in hexane before use. The M_n and M_w of the purified PHB are 8.7×10^4 and 2.3×10^5, respectively. Bis(2-methoxyethyl) ether (Diglyme, 99%), ethylene glycol (99%), dibutyltin dilaurate (95%), 2-bromoisobutyryl bromide (98%), N-isopropylacrylamide (NIPAAm, >99%), 1,1,4,7,10,10-hexamethyltriethylenetetramine (HMTETA, 99%), copper(I) bromide (CuBr, 99%), triethylamine (>99%) and 1,4-dioxane (>99%) were obtained from Aldrich. Diglyme was dried with molecular sieve before use. Methylene chloride was distilled over CaH_2 before use.

Telechelic hydroxylated PHB (PHB-diol) prepolymer was prepared by transesterification from the natural PHB and diethylene glycol with dibutyltin dilaurate as catalyst in diglyme as reported previously (yield, 80%).[3] Purified nitrogen was used in all reactions

6.2.2. Synthesis of Poly(N-isopropylacrylamide)-Poly[(*R*)-3-hydroxybutyrate]-Poly(N-isopropylacrylamide) Triblock Copolymers

PHB-diol (8 g, 4.6 mmol) was dissolved in 10 mL of anhydrous methylene chloride containing 20 mmol of triethylamine in a 250 mL round bottom flask. The reaction flask was kept in an ice/water bath (temperature = 4 ^oC). When the PHB-diol had completely dissolved, 10 mmol of 2-bromoisobutyl bromide was added into the flask dropwise through an equalizing funnel. After addition, the reaction was allowed to proceed at room temperature for 24 h. The resulting Br-PHB-Br macroinitiator was precipitated in excess diethylether/methanol (80:20 v/v). The crude product was redissolved in tetrahydrofuran (THF) and reprecipitated in excess diethylether/methanol (80:20 v/v) to remove any residual reactants. This process was repeated

another time. The yield of this reaction is about 4.2 g (53 %). The Br-PHB-Br macroinitiator for the subsequent ATRP was dried in *vacuo*.

The poly(N-isopropylacrylamide)-poly[(*R*)-3-hydroxybutyrate]-poly(N-isopropylacrylamide) (PNIPAAm-PHB-PNIPAAm) triblock copolymers with different PNIPAAm chain lengths were synthesized using different molar feed ratios. As an example, for the synthesis of NHN(60-17-60), a molar feed ratio of [NIPAAm (6 g)/[Br-PHB-Br (0.5 g, M_n = 1730 g/mol)]/[CuBr (84 mg)]/[HMTETA (266 mg)] of 180:1:2:4. The reaction was performed in a 20 mL flask equipped with a magnetic stirrer. NIPAAm, Br-PHB-Br, and HMTETA were introduced into the flask containing 15 mL of dioxane. After the reactants had dissolved completely, the reaction mixture was degassed by bubbling nitrogen through the reaction mixture for 30 min. CuBr was added into the reaction mixture under nitrogen atmosphere. The reaction mixture was further purged with nitrogen for 10 min. The flask was then sealed and kept under nitrogen atmosphere. The polymerization was allowed to proceed under continuous stirring at 45 ^{o}C for 24 h. The reaction was stopped by diluting with THF and exposing the reaction mixture to air for 4 h. The catalyst complex was removed by passing the dilute polymer solution through a short aluminium oxide column. A colourless solution was obtained. After removal of THF under reduced pressure, the crude copolymer was redissolved in a minimum amount of THF and precipitated in hexane to remove the unreacted NIPAAm monomer. The obtained precipitate was then dissolved in THF and then re-precipitated in diethylether. The copolymers were then dried in *vacuo* for further studies. The triblock copolymer yield (and the conversion of NIPAAm) after purification was 2.23 g (34.3%).

6.2.3. Polymer Characterization

Gel permeation chromatography (GPC). GPC analysis was carried out with a Shimadzu SCL-10A and LC-8A system equipped with two Phenogel 5 μm 50 and 1000 Å

columns (size: 300 x 4.6 mm) in series and a Shimadzu RID-10A refractive index detector. THF was used as eluent at a flow rate of 0.30 mL/min at 40 °C. Monodispersed poly(ethylene glycol) standards were used to obtain a calibration curve. The ^{1}H NMR (400 MHz) and ^{13}C NMR (100 MHz) spectra were recorded on a Bruker AV-400 NMR spectrometer at room temperature. The ^{1}H NMR measurements were carried out with an acquisition time of 3.2 s, a pulse repetition time of 2.0 s, a 30° pulse width, 5208 Hz spectral width, and 32K data points. Chemical shift was referred to the solvent peaks (δ = 7.3 ppm for $CHCl_3$, δ = 4.7 ppm for HOD).

CMC Determination by Fluorescence Spectroscopy. Steady-state fluorescence spectra were recorded on a Shimadzu RF-5301PC spectrofluorophotometer. Excitation spectra were monitored at λ_{em} = 390 nm. Slit widths for both excitation and emission sides were maintained at 3.0 nm. Sample solutions were prepared by dissolving a predetermined amount of block copolymer in an aqueous pyrene solution of known concentration, and the solutions were allowed to stand for 1 day for equilibration. The pyrene concentration was kept at 6.0×10^{-7} M.

Thermal Analysis. Thermogravimetric analyses (TGA) were made using a TA Instruments SDT 2960. Samples were heated at 20 ^{o}C/min from room temperature to 800 ^{o}C in a dynamic nitrogen atmosphere (flow rate = 70 mL/min). Differential scanning calorimetry (DSC) measurements were performed using a TA Instruments 2920 differential scanning calorimeter equipped with an autocool accessory and calibrated using indium. The following protocol was used for each sample: heating from room temperature to 170 ^{o}C at 20 ^{o}C/min, holding at 170 ^{o}C for 2 min, cooling from 170 to -30 ^{o}C at 5 ^{o}C/min, and finally reheating from -30 to 170 ^{o}C at 5 ^{o}C/min. Data were collected during the second heating run. Transition temperatures were taken as peak maxima.

Lower Critical Solution Temperature Determination (LCST). Cloud points were measured with a UV-vis spectrophotometer. Aqueous copolymer solutions (0.5 mg/mL) were heated at 2 ^{o}C/min while both the transmittance at 500 nm (1 cm path length) and the solution temperature were monitored.

Micelle Size Measurements. Measurements of micelle size were performed on micelle solutions (50 mg/L) using a Zetasizer Nano ZS (Malvern Instruments, Southborough, MA, USA) with a laser light wavelength of 633 nm at a 173° scattering angle. The micelle size measurement was performed at 25 °C. The deconvolution of the measured correlation curve to an intensity size distribution was accomplished using a nonnegative least squares algorithm. The decay rate distributions were transformed to an apparent diffusion coefficient (D). From the diffusion coefficient, the apparent hydrodynamic size of the polymer or micelles can be obtained by the Stokes-Einstein equation. The Z-average hydrodynamic diameters of the particles were given by the instrument. The Z-average size is the intensity weighted mean diameter derived from a cumulants or single-exponential fit of the intensity autocorrelation function.

Transmission Electron Microscopy (TEM). The samples were imaged on a JEOL JEM-2010F FasTEM field emission transmission electron microscope, operated at 100 kV. The samples for TEM were prepared by directly depositing one drop of sample solution (50 mg/L or 500mg/L) containing 0.1 wt % phosphotungstic acid (PTA) onto copper grids, which were coated in advance with supportive Formvar films and carbon (Agar Scientific). The samples were kept in an oven for 12 h for drying at 25 ^{o}C or at 35 ^{o}C before TEM imaging.

6.2.4. Cell Culture

Cells and Media. L929 mouse fibroblasts were obtained from ATCC and cultivated in DMEM containing 10% fetal bovine serum (FBS) and 1% penicillin / streptomycin. Cells were

grown as a monolayer and were passaged upon confluence using trypsin (0.5% w/v in PBS). L929 cells were harvested from culture by incubating in trypsin solution for 10 min. The cells were centrifuged and the supernatent was discarded. 3 mL of serum-supplemented DMEM was added to neutralize any residual trypsin. The cells were resuspended in serum-supplemented DMEM at a concentration of 2 x 10^4 cells mL^{-1}. Cells were cultivated at 37 ^oC and 5% CO_2.

Cell Viability Assay. The cytotoxicity of the copolymers was evaluated using the MTT assay in L929 cell lines. The cells were cultured in complete DMEM supplemented with 10% FBS at 37 ^oC, 5% CO_2, and 95% relative humidity. The cells were seeded in a 96-well microtiter plate (Nunc, Wiesbaden, Germany) at densities of 3 x 10^4 cells/well. After 24 h, culture media were replaced with serum-supplemented culture media containing known concentrations of the copolymers, and the cells were incubated for a further 48 h. Then, 10 μL of sterile-filtered MTT stock solution in PBS (5 mg/mL) was added to each well, reaching a final MTT concentration of 0.5 mg/mL. After 5 h, unreacted dye was removed by aspiration. The formazan crystals were dissolved in DMSO (100 μL/well), and the absorbance was measured using a microplate reader (Spectra Plus, TECAN) at a wavelength of 570 nm. The relative cell viability (%) related to control cells cultured in media without polymers was calculated with $[A]_{test}/[A]_{control} \times 100\%$, where $[A]_{test}$ is the absorbance of the wells with polymers and $[A]_{control}$ is the absorbance of the control wells. All experiments were conducted with six repetitions and averaged.

6.3. Results and Discussion

6.3.1. Synthesis of the PNIPAAm-PHB-PNIPAAm Triblock Copolymers

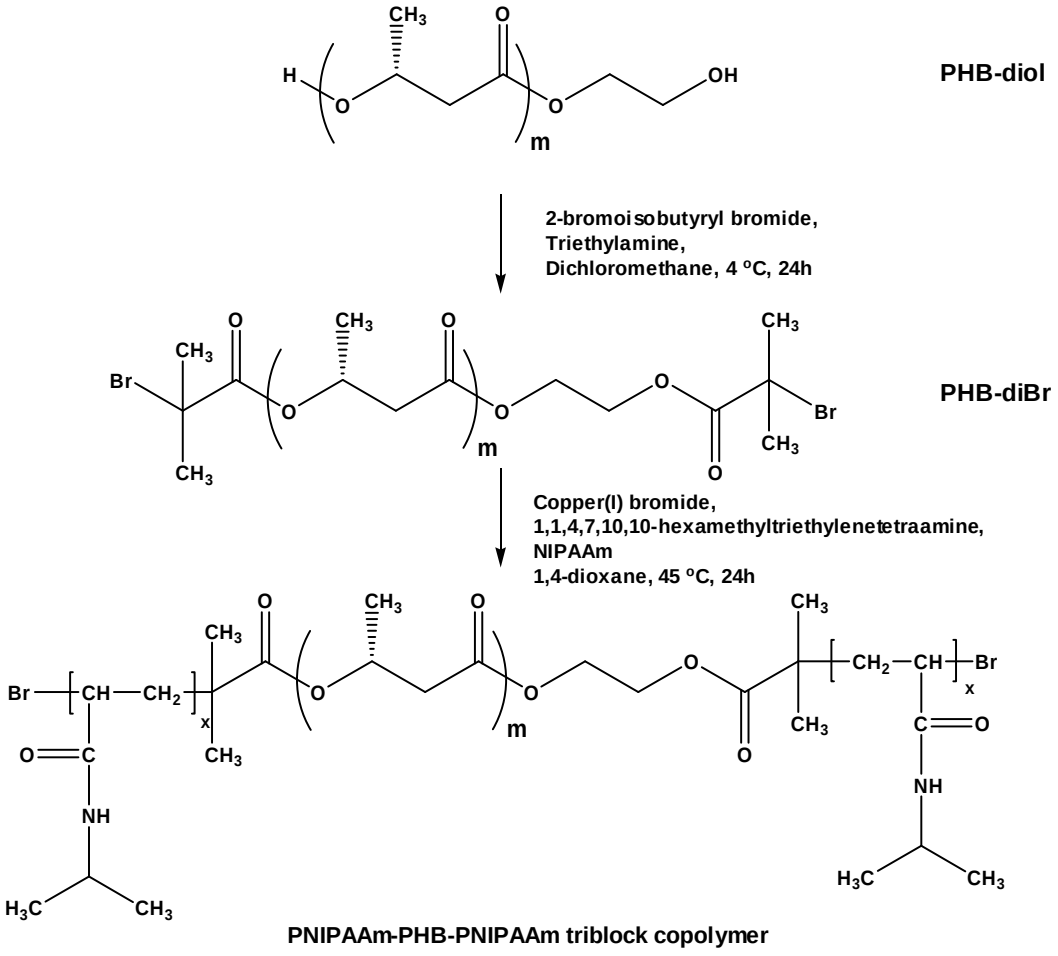

Scheme 6.1. Synthesis of PNIPAAm-PHB-PNIPAAm triblock copolymers by ATRP

The thermo-responsive PNIPAAm-PHB-PNIPAAm triblock copolymers were prepared according to the reaction sequence shown in Scheme 6.1. The starting dibromo-terminated PHB (Br-PHB-Br) macroinitiator for ATRP was prepared from PHB-diol by reaction of the terminal hydroxyl end groups of PHB-diol with 2-bromoisobutyryl bromide. The M_n of Br-PHB-Br is about 1.73×10^3 g/mol (Figure 6.1e). The ^{1}H NMR spectrum shows a signal at 4.25 ppm due to the protons from the ethylene glycol segment in the PHB-diBr and the signal at 1.92 ppm from

the methyl protons of the 2-bromoisobutyryl fragment (Figure 6.2a). By calculating the ratio of these two signals, the extent of substitution of the PHB-diol was obtained. Substitution of the hydroxyl groups was estimated to be about 95 % based on ^{1}H NMR. PNIPAAm-PHB-PNIPAAm triblock copolymer was synthesized via ATRP of NIPAAm from the Br-PHB-Br macroinitiator. The PNIPAAm-PHB-PNIPAAm triblock copolymers were synthesized in dioxane at 45 °C for 24 h via ATRP of NIPAAm from the Br-PHB-Br macroinitiator units. A series of triblock copolymers with different PNIPAAm block lengths were synthesized by varying the monomer feed. The molecular weights of the copolymers are summarized in Table 6.1. In general, the copolymers had low polydispersities and the GPC profiles of the copolymers did not show overlapping peaks with the PHB-diBr precursor, as shown in Figure 6.1. This indicates that the PHB-diBr has reacted with the NIPAAm monomer.

The chemical structure of the PNIPAAm-PHB-PNIPAAm triblock copolymer was characterized by ^{1}H NMR spectroscopy. Figure 6.2b shows the ^{1}H NMR spectrum of the NHN(10-17-10) copolymer. The peaks associated with the methyl protons (δ = 1.14 ppm), methylene protons (δ = 1.4-1.6 ppm), methylidyne protons adjacent to the carbonyl group (δ = 1.78 ppm) and the methylidyne protons adjacent to the amine moiety (δ = 3.95 ppm) of the PNIPAAm blocks were observed. The peaks associated with the methyl proton (δ = 1.32 ppm), methylene proton (δ = 2.49-2.64 ppm) and methine proton (δ = 5.25 ppm) of the PHB segment were also observed. From ^{1}H NMR, the molecular weights and composition of the block copolymers were calculated and summarized in Table 6.1.

Table 6.1. Molecular characteristics of PNIPAAm-PHB-PNIPAAm triblock copolymers

Copolymer[a]	M_n[b] ($\times 10^3$)	M_w/M_n[b]	M_n[c] ($\times 10^3$)	Copolymer composition (wt %)[c]		Copolymer composition (wt %)[d]	
				PHB	NIPAAm	PHB	NIPAAm
PHB-diBr	1.73	1.04	1.63	-	-	-	-
NHN(10-17-10)	3.75	1.09	2.79	58.5	41.5	59.5	40.5
NHN(60-17-60)	13.76	1.49	8.23	19.8	80.2	23.8	76.2
NHN(157-17-157)	33.20	1.30	31.35	5.2	94.8	6.3	93.7
NHN(180-17-180)	37.72	1.50	41.80	3.9	96.1	3.5	96.5

[a] PNIPAAm-PHB-PNIPAAm triblock copolymers are denoted NHN, N for P**N**IPAAm and H for P**H**B, the numbers in brackets show the indicative molecular weight of the respective block in hundred g/mol. [b] Determined by GPC. [c] Calculated from ^{1}H NMR results. [d] Calculated from TGA results.

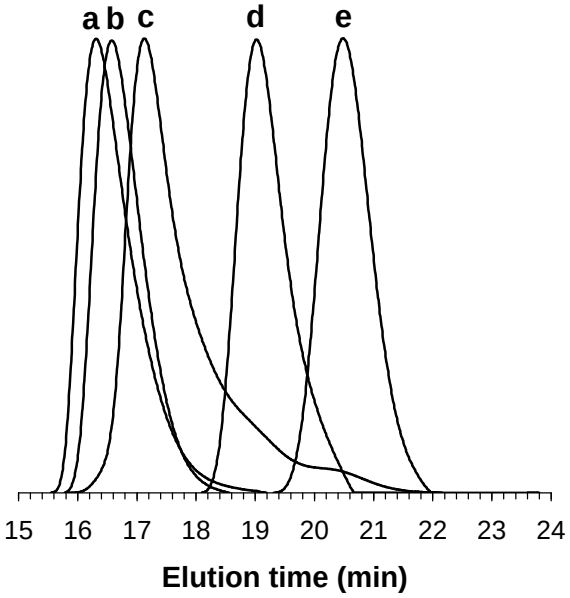

Figure 6.1. GPC traces of the PNIPAAm-PHB-PNIPAAm triblock copolymers and the PHB precursor: (a) NHN(180-17-180); (b) NHN(157-17-157); (c) NHN(60-17-60); (d) NHN(10-17-10); (e) PHB-diBr.

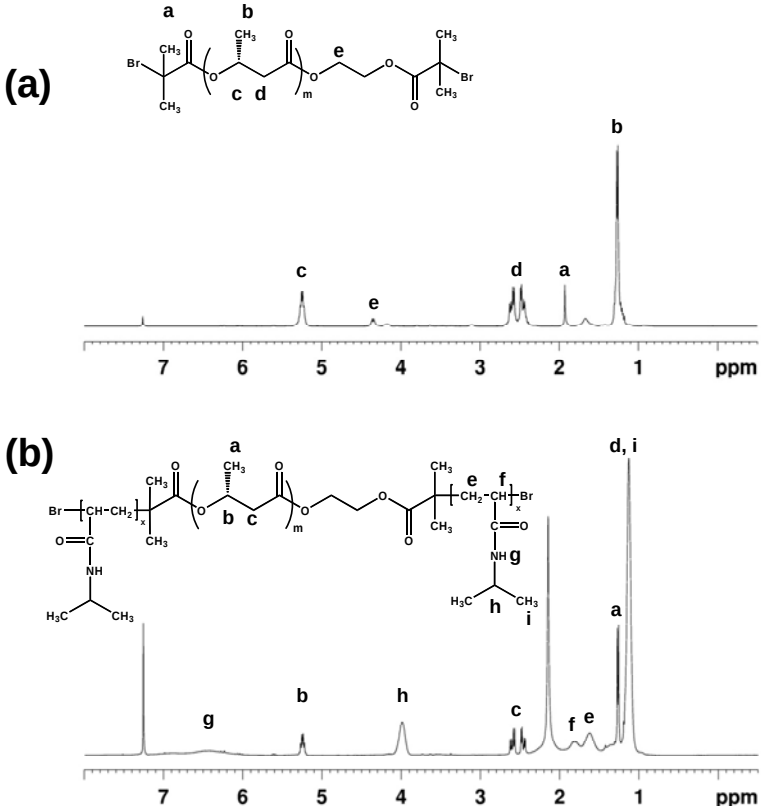

Figure 6.2. ^{1}H NMR spectrum of (a) PHB-diBr, (b) PNIPAAm-PHB-PNIPAAm triblock copolymer, NHN(10-17-10).

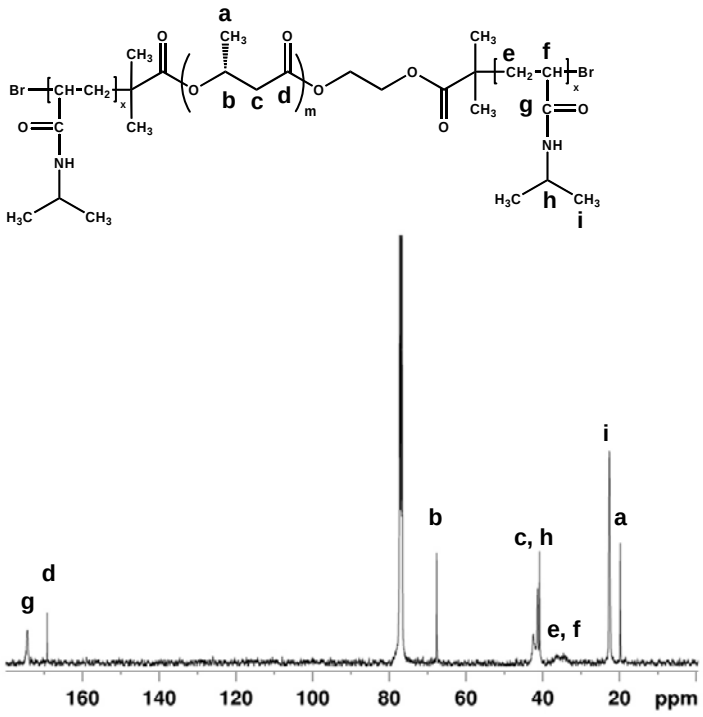

Figure 6.3. ^{13}C NMR spectrum of PNIPAAm-PHB-PNIPAAm triblock copolymer, NHN(10-17-10).

For ^{13}C NMR, the spectrum of NHN(10-17-10) copolymer is shown in Figure 6.3. The peaks associated with the methyl carbons (δ = 22.3 ppm), methylene carbons and methylidyne carbon adjacent to the carbonyl group (δ = 33.4-38.2 ppm), methylidyne carbon adjacent to the amine moiety (δ = 40.1 ppm) and the carbonyl carbon (δ = 175.2 ppm) of the PNIPAAm blocks were observed. The peaks associated with the methyl carbon (δ = 19.9 ppm), methylene carbon (δ = 41.2 ppm), methine carbon (δ = 68.1 ppm) and carbonyl carbon (δ = 170.1 ppm) of the PHB segment were observed. More importantly, the methyl carbon peak associated with the 2-bromoisobutyryl fragment, originally at δ = 31.0 ppm was absent; this indicates that the bromide end of the macroinitiator has reacted with the NIPAAm monomer. Therefore, the NMR results taken together with the GPC results demonstrate the successful synthesis of the triblock copolymers.

6.3.2. Micellization of PNIPAAm-PHB-PNIPAAm Triblock Copolymers

NMR spectroscopy was used to investigate the effect of solvent on the micelle structure.[36-39] $CDCl_3$ is a good nonselective solvent for PHB and PNIPAAm while water is a good selective solvent for PNIPAAm but poor for PHB. In $CDCl_3$, the peaks due to the PHB and PNIPAAm segments were sharp and well defined (Figures 6.4 and 6.5). In D_2O, PNIPAAm is shown as a sharp peak but PHB peaks could not be observed. This shows that the molecular motion of PHB is slow in water, indicating a hydrophobic core structure made up of PHB with the hydrophilic PNIPAAm as the outer corona structure, confirming the core-corona structure of the micelle.[37-39]

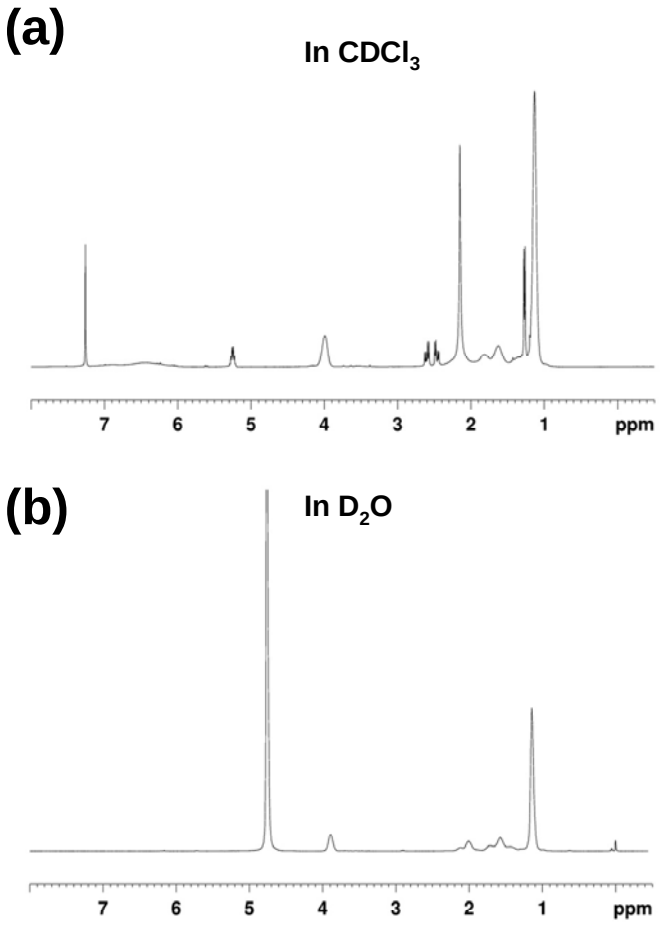

Figure 6.4. ^1H NMR spectra of NHN(10-17-10) (1 mg/mL) in $CDCl_3$ (a) and D_2O (b) at 25 ^oC.

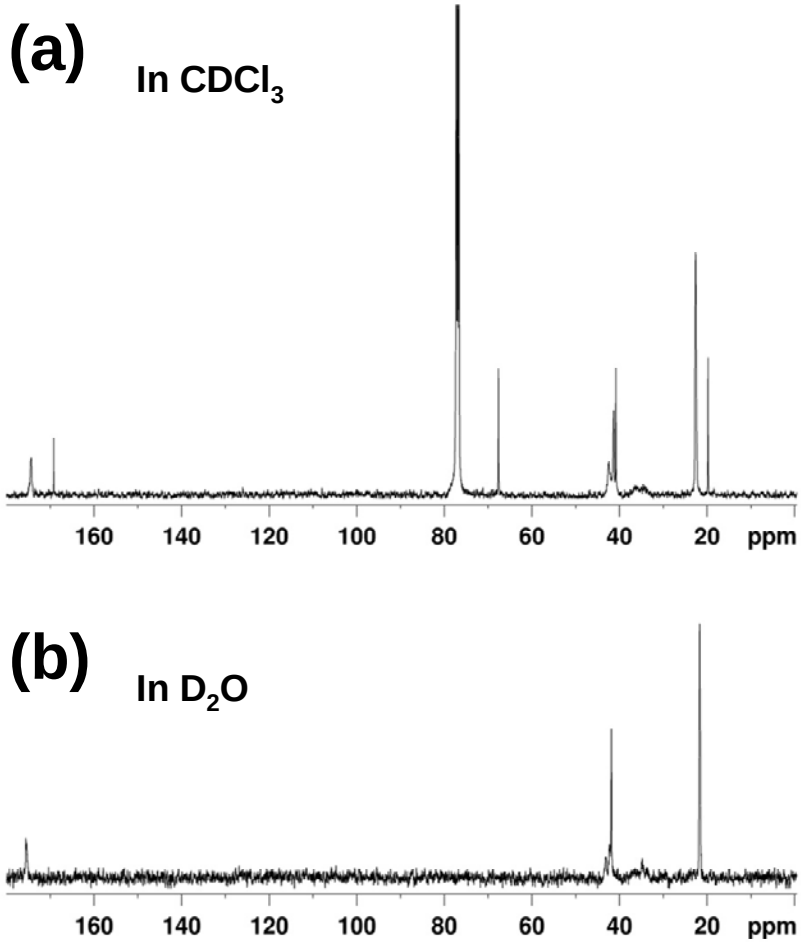

Figure 6.5. ^{13}C NMR spectra of NHN(10-17-10) (1 mg/mL) in $CDCl_3$ (a) and D_2O (b) at 25 ^oC.

The PNIPAAm-PHB-PNIPAAm triblock copolymers were soluble in water. CMC determination was carried out for these copolymers using fluorescence spectroscopy. Fluorescence probe technique is a powerful tool to study micellar properties of amphiphilic block copolymers.[40,41] When the copolymer concentration in an aqueous solution of pyrene is increased, both emission and excitation spectra undergoes significant changes upon micellization of the block copolymer systems.[41] These changes are caused by the transfer of pyrene molecules from the polar aqueous environment to the hydrophobic micellar cores and are related to the location of the pyrene molecules in the solution. The fluorescence excitation spectrum shows a shift of the low-energy band of the L_a ($S_2 \leftarrow S_0$) from 333 to 338 nm. It has

been reported that this (0,0) absorption band change of pyrene is more sensitive to the true onset of aggregation than either lifetime measurements or fluorescence emission changes.[42,43] This change is described in terms of the ratio of the intensities of the first and third bands in the pyrene fluorescence spectrum, I_{338}/I_{333}. Hence, the CMC values of the PNIPAAm-PHB-PNIPAAm triblock copolymers in aqueous solution were determined using the fluorescence excitation spectra of the pyrene probe.

Figure 6.6a shows the excitation spectra for pyrene in water at various concentrations of PNIPAAm-PHB-PNIPAAm triblock copolymer. When the copolymer concentration increased, a red shift of the (0,0) absorption band from 333 to 338 nm was observed. Figure 6.6b shows the intensity ratio of I_{338}/I_{333} of pyrene excitation spectra as a function of the logarithm of copolymer concentrations for NHN(60-17-60) triblock copolymer. The I_{338}/I_{333} vs log C plots present a sigmoid curve. A negligible change of intensity ratio of I_{338}/I_{333} was observed at low concentration range for each triblock copolymer. With an increase in the copolymer concentration, the intensity ratio exhibited a substantial increase at a certain concentration, reflecting the incorporation of pyrene into the hydrophobic core region of the micelles. Therefore, the CMC values were determined form the crossover point at the low concentration range in Figure 6.6b, and the results are listed in Table 6.2. The very low CMC values for PNIPAAm-PHB-PNIPAAm triblock copolymers, indicate a very strong tendency of the triblock copolymers toward formation of micelles in aqueous solution. The CMC values of the triblock copolymers were observed to increase with an increase in the PNIPAAm segment length, due to the increased hydrophilicity of the copolymer. The CMC values of the PNIPAAm-PHB-PNIPAAm triblock copolymers are much lower than the PNIPAAm-PCL-PNIPAAm[30] and PCL-PNIPAAm-PCL[31] copolymers, indicating that the more hydrophobic PHB segments (as

compared to PCL) provide a greater driving force for the self assembly of the copolymers into micelles in aqueous solution.

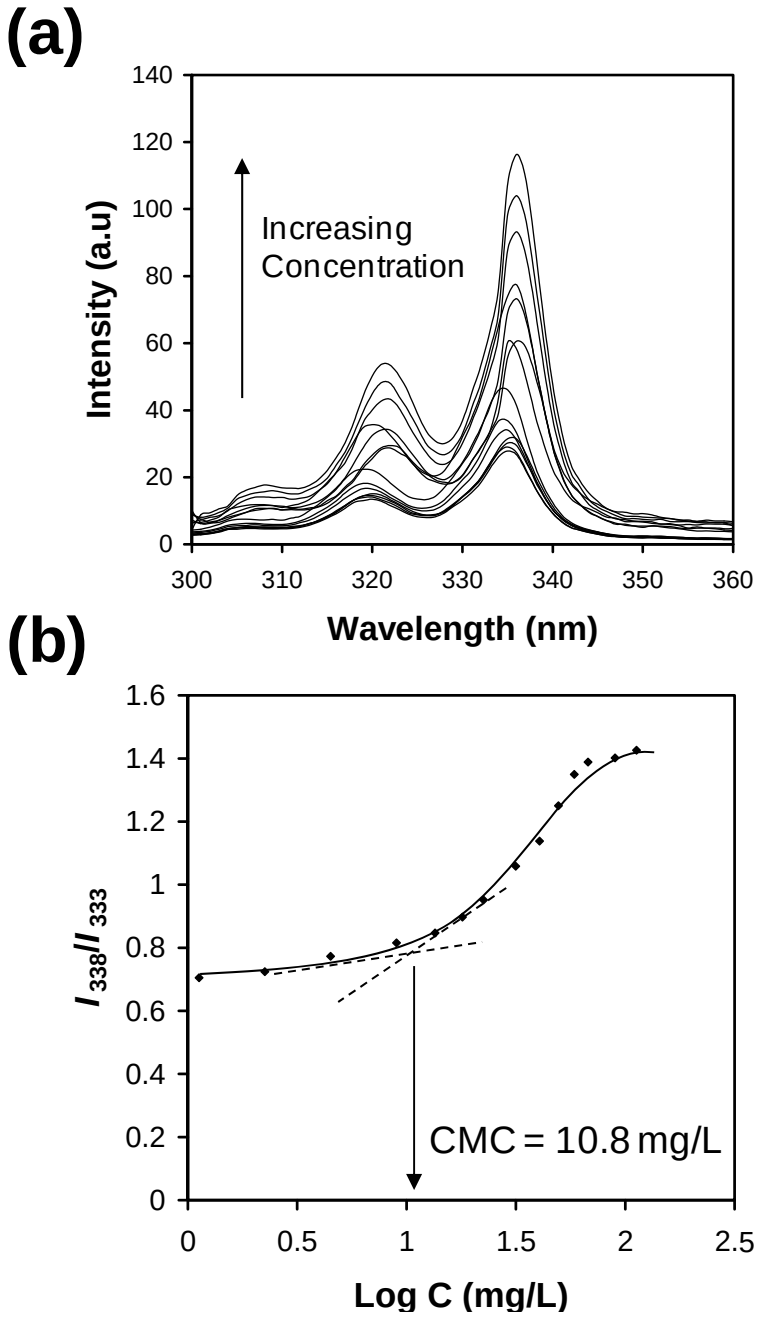

Figure 6.6. (a) Steady-state fluorescence excitation spectra monitored at 390 nm for the pyrene probe in an aqueous solution of NHN(60-17-60) copolymer of various concentrations in water at 25 °C. The concentration of pyrene is 6.0 x 10^{-7} M (b) Plots of the I_{338}/I_{333} ratio of pyrene excitation spectra in water as a function of NHN(60-17-60) triblock copolymer concentration at 25 °C.

These micelles can aid in the encapsulation and aqueous solubilization of hydrophobic drugs. The encapsulation efficiency of the drug is affected by the hydrophobicity of the micelle core. The hydrophobicity of the PHB micellar core can be estimated by determining the partition equilibrium coefficient, K_v of pyrene, in the aqueous PNIPAAm-PHB-PNIPAAm triblock copolymer solutions. The calculations were performed as reported previously.[41, 44-46] This method calculates the partition equilibrium based on the assumption of a simple equilibrium distribution between the micellar phase and the water phase. The ratio of the pyrene concentration in the micellar phase to the water phase ($[Py]_m/[Py]_w$) can be correlated to the ratio of volume of each phase and expressed as follows.

$$([Py]_m/[Py]_w) = K_v V_m/V_w \quad (6.1)$$

This can be rewritten as

$$([Py]_m/[Py]_w) = K_v x(c - CMC)/1000\rho \quad (6.2)$$

where x is the weight fraction of the PHB block in the triblock copolymer, c is the concentration of the triblock copolymer, and ρ is the density of the PHB core of the micelles, which is assumed to be the bulk density of PHB (1.285 g/cm^3). In the intermediate range of the polymer concentrations with substantial increases in the intensity ratios (I_{338}/I_{333}), ($[Py]_m/[Py]_w$) can be written as

$$([Py]_m/[Py]_w) = (F - F_{min})/(F_{max} - F) \quad (6.3)$$

where F_{min} and F_{max} correspond to the average magnitude of the intensity ratio (I_{338}/I_{333}) in the constant region in the low and high concentration ranges in Figure 6.6, respectively. F is the intensity ratio (I_{338}/I_{333}) in the intermediate concentration range of the triblock copolymers. Combining equations 6.2 and 6.3 yields

$$(F - F_{min})/(F_{max} - F) = K_v x(c - CMC)/1000\rho \quad (6.4)$$

K_v values for pyrene were obtained by plotting a graph of $(F - F_{min})/(F_{max} - F)$ vs the concentration of the PNIPAAm-PHB-PNIPAAm triblock copolymer solutions (Figure 6.7). The K_v values are summarized in Table 6.2. The values ranged from 1.64×10^5 to 20.42×10^5 for the triblock copolymers. This indicates that the copolymer can be potentially loaded with a hydrophobic drug with high encapsulation efficiency. As the length of the PNIPAAm chains increased, the K_v values decreased, suggesting that the hydrophobicities of the micellar core decreased. This is related to the hydrophilic/hydrophobic balance in the triblock copolymer, which consequently affects the micelle packing ability of the copolymer. Previously, K_v values of 3.0×10^4 to 3.3×10^5 have been reported for amphiphilic poly[bis(2,2,2-trifluoroethoxy)phosphazene]/poly(propylene glycol) triblock copolymers and K_v values of 1.79×10^5 to 5.88×10^5 have been reported for copolymers of poly(2-ethyl-2-oxazoline)-poly(ε-caprolactone) and poly(2-ethyl-2-oxazoline)-poly(L-lactide).[45,46] The K_v values determined in this work are relatively higher than those reported previously, particularly for NHN(10-17-10). Compared with the K_v values of PNIPAAm-PCL-PNIPAAm micelles, the K_v values of PNIPAAm-PHB-PNIPAAm are much higher.[30] It appears that PNIPAAm-PHB-PNIPAAm micelles have a higher encapsulation capacity than PNIPAAm-PCL-PNIPAAm micelles.

6.3.3. Thermal Stability.

The thermal stability of the triblock copolymers was evaluated using thermogravimetric analysis (TGA). Figure 6.8 shows the weight loss curves for the series of triblock copolymers compared with its PHB precursor. The PNIPAAm-PHB-PNIPAAm triblock copolymers undergo stepwise thermal degradation. The PHB block degrades first at about 230 ^oC, followed by the PNIPAAm block at about 360 ^oC. The PNIPAAm block starts to degrade only after the PHB block has completed its degradation at 310 – 330 ^oC. The compositions of the triblock copolymers can be calculated from the two-step degradation profile. The PHB and PNIPAAm

contents estimated from TGA results are listed in Table 6.1. The results are in excellent agreement with the values calculated from ^{1}H NMR. The thermal stabilities of these polymers were evaluated by observing the temperature at which the onset of thermal degradation occurs. The thermal stability of PHB increased when incorporated in the triblock copolymers as compared with the PHB-diBr precursor. Overall, all the copolymers have better thermal stabilities than their PHB precursor.

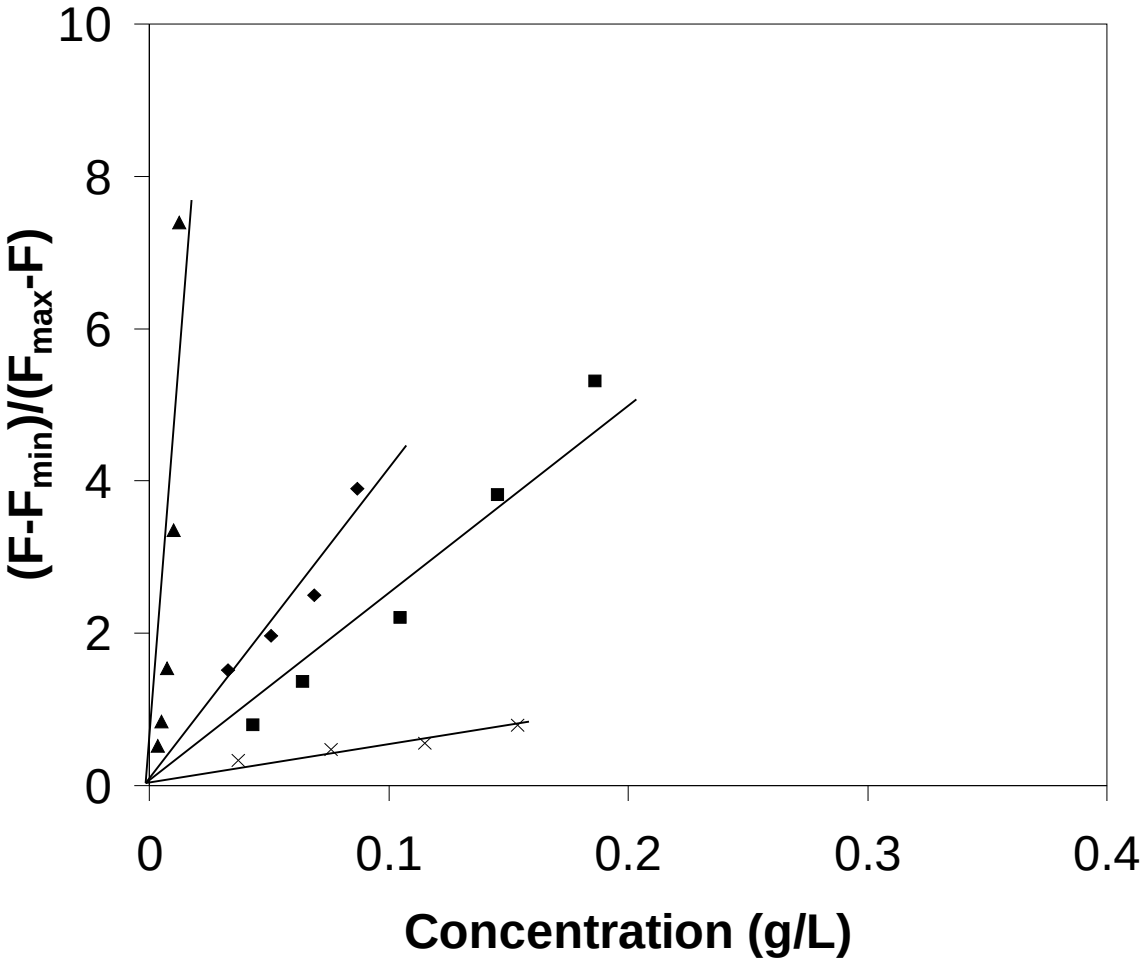

Figure 6.7. Plots of $(F - F_{min})/(F_{max} - F)$ vs concentration of PNIPAAm-PHB-PNIPAAm triblock copolymers, NHN(10-17-10) (▲), NHN(60-17-60) (◆), NHN(157-17-157) (■) and NHN(180-17-180) (×) in water at 25 ^{o}C.

Table 6.2. Solution properties of PNIPAAm-PHB-PNIPAAm triblock copolymers

Copolymer	LCST (^oC)[a]	CMC (mg/L)[b]	K_v (x 10^{-5})	d, 25 ^oC[c] (nm)	d, 35 ^oC [c] (nm)
NHN(10-17-10)	28.0	1.5	20.42	844 ± 24 (0.97)	550 ± 18 (0.47)
NHN(60-17-60)	28.3	10.8	2.71	449 ± 27 (0.77)	215 ± 2 (0.30)
NHN(157-17-157)	28.8	38.1	2.33	342 ± 39 (0.48)	161 ± 2 (0.15)
NHN(180-17-180)	29.0	41.1	1.64	287 ± 22 (0.45)	139 ± 3 (0.14)

[a] Determined from turbidmetry measurements. [b] Determined by pyrene solubilization method. [c] Mean Z-average diameters by dynamic light scattering from 5 individual measurements. Numbers in brackets represent the average polydispersity of the particle size.

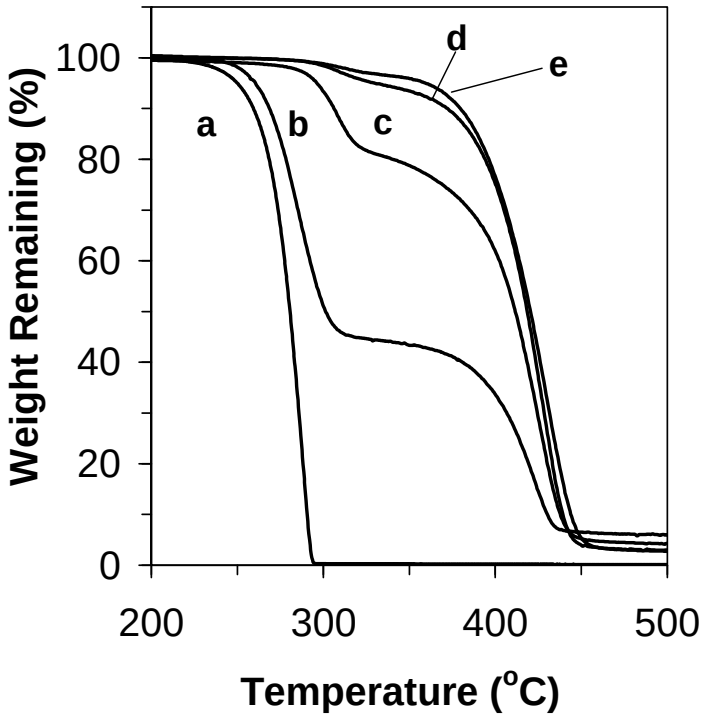

Figure 6.8. TGA curves obtained at a heating rate of 20 ^oC/min under nitrogen atmosphere for (a) PHB-diBr, (b) NHN(10-17-10), (c) NHN(60-17-60), (d) NHN(157-17-157), and (e) NHN(180-17-180).

6.3.4. Solid-State Behavior.

Differential scanning calorimetry (DSC) was carried out to determine the microphase separation and crystallization of the PHB block in the copolymer. The DSC thermograms for the PNIPAAm-PHB-PNIPAAm triblock copolymers are presented (Figure 6.9). Numerical values corresponding to the thermal transitions and the crystallinity of the PHB block are tabulated in Table 6.3.

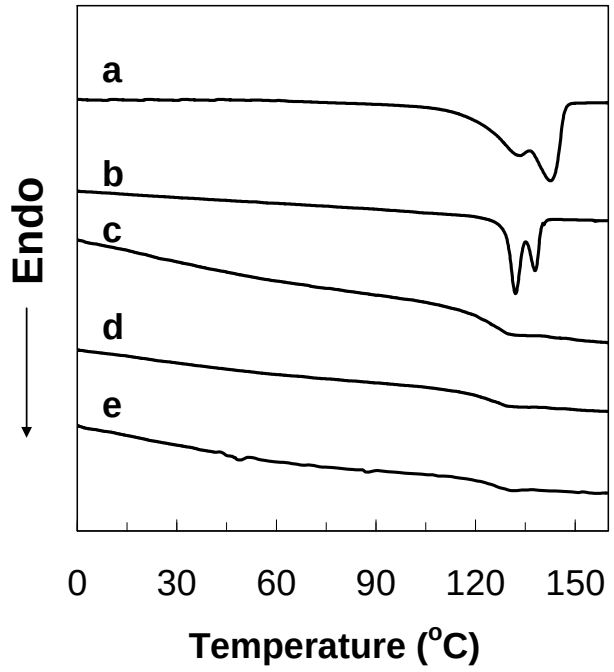

Figure 6.9. DSC second heating curves (5 °C/min) of (a) PHB-diBr, (b) NHN(10-17-10), (c) NHN(60-17-60), (d) NHN(157-17-157), and (e) NHN(180-17-180).

PHB is a crystalline polymer. With the incorporation of PNIPAAm, the crystallization of the PHB block is suppressed. When the length of the PNIPAAm block increased, the fractional crystallinity of the PHB block decreased. The melting transition corresponding to PHB segments shifted to lower temperature with lower crystallinity in comparison with that of their PHB-diBr precursors. The decreases in T_m and crystallinity are determined by the relative fractions of PHB segments in the copolymers. For example, the T_m and crystallinity of the PHB segment decrease

from 137.3 °C and 36.7% for NHN(10-17-10) to 124.3 °C and 10.7% for NHN(180-17-180), respectively. When the copolymers are cooled from the molten state, the PHB segment solidifies and crystallizes However, due to the interference of the PNIPAAm segment, the crystallization of the PHB segment is retarded.

Table 6.3. Transition temperatures, corresponding enthalpies, crystallinity for polymer samples, and their decomposition temperatures

Copolymer	T_m (°C)[a]	ΔH_m (J/g)[b]	X_c (%)[c]	T_d, PHB (°C)[d]	T_d, PNIPAAm (°C)[d]
PHB-diBr	142.2	62.5	42.6	236	-
NHN(10-17-10)	137.3	53.8	36.7	245	361
NHN(60-17-60)	135.6	32.8	22.4	285	365
NHN(157-17-157)	129.5	23.2	15.8	291	366
NHN(180-17-180)	124.3	10.7	7.3	292	368

[a] Melting point determined by DSC second heating run. For PHB-diBr having multipeak endotherm due to melting-recrystallization, the T_m value for the second peak is given. [b] Enthalpy change during melting determined by DSC second heating run. $\Delta H_m = \Delta H_i/w_i$, where ΔH_i is the area of the endothermic peak for PHB block read from Figure 6.9, and w_i is the weight fraction of the corresponding block. [c] Crystallinity calculated from melting enthalpies. Reference values of 146.6 J/g for completely crystallized PHB were used.[3] [d] Temperature at which the onset of thermal degradation occurred.

6.3.5. Thermoresponsive Behavior of Micelles.

The PNIPAAm-PHB-PNIPAAm triblock copolymer micelles were water-soluble at 25 °C with a hydrophobic PHB core and hydrophillic PNIPAAm corona. When the temperature of the solution is increased, the hydrophobicity of PNIPAAm increases and PNIPAAm chains in the micelle corona collapse. The increased hydrophobicity of the micelles leads to micelle aggregation, leading to the formation of larger particles. The thermosensitivity of the PNIPAAm-PHB-PNIPAAm triblock copolymer micelles was demonstrated by observing the change in the optical absorbance of a micellar solution as a function of temperature. PNIPAAm exhibits a

temperature sensitive phase transition in the temperature range of 32 to 33 ^{o}C. This temperature is known as the lower critical solution temperature (LCST).

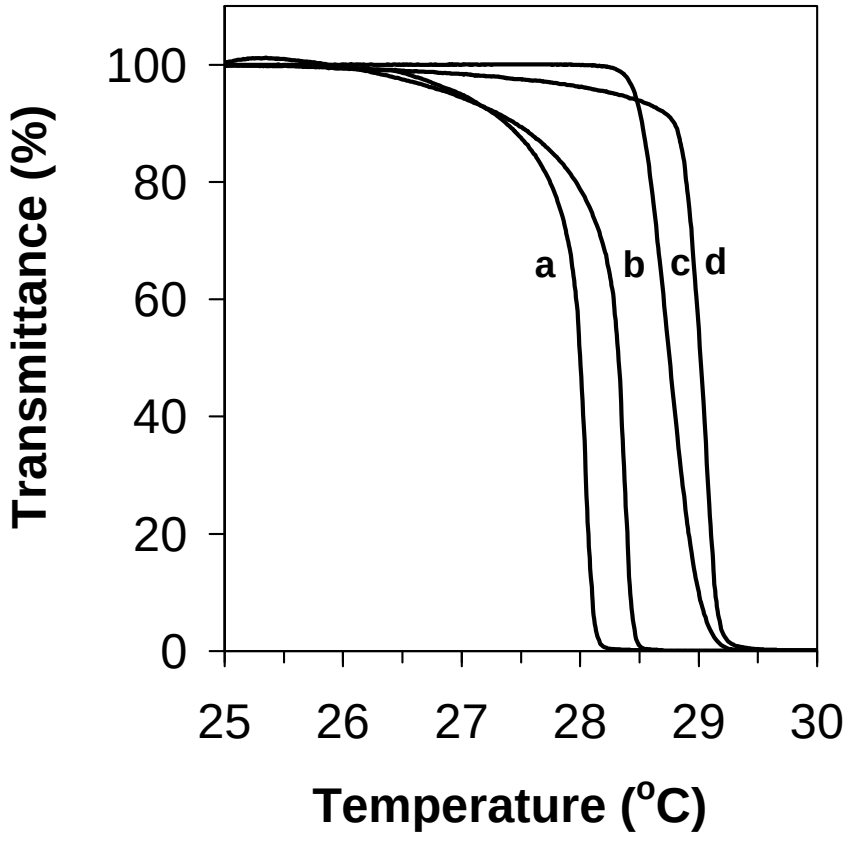

Figure 6.10. Thermoresponsive behavior of PNIPAAm-PHB-PNIPAAm micelles (0.5 mg/mL) (a) NHN(10-17-10), (b) NHN(60-17-60), (c) NHN(157-17-157), and (d) NHN(180-17-180).

The LCST values of the copolymers are presented in Table 6.2. At temperatures below LCST, PNIPAAm is a hydrophilic water-soluble polymer. Above this temperature, PNIPAAm becomes hydrophobic and precipitates out of the aqueous solution. In this thesis, the LCST is defined as the temperature exhibiting a 50% decrease in optical transmittance of an aqueous copolymer solution (0.5 mg/mL) at 500 nm (Figure 6.10). The incorporation of the hydrophobic PHB lowers the LCST compared to the PNIPAAm homopolymer. The copolymer NHN(10-17-

10) exhibits an LCST of 28.0 ^{o}C, on the other hand, the copolymer NHN(180-17-180) shows an LCST of 29.0 ^{o}C. In this work, the LCST values of the copolymers are expected to increase to a constant value with increasing PNIPAAm chain length. The changes observed in this case are due to the changes in the polymer/solvent interactions arising from the change in the hydrophillic/hydrophobic balance of the copolymers. For the PNIPAAm-PHB-PNIPAAm triblock copolymers, the copolymers become more hydrophilic as the PNIPAAm segments become longer, leading to the observed increase in the LCST. Overall, there is no significant change in the LCST values with the incorporation of the hydrophobic PHB segment. This is similar to previously reported studies on PNIPAAm-PCL-PNIPAAm and PCL-PNIPAAm-PCL copolymer micelles.[30,31] From this, it can be hypothesized that the thermosensitive PNIPAAm arms of the micelle behaves like free PNIPAAm in solution, except that it is anchored in a micelle structure by the hydrophobic PHB segments. PCL-PNIPAAm-PCL copolymer micelles showed no decrease in the LCST values upon incorporation of PCL into the copolymer. It was suggested that the copolymers form phase-separated core shell micelle structures in aqueous solution.[31]

The phenomenon of LCST is a complex process which is dependent on the concentration of the copolymer solution.[47] Thermoresponsive behavior of PNIPAAm, such as the coil-to-globule transition, was reported using dilute solutions.[48,49] Therefore for this study of the thermoresponsive behavior of the micelles, very dilute solutions, just slightly above the CMC value, were used. The scheme of the thermoresponsive micelle behavior of these copolymers in a dilute solution is illustrated in Figure 6.11a.

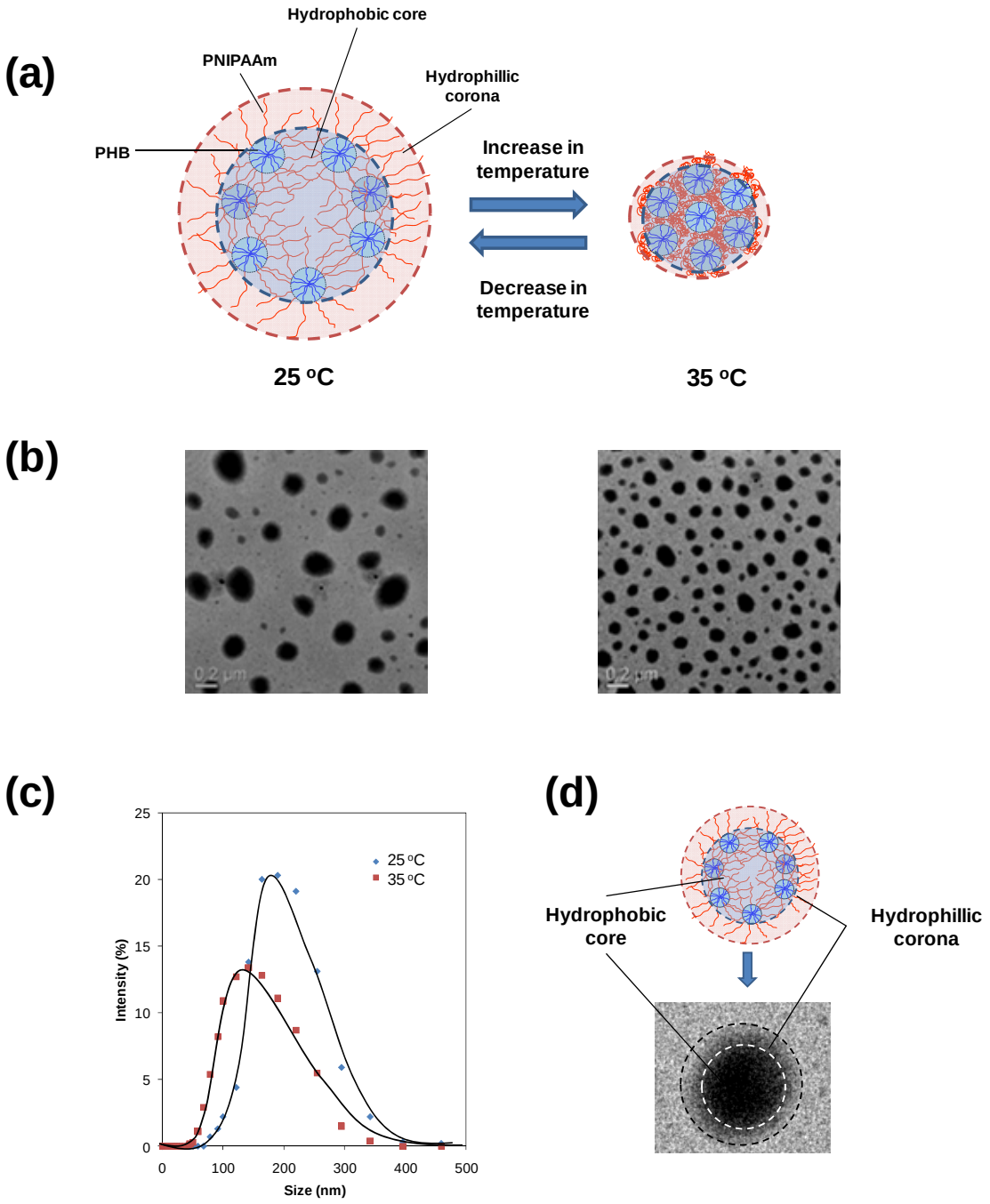

Figure 6.11. (a) Proposed thermoresponsive behavior of PNIPAAm-PHB-PNIPAAm triblock copolymers. (b) TEM micrographs of the NHN(180-17-180) micelles prepared at 25 °C and 35 °C. (c) Particle size distribution of NHN(180-17-180) micelles (Solution concentration = 50 mg/L) at 25 °C and 35 °C. (d) Schematic relation between the proposed structure of the micelle aggregates and the TEM-observed structure.

The morphology and size distribution of the copolymer micelles were investigated by TEM observation (Figure 6.11b), and dynamic light scattering (DLS) (Figure 6.11c), respectively. The schematic relation between the proposed structure of the micelle aggregates and the TEM-observed structure is shown in Figure 6.11d.The results of the DLS measurements are summarized in Table 6.2. From DLS measurements, these diameters of the micelles range from 290 nm to 840 nm, decreasing as the PNIPAAm segment becomes longer. This is an interesting observation. Normally, it is expected that with a longer PNIPAAM chain, the micelle size would increase with increasing micelle interaction with water. However, in this case, the reverse trend is observed. This was attributed to micelle aggregation. PHB is a very hydrophobic copolymer which has a very strong tendency to self-associate.[42] For the copolymers with higher PHB content, there is a great tendency for the PHB segments to associate in the aqueous environment. This observation corroborates with the partition coefficient of pyrene calculated in the earlier section, which showed that the PHB core is very hydrophobic. It is also pertinent to note that in this experiment, the samples were not filtered prior to measurements so that the pristine state of the dissolved copolymer could be analyzed. The contour length of the NHN(180-17-180) is calculated to be about 100 nm, with the PHB segment estimated to be about 8 nm and the PNIPAAm segment estimated to be about 96 nm. However, the observed particle size in the DLS experiment is 290 nm. Therefore, in this experiment, it is very likely that micelle aggregates are observed. When the temperature is increased to 35 ^{o}C, the particle size decreases due to the collapse of the PNIPAAm corona and increased hydrophobic interactions between the PHB cores, leading to an overall decrease in the aggregate size (Figure 6.11a). The diameters of the micelles range from 140 to 550 nm. Lower polydispersities were observed at this temperature. It should be noted that the initial PHB segment used is almost monodisperse, in terms of molecular weight. This observation is most likely caused by the collapse of the

PNIPAAm corona into the PHB core. The particle size remained constant at this temperature for at least 24 h, and did not form aggregates. The solutions were observed to be transparent and very faint blue in color. The micelles of this size are not expected to be readily cleared by renal filtration as inferred by previous in vivo studies.[33-35] The pore size of the glomerular basement membrane is about 3-5 nm, which is too small for the micelles to pass.[35] This allows for the prolonged circulation of the drug-loaded micelles in the system. After the drug cargo is released, the micelles will degrade hydrolytically. Upon complete degradation of the copolymer, only the monomers of D-3-hydroxybutyric acid and the undegraded PNIPAAm segments (molecular weight < 20,000 g/mol) should be left. These fragments can be easily removed by renal filtration.[33-35] The TEM micrographs of NHN(180-17-180) copolymer solution (50 mg/L) dried at 25 ^{o}C and 35 ^{o}C is shown in Figure 6.12. The results support the observations made with DLS. Larger spherical particles (ca. 200 nm) were observed for the sample dried at 25 ^{o}C whereas smaller particles (ca. 100 nm) were observed for the sample dried at 35 ^{o}C. In addition, it was observed that upon drying at 35 ^{o}C, the micelle aggregates were packed more densely, although large micron-sized particles were not observed. This is probably due to the concentration of the solution being too low.

The concentration effect on the aggregation behavior was further evaluated. LCST behavior has been reported to be dependent on the concentration of the solution.[47] When the concentration of the solution is high, there is a great decrease in the optical transmittance of the solution. However, when the concentration of the solution is low, the change in the optical transmitrance of the solution is not so obvious. For example, Fujishige[48] and Hirotsu[49] have reported the collapse of PNIPAAm chains at very dilute polymer concentrations based on light scattering experiments. At very low concentrations, no PNIPAAm aggregation is observed. TEM micrographs of NHN(180-17-180) copolymer solutions (50 mg/L and 500 mg/L) dried at 25 ^{o}C

and 35 ^{o}C are shown in Figure 6.12. Comparing both solutions at 25 ^{o}C, the 500 mg/L solution had slightly larger aggregates. Above the solution LCST, at 35 ^{o}C, the behavior is very different. While smaller dense particles were observed for the sample prepared at 50 mg/L and dried at 35 ^{o}C. Large patchy aggregates were observed for the sample prepared from the 500 mg/L solution and dried at 35 ^{o}C. When the concentration is sufficiently high, the increased temperature leads to the typical LCST behavior. This was demonstrated by the turbidity experiments described earlier. Large irregular aggregates, having sizes larger than 1 μm, are observed. This is similar to another report, in which PDLLA-PNIPAAm diblock copolymers were observed to undergo aggregation at temperatures above the LCST.[32]

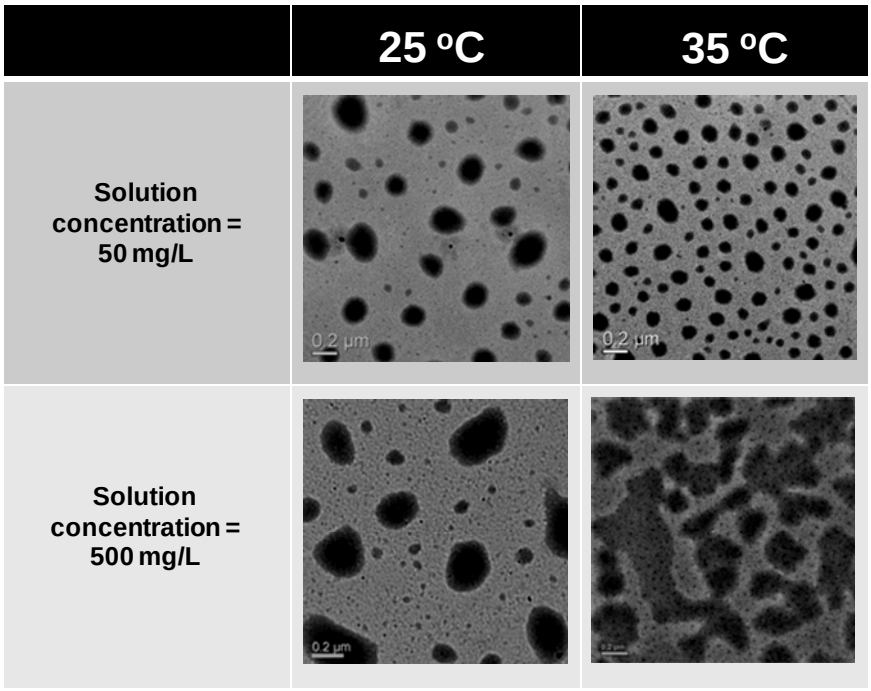

Figure 6.12. TEM micrographs of the NHN(180-17-180) micelles prepared at 25 ^{o}C and 35 ^{o}C at 50 mg/L and 500mg/L.

6.3.6. Cytotoxicity Study.

The cytotoxicity of the triblock copolymers was evaluated by incubating the mouse fibroblast L929 cells with different concentrations of the copolymer solution over a period of 48 h at 37 ^{o}C. The aim of this experiment is to determine the potential toxicological hazard of the copolymers. Quantification of the cytotoxic response was done using the MTT assay, shown in Figure 6.13. The copolymer solutions do not show significant cytotoxicity against L929 cells, over a solution concentration range of 2 – 500 mg/mL. Interestingly, the cell viability increased with increasing PNIPAAm content in the block copolymer. From the MTT assay results of the copolymers, the polymer is expected to be safe for biomedical applications.

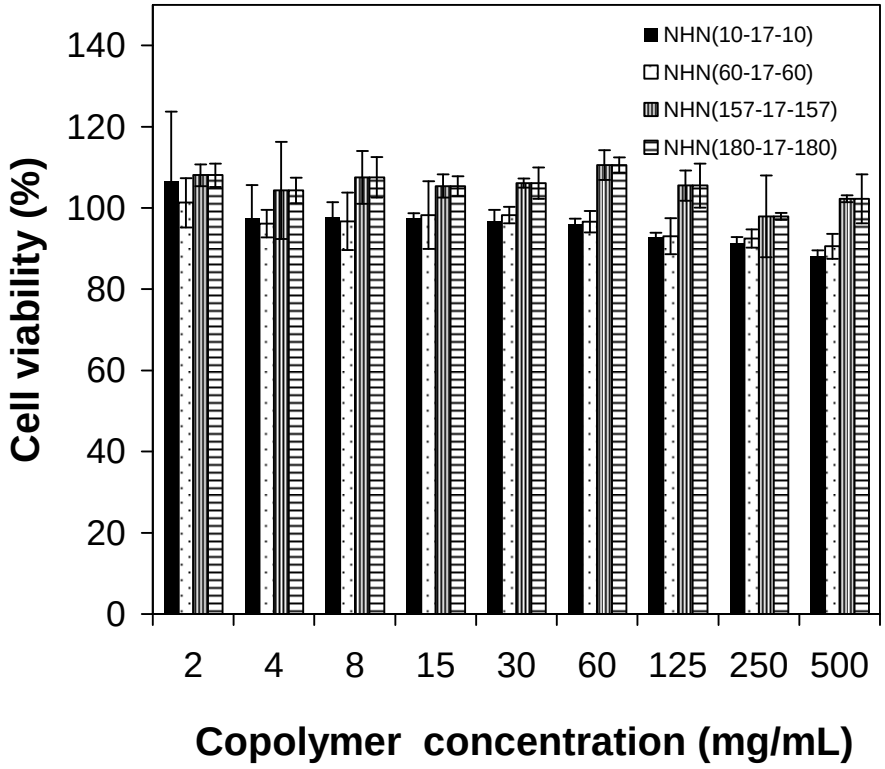

Figure 6.13. Cell viability of L929 cells incubated with known concentrations of PNIPAAm-PHB-PNIPAAm triblock copolymers.

6.4. Conclusions

Thermoresponsive triblock copolymers having two hydrophilic poly(N-isopropylacrylamide) blocks linked to a central hydrophobic poly[(*R*)-3-hydroxybutyrate] block were synthesized by atom transfer radical polymerization. Molecular characterizations of the copolymers were performed by GPC, NMR, TGA and DSC. The triblock copolymers formed micelles with a hydrophobic PHB core and a hydrophilic PNIPAAm shell as inferred from the ^{1}H and ^{13}C NMR spectra derived in two different environments ($CDCl_3$ and D_2O). The CMC of the triblock copolymers were very low and have great stability under high dilution conditions. The hydrophobicity of the micellar cores were estimated by measuring the partition equilibrium constant, K_v of pyrene in the micellar solution of the triblock copolymers. The high values of K_v indicate potential high encapsulation efficiency of hydrophobic drugs. The hydrophobicity of the micellar core could be controlled by adjusting the composition of the copolymer. The temperature sensitivity of the triblock copolymer micelles were studied by the turbimetry method. Preliminary cytotoxicity evaluation of the copolymers indicates that these copolymers are non-toxic. The exciting potential for this copolymer lies in its low critical micelle concentrations, the tunability of these loading capacities by varying its composition, and its potential biodegradability.

6.5. References

1. Torchilin, V. P. *J. Controlled Release* **2001,** *73*, 137-172.

2. Kwon, G. S.; Kataoka, K. *Adv. Drug Delivery Rev.* **1995,** *16*, 295-309.

3. Li, J.; Li, X.; Ni, X.; Leong, K. W. *Macromolecules* **2003,** *36*, 2661-2667.

4. Paria, S. *Adv. Colloid Interface Sci.* **2008,** *131*, 24-58.

5. Walker, L. M.; Kuntz, D. M. *Curr. Opin. Colloid & Interface Sci.* **2007**, *12*, 101-105.

6. Wang, Z. L. *Appl. Microbiol. Biotechnol.* **2007**, *75*, 1-10.

7. Fiamegos, Y. C.; Stalikas, C. D. *Anal. Chim. Acta* **2005**, *550*, 1-12.

8. Doi, Y., Steinbuchel, A., Eds.; *Biopolymers, Polyesters I-III*; Wiley: New York, 2001; Vols. 3, 3b, and 4.

9. Doi, Y. *Microbial Polyesters*; VCH Publishers: New York, 1990.

10. Anderson, A. J.; Dawes, E. A. *Microbiol. Rev.* **1990**, *54*, 450-472.

11. Dawes, E. A. *Novel Biodegradable Microbial Polymers*; Kluwer: Dordrecht, 1990.

12. Satkowski, M. M.; Melik, D. H.; Autran, J. P.; Green, P. R.; Noda, I.; Schechtman, L. A. In *Biopolymers*; Steinbuchel, A., Doi, Y., Eds.; Wiley-VCH: Wienheim, 2001; p 231.

13. Iwata, T.; Doi, Y. *Macromol. Chem. Phys.* **1999**, *200*, 2429-2442.

14. Purnell, M. P.; Petrasovits, L. A.; Nielsen, L. K.; Brumbley, S. M. *Plant Biotechnol. J.* **2007,** *5,* 173-184.

15. Reusch, R. N. *Can. J. Microbiol.* **1995**, *41*, 50-54.

16. Loh, X. J.; Goh, S. H.; Li, J. *Biomacromolecules* **2007,** *8*, 585-593.

17. Loh, X. J.; Goh, S. H.; Li, J. *Biomaterials* **2007,** *28*, 4113-4123.

18. Loh, X. J.; Li, J. *Expert Opin. Ther. Pat.* **2007,** *17*, 965-977.

19. Motokawa, R.; Morishita, K.; Koizumi, S.; Nakahira, T.; Annaka, M. *Macromolecules* **2005,** *38*, 5748-5760.

20. Kim, Y. C.; Kil, D. S.; Kim, J. C. *J. Appl. Polym. Sci.* **2006,** *101*, 1833-1841.

21. Wei, H.; Zhang, X. Z.; Cheng, C.; Cheng, S. X.; Zhuo, R. X. *Biomaterials* **2007,** *28*, 99-107.

22. Li, Y. Y.; Zhang, X. Z.; Cheng, H.; Kim, G. C.; Cheng, S. X.; Zhuo, R. X. *Biomacromolecules* **2006,** *7*, 2956-2960.

23. Wei, H.; Zhang, X. Z.; Cheng, H.; Chen, W. Q.; Cheng, S. X.; Zhuo, R. X. *J. Controlled Release* **2006,** *116*, 266-274.

24. Li, Y. Y.; Zhang, X. Z.; Kim, G. C.; Cheng, H.; Cheng, S. X.; Zhuo, R. X. *Small* **2006,** *2*, 917-923.

25. Kohori, F.; Sakai, K.; Aoyagi, T.; Yokoyama, M.; Yamato, M.; Sakurai, Y.; Okano, T. *Colloids Surf., B* **1999,** 16, 195-205.

26. Liu, S. Q.; Tong, Y. W.; Yang, Y. Y. *Biomaterials* **2005,** 26, 5064-5074.

27. Liu, S. Q.; Tong, Y. W.; Yang, Y. Y. *Mol. Biosyst.* **2005,** 1, 158-165.

28. Nakayama, M.; Okano, T.; Miyazaki, T.; Kohori, F.; Sakai, K.; Yokoyama, M. *J. Controlled Release* **2006,** 115, 46-56.

29. Li, Y. Y.; Zhang, X. Z.; Cheng, H.; Zhu, J. L.; Li, U. N.; Cheng, S. X.; Zhuo, R. X. *Nanotechnology* **2007**, 18, 505101.

30. Loh, X. J.; Wu, Y. L.; Seow, W. T. J.; Norimzan, M. N. I; Zhang, Z. X.; Xu, F. J.; Kang, E. T.; Neoh, K. G.; Li, J., *Polymer* **2008**, doi:10.1016/j.polymer.2008.08.061

31. Chang, C.; Wei, H.; Quan, C. Y.; Li, Y. Y.; Liu, J.; Wang, Z. C.; Cheng, S. X.; Zhang, X. Z.; Zhuo, R. X. *J.Polym. Sci. Part A-Polym. Chem.* **2008**, 46, 3048-3057.

32. Kohori, F.; Sakai, K.; Aoyagi, T.; Yokoyama, M.; Sakurai, Y.; Okano, T. *J. Controlled Release* **1998**, 55, 87-98.

33. Yamaoka, T.; Tabata, Y.; Ikada, Y. *J. Pharm. Sci.* **1994**, 83, 601-606.

34. Yamaoka, T.; Tabata, Y.; Ikada, Y. *J. Pharm. Sci.* **1995**, 84, 349-354.

35. Nakaoka, R.; Tabata, Y.; Yamaoka, T.; Ikada, Y. *J. Controlled Release* **1997**, 46, 253-261.

36. Jeong, B.; Bae, Y. H.; Kim, S. W. *Macromolecules* **1999**, *32*, 7064-7069.

37. Jeong, B.; Bae, Y. H.; Kim, S. W. *Colloids Surf., B* **1999**, *16*, 185-193.

38. Jeong, B.; Windisch, C. F., Jr.; Park, M. J.; Sohn, M. J.; Gutowska, A.; Char, K. *J. Phys. Chem. B* **2003**, *107*, 10032-10039.

39. Lee, B. H.; Lee, Y. M.; Sohn, Y. S.; Song, S. C. *Macromolecules* **2002**, *35*, 3876-3879.

40. Astafieva, I.; Zhong, X. F.; Eisenberg, A. *Macromolecules* **1993**, *26*, 7339-7352.

41. Wilhelm, M.; Zhao, C.; Wang, Y.; Xu, R.; Winnik, M. A.; Mura, J. L.; Riess, G.; Croucher, M. D. *Macromolecules* **1991**, *24*, 1033-1040.

42. Li, J.; Ni, X. P.; Li, X.; Tan, N. K.; Lim, C. T.; Ramakrishna, S.; Leong, K. W. *Langmuir* **2005**, *21*, 8681-8685.

43. Li, X.; Mya, K. Y.; Ni, X.; He, C.; Leong, K. W.; Li, J. *J. Phys. Chem. B* **2006**, *110*, 5920-5926.

44. Chang, Y.; Lee, S. C.; Him, K. T.; Him, C.; Reeves, S. D.; Allcock, H. R. *Macromolecules* **2001,** *34*, 269-274.

45. Allcock, H. R.; Cho, S. Y.; Steely, L. B. *Macromolecules* **2006,** *39*, 8334-8338.

46. Lee, S. C.; Chang, Y. K.; Yoon, J. S.; Kim, C. H.; Kwon, I. C.; Kim, Y. H.; Jeong, S. Y. *Macromolecules* **1999,** *32*, 1847-1852.

47. Xu, J.; Ye, J.; Liu, S. *Macromolecules* **2007,** *40*, 9103-9110.

48. Fujishige, S.; Kubota, K.; Ando, I. *J. Phys. Chem.* **1989**, *93*, 3311-3313

49. Yamamoto, I.; Iwasaki, K.; Hirotsu, S. *J. Phys. Soc. Jpn.* **1989,** *58*, 210-215

CHAPTER SEVEN

POLY(N-ISOPROPYLACRYLAMIDE)-POLY[(R)-3-HYDROXYBUTYRATE]-POLY(N-ISOPROPYLACRYLAMIDE) TRIBLOCK COPOLYMER SURFACE AS A CULTURE SUBSTRATE FOR HUMAN MESENCHYMAL STEM CELLS

7.1. Introduction

Poly(*N*-isopropylacrylamide) (PNIPAAm) is a popular thermally responsive polymer. PNIPAAm exhibits a lower critical solution temperature (LCST) of 32 to 33 °C, being hydrophilic at low temperatures and precipitating above the critical phase transition temperature.[1] This unique change in physical property has been exploited by researchers in the fabrication of thermally responsive surfaces for cell sheet engineering.[2-11] At a cell culture temperature above the LCST, the surface is hydrophobic and cells/tissues are attached to the substrate. When the temperature is lowered below the LCST, the surface becomes hydrophilic and the cells/tissues are detached from the surface. This mild technique of cell detachment preserves cell–cell and cell–extracellular matrix interactions, unlike the typical approach of using proteases, such as trypsin, to detach cells.[12-14]

In earlier reports, PNIPAAm was covalently grafted onto the cell culture substrate and some modifications were required to enhance the cell adhesiveness on PNIPAAm. Here, it was observed found that PHB-incorporated PNIPAAm, a triblock copolymer of poly(*N*-isopropylacrylamide)-poly[(*R*)-3-hydroxybutyrate]-poly(*N*-isopropylacrylamide) (PNIPAAm-PHB-PNIPAAm),[15] self-assembled on a tissue cell culture surface because PHB as a hydrophobic component serves to enhance the copolymer adsorption. Instead of using spin coating, which usually involves wasting large amounts of polymer during the coating process, drop-casting can be used to prepare homogeneous coatings. The chemical modification of natural PHB to water soluble and temperature-sensitive PHB-containing block copolymers was previously reported.[16-21] Extraction of PHB from genetically modified plants has also been reported.[22,23] In addition to biodegradability, PHB-based scaffolds were reported to be suitable for cell adhesion.[24-27] Therefore, PHB is considered applicable for biomedical use, such as tissue engineering scaffolds.

In this chapter, human mesenchymal stem cells (hMSCs) derived from human bone marrow, which have been extensively studied for their potential to differentiate into different connective tissue lineages of mesodermal-osteocyte, chondrocyte and adipocyte,[28-31] were cultured on the thermoresponsive surface. Cells proliferated on the surfaces and could be detached by cooling the substrate to low temperatures. The detached cells maintained their associated state and could be subsequently recultured, transplanted or used for differentiation protocols. For the transplantation of stem cells, trypsinization has usually been employed. However, it reduces the viability of sensitive cells such as stem cells over time.[32] To bypass the use of trypsin, a mild approach, known as cell sheet engineering, has been proposed.[33] By using a substrate that is surface modified with a thermally responsive polymer, the cultured hMSCs were nonenzymatically recovered.

7.2. Experimental Section

7.2.1. Materials

Poly(*N*-isopropylacrylamide)-poly[(*R*)-3-hydroxybutyrate]-poly(*N*-isopropylacrylamide) triblock copolymer was synthesized as described in Chapter 6. The molecular weight of the copolymer was determined by ^{1}H NMR to be 4.18×10^4 g/mol. The PHB content was 3.9 wt% and the PNIPAAm content was 96.1 wt%. The M_n of the copolymer is 3.77×10^4 g/mol and the PDI is 1.50. The LCST of the copolymer was 29.0 °C. The molecular weight of the PNIPAAm homopolymer was determined by ^{1}H NMR to be 4.0×10^4 g/mol. The M_n of the homopolymer is 3.13×10^4 g/mol and the PDI is 1.24. The LCST of PNIPAAm homopolymer was 33.0 °C. Thermanox™ coverslips (15 mm diameter) were purchased from Electron Microscopy Sciences (PA, U.S.A.) and used as the bare substrate. The cell culture medium used was Dulbecco

Minimum Essential Medium (DMEM) (low glucose) (Sigma-Aldrich) supplemented with 10% (vol/vol) fetal bovine serum (FBS) and 1% of 1X penicillin–streptomycin (Wako).

7.2.2. Coating of Substrate

Polymers were dissolved in deionized water at a concentration of between 0.0001 mg/mL and 1 mg/mL. 100 μL of polymer solution was dropped onto a bare substrate. The coverslip was left to dry overnight, sterilized by exposure to UV before cells were seeded onto them and then used as a cell culture substrate.

7.2.3. Illustration of Micelle Attachment on the Substrates

The illustration of the micelle attachment on the substrates was carried out with a simple coarse-grained model for the polymer chains. The calculations were performed on workstations belonging to the Institute of High Performance Computing, Singapore. The programming was done in Fortran, and the graphics were viewed with Diamond (version 3). The course-grained implicit solvent model could simulate the self-assembly of membranes without the need to explicitly simulate water molecules in the model. The effect of water resulting in the hydrophobic and hydrophilic interactions in the copolymer is implicitly considered in the interaction potentials between the polymer chains.[34] The molecular interaction of the polymers and water have been accounted for in the parameterization of this model. Previous simulation studies utilizing this model have been reported.[35, 36] One of these studies shows the assembly of phospholipid–DNA complexes.[35] Another paper reports the self-assembly of artificial viruses.[36] Here, this model was assessed to be suitable for the simulation of the micelles. In this simulation, the original model was modified to simulate the behavior of the polymer chains. Each polymer chain consists of a central hydrophobic segment and two hydrophilic segments at each end of the

polymer chain. All simulation parameters were derived and modified from the parameters obtained from Farago's work.[34]

7.2.4. Contact Angle Measurements

Contact angle measurements were performed with MilliQ water using the Dropmaster 500. The sample was placed on the stage of a CA-W Automatic Contact Angle Meter (Kyowa Interface Co. Ltd.), and a drop of water (0.1 μL) was placed on the sample surface. The static contact angle of the drop on the surface was measured after 2.5 s. At least 10 angles were measured at different areas and averaged.

7.2.5. Attenuated Total Reflectance – Fourier Transform Infra-Red (ATR-FTIR) Of Coated Substrates

ATR-FTIR measurements were performed using a Perkin Elmer FT-IR Spectrometer Spectrum 2000 to characterize the surface of the substrate. Substrates with polymer coating density of 5.66 $\mu g/cm^2$ were used for the stability studies. The substrates were soaked in 1 mL of water at 37 ^oC for 24 h. To further test the stability of the coatings, the substrates were washed. One washing cycle was performed by dipping and swirling the substrate in 10 mL of water at 22 ^oC for 5 times. The process was repeated 3 times, each time in fresh water. ATR-FTIR spectra of the substrates before and after the soaking were recorded. As a control, the bare Thermanox™ coverslip was used.

7.2.6. Thickness Measurements

A Digital Instruments MultiMode atomic force microscope with a Nanoscope IV controller in tapping mode was employed to image the copolymer coated substrate at its edges. All the atomic force microscopy (AFM) images were obtained with a scan rate of 1 Hz. Image

analysis was performed using Nanoscope software after removal of the background slope by flattening the images.

7.2.7. Human Mesenchymal Stem Cell (hMSC) Culture

Passaging Procedures. hMSCs used were the UE6E7T-12 cell line obtained from the JCRB (Japanese Collection of Research Biosciences) cell bank.[37] This hMSC line derived from bone marrow is immortalized by HPV E6, E7, and hTERT and was used in all of the cell culture studies. The hMSCs were cultured on tissue culture plates in supplemented DMEM and incubated at 37 °C in 5% CO_2 in humidified air. For maintenance of the hMSCs, cells were passaged every three days using 0.25% trypsin–1.0 mM EDTA. For the culture of hMSCs on the coated surfaces, three types of surfaces were tested. They were uncoated substrate surface, PNIPAAm-PHB-PNIPAAm copolymer and PNIPAAm homopolymer. For the copolymer and homopolymer coated surfaces, the coating density was 0.566 μg/cm^2.

Cytotoxicity Measurements. The cell viability was determined using the Dojindo Cell Counting Kit. Briefly, 100 μL of cell suspension (5000 cells/well) was dispensed into a 96-well plate. The plate was preincubated for 24 h at 37 °C in 5% CO_2 in humidified air. Following that, the medium was removed and 100 μL of polymer solution of different concentrations was added to the culture medium in the plate. The plate was incubated for a further 48 h before measurements were made using the kit.

Growth Curve Measurements. Cells were seeded at a cell density of 4×10^4 cells/dish in a 60 mm cell culture dish and incubated at 37 °C in 5% CO_2 in humidified air. At different time intervals, the cells were removed by trypsinization with 0.25% trypsin–1.0 mM EDTA and the cell number was measured using a hemocytometer. Three readings were taken and the results

were averaged. For the copolymer and homopolymer coated surfaces, the coating density was 0.566 μg/cm^2.

Cell Detachment Efficiency Determination. Cells were seeded at a cell density of 4 × 10^4 cells/dish in a 60 mm cell culture dish and incubated at 37 °C in 5% CO_2 in humidified air. At different time periods, the cells were detached by cooling. The detached cells were then centrifuged and washed with buffer solution. Following that, the buffer solution was removed and 0.5 mL of 0.25% trypsin was added to the cells and incubated at 37 °C in 5% CO_2 in humidified air for 3 min. The cells were suspended by pipetting several times and the detached cell numbers were counted using a hemocytometer. Cells that were undetached by the cooling process were trypsinized with 0.25% trypsin–1.0 mM EDTA and detached as per passaging procedures. The undetached cell numbers were counted by a hemocytometer. Six readings were taken and the results were averaged. For the copolymer and homopolymer coated surfaces, the coating density was 0.566 μg/cm^2.

7.3. Results and Discussion

7.3.1. Polymer Coating on Substrates

Water soluble thermo-responsive PNIPAAm-PHB-PNIPAAm triblock copolymers were prepared by ATRP as previously described in Chapter 6. The molecular weight of the copolymer used in this study is 4.18 x 10^{-4} g/mol. The critical micelle concentration of the copolymer is 41.1 mg/L. The LCST of the copolymer was 29 ^oC. As for the choice of coating, the copolymer with PHB content of 3.9 wt% was chosen, due to its excellent water solubility and also because the longer PNIPAAm chain segments would give rise to a greater thermal response. In this work, the thermal response is defined as the change in the contact angle of the surface when the

temperature of the substrate is changed. A later section discusses the thermal response of the coated substrates.

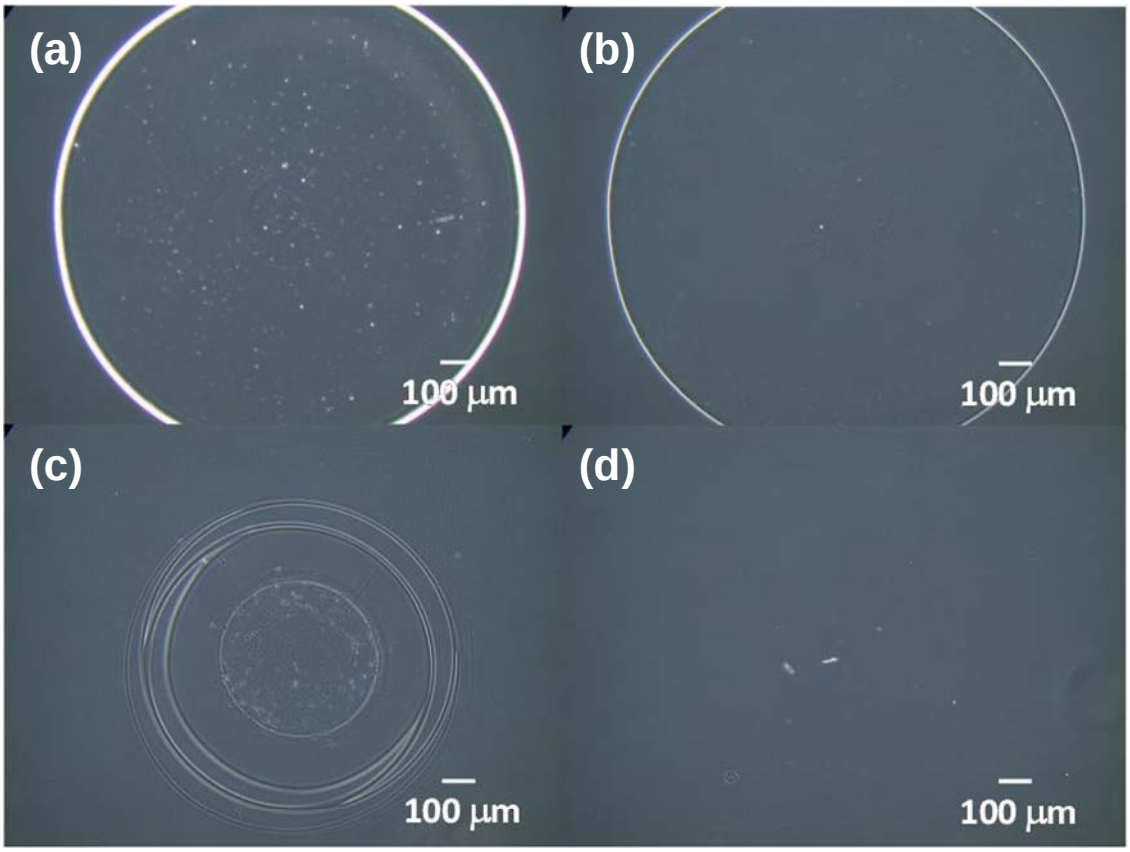

Figure 7.1. Phase contrast microscope images of PNIPAAm-PHB-PNIPAAm triblock copolymer coating (coating density = 5.66 μg/cm^2): a) before soaking in water at 37 °C, b) after soaking in water at 37 °C; PNIPAAm homopolymer coating (coating density = 5.66 μg/cm^2), c) before soaking in water at 37 °C, d) after soaking in water at 37 °C.

During the coating process at room temperature, it was noted that the PNIPAAm-PHB-PNIPAAm copolymer gave a more homogeneous coating than the PNIPAAm homopolymer (Figure 7.1). The interaction between the substrate surface and the polymer solution is an important factor that determines whether the polymer homogeneously coated the surface. In this case, the substrate is made of hydrophobic polyester. Under the coating conditions, PNIPAAm is below its LCST and behaves as a hydrophilic polymer. The homopolymer does not interact well

with the surface, and the coating does not adhere to the surface as the solution evaporates, apparently forming thick layers at the edges. On the other hand, the adsorption of the copolymer to the substrate surface was aided by the presence of the hydrophobic PHB segment, which helps in the adsorption of the copolymer by hydrophobic interactions.

Previously, Deegan *et al.* have sought the answer to the common observation of a "ring" stain observed when a spilled drop of coffee dries on a solid surface.[38] This phenomenon was explained by a form of capillary flow in which the liquid evaporating from the edge of the droplet was replaced by the liquid in the interior. Subsequently, a thick layer was observed at the edges, giving rise to the "ring" stain. This was observed in the case of the PNIPAAm coating. However, Deng *et al.* showed that transport at the air/water interface was responsible for the formation of "ring" stains in protein microarrays.[39] That work was focused on obtaining a homogeneous coating. The researchers obtained a homogeneous protein coating by adding surfactants to disrupt the protein molecules at the air/water interface, showing that the intermolecular forces between the water and protein are an important factor to consider when optimizing for a homogeneous coating.

In a polymeric micelle solution, there are three main forces to consider when considering the coating of a micelle on a substrate. They are micelle–substrate, micelle–micelle and water–micelle interactions. In the case of the PNIPAAm-PHB-PNIPAAm copolymer, the hydrophobic adhesion force provided by the central PHB segment is sufficient to ensure that when the solution evaporates, the polymer is not carried along in solution to the contact line at the edge. The micelle–substrate interaction dominated over the micelle–water interaction. With this, a homogeneous coating on the surface was obtained using the PNIPAAm-PHB-PNIPAAm copolymer. This coating technique is simple to perform with no loss of samples, a problem that

is commonly associated with spin coating. Accurate coating density can be applied on the coverslips by adjusting the concentration of the coating solution.

In this study, the density of the coated copolymers was varied in the range of 5.66×10^{-3} to 56.6 μg/cm^2. The main advantage of using the PNIPAAm-PHB-PNIPAAm copolymer coating was the stability under high dilution conditions when compared with the PNIPAAm homopolymer coating. PNIPAAm-PHB-PNIPAAm copolymers have very low critical micelle concentrations, as described in Chapter 6. These micelles are stable under high dilution conditions. The stability of the coating resulted from the association of the micelles with the substrate surface via the hydrophobic core. In the case of the homopolymer, there is no such association, and it appears that even though PNIPAAm is hydrophobic at 37 °C, it is not sufficiently hydrophobic to anchor the polymer to the substrate surface. From the images in Figure 7.1, it was observed that after soaking in 1 mL of water at 37 ^{o}C for 30 min, the PNIPAAm coatings were washed away whereas the PNIPAAm-PHB-PNIPAAm coatings remained on the substrate.

The stability of the copolymer coating on the surface was evaluated by checking for the presence of the copolymer on the substrate before and after soaking in water at 37 ^{o}C. This was done by using ATR-FTIR. As can be seen in Figure 7.2, the bare Thermonox^{TM} coverslip shows a characteristic peak at 1720 cm^{-1}, which is attributed to the carbonyl peak of the polyester moiety present in the coverslip. When the substrate is coated with either the PNIPAAm-PHB-PNIPAAm copolymer or the PNIPAAm homopolymer, the characteristic peaks of the PNIPAAm segment can be observed at 1650 cm^{-1} (for amide I) and 1530 cm^{-1} (for amide II). When the polymer-coated substrates were immersed in water at 37 ^{o}C for 24 h and taken for surface

characterization, it was observed that the PNIPAAm-PHB-PNIPAAm coated substrate showed a similar spectrum as the one obtained from the substrate before soaking in water.

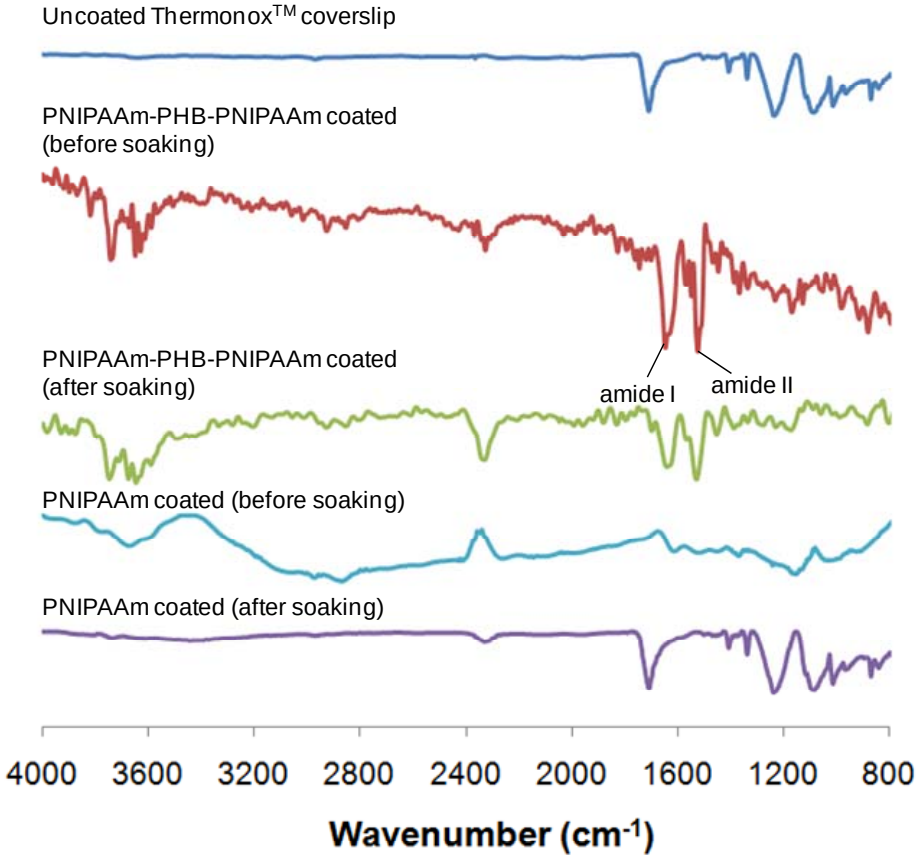

Figure 7.2. ATR-FTIR spectra of the polymer-coated substrates before/after soaking in water at 37 ^{o}C.

On the other hand, for the PNIPAAm coated substrate, after 24 h of soaking in water the FTIR peaks corresponding to amide I and II cannot be observed. Instead, it was observed that a spectrum that is very similar to the bare uncoated Thermonox™ surface was obtained. This indicates that the PNIPAAm-PHB-PNIPAAm copolymer coating is more stable than the PNIPAAm coating when incubated in water at 37 ^{o}C. After the washing treatment, a gravimetric analysis was performed on the substrates to determine the mass of polymer that remains on the substrate. It was observed that for the PNIPAAm-PHB-PNIPAAm copolymer coated substrate (coated at a density of 56.6 μg/cm^2), 90.7 ± 5.8 % of the copolymer mass remained where as for

the PNIPAAm homopolymer coated substrate, only 12.3 ± 6.8 % of the homopolymer mass remained. This shows the enhanced stability of the copolymer coating compared to the homopolymer.

To support the experimental observations, molecular dynamics simulations with a simple coarse-grained implicit-solvent model for the polymer chains was carried out. The coarse-grained implicit-solvent model was previously proven to yield the self-assembly of a membrane.[34] This implicit-solvent model was designed to capture the interaction of the hydrophobic and hydrophilic parts of a polymer without the need to include water molecules in the simulation. A thorough treatment of the model was provided by Farago.[34] In this copolymer, the central hydrophobic core is flanked by two hydrophilic segments. In the simulation, Farago's model was modified to simulate actual PNIPAAm-PHB-PNIPAAm copolymer chains, each with three segments of equal length, consisting of a hydrophobic central segment and two hydrophilic segments, one at each end. Each polymer chain was modeled as 12 spheres or 42 spheres, and each sphere had a diameter of 10 nm tethered by bonds with pair interactions that implicitly account for the hydrophobic effect. For the 12-sphere model (Figure 7.3a), the hydrophilic–hydrophobic–hydrophilic ratio was 4:4:4 (hydrophobic segment % = 33.3%), whereas for the 42-sphere model, the hydrophilic–hydrophobic–hydrophilic ratio was 20:2:20 (hydrophobic segment % = 4.8%). Both models showed the self-assembly of micelles that subsequently deposited on the substrates. For ease of representation of the adhesion of the micelles, the 12-sphere model is presented in Figure 7.3. The blue spheres represent the hydrophilic segments, and the red spheres represent the hydrophobic segments. In these simulations, the polymer strands were initially arranged randomly. After equilibrium was reached, the polymer chains self-assemble to form micelles with a hydrophobic core (in red) and a hydrophilic corona (in blue) (Figure 7.3b).

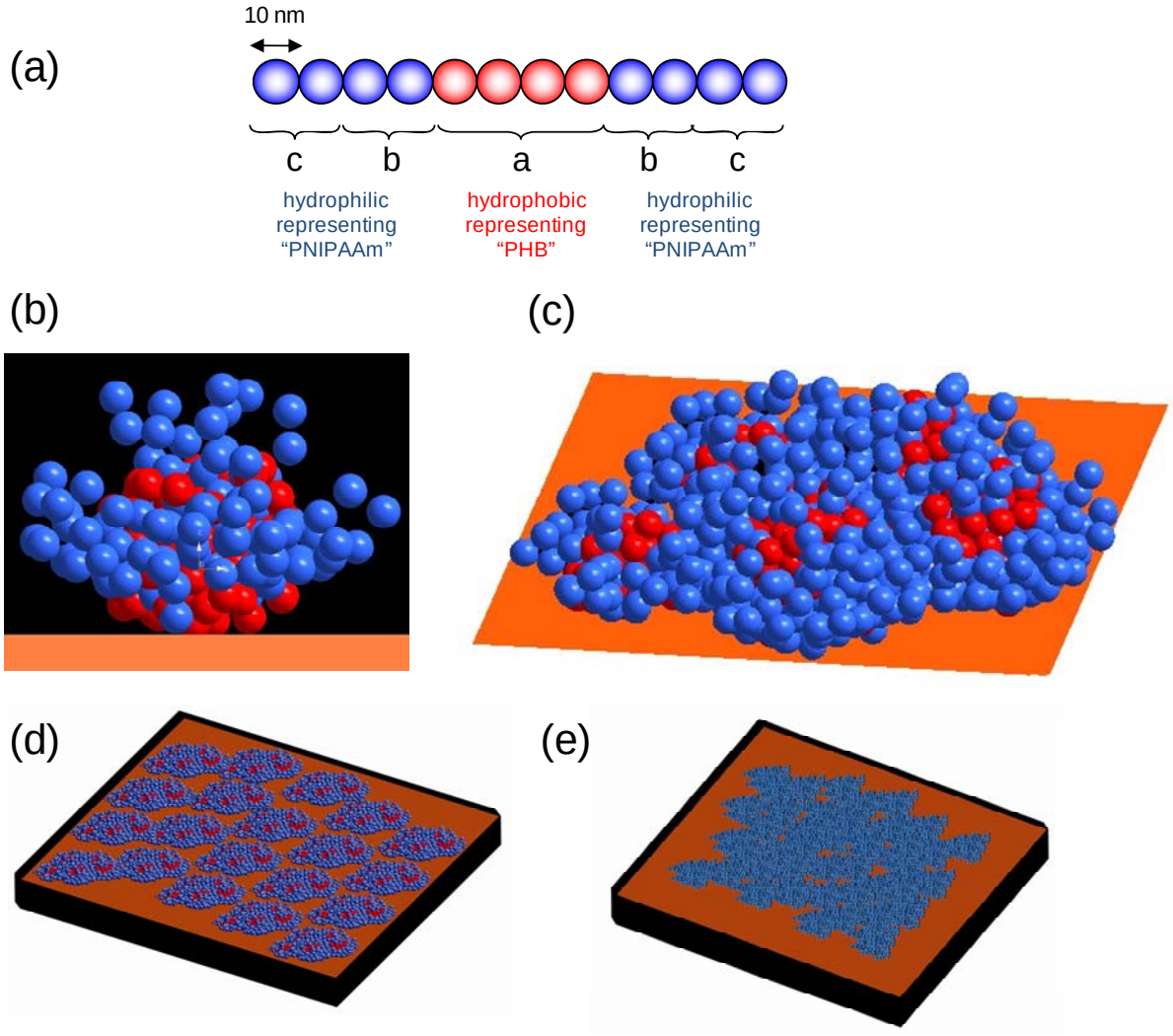

Figure 7.3. Molecular dynamics simulated self-assembly of amphiphilic polymers on a hydrophobic substrate surface. The blue spheres represent the hydrophilic component of the copolymer, and the red spheres represent the hydrophobic component of the copolymer. (a) Model 12-sphere polymer chain used in the simulation, (b) representation of the adhesion of a single micelle on the substrate, (c) representation of the adhesion of a micelle cluster on the substrate, (d) representation of the copolymer coating on the substrate using the 12-sphere model, (e) representation of the copolymer coating on the substrate using the 42-sphere model.

This is consistent with the structure suggested by experimental observations using pyrene probes and NMR studies.[15] When the micelles are brought near a hydrophobic substrate surface, it was observed from the simulation that the micelles deposit and coat the substrate surface.

Figure 7.3b shows a single micelle deposited on the substrate surface. According to the simulation, the micelle assembles itself such that it is shaped like a shuttlecock, with the hydrophobic core assembled in a manner resembling the base of the shuttlecock and the hydrophilic segments outstretched like the feathers of the shuttlecock. The base is anchored to the substrate by hydrophobic interactions. When the simulated polymer chain is made entirely of hydrophilic segments, no substrate attachment was observed. This shows that the hydrophobic core is vital for stable micelle attachment to the substrate. Figure 7.3c shows the deposition of a micellar cluster (with five micelles) on the substrate surface. The micelle cluster is anchored to the surface by the red hydrophobic cores. The hydrophilic segments were found to be entangled, resulting in a surface that is covered almost entirely by the hydrophilic (PNIPAAm) segments. In the actual experiments, there will be single micelles and micellar clusters in solution.[15] However, as the solution evaporates, micelle aggregates will be formed on the surface. Finally, in Figure 7.3d, a representation of the copolymer coating on the substrate is shown. This image shows the micelle clusters coated on the surface of the substrate. In so doing, the surface properties of the substrate are modified and now take on the characteristic of the hydrophilic (PNIPAAm) segments. The representation of the surface coating with the 42-sphere model is shown in Figure 7.3e. Farago's model has been shown to reproduce the three-dimensional structure of the self-assembled lipid–DNA complexes.[35,40,41] By using this implicit-solvent model, complex macromolecular problems can be simulated with less computational resources, and the images generated allow us to gain a qualitative understanding of the processes occurring at the surface molecular level.

Surface hydrophilicity of the coated substrate was evaluated by contact angle measurements. For the bare substrate, the contact angle of a water droplet was measured to be 68.2° ± 1.9° at 37 °C. Any thermal response was observed in its hydrophilicity when cooled to 4

°C. For the PNIPAAm-PHB-PNIPAAm copolymer-coated and the PNIPAAm homopolymer-coated substrate, a change in the hydrophilicity was observed upon cooling. PNIPAAm-PHB-PNIPAAm copolymer coated at a density of 5.66 μg/cm^2 showed a change in the contact angle from 66.1° ± 2.3° at 37 °C to 29.0° ± 3.7° at 4 °C. PNIPAAm homopolymer coated at a density of 5.66 μg/cm^2 showed a change in the contact angle from 57.5° ± 6.5° at 37 °C to 33.1° ± 6.0° at 4 °C. The change in the contact angle of the PNIPAAm-PHB-PNIPAAm coating upon exposure to lower temperature was 37.1°, whereas that of the PNIPAAm coating was 24.4°. The reduced thermal response of the PNIPAAm surface, compared with the PNIPAAm-PHB-PNIPAAm surface, could indicate that the PNIPAAm surface was less homogeneously coated compared with the PNIPAAm-PHB-PNIPAAm surface. The main difference between the two coatings was observed after being soaked in water at 37 °C for 24 h. After the soaking treatment, the PNIPAAm-PHB-PNIPAAm copolymer coating showed a change in the contact angle from 61.9° ± 1.9° at 37 °C to 22.1° ± 6.0° at 4 °C. The PNIPAAm homopolymer coating showed a change in the contact angle from 62.5° ± 1.6° at 37 °C to 56.7° ± 5.2° at 4 °C. Comparing Figures 7.4a and 7.4b, it was observed that the thermal response of the PNIPAAm-PHB-PNIPAAm coating did not significantly change after soaking in water at 37 °C. The slight loss in thermal response could be due to polymer loss from the substrate. However, the PNIPAAm coating lost its ability to respond thermally after the soaking treatment (Figures 7.4c and 7.4d). These results indicate that the PNIPAAm-PHB-PNIPAAm copolymer coating remained on the substrate whereas the PNIPAAm homopolymer coating dissolved, and that the PNIPAAm-PHB-PNIPAAm coating was more stable than the PNIPAAm coating.

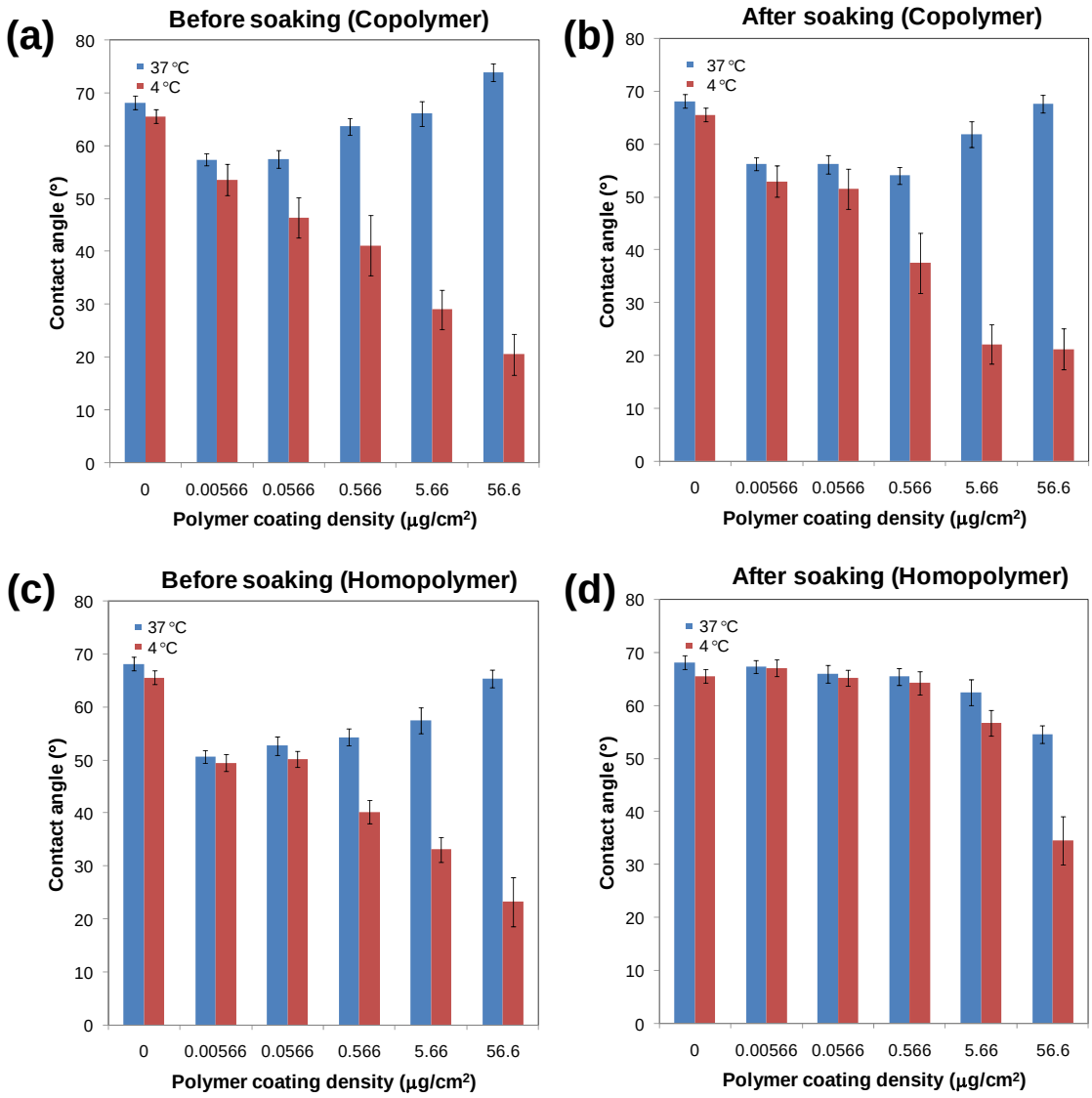

Figure 7.4. a) Effect of coating density on the thermal response of the PNIPAAm-PHB-PNIPAAm surface, b) effect of soaking treatment in water at 37 °C on the thermal response of the PNIPAAm-PHB-PNIPAAm surface, c) effect of coating density on the thermal response of the PNIPAAm surface, d) effect of soaking treatment in water at 37 °C on the thermal response of the PNIPAAm surface.

7.3.2. hMSC Culture on Coated Substrates

The cytotoxicity of the copolymer and homopolymer was tested against the hMSCs (Figure 7.5). The polymers showed no toxicity against hMSCs. The cell viabilities of hMSCs

were in the range of 90% for the concentrations tested up to 2 mg/mL. Therefore, even if the polymers are dissolved in the culture medium, it would not cause toxicity problems to the detached cell suspensions.

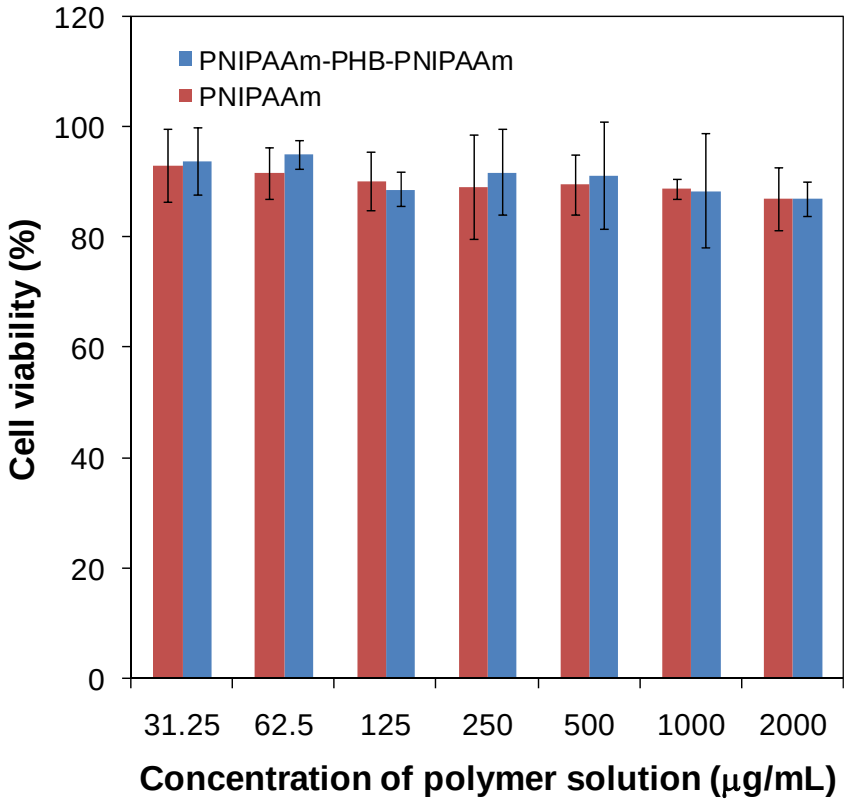

Figure 7.5. Cell viability of hMSCs cultured in the presence of PNIPAAm homopolymer and PNIPAAm-PHB-PNIPAAm copolymer of different concentrations.

The cells were cultured on the surfaces with different coating amounts of PNIPAAm-PHB-PNIPAAm copolymer, as shown in Figure 7.6. Under this condition, the cells grew and adopted a fibroblastic morphology, which was very similar to the morphology observed when the cells are cultured on uncoated substrate. When the copolymer coating density was 566 $\mu g/cm^2$, round cells were observed after three days of culture. On the other hand, the thermal

response decreased when the coating amount became less. Therefore, substrates with coating densities of 0.566 μg/cm^2 was used for these cell culture studies.

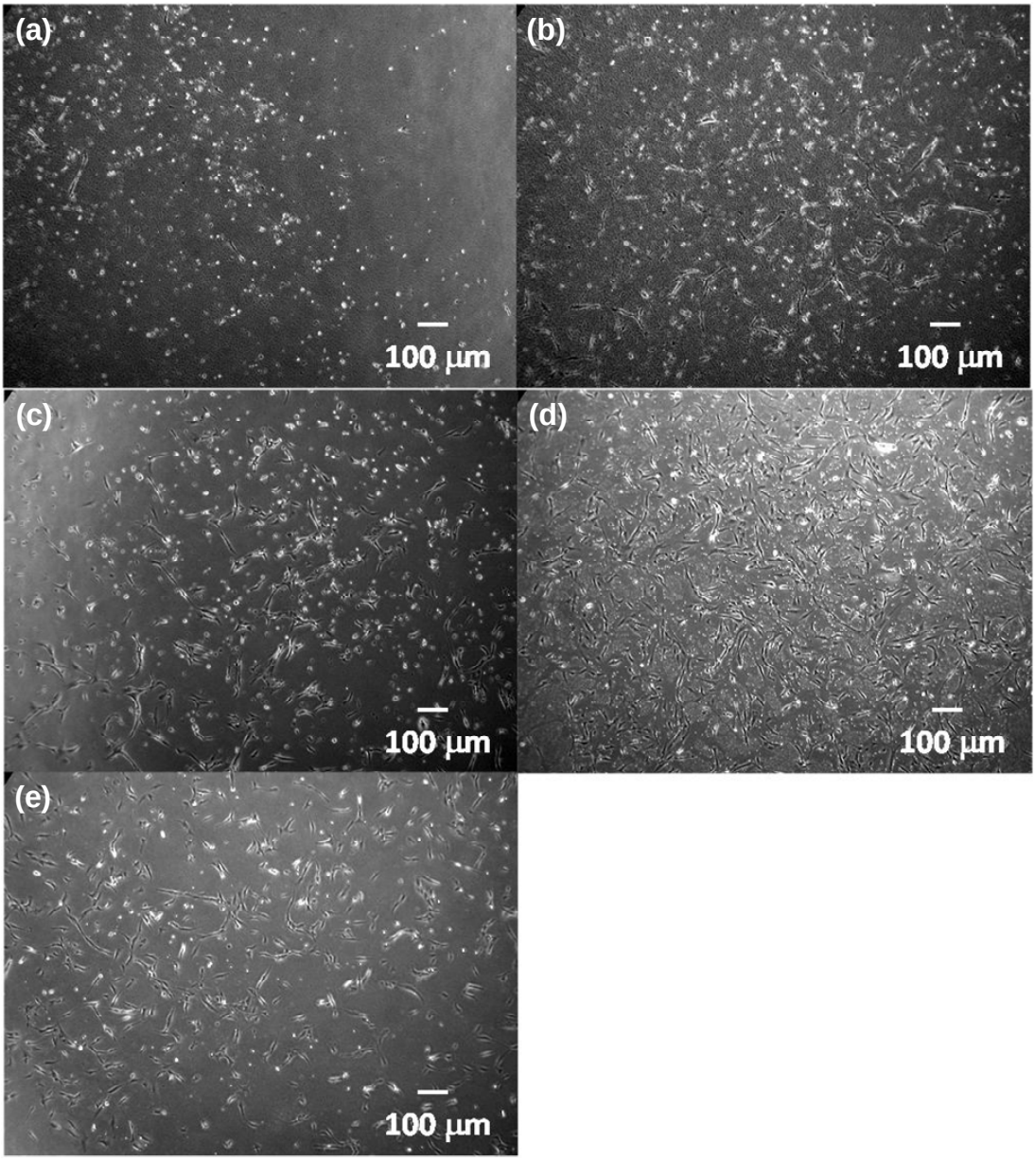

Figure 7.6. Morphology of hMSCs cultured on PNIPAAm-PHB-PNIPAAm surfaces of different thicknesses: a) 566 μg/cm^2, b) 56.6 μg/cm^2, c) 5.66 μg/cm^2, d) 0.566 μg/cm^2, e) uncoated substrate control.

Assuming that the density of the copolymer is 1 to 1.1 g/cm^3, the calculated thickness of the layer used for cell culture studies is about 5 nm. By performing AFM imaging on a copolymer coated substrate, a surface coating thickness of ~ 4-8 nm was observed. (Figure 7.7)

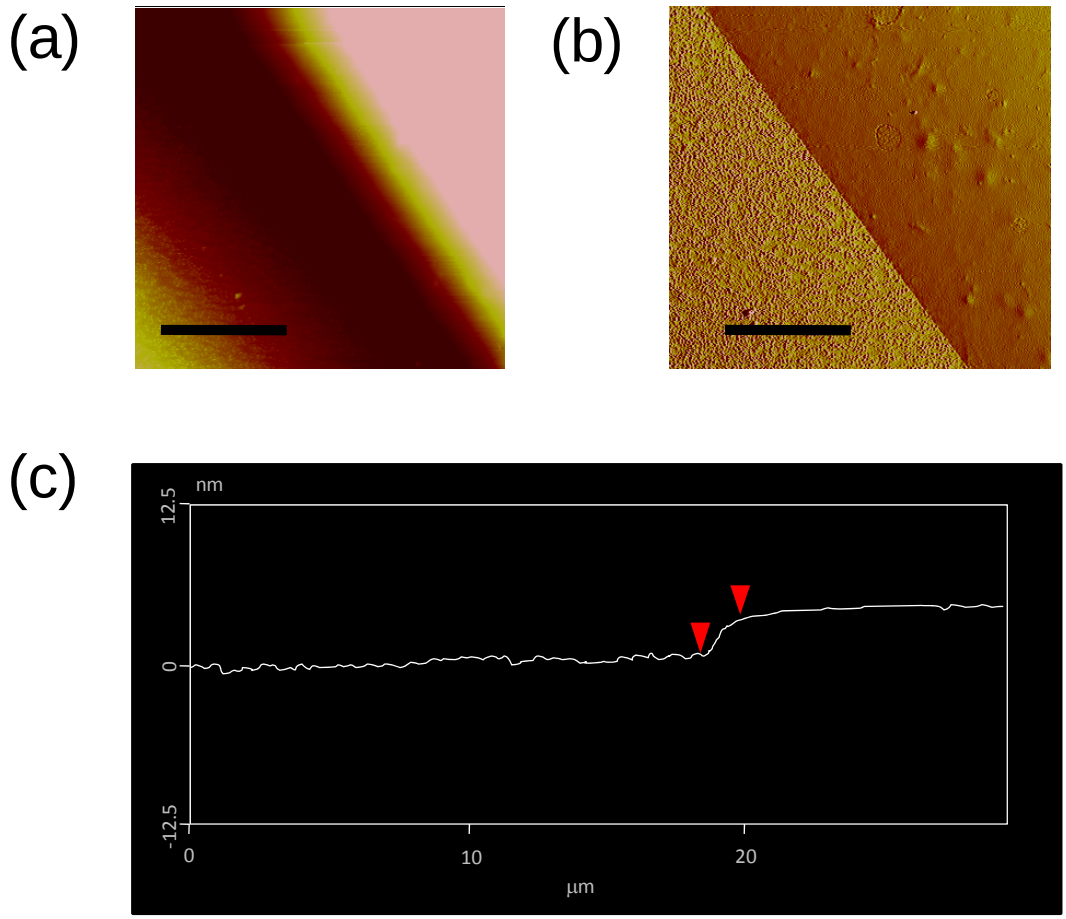

Figure 7.7. AFM micrographs of the copolymer coated substrate used for cell culture (polymer coating density = 0.566 µg/cm^2). Scale bar corresponds to 5 µm. The smooth surface observed on the right side of the image is the copolymer coating. The rough surface on the left side of the image is the surface of the uncoated substrate. (a) Height image of the edge of the coating, (b) Amplitude image of the edge of the coating. (c) Section profile of the image.

Figure 7.8 shows the growth of hMSC on different surfaces over a period of four days. Although there was a lag period, from the second day onward, the cell growth rate proceeded at an exponential rate, with a population doubling time of about 24 h. After the fourth day, the cells

reached confluence and the growth rate of the cells tapered off. The growth rate was found to be in the following order: PNIPAAm-PHB-PNIPAAm > uncoated substrate > PNIPAAm homopolymer. Incorporation of the PHB segment significantly increased the cell proliferation rate of the hMSCs, even outperforming the uncoated substrate in this aspect.

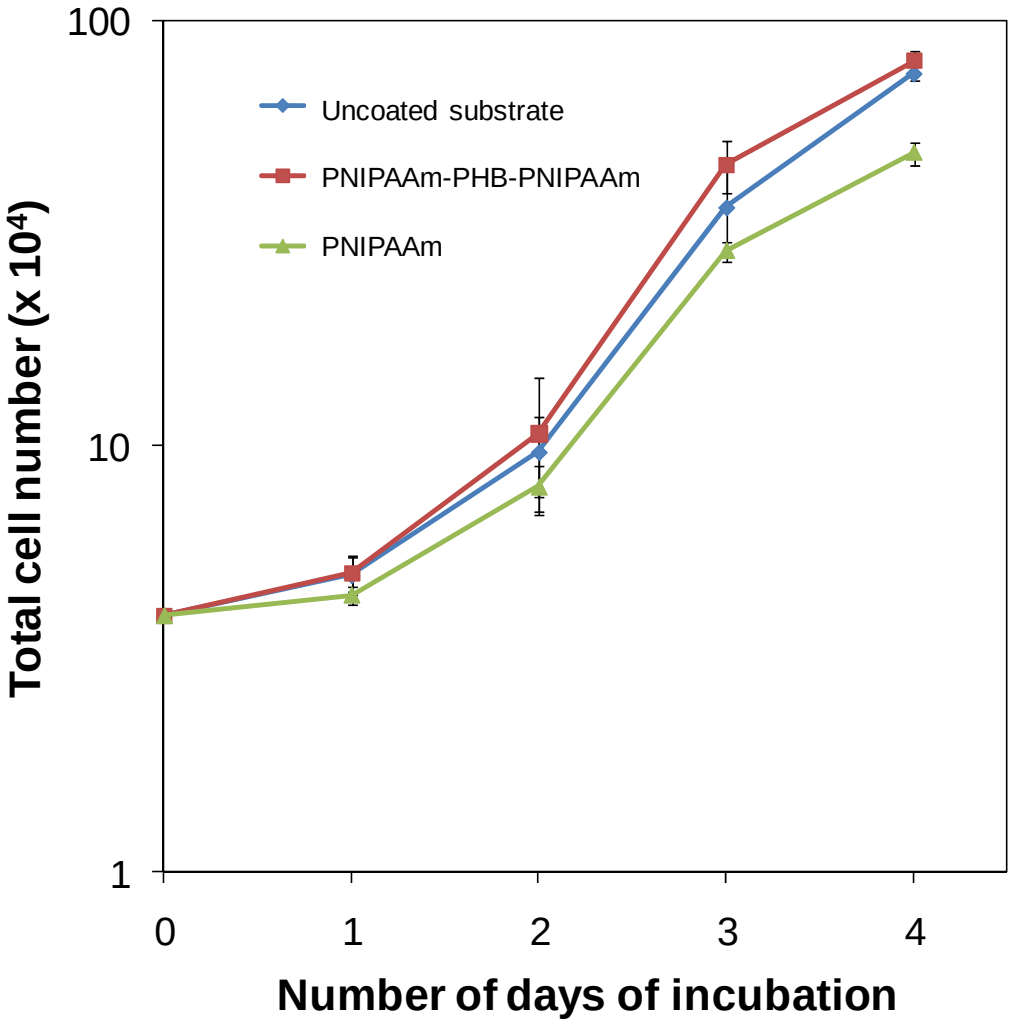

Figure 7.8. Growth curve of hMSCs cultured on three different surfaces (polymer coating density = 0.566 μg/cm^2).

Chen *et al.* have shown that mouse fibroblast cells cultured on polyhydroxyalkanoate-based scaffolds have high adhesivity as well as excellent viability.[24] MC3T3-E1 osteoblasts

cultured on poly(3-hydroxybutyrate-co-3-hydroxyhexanoate) (PHBHHx) films exhibited varying degrees of cell viability and cell adhesion.[25] It was further found that by incorporating hydrophilic components into the blend mixture, the cell viability and adhesion can be enhanced. Films of PHB and PHBHHx have also been shown to support the growth of osteoblasts and fibroblasts much more effectively than poly(lactic acid) scaffolds.[26]

7.3.3. Thermally Induced hMSC Detachment from Coated Substrates

Cell detachment from the thermoresponsive surface was performed on the hMSCs by incubating the copolymer-coated surface at 4 °C for a period of 20 min. Figure 7.9 shows detachment of the cultured cell from the PNIPAAm-PHB-PNIPAAm surface by cooling. As the PNIPAAm-PHB-PNIPAAm surface was cooled, it became hydrophilic and cell adhesion to the surface became weak. The cells were almost completely detached after 20 min. It can be noted that upon detachment, the cells tended to clump up into cell clusters. On the other hand, cells grown on the noncoated substrate surface were not detached after being incubated at 4 °C for a period of 20 min. The cell detachment numbers were evaluated as shown in Figure 7.10. For the PNIPAAm-PHB-PNIPAAm, almost all of the cells were detached by this method, and the cell detachment number was more than three times that for the PNIPAAm surface. This phenomenon was considered to be caused by the heterogeneous coating that results in a smaller area of substrate being coated with PNIPAAm. As shown in the previous section, the coated PNIPAAm dissolved upon contact with an aqueous solution. Therefore, on the homopolymer-coated surface, some cells may grow on the bare substrate while others grow on the PNIPAAm-coated surface.

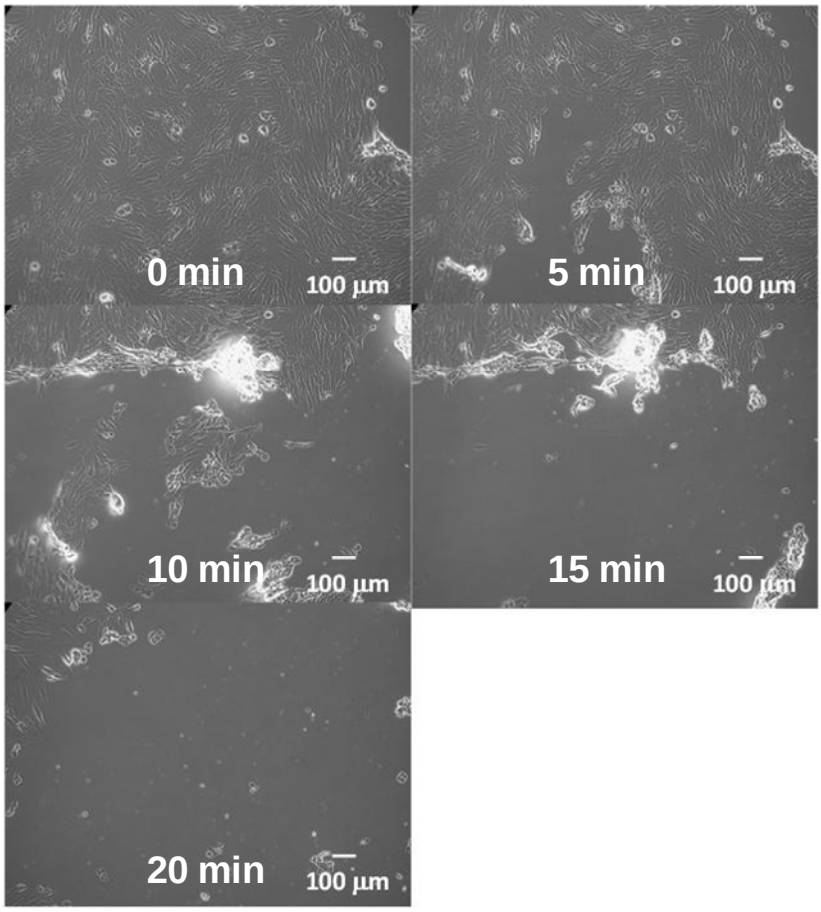

Figure 7.9. Temperature-induced hMSC detachment demonstrated on a PNIPAAm-PHB-PNIPAAm surface (polymer coating density = 0.566 µg/cm^2).

Finally, the thermally detached cells were recovered and compared with those that were obtained by typical trypsin harvesting methods. Figure 7.11 shows the morphology of the cells after one day of culture. The thermally detached cells showed strong intercellular associations and readhered to the tissue culture plates as a sheet of cells. On the other hand, after trypsinization, the cells were suspended and seeded as single cells. This reduced the intercellular connections, and the cells were observed to be growing as isolated cells. This shows that this technique of harvesting the hMSCs by thermal modulation is successful and could be applied to the culture of hMSCs. This technique offers rapid culture and detachment characteristics that would be useful in the culture of hMSCs for future clinical applications.

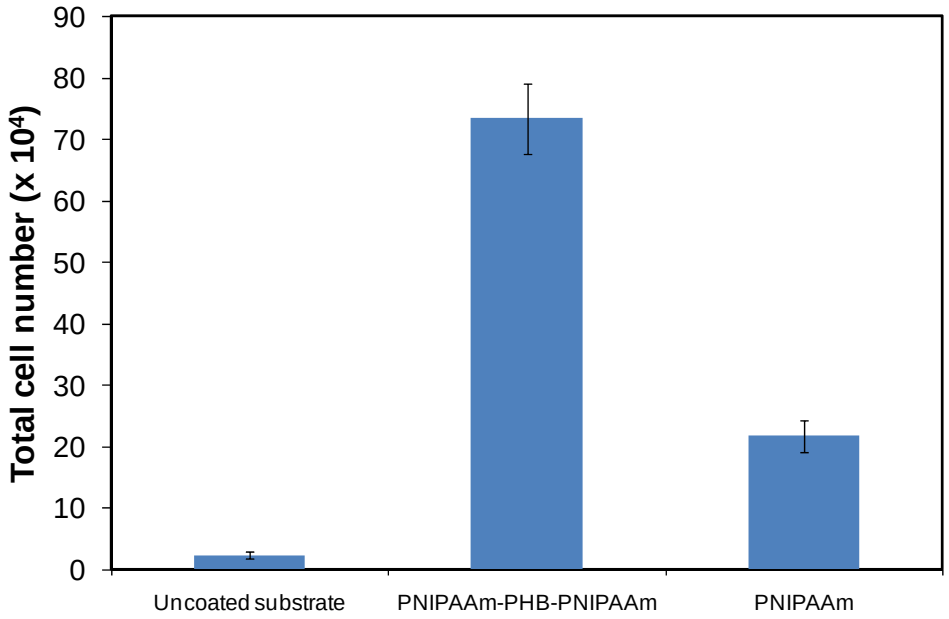

Figure 7.10. Cell detachment number of hMSCs cultured on different surfaces (polymer coating density = 0.566 μg/cm^2).

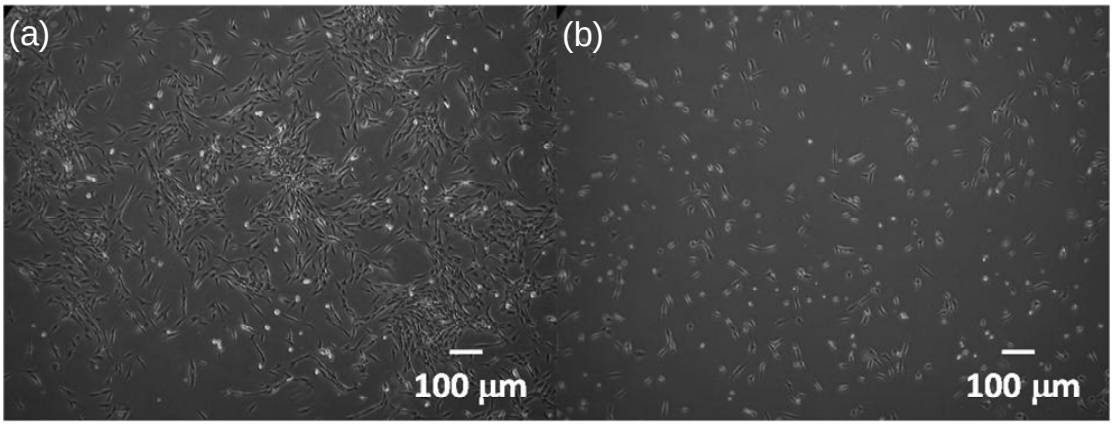

Figure 7.11. (a) Detached hMSCs from PNIPAAm-PHB-PNIPAAm surfaces, replated on tissue culture surface after one day of culture. (b) hMSCs harvested using typical trypsinization methods after one day of culture.

7.4. Conclusions

A thermoresponsive amphiphilic PNIPAAm-PHB-PNIPAAm triblock copolymer was used to coat a substrate. This copolymer offered homogeneous coating as well as excellent stem

cell growth and adhesion characteristics. The stability of the coatings before and after soaking in water was evaluated by ATR-FTIR. Farago's implicit-solvent model of macromolecular self-assembly was used to illustrate the deposition of the copolymer micelles on the substrate. The thermal response was modulated by the coating thickness, with the maximal response obtained when the layer was at its thickest. An optimal coating density for the copolymer was determined. These coated substrates had a thermoresponsive nature; they were hydrophobic at higher temperatures, and they became hydrophilic when cooled to lower temperatures. This allowed for the detachment of the cultured cells from the substrate at lower temperatures without using typical enzymatic methods. This technique allows for the harvesting and replating of entire cell sheets, bypassing the need for the use of trypsin in the cell harvesting process. This will save valuable time in the cell culture process, which could have important implications in clinical applications.

7.5. References

1. Xia, Y.; Yin, X. C.; Burke, N. A. D.; Stover, H. D. H. *Macromolecules* **2005,** 38, (14), 5937-5943.
2. Akiyama, Y.; Kikuchi, A.; Yamato, M.; Okano, T. *Langmuir* **2004,** 20, (13), 5506-5511.
3. Hirose, M.; Kwon, O. H.; Yamato, M.; Kikuchi, A.; Okano, T. *Biomacromolecules* **2000**, 1, (3), 377-381.
4. Okano, T.; Yamada, N.; Okuhara, M.; Sakai, H.; Sakurai, Y. *Biomaterials* **1995**, 16, (4), 297-303.
5. Okano, T.; Yamada, N.; Sakai, H.; Sakurai, Y. *Journal of Biomedical Materials Research* **1993**, 27, (10), 1243-1251.

6. Yamato, M.; Utsumi, M.; Kushida, A.; Konno, C.; Kikuchi, A.; Okano, T. *Tissue Engineering* **2001**, 7, (4), 473-480.

7. Chen, G. P.; Imanishi, Y.; Ito, Y. *Journal of Biomedical Materials Research* **1998**, 42, (1), 38-44.

8. Chen, G. P.; Ito, Y.; Imanishi, Y. *Biotechnology and Bioengineering* **1997**, 53, (3), 339-344.

9. Ito, Y.; Chen, G. P.; Guan, Y. Q.; Imanishi, Y. *Langmuir* **1997**, 13, (10), 2756-2759.

10. Liu, H. C.; Ito, Y. *Lab on a Chip* **2002**, 2, (3), 175-178.

11. Liu, H. C.; Ito, Y. *Journal of Biomedical Materials Research Part A* **2003**, 67A, (4), 1424-1429.

12. Shimizu, T.; Yamato, M.; Akutsu, T.; Shibata, T.; Isoi, Y.; Kikuchi, A.; Umezu, M.; Okano, T. *Journal of Biomedical Materials Research* **2002,** 60, (1), 110-117.

13. Shimizu, T.; Yamato, M.; Kikuchi, A.; Okano, T. *Biomaterials* **2003,** 24, (13), 2309-2316.

14. Kushida, A.; Yamato, M.; Konno, C.; Kikuchi, A.; Sakurai, Y.; Okano, T. *Journal of Biomedical Materials Research* **1999,** 45, (4), 355-362.

15. Loh, X. J.; Zhang, Z. X.; Wu, Y.; Lee, T. S.; Li, J. *Macromolecules* **2009,** 42, (1), 194-202.

16. Li, X.; Loh, X. J.; Wang, K.; He, C. B.; Li, J. *Biomacromolecules* **2005,** 6, (5), 2740-2747.

17. Loh, X. J.; Goh, S. H.; Li, J. *Biomaterials* **2007,** 28, (28), 4113-4123.

18. Loh, X. J.; Goh, S. H.; Li, J. *Biomacromolecules* **2007,** 8, (2), 585-593.

19. Loh, X. J.; Li, J. *Expert Opinion on Therapeutic Patents* **2007,** 17, (8), 965-977.

20. Loh, X. J.; Tan, K. K.; Li, X.; Li, J. *Biomaterials* **2006,** 27, (9), 1841-1850.

21. Loh, X. J.; Wang, X.; Li, H. Z.; Li, X.; Li, J. *Materials Science & Engineering C-Biomimetic and Supramolecular Systems* **2007,** 27, (2), 267-273.

22. Petrasovits, L. A.; Purnell, M. P.; Nielsen, L. K.; Brumbley, S. M. *Plant Biotechnology Journal* **2007,** 5, (1), 162-172.

23. Purnell, M. P.; Petrasovits, L. A.; Nielsen, L. K.; Brumbley, S. M. *Plant Biotechnology Journal* **2007,** 5, (1), 173-184.

24. Chen, X. Y.; Zhang, X. F.; Zhu, Y.; Zhang, J. Z.; Hu, P. *Polymer Journal* **2003,** 35, (2), 148-154.

25. Jing, X.; Kong, L. J.; Gao, Y.; Gong, Y. D.; Zhao, N. M.; Zhang, X. F. *Journal of Biomaterials Science-Polymer Edition* **2005,** 16, (11), 1395-1408.

26. Wang, Y. W.; Yang, F.; Wu, Q.; Cheng, Y. C.; Yu, P. H. F.; Chen, J.; Chen, G. Q. *Biomaterials* **2005,** 26, (7), 755-761.

27. Wu, L. P.; Chen, S. T.; Li, Z. B.; Xu, K. T.; Chen, G. Q. *Polymer International* **2008,** 57, (7), 939-949.

28. Reyes, M.; Lund, T.; Lenvik, T.; Aguiar, D.; Koodie, L.; Verfaillie, C. M. *Blood* **2001,** 98, (9), 2615-2625.

29. Jackson, K. A.; Majka, S. M.; Wang, H. G.; Pocius, J.; Hartley, C. J.; Majesky, M. W.; Entman, M. L.; Michael, L. H.; Hirschi, K. K.; Goodell, M. A. *Journal of Clinical Investigation* **2001,** 107, (11), 1395-1402.

30. Kovacic, J. C.; Graham, R. M. *Lancet* **2004,** 363, (9422), 1735-1736.

31. Petersen, B. E.; Bowen, W. C.; Patrene, K. D.; Mars, W. M.; Sullivan, A. K.; Murase, N.; Boggs, S. S.; Greenberger, J. S.; Goff, J. P. *Science* **1999,** 284, (5417), 1168-1170.

32. Heng, B. C.; Liu, H.; Ge, Z. G.; Cao, T. *Biotechnology and Applied Biochemistry* **2007,** 47, 33-37.

33. Okano, T. *Advances in Polymer Science* **1993,** 110, 179-197.

34. Farago, O. *Journal of Chemical Physics* **2003,** 119, (1), 596-605.

35. Tresset, G.; Cheong, W. C. D.; Lam, Y. M. *Journal of Physical Chemistry B* **2007,** 111, (51), 14233-14238.

36. Tresset, G.; Cheong, W. C. D.; Tan, Y. L. S.; Boulaire, J.; Lam, Y. M. *Biophysical Journal* **2007,** 93, (2), 637-644.

37. Mori, T.; Kiyono, T.; Imabayashi, H.; Takeda, Y.; Tsuchiya, K.; Miyoshi, S.; Makino, H.; Matsumoto, K.; Saito, H.; Ogawa, S.; Sakamoto, M.; Hata, J. I.; Umezawa, A. *Molecular and Cellular Biology* **2005,** 25, (12), 5183-5195.

38. Deegan, R. D.; Bakajin, O.; Dupont, T. F.; Huber, G.; Nagel, S. R.; Witten, T. A. *Nature* **1997,** 389, (6653), 827-829.

39. Deng, Y.; Zhu, X. Y.; Kienlen, T.; Guo, A. *Journal of the American Chemical Society* **2006,** 128, (9), 2768-2769.

40. Farago, O.; Gronbech-Jensen, N. *Biophysical Journal* **2007,** 92, (9), 3228-3240.

41. Farago, O.; Gronbech-Jensen, N.; Pincus, P. *Physical Review Letters* **2006,** 96, (1), 018102.

CHAPTER EIGHT

POLY(N-ISOPROPYLACRYLAMIDE)-POLY[(R)-3-HYDROXYBUTYRATE]-POLY(N-ISOPROPYLACRYLAMIDE) TRIBLOCK COPOLYMER SURFACE AS A CULTURE SUBSTRATE FOR MOUSE EMBRYONIC STEM CELLS

8.1. Introduction

Recently, there is great interest in using embryonic stem (ES) cells for tissue regeneration. ES cells were first derived from the inner cell mass of mouse blastocysts in the early 1980s.[1] They can differentiate into a variety of cells of any somatic cell linage and act as a renewable source of cells for tissue regeneration and cell-based treatment therapies. The culture and maintenance of ES cells is therefore of vital importance to the success of these technologies. For the culture of some mouse ES cells, gelatin coated polystyrene tissue culture dishes are used in the presence of the interleukin-6 family member cytokine leukemia inhibitory factor (LIF).[2] It is known that human ES cells require close intercellular communication for the maintenance of cell viability during *in vitro* cell culture, including close physical contact and other cooperative interactions.[3] Trypsinization dissociates the cells into single-cell suspensions and an excessive exposure to the enzyme reduces the number of viable stem cells over time.[4]

In this work, a thermal responsive coating was tested for the culture of mouse ES cells. Cells were able to grow and colonize on the surfaces and could be detached by cooling the culture dish. The detached cells maintained their colonized state and could be subsequently re-cultured or used in differentiation protocols. Aggregation of ES cells induces repression of Nanog at the outer layer of the cells. This factor is essential for the formation of aggregation-induced primitive endoderm,[2] and keeping the colonized state of ES cells is important for expansion under an undifferentiated state. Several other papers have reported that the formation of ES cell aggregates is essential prior to the differentiation of these cells.[5-9] The formation of ES cell aggregates takes a minimum of 3 days, thus cells which are freshly trypsinized cannot be used for immediate differentiation.

An approach known as cell sheet engineering has been proposed for culturing and passaging cells without the use of trypsin.[10] Using a coating of a thermally responsive polymer,

the surface properties of the substrate can be changed by changing the temperature of the environment. Poly(*N*-isopropylacrylamide) (PNIPAAm) is a popular polymer of this type. It exhibits a lower critical solution temperature (LCST) of 32–33 °C, being hydrophilic at low temperatures and precipitating above the critical phase transition temperature.[11] This unique physical property has been exploited in the fabrication of thermally responsive surfaces for cell sheet engineering.[12-21] At cell culture temperatures above the LCST, the surface is hydrophobic, and cells or tissues attach to the substrate. When the temperature is lowered below the LCST, the surface becomes hydrophilic, and they detach. This mild technique of cell detachment preserves cell–cell and cell–extracellular matrix (ECM) interactions, unlike trypsinization.[22-24]

The polymer used is a thermally responsive triblock copolymer of poly(*N*-isopropylacrylamide)–poly[(*R*)-3-hydroxybutyrate]–poly(*N*-isopropylacrylamide) (PNIPAAm-PHB-PNIPAAm), which was described in Chapter 6.[25] PHB belongs to a class of naturally derived biologically synthesized polyesters known as poly[(*R*)-3-hydroxyalkanoate]s.[26-31] PHB has also been extracted from genetically modified plants.[32,33] Based on its advantageous properties, PHB might be suitable for a variety of biomedical applications such as tissue engineering scaffolds, and these have been reported to be suitable for enabling cell adhesion.[34-37]

In this chapter, a simple drop-casting technique for the preparation of a homogeneous thermoresponsive surface is described. This method is preferred over conventional spin coating methods because it reduces wastage of large amounts of polymer during the coating process. Furthermore, this method is easier to perform than other types of substrate preparation processes, such as chemical immobilization or plasma treatment.[38,39] The objective in this study is to develop a thermoresponsive stem cell culture substrate for the attachment and the nonenzymatic recovery of mouse ES cells, prior to differentiation of the cells. Currently, there has been no precedent report on this approach.

8.2. Experimental Section

8.2.1. Materials

A series of poly(*N*-isopropylacrylamide)-poly[(*R*)-3-hydroxybutyrate]-poly(*N*-isopropylacrylamide) triblock copolymers was synthesized as described in Chapter 6. Thermanox^{TM} coverslips (15 mm diameter) were purchased from Electron Microscopy Sciences (Hatfield, PA, U.S.A.) and used as bare substrates. The cell culture medium used was Glasgow Minimum Essential Medium (GMEM; Sigma-Aldrich, St Louis, MO, U.S.A.) supplemented with 2 mM L-glutamine, 1 mM nonessential amino acids (Lonza Ltd, Basel, Switzerland), 0.5 mM β-mercaptoethanol (GIBCO BRL), 10% (v/v) fetal bovine serum (FBS) and 1000 units/mL of LIF (Chemicon). All media contained 1 mM sodium pyruvate (GIBCO BRL) and 1% of 1× penicillin-streptomycin (Wako Pure Chemical Industries Ltd, Osaka, Japan).

8.2.2. Coating of Copolymer On Cell Culture Substrates

Polymers were dissolved in deionized water at a concentration of between 0.0001 mg/mL and 1 mg/mL. Aliquots of 100 μL of polymer solution were dropped onto bare substrates, left to dry overnight and sterilized by exposure to UV for 1 h before cell seeding. For the gelatin blended coatings, PNIPAAm or PNIPAAm-PHB-PNIPAAm were first dissolved in 0.001%, 0.01% or 0.1% gelatin solution before being drop-casted.

8.2.3. Contact Angle Measurements

Contact angles were measured using a CA-W Automatic Contact Angle Meter (Kyowa Interface Co. Ltd, Saitama, Japan). Solutions were prepared with MilliQ water (Millipore Corp., Billerica, MA, U.S.A.). Uniform droplets with volume of 0.1 μL was dropped on the sample surface using a Dropmaster 500 (Kyowa Interface Co. Ltd, Saitama, Japan). The static contact angle of the drop on the surface was measured after 2.5 s. At least 10 angles were measured at

different areas and averaged. Optimization studies were carried out for maximum thermal response using the different copolymers with molecular weights and composition as described in Table 6.1.

8.2.4. Attenuated Total Reflectance – Fourier Transform Infra-Red (ATR-FTIR) Of Coated Substrates

ATR-FTIR measurements were performed using a Perkin Elmer FT-IR Spectrometer Spectrum 2000 to characterize the surface of the substrate. Substrates with polymer coating density of 5.66 μg/cm^2 and gelatin coating of 0.566 μg/cm^2 were used for the stability studies. The substrates were soaked in 1 mL of water for 24 h. One washing cycle was performed by dipping and swirling the substrate in 10 mL of water 5 times. The process was repeated 3 times, each time in fresh water. ATR-FTIR spectra of the substrates before and after the soaking were recorded. As a control, the bare Thermanox^{TM} coverslip was used. Samples were dried after washing prior to the recording of the spectra.

8.2.5. ES Cell Culture

Feeder-free mouse embryonic stem cells (EB3) were used in all the cell culture studies. They were cultured on gelatin-coated plates in supplemented GMEM. The ES cells were cultured on the coated substrates at a cell seeding density of 5×10^4 cells per coverslip and incubated at 37 °C in 5% CO_2, in humidified air. For maintenance of the ES cells, cells were passaged every 3 days using 0.25% trypsin/1.0 mM EDTA. Three types of coatings were tested for culture: gelatin, gelatin/PNIPAAm-PHB-PNIPAAm copolymer and gelatin/PNIPAAm homopolymer.

Cytotoxicity Measurements

Cell viability was determined using the Dojindo Cell Counting Kit (Dojindo Laboratories, Kumamoto, Japan). Briefly, 100 μL of cell suspension (5000 cells/well) was

dispensed into a 96-well plate. Each plate was preincubated for 24 h at 37 °C under 5% CO_2, in humidified air. The medium was removed, and 100 μL aliquots of polymer solutions at different concentrations were added. Plates were incubated for a further 48 h before measurements were made using the kit.

Growth Curve Measurements

Cells were seeded at 4×10^5 per dish in a 60 mm culture dish and incubated at 37 °C under 5% CO_2, in humidified air. At different times, the cells were removed by trypsinization with 0.25% trypsin/1.0 mM EDTA, and the cell number was measured using a hemocytometer. Three readings were taken, and the results were averaged. For culture on the coated surfaces, five types of coatings were tested: gelatin, PNIPAAm-PHB-PNIPAAm copolymer, PNIPAAm homopolymer, gelatin/PNIPAAm-PHB-PNIPAAm copolymer and gelatin/PNIPAAm homopolymer.

Cell Detachment

Cells were seeded at 4×10^5 per dish in a 60 mm culture dish and incubated at 37 °C under 5% CO_2, in humidified air. After 3 days, the cells were detached by cooling. The detached cells were then centrifuged at 1000 rpm for 3 minutes and washed with buffer solution. Following that, the buffer solution was removed, and 0.5 mL of 0.25% trypsin was added to the cells and incubated at 37 °C in 5% CO_2, in humidified air for 3 min. The cells were suspended by pipetting several times, and the detached cell numbers were counted using a hemocytometer. Cells left undetached by the cooling process were removed with 0.25% trypsin/1.0 mM EDTA and detached as with the passaging procedures above. The undetached cell numbers were counted using a hemocytometer. Six readings were taken, and the results were averaged.

8.2.6. Characterization of Pluripotency of ES Cells

Staining For Alkaline Phosphatase (ALP)

Staining for ALP was performed as described.[40,41] Cells were cultured for 3 days and detached from the surface by incubating it at 4 °C for 20 min. The cells were transferred to a gelatin coated tissue culture dish and incubated for 1 day at 37 °C under 5% CO_2, in humidified air. The adhered cells were stained using an ALP staining kit (Vector® Red Alkaline Phosphatase Substrate Kit I, Cat. No. SK-5100) purchased from Vector Laboratories (Burlingame, CA, U.S.A.).

Western Blot Assay

Total protein was extracted from the cells that had been cultured for 3 days, using lysis buffer (50 mM Tris, 150 mM NaCl, 0.1% Triton X-100, 0.1 mM dithiothreitol and proteinase inhibitors). The extracted proteins were separated by 10% sodium dodecyl sulfate–polyacrylamide gel electrophoresis and transferred onto polyvinylidene fluoride membranes. The membranes were incubated with antibodies against STAT3 and phosphorylated STAT3 (BD Biosciences, San Jose, CA, U.S.A.), followed by incubation with peroxidase-conjugated goat anti-mouse immunoglobin and visualized with ECL Advance reagents purchased from Amersham Biosciences (Piscataway, NJ, U.S.A.).

Reverse Transcription Polymerase Chain Reaction (RT–PCR)

ES cells that had been cultured for 3 days were collected by trypsinization, and total RNA was extracted using the RNeasy Protect Mini kit (Qiagen, Hilden, Germany). For the RT–PCR analysis, cDNA was prepared from 5 μg of total RNA, with an oligo-dT primer, using the SuperScript III First-Strand Synthesis System for RT-PCR (Invitrogen, Carlsbad, CA, U.S.A.). RT–PCR data were first normalized to β-actin mRNA levels. The sequences of the gene-specific primers were as follows: octamer-binding protein 3/4 (Oct3/4; 468 bp, NM_013633) (forward:

agctgctgaagcagaagagg, reverse: cctgggaaaggtgtccctgta) and GATA4 (443 bp, U85046) (forward: ctgtgccaactgccagacta, reverse: gcgatgtctgagtgacagga).

Quantification Of RNA Expression In Mouse ES Cells

The images of the gels after electrophoresis were captured in JPEG format and analyzed using Adobe Photoshop CS3 Extended. The Image Analysis option was utilized for the measurement of the grey value intensity. Grey value intensity range from 0 (black) to 255 (white). An area with height of 7 pixels by width of 22 pixels was used at all times for the intensity determination. The values reported are the average grey intensity values of a total of 154 pixels.

8.2.7. Statistical Analysis

Data are expressed as mean ± SD. Analysis of variance, followed by Student's t test, was used to determine the significant differences among the groups, and p-values less than 0.05 were considered significant.

8.3. Results and Discussion

8.3.1. Copolymer Coatings

Three types of surfaces, gelatin, gelatin/PNIPAAm-PHB-PNIPAAm copolymer and gelatin/PNIPAAm homopolymer were prepared. Gelatin-coated substrates have been widely used for the culture of a mouse ES cell line, EB3 cells, as the interaction with gelatin is important for cell growth.[40] However, the gelatin-coated substrate is unable to give the thermal response that is required for the nonenzymatic recovery of cells. Because gelatin is an important component for stem cell culture, it was important to compare cell growth rates on substrates coated only with the copolymers or with gelatin-blended copolymers.

During the coating process at room temperature, it was noted that the PNIPAAm-PHB-PNIPAAm copolymer gave a more homogeneous coating than the PNIPAAm homopolymer as

described in Chapter 7. This was also observed with the gelatin-blended coatings. The interaction between the substrate surface and the polymer solution is an important factor that determines whether the surface is homogeneously coated with the polymer or not. In this case, the substrate was a hydrophobic polyester, and PNIPAAm at temperatures below the LCST is hydrophilic. Therefore, the homopolymer formed a thick layer at the edges. However, it did not interact well with the surface and did not adhere to the surface as the solution evaporated.

A 'ring' stain resembling that seen when a coffee droplet dries on a solid surface was also studied.[42] The drying process is attributed to a form of capillary flow in which the liquid evaporating from the edge is replenished by the liquid from the interior. The movement of the liquid in this manner transports along with it the polymer solute to the edges, leading to a thicker layer at the edges for the PNIPAAm coating. However, the copolymer used here has a hydrophobic PHB segment, which helps in the immobilization of the copolymer to the substrate surface by hydrophobic interactions. The addition of surfactants has been shown to help in obtaining homogeneous protein drop coatings.[43] It should be noted that this coating technique was simple to perform with no loss of samples, a problem commonly associated with spin coating. Therefore, accurate coating density can be applied to the substrates by adjusting the concentration of the coating solution. When the coatings were performed at a temperature above the LCST (37 °C), large particles were deposited on the plates. This resulted in the formation of a very rough and uneven surface.

The main advantage of using the PNIPAAm-PHB-PNIPAAm copolymer coating is that it was more stable under high dilution conditions than the PNIPAAm homopolymer coating. The critical micelle-forming concentration of PNIPAAm-PHB-PNIPAAm copolymers used in this study is 41.1 mg/L. Therefore, even when exposed to high amounts of buffer, the micelles are stable. This stability of the coating results from the association of the micelles with the substrate

surface via the hydrophobic core. For the homopolymer, there was no such association, and it appeared that even though PNIPAAm is hydrophobic at 37 °C, this was not sufficient to anchor it to the substrate. The PNIPAAm-PHB-PNIPAAm copolymer coating remained on the substrate after being incubated with buffer at 37 °C for 24 h, whereas the PNIPAAm coating dissolved after 24 h.

8.3.2. Contact Angle Measurements

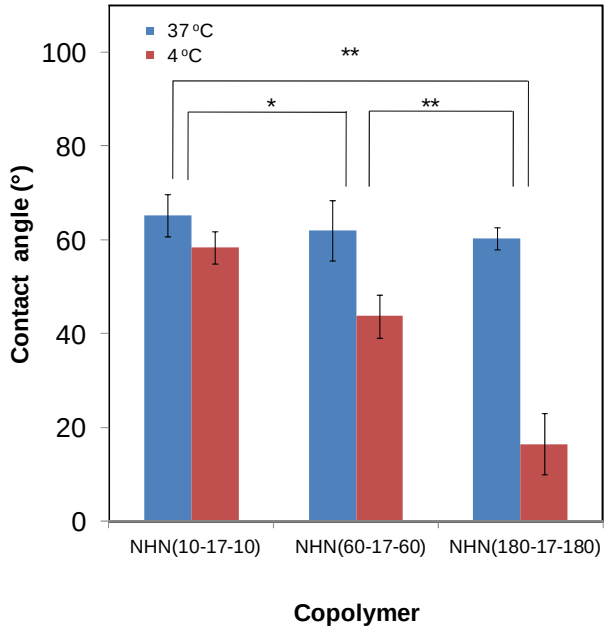

Figure 8.1. (a) Thermal response of the gelatin/PNIPAAm-PHB-PNIPAAm using copolymers of different composition. (Gelatin coating density = 0.566 μg/cm^2; Copolymer coating density = 5.66 μg/cm^2). *$p < 0.05$. **$p < 0.01$.

The PNIPAAm-PHB-PNIPAAm triblock copolymer used in this work has a molecular weight of 4.18 x 10^4 g/mol. The central PHB block has a molecular weight of 1.73 x 10^3 g/mol. The use of this copolymer was decided after contact angle measurements revealed that this copolymer had the highest thermal response among the 3 copolymers tested, based on the contact angle change when the temperature was changed ($p < 0.05$) (Figure 8.1). All coatings

tested in the optimization study were based on gelatin and polymer coating densities of 0.566 and 5.66 μg/cm^2, respectively. The incorporation of a higher PHB content rendered the surface more hydrophobic. At the same time, upon cooling, the hydrophilic effect of PNIPAAm was reduced.

Table 8.1. Contact angle values of the different coatings (coating density = 5.66 μg/cm^2).

Polymer coating	Contact angle (37 °C)	Contact angle (4 °C)
Gelatin/PNIPAAm-PHB-PNIPAAm (1/10)	60.3 ± 2.4° [a] 55.1 ± 3.9° [b]	16.5 ± 6.6° [a] 22.2 ± 9.9° [b]
Gelatin/PNIPAAm (1/10)	57.0 ± 3.1° [a] 57.1 ± 2.9° [b]	32.0 ± 7.6° [a] 53.9 ± 6.2° [b]
Gelatin	48.1 ± 5.6°	47.2 ± 7.3°

[a] Before soaking in buffer.
[b] After soaking in buffer at 37 °C for 24 h.

Having decided on the copolymer to be used, the hydrophilicity of the coated surfaces was evaluated by contact angle measurements (Table 8.1). For bare substrate, the contact angle of a water droplet was measured to be 68.2° ± 1.9° at 37 °C. Water droplets on the gelatin coated substrates had a contact angle of 48.1° ± 5.6° at 37 °C. Neither showed thermal response in their hydrophilicities when cooled to 4 °C ($p > 0.05$). For the gelatin/PNIPAAm-PHB-PNIPAAm copolymer coated and the gelatin/PNIPAAm homopolymer coated substrates, changes in the hydrophilicities were observed upon cooling. The gelatin/PNIPAAm-PHB-PNIPAAm copolymer when coated at 5.66 μg/cm^2 showed a change in the contact angle from 60.3° ± 2.4° at 37 °C to 16.5° ± 6.6° at 4 °C. The gelatin/PNIPAAm homopolymer coated at 5.66 μg/cm^2 showed a change in the contact angle from 57.0° ± 3.1° at 37 °C to 32.0° ± 7.6° at 4 °C. The main difference between the two coatings was that after being soaked in water at 37 °C for 24 h,

the gelatin/PNIPAAm-PHB-PNIPAAm copolymer remained on the surface whereas the gelatin/PNIPAAm homopolymer dissolved. After the soaking treatment, the gelatin/PNIPAAm-PHB-PNIPAAm copolymer coating showed a change in the contact angle from 55.1° ± 3.9° at 37 °C to 22.2° ± 9.9° at 4 °C whereas the gelatin/PNIPAAm homopolymer coating showed a change in the contact angle from 57.1° ± 2.9° at 37 °C to 53.9° ± 6.2° at 4 °C.

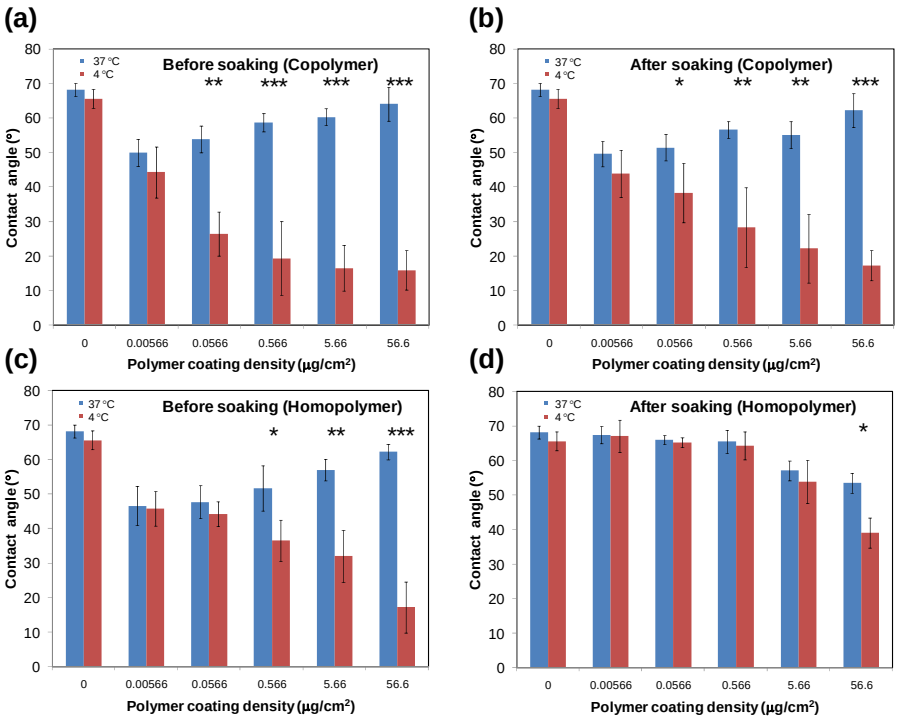

Figure 8.2. (a) Effect of coating density on the thermal response of the gelatin/PNIPAAm-PHB-PNIPAAm surface. (b) Effect of soaking in water at 37 °C on the thermal response of the gelatin/PNIPAAm-PHB-PNIPAAm surface. (c) Effect of coating density on the thermal response of the gelatin/PNIPAAm surface. (d) Effect of soaking treatment in water at 37 °C on the thermal response of the gelatin/PNIPAAm surface. (Gelatin coating density = 0.566 µg/cm^2). *$p < 0.05$ vs. non-coated substrate. ** $p < 0.01$ vs. non-coated substrate. *** $p < 0.001$ vs. non-coated substrate.

Based on these values, it is evident that the thermal response of the gelatin/PNIPAAm-PHB-PNIPAAm coating did not change much after soaking in water at 37 °C ($p < 0.05$). However, gelatin/PNIPAAm lost its ability to respond thermally after this treatment (Fig. 8.2c, d) ($p > 0.05$). This suggests that the gelatin/PNIPAAm-PHB-PNIPAAm coating was more stable

than the gelatin/PNIPAAm coating. The effect of increasing the amount of gelatin in the coating mixture resulted in a decrease in the thermal response (Figure 8.3). The hydrophilic gelatin reduced the contact angle made at 37 °C. However, at 4 °C, the contact angles were in the range of 20°. Overall, the temperature-induced change in contact angle of the surface decreased with increasing amount of gelatin incorporated ($p < 0.05$).

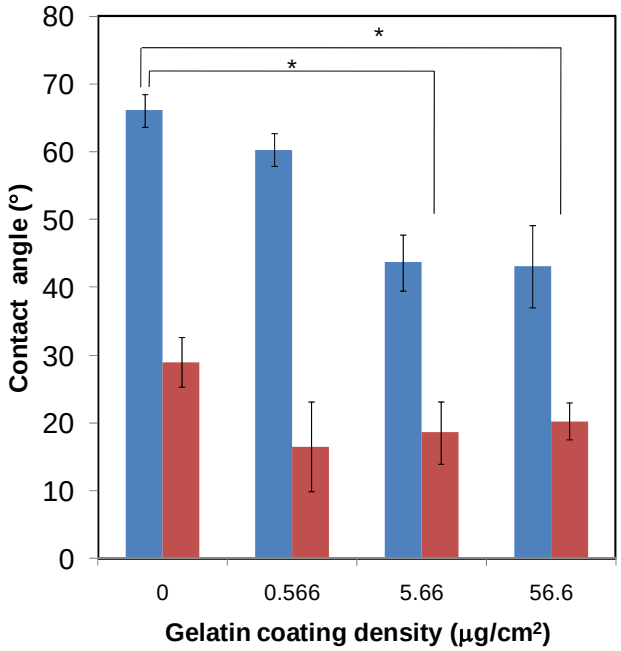

Figure 8.3. Effect of gelatin content on the thermal response of the gelatin/PNIPAAm-PHB-PNIPAAm coating. (Copolymer coating density = 5.66 µg/cm^2). *$p < 0.05$.

8.3.3. ATR-FTIR Evaluation of the Coated Surfaces

ATR-FTIR was used to investigate the surface characteristics of the substrate before and after coating. The data is presented in Figure. 8.4. When the surface is uncoated, the spectrum reveals a peak at 1715 cm^{-1}, which is attributed to the ester group belonging to the material of the substrate. When gelatin is applied as a coating, the ester bond of the material of the substrate can be observed, as well as a very faint amide II of gelatin observed at 1570 cm^{-1}. This indicates inhomogeneous coating of gelatin on the substrate surface. When the gelatin/PNIPAAm-PHB-

PNIPAAm coating is applied, this peak at 1715 cm^{-1} disappears, showing that the copolymer completely coated the surface. In addition, peaks were observed at 1630 and 1550 cm^{-1}. These are assigned to the amide I and amide II peaks of PNIPAAm, respectively. Additionally, a very small peak is observed at 1739 cm^{-1}, this is attributed to the ester bond of PHB. Even after 1 day of soaking in water, followed by 5 repeated washes, the FTIR peaks of the substrate remained almost unchanged, indicating the stability of the coating on the surface. On the other hand, when gelatin/PNIPAAm homopolymer was coated on the surface, the peak attributed to the ester bond of the material of the substrate as well as the amide I and II peaks of PNIPAAm and gelatin can be observed (Figure 8.4e). This shows that there is also an inhomogeneous coating of PNIPAAm on the surface. Upon soaking, followed by 3 cycles of washing, a spectra qualitatively resembling the uncoated substrate is obtained.

8.3.4. Cytotoxicity of Copolymers

The copolymer and homopolymer were first tested for toxicity against mouse ES cells. This was done by incubating adhered cells with different concentrations of the polymers. The copolymer and homopolymer were found to be nontoxic to the cells as indicated by cell viability over 90% at concentrations below 2 mg/mL (Figure 8.5). The range of exposure of the cells to the copolymers was much lower than 1 mg/mL in the cell adhesion and detachment studies. Studies of PNIPAAm copolymers using human vein endothelial cells have also shown that they are nontoxic.[44,45]

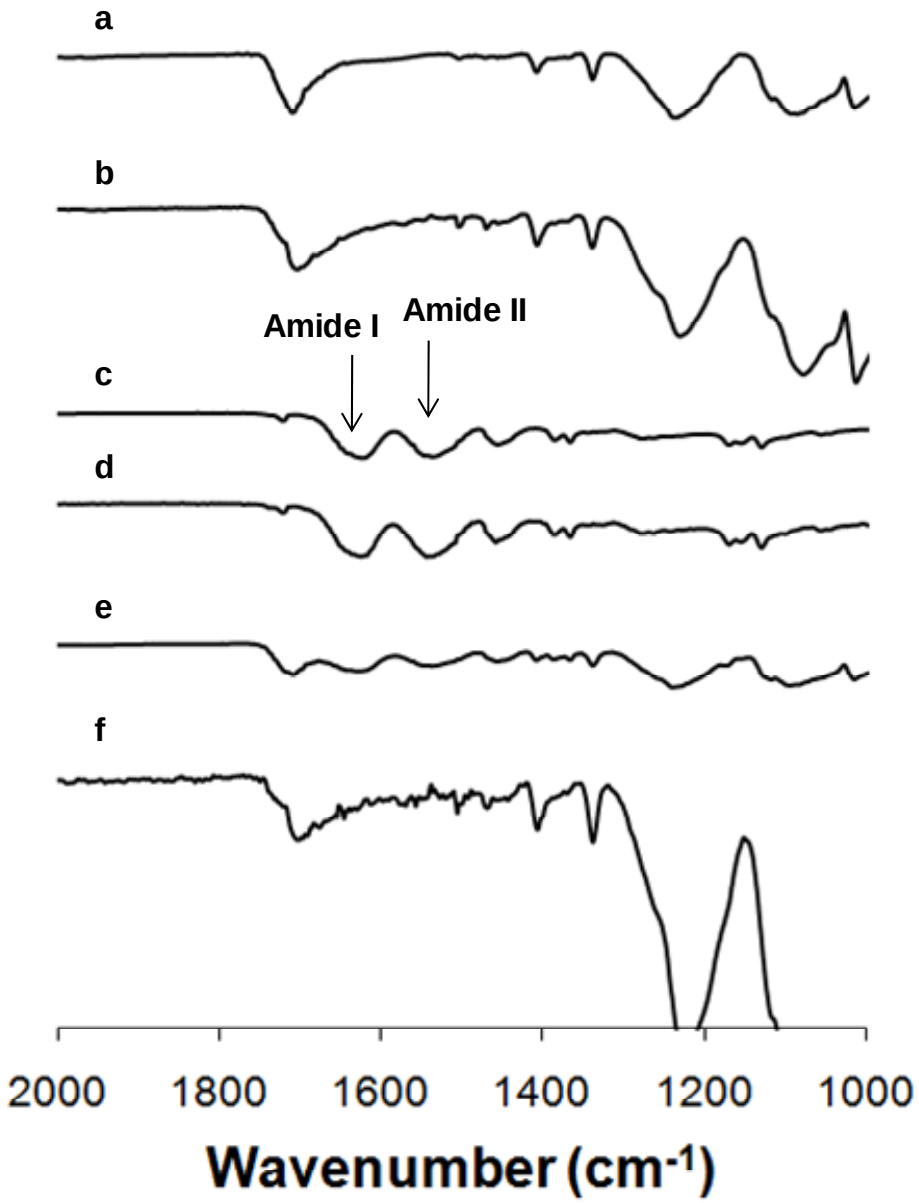

Figure 8.4. ATR-FTIR profiles of the different surfaces: (a) uncoated substrate. (b) gelatin coated substrate (0.566 μg/cm^2) (c) gelatin/PNIPAAm-PHB-PNIPAAm coated substrate (gelatin coating density = 0.566 μg/cm^2, copolymer coating density = 5.66 μg/cm^2) before soaking and washing. (d) gelatin/PNIPAAm-PHB-PNIPAAm coated substrate (gelatin coating density = 0.566 μg/cm^2, copolymer coating density = 5.66 μg/cm^2) after soaking and washing. (e) gelatin/PNIPAAm coated substrate (gelatin coating density = 0.566 μg/cm^2, polymer coating density = 5.66 μg/cm^2) before soaking and washing. (f) gelatin/PNIPAAm coated substrate (gelatin coating density = 0.566 μg/cm^2, polymer coating density = 5.66 μg/cm^2) after soaking and washing.

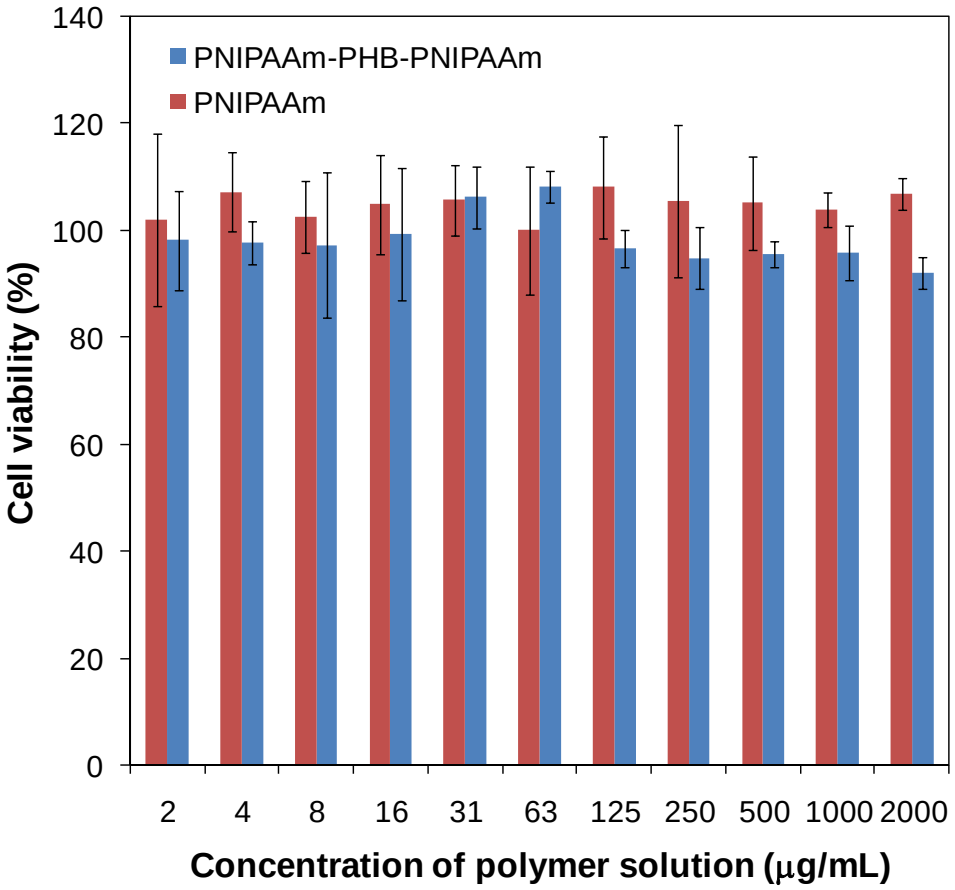

Figure 8.5. Cell viability of mouse embryonic stem cells cultured in the presence of polymer solutions at different concentrations.

8.3.5. ES Cell Culture On Polymer Coated Surfaces

Comparing the morphology of the cells cultured on the surfaces at 56.6 μg/cm^2 and at 5.66 μg/cm^2, the cells cultured on the latter layer resembled cells cultured on the gelatin-coated dishes, whereas the cells cultured on the former layers presented a clearly different morphology (compare Figure 8.6a and Figure 8.6b). Cell numbers were counted for the layers with different surface densities and are shown in Figure 8.6c. The cell numbers were generally similar up to 5.66 μg/cm^2, above which they decreased. Cells grew on the layers at 56.6 μg/cm^2, but the cell

proliferation rate was much lower than on layers of lower coating density (Fig. 8.6c). The amount of gelatin incorporated into the coating also affected cell proliferation (Fig. 8.6d).

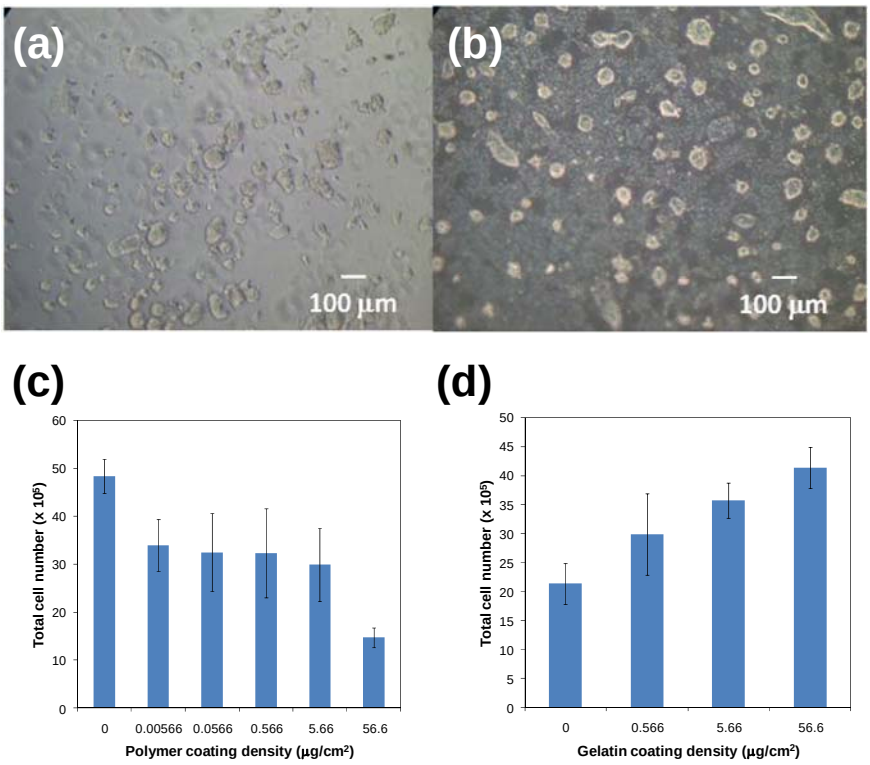

Figure 8.6. Morphology of mouse embryonic stem cells cultured on gelatin/PNIPAAm-PHB-PNIPAAm surfaces of different thicknesses: (a) 5.66 µg/cm^2 and (b) 56.6 µg/cm^2. (c) Cell growth on different copolymer coating densities of gelatin/PNIPAAm-PHB-PNIPAAm after 3 days. (Gelatin coating density = 0.566 µg/cm^2). (d) Cell growth on different gelatin coating densities of gelatin/PNIPAAm-PHB-PNIPAAm after 3 days (Copolymer coating density = 5.66 µg/cm^2).

Considering that the aim was to achieve a high growth rate of ES cells as well as a maximal thermal response, substrates with gelatin and polymer coating densities of 0.566 and 5.66 µg/cm^2, respectively, were used. Mouse ES cells were cultured on five different coated surfaces as detailed above. The cell growth was monitored over 4 days as shown in Figure 8.7.

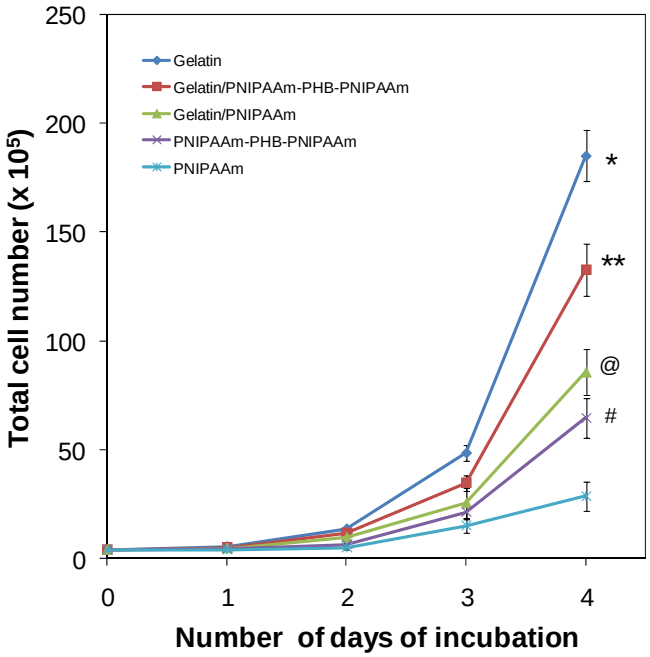

Figure 8.7. Growth curve of mouse embryonic stem cells cultured on five different surfaces. $^{\#}p < 0.05$ vs. the growth rate of gelatin coated surface. $^{@}p < 0.05$ vs. the growth rate of PNIPAAm coated surface. $^{**}p < 0.05$ vs. the growth rate of PNIPAAm-PHB-PNIPAAm coated surface. $^{*}p < 0.05$ significant vs. the growth rate of gelatin/PNIPAAm coated surface.

Initially, the cells grew at about the same rate. From the second day onwards, the cell growth rate proceeded at an exponential rate. The growth rate was found to be in the following order: gelatin > gelatin/PNIPAAm-PHB-PNIPAAm > gelatin/PNIPAAm homopolymer > PNIPAAm-PHB-PNIPAAm > PNIPAAm homopolymer ($p < 0.05$). It is known that gelatin is essential for culture of the EB3 ES cell line. Gelatin immobilized on acrylic acid grafted poly(L-lactide-co-ε-caprolactone) aided in the growth and adhesion of human mesenchymal stem cells, compared with the nonimmobilized polymer.[46] These results showed that although cells could be cultured on the plain polymer surfaces, incorporation of the gelatin coating significantly improved both cell growth and adhesion. On the other hand, it appeared that incorporation of the polymers stunted the growth of the cells compared with the substrate coated with gelatin.

The highest growth rate of ES cell was obtained with the gelatin/PNIPAAm-PHB-PNIPAAm coating. This was more effective than the PNIPAAm coating, probably because of the presence of the PHB segment. As PHB-based scaffolds are suitable for cell adhesion,[34-37] the PHB segment might contribute to the growth enhancement of anchorage-dependent cells, although the effect was less than that of gelatin.

8.3.6. Cell Detachment From Thermoresponsive Surfaces

Cell detachment was tested by incubating the culture dish at 4 °C for 20 min. As a control, cells growing on the gelatin-coated dish were also incubated at 4 °C for the same period. Figure 8.8a shows the thermoresponsive cell detachment from the cooled gelatin/PNIPAAm-PHB-PNIPAAm surface. The cell colonies eventually detached after 20 min. On the other hand, as shown in Figure 8.8b, cells grown on the control gelatin surface did not detach. The cell detachment numbers were evaluated as shown in Figure 8.9a. The percentages of cells detached were 91.3% ± 17.6% from gelatin/PNIPAAm-PHB-PNIPAAm, 59.2% ± 10.4% from gelatin/PNIPAAm, and 4.8% ± 1.2% from the gelatin surface (Figure 8.9b). The detachment of cells was significantly higher from the gelatin/PNIPAAm-PHB-PNIPAAm surface than from either the gelatin/PNIPAAm or gelatin surfaces ($p < 0.01$). Very few cells detached from the gelatin control surface. For the gelatin/PNIPAAm-PHB-PNIPAAm surface, almost three times more cells detached than from the gelatin/PNIPAAm surface; in fact, almost all the cells were removed by this method. However, cell detachment from the gelatin/PNIPAAm surface was not as efficient as from the gelatin/PNIPAAm-PHB-PNIPAAm surface. This could have been caused by the inhomogeneous coating, leading to regions with very little PNIPAAm coating and a high concentration of gelatin. This would have reduced the thermal response, and so some of the cells did not detach easily.

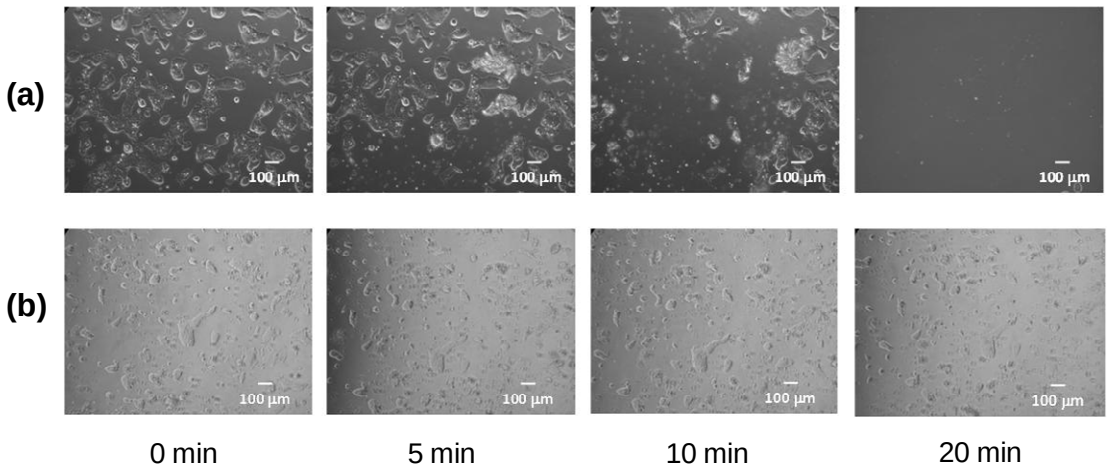

Figure 8.8. Mouse embryonic stem cell detachment demonstrated on (a) a gelatin/PNIPAAm-PHB-PNIPAAm surface compared with (b) a gelatin-coated substrate.

In Scheme 8.1, a schematic diagram of the likely cell detachment process is shown. The cells adhere on the substrate coated with copolymer micelles, which have a hydrophobic core and a collapsed PNIPAAm corona at 37 °C. When the substrate is cooled, the PNIPAAm segment relaxes and becomes more hydrophilic. This hydrophilic surface is not suitable for the attachment of the cells, and so they detach.

8.3.7. Status of Cultured ES Cells

It has been reported that substrates used for the culture of ES cells can affect cell pluripotency.[47,48] Therefore, it was important to check the undifferentiated state of the mouse ES cells after being cultured on the gelatin/copolymer surfaces. First, ALP activity was tested, because this enzyme can be used as a cell marker to determine the differentiation status of mouse ES cells.[49] Cells cultured on the different surfaces were tested for ALP activity after three days of culture as shown in Figure 8.10. Staining for ALP was positive, indicating the undifferentiated state of the stem cells when cultured on the coated substrates.

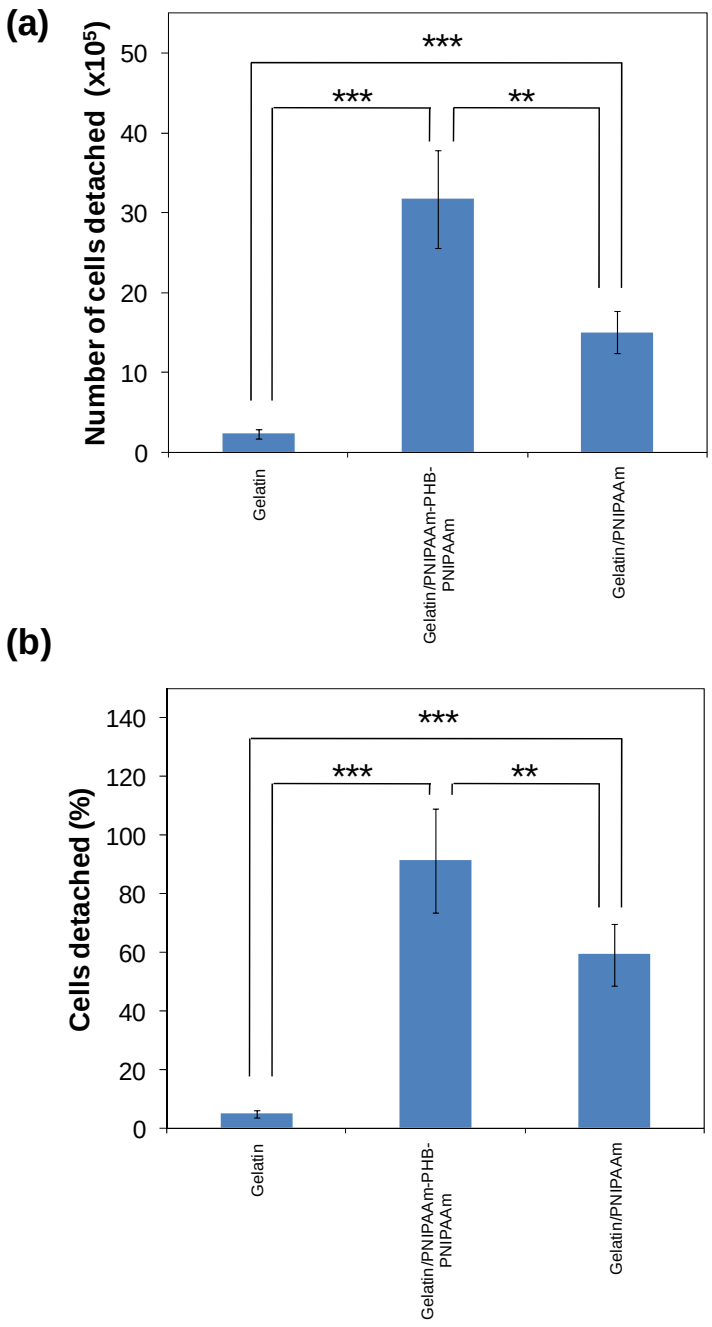

Figure 8.9. (a) Comparison of numbers of mouse embryonic stem cells detaching after being cultured for 3 days on the different surfaces. (b) Comparison of percentage of mouse embryonic stem cells detaching after being cultured for 3 days on the different surfaces. ** $p < 0.01$. *** $p < 0.001$.

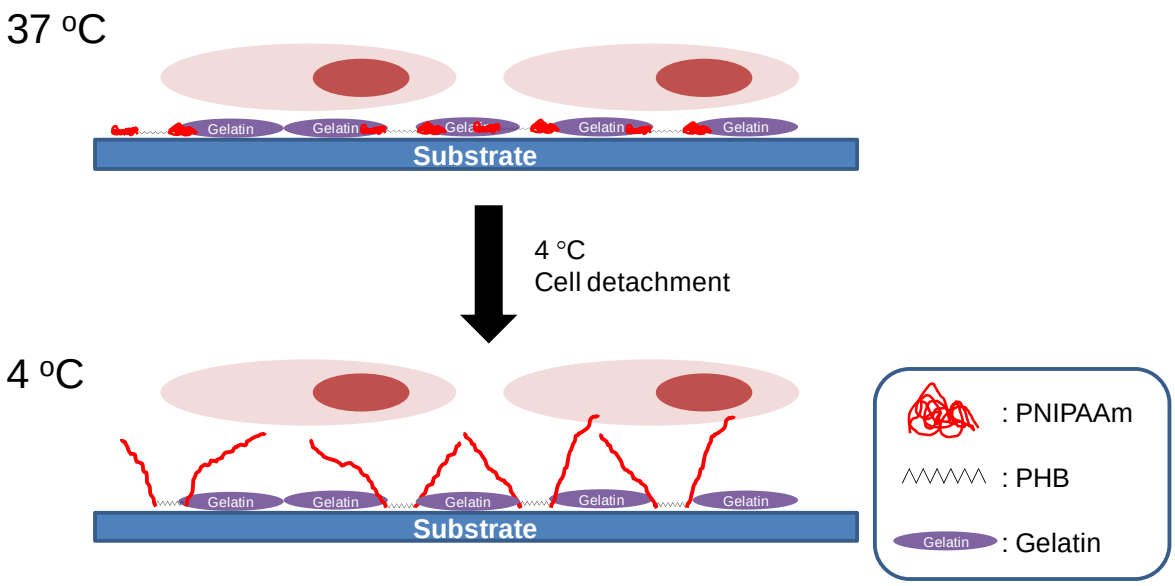

Scheme 8.1. Illustration of the cell detachment process.

The control used was cells cultured on gelatin surface alone (Figure 8.11). Cells that were recultured on normal gelatin-coated substrates after detachment also tested positive for ALP activity.

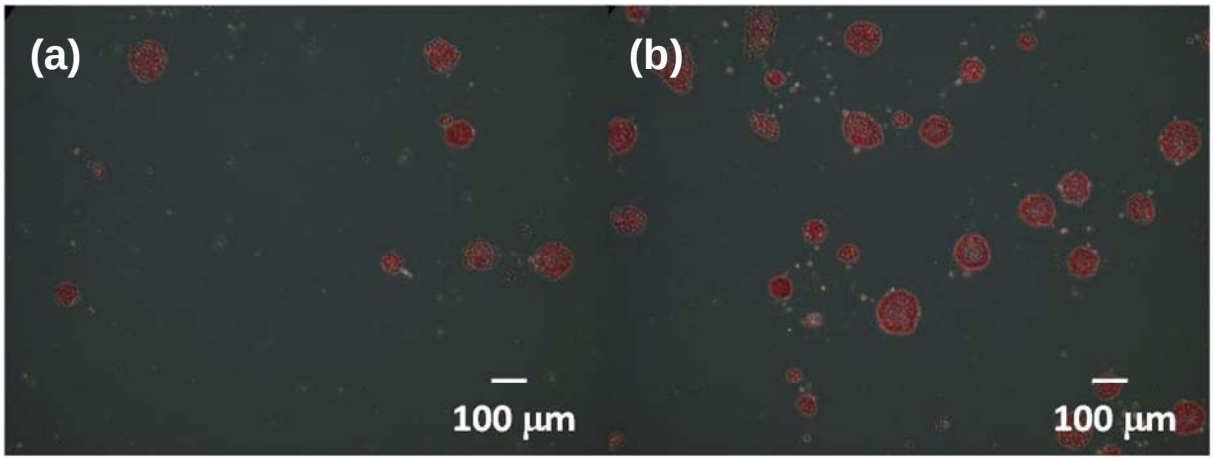

Figure 8.10. Phase contrast microscope images mouse embryonic stem cells stained for alkaline phosphatase after being cultured for 3 days on the different surfaces: (a) Gelatin/PNIPAAm and (b) Gelatin/PNIPAAm-PHB-PNIPAAm.

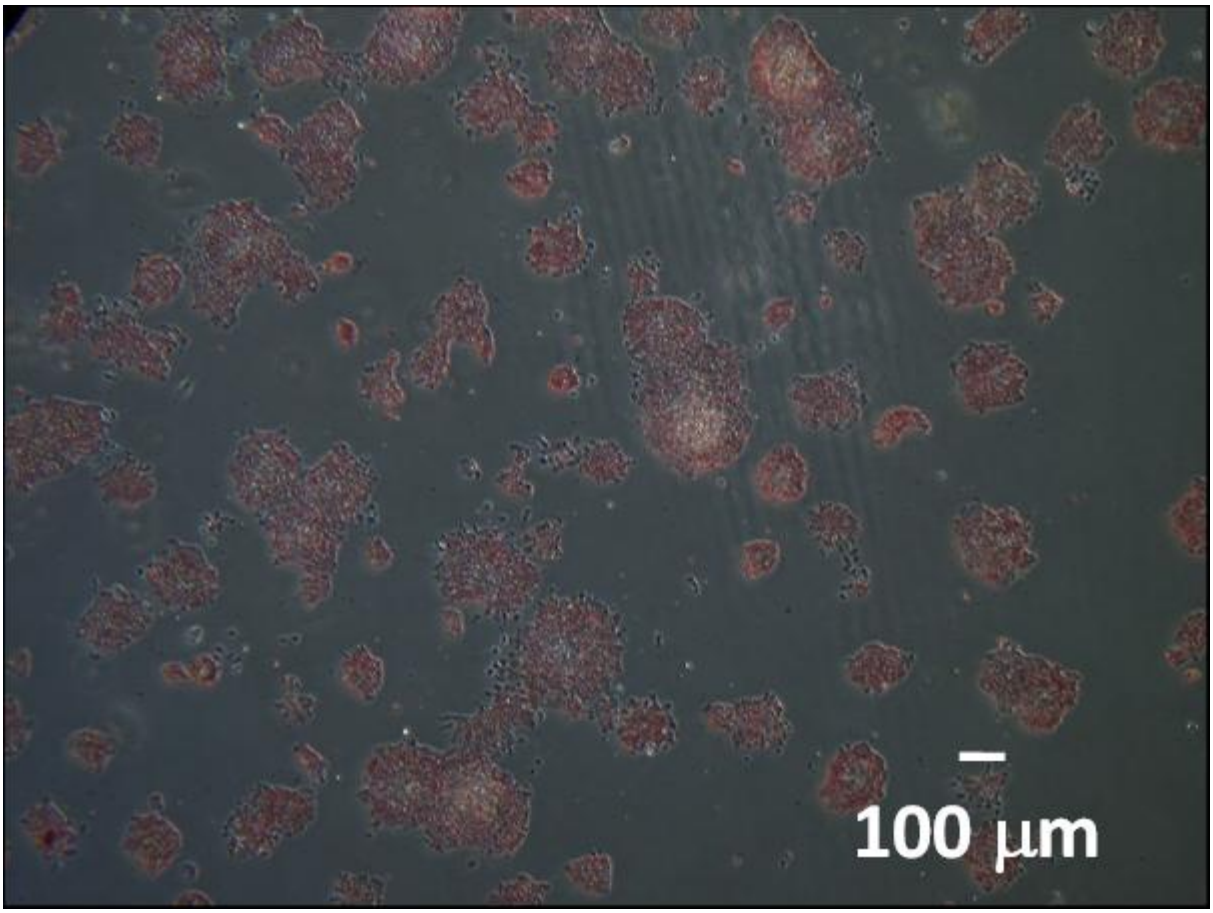

Figure 8.11. Phase contrast microscope images mouse embryonic stem cells stained for alkaline phosphatase after being cultured for 3 days on gelatin surface.

Second, the presence of STAT3 and its activated counterpart, phosphorylated STAT3, were determined. In mouse ES cells, LIF signaling begins when the cytokine receptors LIF-R and gp130 are assembled together with the cytokine. The Janus kinase (Jak) family of tyrosine kinases are activated, leading to the phosphorylation of LIF-R and gp130 at tyrosine residues.[50] These receptor molecules that bind Jak then recruit STAT3 molecules. STAT3 is phosphorylated by Jak, leading to its dimerization, nuclear translocation and target gene activation.[51] Phosphorylated or activated STAT3 induces the expression of Oct3/4, a well-known marker for undifferentiated embryonic stem cells. STAT3 activation results in the phosphorylation of STAT3, which maintains the undifferentiated state of mouse ES cells.[52] Here, phosphorylated

STAT3 (p-STAT3) and total STAT3 (t-STAT3) in the cells were detected by western blot assays from cells obtained after 3 days of culture. Figure 8.12 shows the relative intensities of the p-STAT3 and the t-STAT3 bands. A band corresponding to the p-STAT3 was observed for the gelatin control, the gelatin/PNIPAAm-PHB-PNIPAAm and the gelatin/PNIPAAm coatings. For the STO mouse embryonic fibroblasts used as negative controls, the t-STAT3 band was evident, but the p-STAT3 band was absent. This confirmed the undifferentiated state of the cells at a molecular level. In addition, it was observed that cells cultured on gelatin/PNIPAAm-PHB-PNIPAAm surface showed a stronger band for p-STAT3 than did cells grown on gelatin/PNIPAAm. This indicates that the gelatin/PNIPAAm-PHB-PNIPAAm surfaces could be more suitable for the culture of ES cells than gelatin/PNIPAAm surfaces.

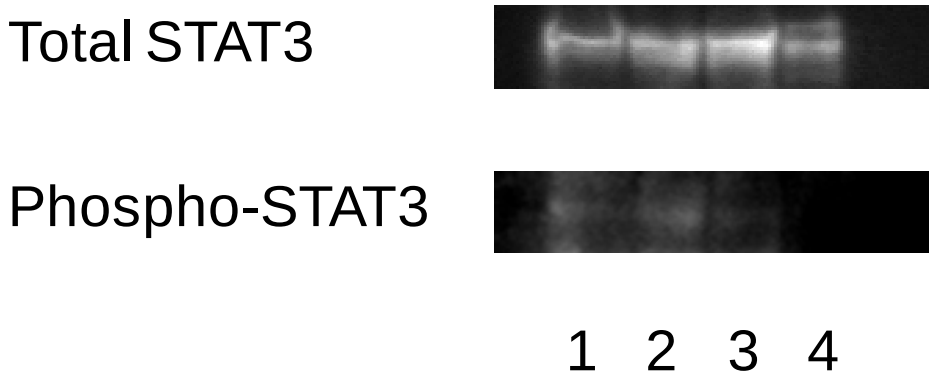

Figure 8.12. Detection of phosphorylated STAT3 and total STAT3 in mouse ES cells cultured on the different substrates, using western blotting. Lane 1: Gelatin control, lane 2: gelatin/PNIPAAm-PHB-PNIPAAm, lane 3: gelatin/PNIPAAm, lane 4: STO mouse embryonic fibroblast cell (negative control).

Third, RT–PCR was performed to check the expression level of Oct3/4 and thus to confirm the undifferentiated state of the ES cells. It is known that ES cells express Oct3/4 to maintain their undifferentiated state[53] and that phosphorylation of STAT3 induces the expression of Oct3/4. Oct3/4 is widely regarded as a marker for totipotent embryonic stem cells[54,55]. The mRNA level was normalized against β-actin mRNA level. The Oct3/4 bands of the cells cultured

on the gelatin, gelatin/PNIPAAm-PHB-PNIPAAm and the gelatin/PNIPAAm surfaces were of almost equal intensity, as shown in Figure 8.13. The quantitative values are tabulated in Table 8.2. The negative control used in this experiment was mRNA extracted from STO mouse embryonic fibroblast cells. Next, the expression of GATA4 was tested. Cells express GATA4 during the early endodermal state or while differentiating to embryoid bodies.[56,57] A weak band of GATA4 was detected from the ES cells cultured on the gelatin, gelatin/PNIPAAm-PHB-PNIPAAm and gelatin/PNIPAAm surfaces. Overall, the ES cells showed a lower expression of GATA4 than the STO cells. Incorporation of the polymers as a surface coating reduced the intensity of the band compared with the pure gelatin surface. Taken in total, the ALP, western blotting and the RT–PCR results show that the mouse ES cells remained in an undifferentiated state after culture on these thermosensitive coatings.

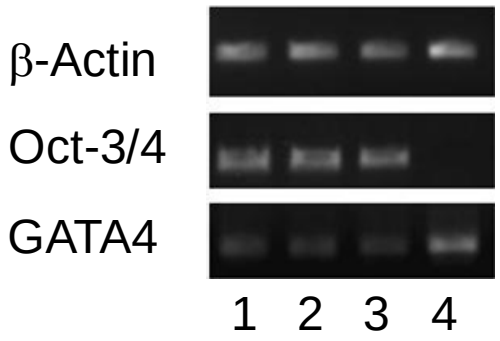

Figure 8.13. Expression levels of β-actin, Oct3/4 and GATA4 in mouse ES cells cultured on the different substrates, measured by reverse transcription polymerase chain reaction. Lane 1, gelatin control; lane 2, gelatin/PNIPAAm-PHB-PNIPAAm; lane 3, gelatin/PNIPAAm and lane 4, STO mouse embryonic fibroblast cells (negative control).

Table 8.2. Quantitative grey value measurements of the expression levels of β-actin, Oct3/4 and GATA4 in mouse ES cells cultured on the different substrates, measured by reverse transcription polymerase chain reaction. Lane 1, gelatin control; lane 2, gelatin/PNIPAAm-PHB-PNIPAAm; lane 3, gelatin/PNIPAAm and lane 4, STO mouse embryonic fibroblast cells (negative control).

	Lane 1	Lane 2	Lane 3	Lane 4
β-actin	80.9	81.3	82.0	80.6
Oct3/4[a]	70.5 (87.1%)	68.8 (84.6%)	61.3 (74.8%)	16.1 (20.0%)
GATA4[b]	31.2 (38.6%)	27.7 (34.1%)	26.6 (32.4%)	63.3 (78.5%)

[a] Percentage in parenthesis calculated by the following relation: Grey value intensity$_{(Oct3/4)}$ / Grey value intensity$_{(\beta\text{-actin})}$ x 100%

[b] Percentage in parenthesis calculated by the following relation: Grey value intensity$_{(GATA4)}$ / Grey value intensity$_{(\beta\text{-actin})}$ x 100%

8.4. Conclusions

A thermo-responsive amphiphilic PNIPAAm-PHB-PNIPAAm triblock copolymer was used to coat a cell culture substrate. When mixed with gelatin, this copolymer offers a homogeneous coating as well as excellent stem cell growth and adhesion characteristics. The thermal response is modulated by the coating thickness, with the maximal response obtained when the layer is thickest. The optimal coating densities for the gelatin and the copolymer were determined. Mouse ES cells maintained their undifferentiated state when cultured on the coated substrates, based on ALP activity, the detection of phosphorylated STAT3 and the presence of Oct3/4. These coated substrates are thermoresponsive in that they are hydrophobic at higher temperatures and become hydrophilic when cooled. This allows for the detachment of the cultured cells from the substrate at lower temperatures without using the routine deleterious enzymatic methods. Almost all cells can be detached by this mild technique, which could be useful for the culture and maintenance of stem cells.

8.5. References

1. Evans, M. J.; Kaufman, M. H. *Nature* **1981,** 292, (5819), 154-156.
2. Hamazaki, T.; Oka, M.; Yamanaka, S.; Terada, N. *Journal of Cell Science* **2004,** 117, (23), 5681-5686.
3. Schatten, G.; Smith, J.; Navara, C.; Park, J. H.; Pedersen, R. *Nature Methods* **2005,** 2, (6), 455-463.
4. Heng, B. C.; Liu, H.; Ge, Z. G.; Cao, T. *Biotechnology and Applied Biochemistry* **2007,** 47, 33-37.
5. Levenberg, S.; Huang, N. F.; Lavik, E.; Rogers, A. B.; Itskovitz-Eldor, J.; Langer, R. *Proceedings of the National Academy of Sciences of the United States of America* **2003,** 100, (22), 12741-12746.
6. Dang, S. M.; Gerecht-Nir, S.; Chen, J.; Itskovitz-Eldor, J.; Zandstra, P. W. *Stem Cells* **2004,** 22, (3), 275-282.
7. Miyazaki, S.; Yamato, E.; Miyazaki, J. *Diabetes* **2004,** 53, (4), 1030-1037.
8. Lee, S. H.; Lumelsky, N.; Studer, L.; Auerbach, J. M.; McKay, R. D. *Nature Biotechnology* **2000,** 18, (6), 675-679.
9. Konno, T.; Akita, K.; Kurita, K.; Ito, Y. *Journal of Bioscience and Bioengineering* **2005,** 100, (1), 88-93.
10. Okano, T. *Advances in Polymer Science* **1993,** 110, 179-197.
11. Xia, Y.; Yin, X. C.; Burke, N. A. D.; Stover, H. D. H. *Macromolecules* **2005,** 38, (14), 5937-5943.
12. Akiyama, Y.; Kikuchi, A.; Yamato, M.; Okano, T. *Langmuir* **2004,** 20, (13), 5506-5511.
13. Hirose, M.; Kwon, O. H.; Yamato, M.; Kikuchi, A.; Okano, T. *Biomacromolecules* **2000**, 1, (3), 377-381.

14. Okano, T.; Yamada, N.; Okuhara, M.; Sakai, H.; Sakurai, Y. *Biomaterials* **1995**, 16, (4), 297-303.

15. Okano, T.; Yamada, N.; Sakai, H.; Sakurai, Y. *Journal of Biomedical Materials Research* **1993**, 27, (10), 1243-1251.

16. Yamato, M.; Utsumi, M.; Kushida, A.; Konno, C.; Kikuchi, A.; Okano, T. *Tissue Engineering* **2001**, 7, (4), 473-480.

17. Chen, G. P.; Imanishi, Y.; Ito, Y. *Journal of Biomedical Materials Research* **1998**, 42, (1), 38-44.

18. Chen, G. P.; Ito, Y.; Imanishi, Y. *Biotechnology and Bioengineering* **1997**, 53, (3), 339-344.

19. Ito, Y.; Chen, G. P.; Guan, Y. Q.; Imanishi, Y. *Langmuir* **1997**, 13, (10), 2756-2759.

20. Liu, H. C.; Ito, Y. *Lab on a Chip* **2002**, 2, (3), 175-178.

21. Liu, H. C.; Ito, Y. *Journal of Biomedical Materials Research Part A* **2003**, 67A, (4), 1424-1429.

22. Shimizu, T.; Yamato, M.; Akutsu, T.; Shibata, T.; Isoi, Y.; Kikuchi, A.; Umezu, M.; Okano, T. *Journal of Biomedical Materials Research* **2002,** 60, (1), 110-117.

23. Shimizu, T.; Yamato, M.; Kikuchi, A.; Okano, T. *Biomaterials* **2003,** 24, (13), 2309-2316.

24. Kushida, A.; Yamato, M.; Konno, C.; Kikuchi, A.; Sakurai, Y.; Okano, T. *Journal of Biomedical Materials Research* **1999,** 45, (4), 355-362.

25. Loh, X. J.; Zhang, Z. X.; Wu, Y.; Lee, T. S.; Li, J. *Macromolecules* **2009,** 42, (1), 194-202.

26. Li, X.; Loh, X. J.; Wang, K.; He, C. B.; Li, J. *Biomacromolecules* **2005,** 6, (5), 2740-2747.

27. Loh, X. J.; Goh, S. H.; Li, J. *Biomaterials* **2007,** 28, (28), 4113-4123.

28. Loh, X. J.; Goh, S. H.; Li, J. *Biomacromolecules* **2007,** 8, (2), 585-593.

29. Loh, X. J.; Li, J. *Expert Opinion on Therapeutic Patents* **2007,** 17, (8), 965-977.

30. Loh, X. J.; Tan, K. K.; Li, X.; Li, J. *Biomaterials* **2006,** 27, (9), 1841-1850.

31. Loh, X. J.; Wang, X.; Li, H. Z.; Li, X.; Li, J. *Materials Science & Engineering C-Biomimetic and Supramolecular Systems* **2007,** 27, (2), 267-273.

32. Petrasovits, L. A.; Purnell, M. P.; Nielsen, L. K.; Brumbley, S. M. *Plant Biotechnology Journal* **2007,** 5, (1), 162-172.

33. Purnell, M. P.; Petrasovits, L. A.; Nielsen, L. K.; Brumbley, S. M. *Plant Biotechnology Journal* **2007,** 5, (1), 173-184.

34. Chen, X. Y.; Zhang, X. F.; Zhu, Y.; Zhang, J. Z.; Hu, P. *Polymer Journal* **2003,** 35, (2), 148-154.

35. Jing, X.; Kong, L. J.; Gao, Y.; Gong, Y. D.; Zhao, N. M.; Zhang, X. F. *Journal of Biomaterials Science-Polymer Edition* **2005,** 16, (11), 1395-1408.

36. Wang, Y. W.; Yang, F.; Wu, Q.; Cheng, Y. C.; Yu, P. H. F.; Chen, J.; Chen, G. Q. *Biomaterials* **2005,** 26, (7), 755-761.

37. Wu, L. P.; Chen, S. T.; Li, Z. B.; Xu, K. T.; Chen, G. Q. *Polymer International* **2008,** 57, (7), 939-949.

38. Nitschke, M.; Gramm, S.; Gotze, T.; Valtink, M.; Drichel, J.; Voit, B.; Engelmann, K.; Werner, C. *Journal of Biomedical Materials Research Part A* **2007,** 80A, (4), 1003-1010.

39. Xu, F. J.; Zhong, S. P.; Yung, L. Y. L.; Kang, E. T.; Neoh, K. G. *Biomacromolecules* **2004,** 5, (6), 2392-2403.

40. Konno, T.; Kawazoe, N.; Chen, G. P.; Ito, Y. *Journal of Bioscience and Bioengineering* **2006,** 102, (4), 304-310.

41. Makino, H.; Hasuda, H.; Ito, Y. *Journal of Bioscience and Bioengineering* **2004,** 98, (5), 374-379.

42. Deegan, R. D.; Bakajin, O.; Dupont, T. F.; Huber, G.; Nagel, S. R.; Witten, T. A. *Nature* **1997,** 389, (6653), 827-829.

43. Deng, Y.; Zhu, X. Y.; Kienlen, T.; Guo, A. *Journal of the American Chemical Society* **2006,** 128, (9), 2768-2769.

44. Li, Y. Y.; Zhang, X. Z.; Cheng, H.; Zhu, J. L.; Li, U. N.; Cheng, S. X.; Zhuo, R. X. *Nanotechnology* **2007,** 18, (50).

45. Li, Y. Y.; Zhang, X. Z.; Zhu, J. L.; Cheng, H.; Cheng, S. X.; Zhuo, R. X. *Nanotechnology* **2007,** 18, (21).

46. Shin, Y. M.; Kim, K. S.; Lim, Y. M.; Nho, Y. C.; Shin, H. *Biomacromolecules* **2008,** 9, (7), 1772-1781.

47. Harrison, J.; Melville, A. J.; Forsythe, J. S.; Muddle, B. C.; Trounson, A. O.; Gross, K. A.; Mollard, R. *Biomaterials* **2004,** 25, (20), 4977-4986.

48. Harrison, J.; Pattanawong, S.; Forsythe, J. S.; Gross, K. A.; Nisbet, D. R.; Beh, H.; Scott, T. F.; Trounson, A. O.; Mollard, R. *Biomaterials* **2004,** 25, (20), 4963-4970.

49. Berrill, A.; Tan, H. L.; Wuang, S. C.; Fong, W. J.; Choo, A. B. H.; Oh, S. K. W. *Cytotechnology* **2004,** 44, (1-2), 77-91.

50. Boulton, T. G.; Stahl, N.; Yancopoulos, G. D. *Journal of Biological Chemistry* **1994,** 269, (15), 11648-11655.

51. Darnell, J. E. *Science* **1997,** 277, (5332), 1630-1635.

52. Matsuda, T.; Nakamura, T.; Nakao, K.; Arai, T.; Katsuki, M.; Heike, T.; Yokota, T. *Embo Journal* **1999,** 18, (15), 4261-4269.

53. Niwa, H.; Toyooka, T.; Shimosato, D.; Strumpf, D.; Takahashi, K.; Yagi, R.; Rossant, J. *Cell* **2005,** 123, (5), 917-929.

54. Ginis, I.; Luo, Y. Q.; Miura, T.; Thies, S.; Brandenberger, R.; Gerecht-Nir, S.; Amit, M.; Hoke, A.; Carpenter, M. K.; Itskovitz-Eldor, J.; Rao, M. S. *Developmental Biology* **2004,** 269, (2), 360-380.

55. Shimozaki, K.; Nakashima, K.; Niwa, H.; Taga, T. *Development* **2003,** 130, (11), 2505-2512.

56. Grepin, C.; Nemer, G.; Nemer, M. *Development* **1997,** 124, (12), 2387-2395.

57. Kelley, C.; Blumberg, H.; Zon, L. I.; Evans, T. *Development* **1993,** 118, (3), 817-827.

CHAPTER NINE

CONCLUSIONS

9.1. Conclusions

In the first part of the work, biodegradable multiblock amphiphilic and thermoresponsive poly(ester urethane)s comprising PHB, PEG and PPG blocks were synthesized. Aqueous solutions of this new poly(ester urethane)s underwent a reversible sol-gel-sol transition as the temperature increased from 4 to 80 °C, and showed a very low critical gelation concentration (CGC) ranging from 2 to 5 wt %. This is much lower than current reported values obtained in literature. As a result of its multiblock architecture, a novel associated micelle packing model has been proposed for the sol-gel transition for the copolymer gels of this system. In order to understand the molecular mechanism of the micellization and gelation process at elevated temperatures, the thermodynamics of micellization of the poly(ester urethane)s was studied. The CMCs of these water-soluble poly(ester urethane)s was determined at different temperatures using a dye solubilization method. From these values, the thermodynamic parameters for micelle formation were calculated. The micellization process was entropy-driven and that an entropy gain threshold had to be crossed before the thermogelling effect could be observed. The hydrolytic degradation and protein release studies for these copolymer hydrogels were carried out at pH 7.4 and 37 °C for up to 6 months. The mass-loss profiles of the copolymer hydrogels were obtained. The hydrogel residues at different time periods of hydrolysis were visualized by

scanning electron microscopy, showing increasing porosity with increasing periods of hydrolysis. Hydrolysis occurs by a random chain scission of the ester backbone bonds of the PHB segments. The constituents of degradation products were 3-hydroxybutyric acid monomer and oligomers of various lengths. These products are naturally found in the human body. The protein release studies of the copolymer hydrogels were conducted using bovine serum albumin (BSA) as model protein. The length of drug release is longer than any precedent report in current literature. The release rate was controllable by varying the composition of the poly(ester urethane)s or by adjusting the concentration of the copolymer in the hydrogels. A correlation exists between the protein release rate of the thermogelling copolymers and the hydrolytic degradation rate of these copolymers. This work represents the first time that such a correlation has been elucidated for a biodegradable thermogelling copolymer system. Cytotoxicity studies performed on the copolymer or the extracts of the copolymer gel indicate good cell compatibility. Excellent cell attachment was observed on the surface of the gel. The results are significantly better than on the commercially available PEG-PPG-PEG triblock copolymer. These studies indicate a potential for the copolymer gel to be used for tissue engineering applications or for 3D cell culture.

In the second part of the work, novel thermoresponsive amphiphilic triblock copolymers with two hydrophilic PNIPAAm blocks flanking a central hydrophobic PHB block were synthesized by ATRP. The water soluble copolymers formed core-corona type micelle aggregates in water at very low CMCs owing to the very hydrophobic PHB segment block. Transmission electron microscopy showed that the self-assembled micelle aggregates had well-defined spherical shapes. The temperature sensitivity of the micelles was demonstrated by the phase transition of a 0.5 mg/mL aqueous polymer solution at the LCST. Preliminary cytotoxicity studies showed that these micelles were not toxic.

Using this copolymer, a thermoresponsive substrate was fabricated by drop-coating with an aqueous polymer solution, and used for the attachment and nonenzymatic temperature-induced detachment of human mesenchymal stem cells. Micelles self-assembled in solution and formed stable attachments to the substrate by hydrophobic interactions between the micelle core and the substrate surface. The copolymer coating on the cell culture substrate was visualized by applying Farago's water-free model for studying the self-assembly of large molecules. Coating of the copolymer enhanced the proliferation of human mesenchymal stem cells compared with either the PNIPAAm homopolymer-coated or the noncoated surface. The copolymer-coated substrate showed a change in the surface hydrophilicity when the temperature was changed. After a period of culture, the cells could be detached by cooling at 4 °C for 20 min without trypsinization.

In developing this technology further, a thermoresponsive substrate using the triblock copolymer co-coated with gelatin was used for the culture and nonenzymatic recovery of mouse ES cells. Coatings of this copolymer with gelatin on a cell culture substrate were studied by measuring water contact angles. High proliferation rates of mouse ES cells were observed on these gelatin/copolymer coated surfaces. After a period of culture, the cells could be detached by cooling at 4 °C for 20 min without the need for trypsin digestion. The growth of the mouse ES cells on the gelatin/copolymer coated surface was analyzed in terms of cell morphology, growth rate, activation of the transcription factor STAT3 and expression of the transcription factor octamer-binding protein 3/4 (Oct3/4). The ES cells remained undifferentiated after culture on the gelatin/copolymer coated surface, similar to standard culture techniques. Overall, the PNIPAAm-PHB-PNIPAAm copolymer coating was superior to the PNIPAAm homopolymer coating in terms of supporting better cell growth, being more stable, presenting a more homogeneous surface coating, and maintaining pluripotency of the ES cells.

9.2. Future Directions

The work presented in this thesis opens new avenues for the development of other "smart biomaterials". From the scientific research point of view, the synthesis strategy demonstrated in this thesis can be utilized for the synthesis of other novel thermogelling copolymers whereby other biodegradable groups can be attached instead of the biopolyesters currently studied. This could give rise to copolymers with very different and interesting properties. In addition, the ATRP technique used in this thesis can be applied to the preparation of biodegradable block copolymers which respond to other stimuli. In terms of the synthesis of materials, other block polyesters such as poly(lactic acid) or poly(ε-caprolactone) can be used as the biodegradable segments. In order to develop materials which are similar to natural proteins, poly(amide)s can be considered as the biodegradable block. As the self assembly behavior of these materials has not been well studied, it could be a potentially rich area to explore. This could include rheological studies to understand the mechanism of gelation, small angle neutron scattering studies to probe the transition from unimer $\rightarrow$ micelle $\rightarrow$ gel and thermal analysis of the micellization and gelation process. These studies could lend insights into the thermodynamic basis of self assembly and can be compared to conventional Pluronics thermogels. In the area of drug delivery, applicative studies into the delivery of bioactive proteins such as the basic fibroblast growth factor could be the next investigative step. The combination of the drug delivery and the tissue engineering aspects of this thesis can be explored as potential wound healing strategies. Concurrently, the safe *in vivo* use of these thermogelling copolymers must be ascertained. The potential biocompatibility issues, such as, histocompatibility, foreign body response, polymer/tissue interfacial properties and the presence of residual contaminants should be clarified for practical applications. It is a long journey for this material from bench to bedside. Issues such as the body's hypersensitivity to the copolymer have to be carefully studied before

this material can be used by the masses as consumers would expect absolute assurance that the material is safe for use. An entire battery of tests followed by regulatory approval from organizations, such as the U.S. Food and Drug Administration (FDA) is required before the product can be marketed. This work represents a first step in a multi-disciplinary field which can lead to two basic interlinked paths. Along one path, significant scientific progress in uncharted domains can be envisioned with the combination of the biological, chemical and physical aspects of this work. Along the other path, the successful utilization of these "smart biomaterials" by mankind would lead to reduced human suffering and ultimately, a better quality of life.